

Some pages of this thesis may have been removed for copyright restrictions.

If you have discovered material in Aston Research Explorer which is unlawful e.g. breaches copyright, (either yours or that of a third party) or any other law, including but not limited to those relating to patent, trademark, confidentiality, data protection, obscenity, defamation, libel, then please read our [Takedown policy](#) and contact the service immediately (openaccess@aston.ac.uk)

Structures and Magnetic Properties of Iron(III) Spin-
Crossover Compounds

ROBYN ELIZABETH POWELL

Doctor of Philosophy

ASTON UNIVERSITY

June 2016

© Robyn Elizabeth Powell, 2016

Robyn Elizabeth Powell asserts her moral right to be
identified as the author of this thesis.

This copy of the thesis has been supplied on condition that
anyone who consults it is understood to recognise that its
copyright rests with its author and that no quotation from the
thesis and no information derived from it may be published
without appropriate permission or acknowledgement.

Structures and Magnetic Properties of Iron(III) Spin-Crossover Compounds

Robyn Elizabeth Powell

Doctor of Philosophy

2016

Summary

Transition metal fragments displaying switching behaviour are appealing materials, which may be used in a functional way in research and technology. Some molecular species containing transition metal ions may exhibit a crossover between states having a different magnetic moment, the magnetic interconversion between the low-spin and high-spin state in Fe^{III} systems which can be triggered by a change in temperature, pressure or by light irradiation.

The research presented in this thesis focuses on using substituted derivatives of R-salicylaldehyde 4R'-thiosemicarbazone (H₂L, H₂-R-thsa-R') for generating Fe^{III} spin crossover. The aim was to design mononuclear Fe^{III} compounds with a view of studying their structural features and magnetic properties. The results present the full structural analysis of differently charged Fe^{III}-bis(ligand) complexes, these include: (i) (cation⁺)[Fe^{III}(L²⁻)₂].x(solvent), (ii) [Fe^{III}(HL⁻)(L²⁻)].x(solvent) and (iii) [Fe^{III}(HL⁻)₂](anion⁻).x(solvent). The studies discuss several influences on the structural features and the magnetic properties of the reported Fe^{III} compounds, these include: the nature of the anion or cation associated with the Fe^{III} complex, the degree of solvation of the complex and the variations in the ligand substituents.

The magnetic studies of the (cation⁺)[Fe^{III}(L²⁻)₂].x(solvent) compounds have presented one high-spin compound ((CH₃)₂NH₂[Fe(3-OEt-thsa)₂]) and four low-spin compounds (Cs[Fe(3-OEt-thsa-Me)₂].CH₃OH, Cs[Fe(5-Br-thsa)₂], NH₄[Fe(thsa)₂] and NH₄[Fe(5-Br-thsa)₂]), of which NH₄[Fe(5-Br-thsa)₂] revealed a fraction of the Fe^{III} ions convert into the high-spin state. Three [Fe^{III}(HL⁻)(L²⁻)].x(solvent) compounds have been studied, of which a rare two-step spin transition has been observed for [Fe(H-5-Cl-thsa-Me)(5-Cl-thsa-Me)].H₂O, while the isostructural compounds [Fe(H-thsa-Me)(thsa-Me)].H₂O undergoes an incomplete spin transition and [Fe(H-3-OEt-thsa-Me)(3-OEt-thsa-Me)].H₂O remains in the high-spin state. It was recognised that the steric and electronic features imposed by the R,R'-substituents may have an impact on the spin state of Fe^{III} cations, and affect at which temperature the spin transition occurs. Furthermore, the Fe^{III} cation of both [Fe^{III}(HL⁻)₂](anion⁻).x(solvent) compounds, [Fe(H-5-Br-thsa-Et)₂](NO₃).H₂O and [Fe(H-4-OH-thsa)₂]₄.(SO₄)₂.9H₂O, were found to be in the high-spin state.

Collectively, the described research has provided new insight into this family of Fe^{III} bis(R-salicylaldehyde 4R'-thiosemicarbazone) compounds and provides a strong foundation for further studies.

Keywords: Fe^{III}, spin-crossover, R-salicylaldehyde 4R'-thiosemicarbazone, intermolecular interactions, two-step spin transition

To my family

Acknowledgements

First and foremost, I would like to thank my supervisor, Dr Petra van Koningsbruggen, for all of her support, guidance and knowledge over the past four years which has been invaluable during my time studying for a PhD.

Secondly, my thanks to my associate supervisor Professor Sahar Al-Malaika for her wisdom and constant support, no matter when I may have needed help.

Thirdly, I would like to express my gratitude to Dr Peter Weinberger, Dr Danny Müller, Dr Berthold Stöger and Christian Knoll from the Institute of Applied Synthetic Chemistry, Vienna University of Technology, for their help in the early days of my PhD with crystallographic and magnetic studies and for making my visit to Vienna, so very enjoyable.

I must thank Professor Carl Schwalbe for his help, but especially for imparting his invaluable knowledge of crystallography to me during my studies.

I would like to acknowledge and thank Dr Graham Tizzard whom has taken great care of my samples over the past four years, in association with the EPSRC research grant held with the UK National Crystallography Service, University of Southampton.

My thanks to Dr Martin Lees at the University of Warwick, for the SQUID studies.

Special gratitude belongs to my dear friend Dr Gwen Welsh whose advice and sense of humour has been a motivation to keep me working in the right direction. Of course, many thanks to the rest of the post-graduates in the CEAC department, who made the hard times bearable and the good times great.

I wish to extend my thanks to James, your love, optimism, understanding and support made the hard times of doing this PhD seem inconsequential.

Lastly, I thank my parents, Maria and Alan, and my brothers, Joshua and Thomas, for their unwavering confidence in me, encouragement, love, and support throughout my studies. Without their motivation, I do not think I would have made it past the finish line.

List of Contents

Summary	2
Dedication	3
Acknowledgements	4
List of Contents	5
List of Figures	11
List of Tables	17
Abbreviations	20
Chapter I	23
1.0 Introduction	24
1.1 Introduction to the spin-crossover phenomenon.....	24
1.2 Iron(III) spin-crossover.....	28
1.2.1 R-salicylaldehyde 4R'-thiosemicarbazone ligand system	29
1.3 Factors affecting spin-crossover	30
1.3.1 Chemical Influences	31
1.3.2 Physical Influences	32
1.3.3 Detection of spin-crossover	37
1.3.3.1 Experimental techniques.....	38
1.4 Iron(III) spin-crossover systems with bis(R-salicylaldehyde 4R'-thiosemicarbazone) ligands.....	41
1.4.1 Structural Aspects.....	41
1.4.2 Characterisation by Spectroscopic Techniques	49
1.4.3 Magnetic Studies	50
1.5 Applications of Spin-Crossover Materials.....	53
1.6 Objectives and Scope of Research.....	57
1.7 References	58
Chapter II	63
2.0 Materials and Methods	64
2.1 Introduction	64
2.2 Materials	64
2.3 Ligand Synthesis.....	67
2.3.1 Synthesis of R-salicylaldehyde 4R'-thiosemicarbazone (H ₂ L) based ligands.....	67
2.4 Synthesis of Iron(III) Coordination Compounds	69
2.4.1 Cation[Fe ^{III} (L) ₂]-solvate Complexes	69
2.4.2 [Fe ^{III} (HL)(L)]-solvate Complexes	71

2.4.3 [Fe ^{III} (HL) ₂ ·anion·solvate Complexes	72
2.5 Analytical Techniques	73
2.5.1 Fourier Transform Infrared Spectroscopy	73
2.5.2 Nuclear Magnetic Resonance Spectroscopy.....	73
2.5.3 Single Crystal X-ray Diffraction Measurements	73
2.6 Physical Measurements	74
2.6.1 Differential Scanning Calorimetry	74
2.6.2 Magnetic Measurements.....	75
2.7 References	75
Chapter III	77
3.0 Anionic Fe(III) Complexes of R-salicylaldehyde 4R'-thiosemicarbazones	78
3.1 Introduction	78
3.2 The crystal structure and magnetic properties of caesium bis(3-ethoxysalicylaldehyde 4-methylthiosemicarbazone(2-)-κ ³ -O ² ,N ¹ ,S)ferrate(III) methanol monosolvate.....	79
3.2.1 Crystal Data and Structure Refinement Details of Cs[Fe(3-OEt-thsa-Me) ₂]·CH ₃ OH.....	80
3.2.2 Crystallographic study of Cs[Fe(3-OEt-thsa-Me) ₂]·CH ₃ OH.....	81
3.2.3 Magnetic Studies of Cs[Fe(3-OEt-thsa-Me) ₂]·CH ₃ OH	85
3.3 The crystal structure and magnetic properties of caesium bis(5-bromosalicylaldehyde thiosemicarbazone(2-)-κ ³ -O,N ¹ ,S)ferrate(III)	86
3.3.1 Crystal Data and Structure Refinement Details of Cs[Fe(5-Br-thsa) ₂].....	87
3.3.2 Crystallographic study of Cs[Fe(5-Br-thsa) ₂].....	88
3.3.3 Magnetic Studies of Cs[Fe(5-Br-thsa) ₂]	94
3.4 The crystal structure and magnetic properties of ammonium bis(salicylaldehyde thiosemicarbazone(2-)-κ ³ -O,N ¹ ,S)ferrate(III)	94
3.4.1 Crystal Data and Structure Refinement Details of NH ₄ [Fe(thsa) ₂]	95
3.4.2 Crystallographic study of NH ₄ [Fe(thsa) ₂]	97
3.4.3 Magnetic Studies of NH ₄ [Fe(thsa) ₂]	100
3.5 The crystal structure and magnetic properties of ammonium bis(5-bromosalicylaldehyde thiosemicarbazone(2-)-κ ³ -O,N ¹ ,S)ferrate(III)	100
3.5.1 Crystal Data and Structure Refinement Details of NH ₄ [Fe(5-Br-thsa) ₂].....	102
3.5.2 Crystallographic study of NH ₄ [Fe(5-Br-thsa) ₂].....	102
3.5.3 Magnetic Studies of NH ₄ [Fe(5-Br-thsa) ₂]	107
3.6 The crystal structure and magnetic properties of dimethylammonium bis(3-ethoxy-salicylaldehyde thiosemicarbazone(2-)-κ ³ -O ² ,N ¹ ,S)ferrate(III)	108
3.6.1 Crystal Data and Structure Refinement Details of (CH ₃) ₂ NH ₂ [Fe(3-OEt-thsa) ₂].....	109
3.6.2 Crystallographic study of (CH ₃) ₂ NH ₂ [Fe(3-OEt-thsa) ₂].....	110
3.6.3 Magnetic Studies of (CH ₃) ₂ NH ₂ [Fe(3-OEt-thsa) ₂]	114

3.7 Discussion of Fe ^{III} bis(ligand) compounds of R-salicylaldehyde 4R'-thiosemicarbazone ...	116
3.8 References	120
Chapter IV	122
4.0 Neutral Fe(III) Complexes of R-salicylaldehyde 4R'-thiosemicarbazones.....	123
4.1 Introduction	123
4.2 The crystal structure and magnetic properties of [Fe(H-thsa-Me)(thsa-Me)]·H ₂ O	125
4.2.1 Crystal Data and Structure Refinement Details of [Fe(H-thsa-Me)(thsa-Me)]·H ₂ O.....	125
4.2.2 Crystallographic study of [Fe(H-thsa-Me)(thsa-Me)]·H ₂ O.....	126
4.2.3 Infrared spectroscopic studies of [Fe(H-thsa-Me)(thsa-Me)]·H ₂ O and the ligand salicylaldehyde 4-methylthiosemicarbazone, H ₂ -thsa-Me	130
4.2.4 Magnetic Studies of [Fe(H-thsa-Me)(thsa-Me)]·H ₂ O	131
4.3 The crystal structure and magnetic properties of [Fe(H-3-OEt-thsa-Me)(3-OEt-thsa-Me)]·H ₂ O.....	132
4.3.1 Crystal Data and Structure Refinement Details of [Fe(H-3-OEt-thsa-Me)(3-OEt-thsa-Me)]·H ₂ O.....	132
4.3.2 Crystallographic study of [Fe(H-3-OEt-thsa-Me)(3-OEt-thsa-Me)]·H ₂ O.....	133
4.3.3 Infrared spectroscopic studies of [Fe(H-3-OEt-thsa-Me)(3-OEt-thsa-Me)]·H ₂ O and the ligand 3-ethoxysalicylaldehyde 4-methylthiosemicarbazone, H ₂ -3-OEt-thsa-Me	138
4.3.4 Magnetic Studies of [Fe(H-3-OEt-thsa-Me)(3-OEt-thsa-Me)]·H ₂ O	139
4.4 The crystal structure and magnetic properties of [Fe(H-5-Cl-thsa-Me)(5-Cl-thsa-Me)]·H ₂ O	141
4.4.1 Crystal Data and Structure Refinement Details of [Fe(H-5-Cl-thsa-Me)(5-Cl-thsa-Me)]·H ₂ O.....	141
4.4.2 Crystallographic study of [Fe(H-5-Cl-thsa-Me)(5-Cl-thsa-Me)]·H ₂ O	143
4.4.3 Infrared spectroscopic studies of [Fe(H-5-Cl-thsa-Me)(5-Cl-thsa-Me)]·H ₂ O and the ligand 5-chlorosalicylaldehyde 4-methylthiosemicarbazone, H ₂ -5-Cl-thsa-Me.....	148
4.4.4 Magnetic Studies of [Fe(H-5-Cl-thsa-Me)(5-Cl-thsa-Me)]·H ₂ O	148
4.5 Discussion.....	150
4.5.1 Electronic effects of the R and R'-substituents of the R-salicylaldehyde 4R'- thiosemicarbazone ligand	152
4.5.2 Steric effects of the R and R'-substituents of the R-salicylaldehyde 4R'- thiosemicarbazone ligand	154
4.5.3 R and R'-substituents as hydrogen bonding donor or acceptor atoms and π-π stacking interactions	156
4.6 Conclusion	157
4.7 References	158
Chapter V	161
5.0 Cationic Fe(III) Complexes of R-salicylaldehyde 4R'-thiosemicarbazones	162

5.1 Introduction	162
5.2 The crystal structure and magnetic properties of $[\text{Fe}(\text{H-5-Br-thsa-Et})_2](\text{NO}_3) \cdot \text{H}_2\text{O}$	163
5.2.1 Crystal Data and Structure Refinement Details of $[\text{Fe}(\text{H-5-Br-thsa-Et})_2](\text{NO}_3) \cdot \text{H}_2\text{O}$...	163
5.2.2 Crystallographic study of $[\text{Fe}(\text{H-5-Br-thsa-Et})_2](\text{NO}_3) \cdot \text{H}_2\text{O}$	164
5.2.3 Infrared spectroscopic studies of $[\text{Fe}(\text{H-5-Br-thsa-Et})_2](\text{NO}_3) \cdot \text{H}_2\text{O}$ and the free ligand 5-bromosalicylaldehyde 4-ethylthiosemicarbazone, $\text{H}_2\text{-5-Br-thsa-Et}$	169
5.2.4 Magnetic Studies of $[\text{Fe}(\text{H-5-Br-thsa-Et})_2](\text{NO}_3) \cdot \text{H}_2\text{O}$	169
5.3 The crystal structure and magnetic properties of $[\text{Fe}(\text{H-4-OH-thsa})_2]_4 \cdot (\text{SO}_4)_2 \cdot 9\text{H}_2\text{O}$	171
5.3.1 Crystal Data and Structure Refinement Details of $[\text{Fe}(\text{H-4-OH-thsa})_2]_4 \cdot (\text{SO}_4)_2 \cdot 9\text{H}_2\text{O}$.	171
5.3.2 Crystallographic study of $[\text{Fe}(\text{H-4-OH-thsa})_2]_4 \cdot (\text{SO}_4)_2 \cdot 9\text{H}_2\text{O}$	173
5.3.3 Infrared spectroscopic studies of $[\text{Fe}(\text{H-4-OH-thsa})_2]_4 \cdot (\text{SO}_4)_2 \cdot 9\text{H}_2\text{O}$ and the free ligand 2,4-dihydroxybenzaldehyde thiosemicarbazone, $\text{H}_2\text{-4-OH-thsa}$	178
5.3.4 Magnetic Studies of $[\text{Fe}(\text{H-4-OH-thsa})_2]_4 \cdot (\text{SO}_4)_2 \cdot 9\text{H}_2\text{O}$	179
5.4 Discussion.....	180
5.5 References	184
Chapter VI	186
6.0 Conclusions and Outlook.....	187
6.1 Conclusions	187
6.1.1 Anionic Fe(III) complexes of R-salicylaldehyde 4R'-thiosemicarbazones.....	189
6.1.2 Neutral Fe(III) complexes of R-salicylaldehyde 4R'-thiosemicarbazones.....	189
6.1.3 Cationic Fe(III) complexes of R-salicylaldehyde 4R'-thiosemicarbazones	190
6.2 Outlook	191
6.3 References	194
Appendix	196
Appendix A. List of Publications.....	197
Appendix B. Infrared Spectra of R-salicylaldehyde 4R'-thiosemicarbazone ligands and ferric complexes.....	198
B1. Infrared spectrum of 3-ethoxysalicylaldehyde 4-methylthiosemicarbazone, $\text{H}_2\text{-3-OEt-thsa-Me}$	198
B2. Infrared spectrum of $\text{Cs}[\text{Fe}(\text{3-OEt-thsa-Me})_2] \cdot \text{CH}_3\text{OH}$	198
B3. Infrared spectrum of 5-bromosalicylaldehyde thiosemicarbazone, $\text{H}_2\text{-5-Br-thsa}$	199
B4. Infrared spectrum of $\text{Cs}[\text{Fe}(\text{5-Br-thsa})_2]$	199
B5. Infrared spectrum of salicylaldehyde thiosemicarbazone, $\text{H}_2\text{-thsa}$	200
B6. Infrared spectrum of $\text{NH}_4[\text{Fe}(\text{thsa})_2]$	200
B7. Infrared spectrum of $\text{NH}_4[\text{Fe}(\text{5-Br-thsa})_2]$	201
B8. Infrared spectrum of 3-ethoxysalicylaldehyde thiosemicarbazone, $\text{H}_2\text{-3-OEt-thsa}$	201
B9. Infrared spectrum of $(\text{CH}_3)_2\text{NH}_2[\text{Fe}(\text{3-OEt-thsa})_2]$	202

B10. Infrared spectrum of salicylaldehyde 4-methylthiosemicarbazone, H ₂ -thsa-Me	202
B11. Infrared spectrum of [Fe(H-thsa-Me)(thsa-Me)]·H ₂ O	203
B12. Infrared spectrum of [Fe(H-3-OEt-thsa-Me)(3-OEt-thsa-Me)]·H ₂ O	203
B13. Infrared spectrum of 5-chlorosalicylaldehyde 4-methylthiosemicarbazone, H ₂ -5-Cl-thsa-Me.....	204
B14. Infrared spectrum of [Fe(H-5-Cl-thsa-Me)(5-Cl-thsa-Me)]·H ₂ O	204
B15. Infrared spectrum of 5-bromosalicylaldehyde 4-ethylthiosemicarbazone, H ₂ -5-Br-thsa-Et	205
B16. Infrared spectrum of [Fe(H-5-Br-thsa-Et) ₂](NO ₃)·H ₂ O	205
B17. Infrared spectrum of 2,4-dihydroxybenzaldehyde thiosemicarbazone, H ₂ -4-OH-thsa	206
B18. Infrared spectrum of [Fe(H-4-OH-thsa) ₂] ₄ ·(SO ₄) ₂ ·9H ₂ O	206
Appendix C. ¹H NMR Spectra of R-salicylaldehyde 4R'-thiosemicarbazone ligands.....	207
C1. ¹ H NMR spectrum of 3-ethoxysalicylaldehyde 4-methylthiosemicarbazone, H ₂ -3-OEt-thsa-Me.....	207
C2. ¹ H NMR spectrum of 5-bromosalicylaldehyde thiosemicarbazone, H ₂ -5-Br-thsa	207
C3. ¹ H NMR spectrum of salicylaldehyde thiosemicarbazone, H ₂ -thsa.....	208
C4. ¹ H NMR spectrum of 3-ethoxysalicylaldehyde thiosemicarbazone, H ₂ -3-OEt-thsa.....	208
C5. ¹ H NMR spectrum of salicylaldehyde 4-methylthiosemicarbazone, H ₂ -thsa-Me.....	209
C6. ¹ H NMR spectrum of 5-chlorosalicylaldehyde 4-methylthiosemicarbazone, H ₂ -5-Cl-thsa-M	209
C7. ¹ H NMR spectrum of 5-bromosalicylaldehyde 4-ethylthiosemicarbazone, H ₂ -5-Br-thsa-Et	210
C8. ¹ H NMR spectrum of 2,4-dihydroxybenzaldehyde thiosemicarbazone, H ₂ -4-OH-thsa.....	210
Appendix D. ¹³C NMR Spectra of R-salicylaldehyde 4R'-thiosemicarbazone ligands	211
D1. ¹³ C NMR spectrum of 3-ethoxysalicylaldehyde 4-methylthiosemicarbazone, H ₂ -3-OEt-thsa-Me.....	211
D2. ¹³ C NMR spectrum of 5-bromosalicylaldehyde thiosemicarbazone, H ₂ -5-Br-thsa	211
D3. ¹³ C NMR spectrum of salicylaldehyde thiosemicarbazone, H ₂ -thsa.....	212
D4. ¹³ C NMR spectrum of 3-ethoxysalicylaldehyde thiosemicarbazone, H ₂ -3-OEt-thsa	212
D5. ¹³ C NMR spectrum of salicylaldehyde 4-methylthiosemicarbazone, H ₂ -thsa-Me	213
D6. ¹³ C NMR spectrum of 5-chlorosalicylaldehyde 4-methylthiosemicarbazone, H ₂ -5-Cl-thsa-Me.....	213
D7. ¹³ C NMR spectrum of 5-bromosalicylaldehyde 4-ethylthiosemicarbazone, H ₂ -5-Br-thsa-Et	214
D8. ¹³ C NMR spectrum of 2,4-dihydroxybenzaldehyde thiosemicarbazone, H ₂ -4-OH-thsa	214
Appendix E. Synthesis of R-salicylaldehyde 4R'-thiosemicarbazone and Fe^{III} compounds not presented in the thesis	215

E1. Synthesis of R-salicylaldehyde 4R'-thiosemicarbazone (H ₂ L) based ligands	215
E1.1. List of Ligands	215
E2. Attempted syntheses of Fe ^{III} compounds containing the ligand system: R-salicylaldehyde 4R'-thiosemicarbazone (H ₂ -R-thsa-R')	218

List of Figures

Figure	Page
Figure 1.1 The effect of the splitting of the d-orbitals when placing a metal ion into an octahedral crystal field (Δ_o splitting energy of the octahedral crystal field).	24
Figure 1.2 The two possible ground state electronic configurations for a d^5 metal ion in an octahedral crystal field.	25
Figure 1.3 Spin-crossover dependent upon external perturbations of temperature (T), pressure (p) or light irradiation (hv) for octahedral compounds of Fe^{III} , a $3d^5$ system. The high-spin and low-spin form differ in electronic population of the 3d orbitals with an associated alteration of the magnetic and structural characteristics.	26
Figure 1.4 The potential wells for the high-spin (6A_1) and the low-spin (2T_2) states as a function of the Fe^{III} -donor atom distance, along the symmetric metal-ligand stretching vibration ($r(M-L)$ where M = metal cation and L = ligand). The change in metal-ligand bond distance (<i>i.e.</i> the horizontal displacement of the wells) is represented by $\Delta r(HL)$, and $\Delta E^\circ(HL)$ represents the zero point energy difference between the two spin states. (Adapted from reference [2]).	27
Figure 1.5 $\gamma_{HS}(T)$ plots of the possible different types of thermal spin transition curve i) smooth and continuous, ii) abrupt, iii) with hysteresis, iv) with steps and v) incomplete.	28
Figure 1.6 The two tautomeric forms of R-salicylaldehyde 4R'-thiosemicarbazone, the thione (left) and the thiol (right).	29
Figure 1.7 The dianion of R-salicylaldehyde 4R'-thiosemicarbazone, together with the atom labelling of the R-salicylaldehyde unit.	29
Figure 1.8 Schematic representation of the mechanism for LIESST (green arrow) and reverse-LIESST (red arrow) for Fe^{II} systems. The solid lines indicate excitation by irradiation while dotted lines represent relaxation pathways. (Adapted from reference [20]).	33
Figure 1.9 <i>Trans</i> (left)/ <i>cis</i> (right) isomerisation in 4-styrylpyridine (stpy).	34
Figure 1.10 Schematic representation of the effect of pressure (p) on Fe^{II} spin-crossover systems. (Adapted from reference [43]).	36
Figure 1.11 The strongest intermolecular contacts between $[Fe(5-Br-thsa)_2]^-$ complexes at (a) 150 K and (b) 373 K, adapted from reference [59].	45
Figure 1.12 (a) The molecular packing arrange of $[Fe(H-thsa)(thsa)] \cdot H_2O$ and (b) illustrates the 2D networks of $[Fe(H-5-Cl-thsa)(5-Cl-thsa)] \cdot H_2O$. (c) and (d) illustrate the π - π stacking interactions of $[Fe(H-thsa)(thsa)] \cdot H_2O$ and $[Fe(H-5-Cl-thsa)(5-Cl-thsa)] \cdot H_2O$ at 295 K, respectively. (Adapted from reference [18]).	46

Figure 1.13 (a) 1D supramolecular chain connected by the hydrogen bonds N(azomethine)-H \cdots Ow and N(amide)-H \cdots O at 123 K. (b) 2D supramolecular packing structure of [Fe(H-5-Br-thsa)(5-Br-thsa)] \cdot H $_2$ O along the <i>c</i> axis at 183 K. (Adapted from reference [60]).	47
Figure 1.14 Supramolecular hydrogen bonding packing arrangement of [Fe(H-5-Cl-thsa-Me)(5-Cl-thsa-Me)] \cdot H $_2$ O. (Adapted from reference [19]).	48
Figure 1.15 Temperature dependence of the χ_{MT} product for Li[Fe(5-Br-thsa) $_2$] \cdot H $_2$ O. (Adapted from reference [59]).	51
Figure 1.16 Temperature dependence of the χ_{MT} product for (a) [Fe(H-thsa)(thsa)] \cdot H $_2$ O and (b) [Fe(H-5-Cl-thsa)(5-Cl-thsa)] \cdot H $_2$ O. (Adapted from reference [18]).	52
Figure 1.17 Temperature dependence of the χ_{MT} product for [Fe(H-5-Br-thsa)(5-Br-thsa)] \cdot H $_2$ O. (Adapted from reference [60]).	52
Figure 1.18 Temperature dependence of the χ_{MT} product for [Fe(H-5-Cl-thsa)(5-Cl-thsa)] \cdot H $_2$ O. (Adapted from reference [19]).	53
Figure 3.1.1 Structure of R-salicylaldehyde 4R'-thiosemicarbazone ligands.	79
Figure 3.2.1 The molecular structure and atom-numbering scheme for Cs[Fe(3-OEt-thsa-Me) $_2$] \cdot CH $_3$ OH. The Cs $^+$, CH $_3$ OH and alternative orientation for C110-C111 have been omitted for clarity. Displacement ellipsoids are drawn at the 50% probability level.	82
Figure 3.2.2 A projection showing the unit cell of Cs[Fe(3-OEt-thsa-Me) $_2$] \cdot CH $_3$ OH. An alternative orientation for C110-C111 has been omitted for clarity. Displacement ellipsoids are drawn at the 50% probability level. [Symmetry codes: (i) $-x + 1, -y + 1, -z + 1$; (ii) $-x, -y + 1, -z + 1$.]	85
Figure 3.2.3 χ_{MT} vs T plot of Cs[Fe(3-OEt-thsa-Me) $_2$] \cdot CH $_3$ OH. [The sample was heated (\blacktriangle) and subsequently cooled (\blacktriangledown).]	86
Figure 3.3.1 The molecular structure and atom-numbering scheme for Cs[Fe(5-Br-thsa) $_2$]. Displacement ellipsoids are drawn at 50% probability level.	89
Figure 3.3.2 A projection showing the unit cell of Cs[Fe(5-Br-thsa) $_2$]. The Cs $^+$ cation has been omitted for clarity. Displacement ellipsoids are drawn at the 50% probability level. Dashed lines indicate hydrogen bonds. [Symmetry codes: (iv) $x, -y + 1/2, z + 1/2$; (v) $-x + 1, y - 1/2, -z + 3/2$; (vi) $x, -y + 3/2, z + 1/2$; (vii) $-x + 2, y + 1/2, -z + 3/2$; (viii) $-x + 2, y + 1/2, -z + 1/2$; (ix) $-x + 1, y - 1/2, -z + 1/2$.]	93
Figure 3.3.3 χ_{MT} vs T plot of Cs[Fe(5-Br-thsa) $_2$]. [The sample was heated (\blacktriangle) and subsequently cooled (\blacktriangledown).]	94
Figure 3.4.1 The molecular structure and atom-numbering scheme for NH $_4$ [Fe(thsa) $_2$]. The N atom of the NH $_4^+$ cation has been omitted from the figure for clarity. Displacements ellipsoids are drawn at the 50% probability level.	97

Figure 3.4.2	A projection showing the unit cell of NH ₄ [Fe(thsa) ₂]. The N atom of the ammonium cation has been omitted for clarity. Displacement ellipsoids are drawn at the 50% probability level. Dashed lines indicate hydrogen bonds. [Symmetry codes: (i) $x - 1/2, 1/2 - y, z - 1/2$; (ii) $x - 1/2, 1/2 - y, 1/2 + z$.]	99
Figure 3.4.3	$\chi_M T$ vs T plot of NH ₄ [Fe(thsa) ₂]. [The sample was heated (▲) and subsequently cooled (▼).]	100
Figure 3.5.1	The molecular structure and atom-numbering scheme for NH ₄ [Fe(5-Br-thsa) ₂]. The N atom of the NH ₄ ⁺ cation, and alternative orientation for O1', S1', C2', C3' and C4' have been omitted from the figure for clarity. Displacements ellipsoids are drawn at the 50% probability level. [Symmetry code: (i) $-x, y, -z - 1/2$.]	104
Figure 3.5.2	A projection showing the unit cell of NH ₄ [Fe(5-Br-thsa) ₂]. The N atom of the NH ₄ ⁺ cation, and alternative orientation for O1', S1', C2', C3' and C4' have been omitted for clarity. Displacements ellipsoids are drawn at the 50% probability level. Dashed lines indicate hydrogen bonds. [Symmetry codes: (i) $1/2 + x, 3/2 - y, -1 - z$; (ii) $1/2 + x, 3/2 - y, -1 - z$.]	106
Figure 3.5.3	$\chi_M T$ vs T plot of NH ₄ [Fe(5-Br-thsa) ₂]. [The sample was heated (▲) and subsequently cooled (▼).]	107
Figure 3.5.4	DSC curves obtained for NH ₄ [Fe(5-Br-thsa) ₂] in the temperature range 100-300 K, measured at a scan rate of 5 K min ⁻¹ .	108
Figure 3.6.1	The molecular structure and atom-numbering scheme for (CH ₃) ₂ NH ₂ [Fe(3-OEt-thsa) ₂]. Displacement ellipsoids are drawn at the 50 % probability level.	111
Figure 3.6.2	A projection showing the unit cell of (CH ₃) ₂ NH ₂ [Fe(3-OEt-thsa) ₂]. Displacement ellipsoids are drawn at 50% probability level. Dashed lines indicate hydrogen bonds.	114
Figure 3.6.3	$\chi_M T$ vs T plot of (CH ₃) ₂ NH ₂ [Fe(3-OEt-thsa) ₂]. [The sample was heated (▲) and subsequently cooled (▼).]	114
Figure 3.6.4	Temperature dependence of the molar magnetic susceptibility, χ_M , for the compound (CH ₃) ₂ NH ₂ [Fe(3-OEt-thsa) ₂] in the range 5-150 K. Points are the experimental data; solid red line represents the least-squares fit of the data to Equation (1), where $D = 0.80 \text{ cm}^{-1}$ and $g = 2.20$.	116
Figure 4.1.1	Molecular structure of the R-salicylaldehyde 4R'-thiosemicarbazone ligands (i) H ₂ -3-OEt-thsa-Me and (ii) H ₂ -thsa-Me.	124
Figure 4.2.1	The molecular structure and atom-numbering scheme of [Fe(H-thsa-Me)(thsa-Me)]·H ₂ O, whereby the ligand bound to Fe1 atom are related by the symmetry operation: (i) $-x + 1, -y + 1, z$. The hydrogen atom bound to N2 and N2 ⁱ atoms has a site	127

occupancy factor of 0.5, <i>i.e.</i> the atom is disordered over the N2 and N2 ⁱ sites (50:50). Displacement ellipsoids are drawn at the 50% probability level.	
Figure 4.2.2 A projection showing the unit cell of [Fe(H-thsa-Me)(thsa-Me)]·H ₂ O. The disordered H ₂ O molecule has been omitted for clarity. Displacement ellipsoids are drawn at the 50% probability level. Dashed lines indicate hydrogen bonds. [Symmetry codes: (i) $-x + 1, -y + 1, z$; (ii) $x - 1/2, -y + 1, z + 1/2$]	129
Figure 4.2.3 $\chi_M T$ vs T plot of [Fe(H-thsa-Me)(thsa-Me)]·H ₂ O (left). The sample was warmed (\blacktriangle) and then subsequently cooled (\blacktriangledown) in the temperature region of 5-300 K, at a rate of 2 K min ⁻¹ . DSC curves (right) obtained for [Fe(H-thsa-Me)(thsa-Me)]·H ₂ O at a scan rate of 5 K min ⁻¹ .	131
Figure 4.2.4 $\chi_M T$ vs T plot of [Fe(H-thsa-Me)(thsa-Me)]·H ₂ O. The sample was warmed (\blacktriangle) in the temperature region of 200–400 K, at a rate of 2 K min ⁻¹ .	132
Figure 4.3.1 The molecular structure and atom-numbering scheme for the asymmetric unit of [Fe(H-3-OEt-thsa-Me)(3-OEt-thsa-Me)]·H ₂ O. The two H ₂ O molecules has been omitted for clarity. Displacement ellipsoids are drawn at the 50% probability level.	135
Figure 4.3.2 A projection of the unit cell of [Fe(H-3-OEt-thsa-Me)(3-OEt-thsa-Me)]·H ₂ O. Displacement ellipsoids are drawn at the 50% probability level.	138
Figure 4.3.3 $\chi_M T$ vs T plot of [Fe(H-3-OEt-thsa-Me)(3-OEt-thsa-Me)]·H ₂ O in the temperature range of 5 – 300 K, measured at a rate of 2 K min ⁻¹ . (i) The heating mode is shown on the left and represented by the symbol (Δ) and (ii) the cooling mode on the right is represented by the symbol (\blacktriangledown).	139
Figure 4.3.4 DSC curves obtained for [Fe(H-3-OEt-thsa-Me)(3-OEt-thsa-Me)]·H ₂ O in the temperature range 150-350 K, measured at a scan rate of 5 K min ⁻¹ .	140
Figure 4.3.5 Temperature dependence of the molar magnetic susceptibility, χ_M , for the compound [Fe(H-3-OEt-thsa-Me)(3-OEt-thsa-Me)]·H ₂ O in the range 5-150 K. Points represent the cooling mode experimental data; solid red line represents the least-squares fit of the data to Equation (1), where $D = 2.85$ cm ⁻¹ and $g = 2.18$.	141
Figure 4.4.1 The molecular structure and atom-numbering scheme for [Fe(H-5-Cl-thsa-Me)(5-Cl-thsa-Me)]·H ₂ O, whereby the second ligand bound to Fe1 atom is generated by the symmetry operation (i) $-x + 1, -y + 1, z$. The hydrogen atom bound to N2 and N2 ⁱ atoms has a site occupancy factor of 0.5, <i>i.e.</i> the atom is disordered over the N2 and N2 ⁱ sites (50:50). The H ₂ O molecule has been omitted for clarity. Displacement ellipsoids are drawn at the 50% probability level.	143
Figure 4.4.2 A projection showing the unit cell of [Fe(H-5-Cl-thsa-Me)(5-Cl-thsa-Me)]·H ₂ O. The disordered H ₂ O molecule has been omitted for clarity. The displacement ellipsoids are drawn at the 50% probability level.	146

Figure 4.4.3 Hydrogen bonding system of [Fe(H-5-Cl-thsa-Me)(5-Cl-thsa-Me)]·H ₂ O in the <i>a</i> direction. An alternative orientation for H1WA and H1WB has been omitted for clarity. The displacement ellipsoids are drawn at the 50% probability level. [Symmetry codes: (i) $-x + 1, -y + 1, z$; (ii) $-x + 3/2, y, z + 1/2$; (iii) $x + 1/2, -y + 1, z + 1/2$; (iv) $-x + 3/2, y, z - 1/2$.]	147
Figure 4.4.4 $\chi_M T$ vs <i>T</i> plot of [Fe(H-5-Cl-thsa-Me)(5-Cl-thsa-Me)]·H ₂ O. The sample was warmed (\blacktriangle) and then subsequently cooled (\blacktriangledown) in the temperature region of 5–320 K, at a rate of 2 K min ⁻¹ .	149
Figure 4.4.5 DSC curves obtained for [Fe(H-5-Cl-thsa-Me)(5-Cl-thsa-Me)]·H ₂ O in the temperature range 200-350 K, measured at a scan rate of 5 K min ⁻¹ .	149
Figure 4.5.1 Atom labelling of the benzene ring of the R-salicylaldehyde 4R'-thiosemicarbazone ligand.	153
Figure 5.1.1 Molecular structure of the R-salicylaldehyde 4R'-thiosemicarbazone ligands (i) H ₂ -5-Br-thsa-Et and (ii) H ₂ -4-OH-thsa	163
Figure 5.2.1 The molecular structure and atom-numbering scheme for [Fe(H-5-Br-thsa-Et) ₂](NO ₃)·H ₂ O. Displacement ellipsoids are drawn at the 50% probability level.	165
Figure 5.2.2 A projection showing the hydrogen bonding interactions of [Fe(H-5-Br-thsa-Et) ₂](NO ₃)·H ₂ O. Displacement ellipsoids are drawn at the 50% probability level. Dashed lines indicate hydrogen bonds. [Symmetry codes: (i) $x + 1, -y + 1/2, -z + 3/2$; (ii) $x - 1/2, y, -z + 1$; (iii) $x, -y + 1/2, -z + 3/2$.]	167
Figure 5.2.3 A projection showing the unit cell of [Fe(H-5-Br-thsa-Et) ₂](NO ₃)·H ₂ O. Displacement ellipsoids are drawn at the 50% probability level.	168
Figure 5.2.4 $\chi_M T$ vs <i>T</i> plot of [Fe(H-5-Br-thsa-Et) ₂](NO ₃)·H ₂ O in the temperature range 5-300 K. The data were measured at a rate of 2 K min ⁻¹ .	170
Figure 5.2.5 Temperature dependence of the molar magnetic susceptibility, χ_M , for the compound [Fe(H-5-Br-thsa-Et) ₂](NO ₃)·H ₂ O in the range 5-300 K. Points are the experimental data; solid red line represents the least-squares fit of the data to Equation (1), where $D = 2.12$ cm ⁻¹ and $g = 2.22$.	171
Figure 5.3.1 The molecular structure and atom-numbering scheme of the Fe1 unit for [Fe(H-4-OH-thsa) ₂] ₄ ·(SO ₄) ₂ ·9H ₂ O. Displacement ellipsoids are drawn at the 50% probability level.	173
Figure 5.3.2 The molecular structure of the asymmetric unit of [Fe(H-4-OH-thsa) ₂] ₄ ·(SO ₄) ₂ ·9H ₂ O.	174
Figure 5.3.3 A projection of selected hydrogen bonding ring systems within the asymmetric unit of [Fe(H-4-OH-thsa) ₂] ₄ ·(SO ₄) ₂ ·9H ₂ O. Displacement ellipsoids are drawn at the 50% probability level.	178

Figure 5.3.4 $\chi_M T$ vs T plot of $[\text{Fe}(\text{H-4-OH-thsa})_2]_4 \cdot (\text{SO}_4)_2 \cdot 9\text{H}_2\text{O}$ in the temperature range 5-300 K. the data were measured at a rate of 2 K min⁻¹. 179

Figure 5.3.5 Temperature dependence of the molar magnetic susceptibility, χ_M , for the compound $[\text{Fe}(\text{H-4-OH-thsa})_2]_4 \cdot (\text{SO}_4)_2 \cdot 9\text{H}_2\text{O}$ in the range 5-300 K. Points are the experimental data; solid red line represents the least-squares fit of the data to Equation (1), where $D = 2.78 \text{ cm}^{-1}$ and $g = 2.10$. 180

List of Tables

Table	Page
Table 1.1 Crystallographic data of R-salicylaldehyde 4R'-thiosemicarbazone Fe ^{III} bis(ligand) compounds.	42
Table 2.1 Salicylaldehyde derivatives utilised in the synthesis of the various R-salicylaldehyde 4R'-thiosemicarbazone ligands.	64
Table 2.2 Thiosemicarbazone derivatives utilised in the synthesis of the various R-salicylaldehyde 4R'-thiosemicarbazone ligands.	65
Table 2.3 Various Fe ^{III} salts used in the synthesis of the Fe ^{III} bis(ligand) compounds.	66
Table 2.4 Different bases used in the synthesis of the Fe ^{III} bis(ligand) complexes.	66
Table 3.2.1 Crystal data and structure refinement details of Cs[Fe(3-OEt-thsa-Me) ₂].CH ₃ OH.	80
Table 3.2.2 Selected geometric parameters of Cs[Fe(3-OEt-thsa-Me) ₂].CH ₃ OH (Å, °).	83
Table 3.2.3 Hydrogen bond geometry of Cs[Fe(3-OEt-thsa-Me) ₂].CH ₃ OH (Å, °).	85
Table 3.3.1 Crystal data and structure refinement details of Cs[Fe(5-Br-thsa) ₂].	87
Table 3.3.2 Selected geometric parameters of Cs[Fe(5-Br-thsa) ₂] (Å, °).	89
Table 3.3.3 Hydrogen-bond geometry of Cs[Fe(5-Br-thsa) ₂] (Å, °).	93
Table 3.4.1 Crystal data and structure refinement details of NH ₄ [Fe(thsa) ₂].	96
Table 3.4.2 Selected geometric parameters of NH ₄ [Fe(thsa) ₂] (Å, °).	98
Table 3.4.3 Hydrogen bond geometry of NH ₄ [Fe(thsa) ₂] (Å, °).	100
Table 3.5.1 Crystal data and structure refinement details of NH ₄ [Fe(5-Br-thsa) ₂].	103
Table 3.5.2 Selected geometric parameters of NH ₄ [Fe(5-Br-thsa) ₂] (Å, °).	104
Table 3.5.3 Hydrogen bond geometry of NH ₄ [Fe(5-Br-thsa) ₂] (Å, °).	106
Table 3.6.1 Crystal data and structure refinement details of (CH ₃) ₂ NH ₂ [Fe(3-OEt-thsa) ₂].	109
Table 3.6.2 Selected geometric parameters of (CH ₃) ₂ NH ₂ [Fe(3-OEt-thsa) ₂] (Å, °).	112
Table 3.6.3 Hydrogen bond geometry of (CH ₃) ₂ NH ₂ [Fe(3-OEt-thsa) ₂] (Å, °).	114
Table 3.7.4 Fe-donor atom bond for various (cation ⁺)[Fe(ligand) ₂].nH ₂ O compounds of R-salicylaldehyde thiosemicarbazone described in this chapter.	117
Table 3.7.5 Selected average Fe-donor atom bond distances for non-solvated Fe ^{III} bis(ligand) compounds of R-salicylaldehyde thiosemicarbazone described in the literature.	118
Table 4.2.1 Crystal data and structure refinement details of [Fe(H-thsa-Me)(thsa-Me)].H ₂ O	125
Table 4.2.2 Selected geometric parameters of [Fe(H-thsa-Me)(thsa-Me)].H ₂ O (Å, °)	128
Table 4.2.3 Hydrogen bond geometry of [Fe(H-thsa-Me)(thsa-Me)].H ₂ O (Å, °)	130

Table 4.3.1 Crystal data and structure refinement details of [Fe(H-3-OEt-thsa-Me)(3-OEt-thsa-Me)]·H ₂ O	134
Table 4.3.2 Selected geometric parameters of [Fe(H-3-OEt-thsa-Me)(3-OEt-thsa-Me)]·H ₂ O (Å, °)	135
Table 4.3.3 The average Fe–O, Fe–N and Fe–S bond distances (Å), and the bond distances differences between the low-spin and high-spin state for selected [Fe ^{III} (HL)(L)]·H ₂ O spin-crossover compounds.	137
Table 4.3.4 Hydrogen bond geometry of [Fe(H-3-OEt-thsa-Me)(3-OEt-thsa-Me)]·H ₂ O (Å, °)	138
Table 4.3.5 Selected infrared spectroscopic bands (cm ⁻¹) with assignments of [Fe(H-3-OEt-thsa-Me)(3-OEt-thsa-Me)]·H ₂ O and H ₂ L ligand, 3-ethoxysalicylaldehyde 4-methylthiosemicarbazone.	139
Table 4.4.1 Crystal data and structure refinement details of [Fe(H-5-Cl-thsa-Me)(5-Cl-thsa-Me)]·H ₂ O	142
Table 4.4.2 Selected geometric parameters of [Fe(H-5-Cl-thsa-Me)(5-Cl-thsa-Me)]·H ₂ O (Å, °)	144
Table 4.4.3 Hydrogen bond geometry of [Fe(H-5-Cl-thsa-Me)(5-Cl-thsa-Me)]·H ₂ O (Å, °)	147
Table 4.5.1 Selected crystallographic data and spin state for [Fe(HL)(L)]·H ₂ O type complexes of R-salicylaldehyde 4R'-thiosemicarbazone ligands described in this chapter.	151
Table 4.5.2 Selected average Fe-donor atom bond distances and spin state for [Fe(HL)(L)]·H ₂ O type complexes of R-salicylaldehyde 4R'-thiosemicarbazone ligands described in the literature.	152
Table 4.5.3 Transition temperatures (K) for selected spin-crossover [Fe(HL)(L)]·H ₂ O compounds.	156
Table 5.2.1 Crystal data and structure refinement details of [Fe(H-5-Br-thsa-Et) ₂](NO ₃)·H ₂ O.	164
Table 5.2.2 Selected geometric parameters of [Fe(H-5-Br-thsa-Et) ₂](NO ₃)·H ₂ O (Å, °).	165
Table 5.2.3 Hydrogen bond geometry of [Fe(H-5-Br-thsa-Et) ₂](NO ₃)·H ₂ O (Å, °).	168
Table 5.3.1 Crystal data and structure refinement details of [Fe(H-4-OH-thsa) ₂] ₄ ·(SO ₄) ₂ ·9H ₂ O.	172
Table 5.3.2 Selected bond lengths and angles of [Fe(H-4-OH-thsa) ₂] ₄ ·(SO ₄) ₂ ·9H ₂ O (Å, °)	175
Table 5.3.3 Hydrogen-bond geometry of [Fe(H-4-OH-thsa) ₂] ₄ ·(SO ₄) ₂ ·9H ₂ O (Å, °).	176

Table 5.3.4 Selected infrared spectroscopic bands (cm^{-1}) with assignments of $[\text{Fe}(\text{H}-4\text{-OH-thsa})_2]_4 \cdot (\text{SO}_4)_2 \cdot 9\text{H}_2\text{O}$ and H_2L ligand, 2,4-dihydroxybenzaldehyde thiosemicarbazone.	178
Table 5.4.1 Fe-donor atom bonds for high-spin (HS) $[\text{Fe}(\text{HL}^-)_2](\text{anion}^-) \cdot n\text{H}_2\text{O}$ type compounds of R-salicylaldehyde 4R-thiosemicarbazone.	181
Table 6.1 Selected crystallographic data and spin state of the Fe^{III} bis(R-salicylaldehyde 4R'-thiosemicarbazone) compounds.	188
Table E2.1 Quantities used in the synthesis of Fe^{III} complexes with R-salicylaldehyde 4R'-thiosemicarbazone ($\text{H}_2\text{-R-thsa-R}'$) ligands.	219

Abbreviations

2D	Two-dimensional
A	Acceptor atom
ATR	Attenuated Total Reflectance
B.M.	Bohr Magneton
<i>D</i>	Donor atom
DSC	Differential Scanning Calorimetry
H	Applied magnetic field
ΔH	Enthalpy
<i>H</i>	Hydrogen atom
HS	High-spin
H ν	Light irradiation
IR	Infrared
k_B	Boltzmann constant
KBr	Potassium Bromide
$k_B T$	Thermal energy
<i>L</i>	Generic ligand
LD-LISC	Ligand Driven-Light Induced Spin Changes
LIESST	Light Induced Excited Spin State Trapping
LS	Low-spin
<i>M</i>	Generic metal cation
M	Magnetisation
M	Mass of sample
Mp	Melting point
M_r	Molar mass
NCS	Isothiocyanate
NMR	Nuclear Magnetic Resonance
<i>P</i>	Spin pairing energy
P	Pressure
phen	1,10-Phenanthroline
R	R factor
$r(M-L)$	Symmetric metal-ligand stretching bond distance
ΔS	Entropy
S	Goodness of fit
Sco	Spin-crossover

SQUID	Superconducting Quantum Interference Device
Stpy	4-styrylpyridine
T	Temperature
$T_{1/2}$	Spin transition temperature
V	Volume
VSM	Vibrating Sample Magnetometer
wR	Weighted R factor
Z	Number of formula units per unit cell
Z'	Number of formula units per asymmetric unit
γ_{HS}	High-spin fraction
Δ	Isomer shift
$\Delta E^\circ(HL)$	Change in zero-point energies of the two spin states
ΔE_Q	Quadrupole splitting
Δ_o	Octahedral splitting field parameter
$\Delta r(HL)$	Change in metal-ligand bond distance
ΔW_{HL}	Activation energy
M	Absorption coefficient
μ_{eff}	Effective magnetic moment
μ_{HS}	Magnetic moment of the high-spin state
P	Density
χ_M	Molar magnetic susceptibility
%	Percentage
°	Degrees
°C	Degrees Celsius
Å	Angstrom
Cm	Centimetre
G	Gram
J	Joules
K	Kelvin
Mg	Milligrams
mL	Millilitres
Mm	Millimetre
mmol	Millimoles
Mol	Moles
Nm	Nanometres

ppm	Parts per million
S	Second
μL	Microlitres
Mm	Micrometres
H ₂ L	Ligand (R-salicylaldehyde 4R'-thiosemicarbazone)
HL ⁻	Anionic ligand (R-salicylaldehyde 4R'-thiosemicarbazonate(1-))
L ²⁻	Dianionic ligand (R-salicylaldehyde 4R'-thiosemicarbazonate(2-))
H ₂ -thsa	salicylaldehyde thiosemicarbazone
H ₂ -5-Br-thsa	5-bromosalicylaldehyde thiosemicarbazone
H ₂ -5-Cl-thsa	5-chlorosalicylaldehyde thiosemicarbazone
H ₂ -3-OEt-thsa	3-ethoxysalicylaldehyde thiosemicarbazone
H ₂ -4-OH-thsa	2,4-dihydroxybenzaldehyde thiosemicarbazone
H ₂ -thsa-Me	salicylaldehyde 4-methylthiosemicarbazone
H ₂ -5-Cl-thsa-Me	5-chlorosalicylaldehyde 4-methylthiosemicarbazone
H ₂ -3-OEt-thsa-Me	3-ethoxysalicylaldehyde 4-methylthiosemicarbazone
H ₂ -5-Br-thsa-Et	5-bromosalicylaldehyde 4-ethylthiosemicarbazone
Me	Methyl, -CH ₃
Et	Ethyl, -C ₂ H ₅

Chapter I

Introduction

1.0 Introduction

1.1 Introduction to the spin-crossover phenomenon

The spin-crossover phenomenon which occurs in $3d^4$ - $3d^7$ transition metal systems is described as a change in spin state (low-spin to high-spin) due to an external perturbation [1]. Spin transitions can be caused by a change in temperature, pressure or light irradiation [1].

In order to describe the occurrence of a spin transition of a metal complex, one has to consider crystal field theory. For the purpose of this thesis, the crystal field considerations will be explained with respect to an octahedral transition metal complex. Firstly, if we consider an isolated metal ion or one exposed to a spherical crystal field, all five d-orbitals have the same energy, *i.e.* the d-orbitals of the transition metal ion are energetically degenerate. However, when the transition metal ion is part of a complex system, so bound to six ligand donor atoms in octahedral symmetry, the ion is now exposed to a non-spherical octahedral crystal field. A rise in energy to form the degenerate doublet, the e_g set, is due to the energy of the d_z^2 and the $d_{x^2-y^2}$ orbitals increasing due to the repulsion between electrons in their d-orbitals and the ligand atoms, considered as negative point charges, along the metal-ligand direction. However, the energy of the electrons in the remaining orbitals, the d_{xy} , d_{yz} and d_{xz} orbitals, that lie between the metal ligand axes are less affected by the crystal field, thus the energy is decreased to form a degenerate triplet, the t_{2g} set, at a lower energy with respect to the spherical crystal field. This splitting of the d-orbitals is illustrated in Figure 1.1.

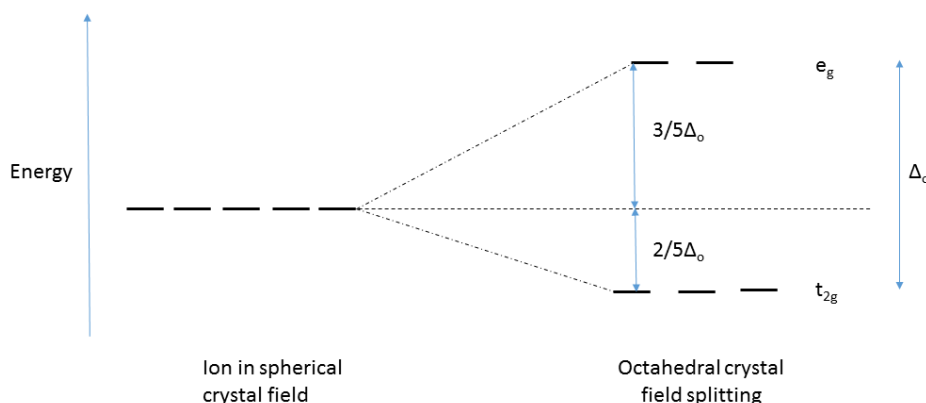


Figure 1.1 The effect of the splitting of the d-orbitals when placing a metal ion into an octahedral crystal field (Δ_o splitting energy of the octahedral crystal field).

Due to the splitting of the d-orbitals into the e_g and t_{2g} subsets when the $3d^4$ - d^7 transition metal ion is exposed to an octahedral crystal field there are two possible arrangements of the electrons in the

ground state *i.e.* low-spin or high-spin state. The energy gap or difference between the e_g and t_{2g} levels is the octahedral crystal field strength, Δ_o , and can be affected dependent upon the ligand bound to the metal ion. The two configurations of the electronic ground states are classed as the high-spin and low-spin state, as displayed in Figure 1.2 for the d^5 metal ion.

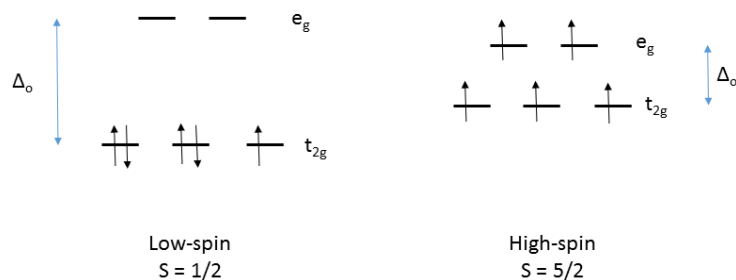


Figure 1.2 The two possible ground state electronic configurations for a d^5 metal ion in an octahedral crystal field.

The low-spin state is the ground state when the crystal field is strong and the energy required to pair electrons in the lower energy t_{2g} orbitals is less than that required to promote it to a higher energy e_g orbital, *i.e.* the electrons occupy the orbitals of lower energy. The high-spin state arrangement for the d^5 ion contains the maximum amount of unpaired electrons. The arrangement of the electrons in the high-spin state d^5 ion is when the energy required to promote electrons to a higher energy e_g orbital is less than the energy to pair the electrons in the lower energy t_{2g} orbitals. This is when Δ_o is smaller than P (the spin pairing energy), the d-orbitals will each contain one electron prior to spin-pairing of electrons within the same orbital, in accordance with Hund's Rule. The low-spin state has the minimum spin possible for the complex system and the high-spin state possesses the maximum spin, with respect to the two configurations of the electronic ground states of $3d^4$ - d^7 metal ions. If the energy difference between the high-spin and low-spin states reaches the thermal energy, $k_B T$, where k_B is the Boltzmann constant and T is temperature, then the compound can interconvert between spin states on the application of an external perturbation. This interconversion of the electrons between the e_g and t_{2g} orbitals of the low-spin and high-spin states is known as a spin-crossover, as illustrated in Figure 1.3.

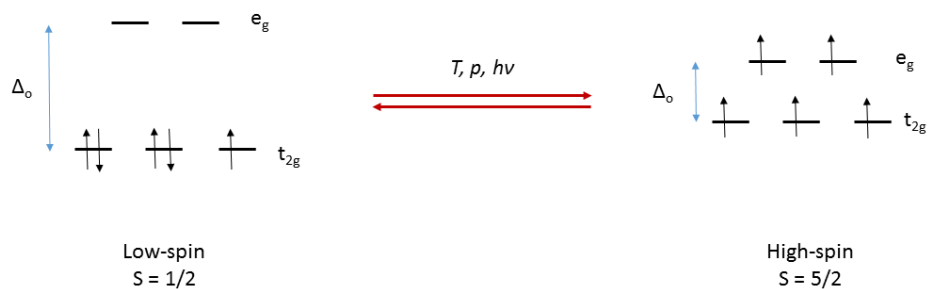


Figure 1.3 Spin-crossover dependent upon external perturbations of temperature (T), pressure (p) or light irradiation (hv) for octahedral compounds of Fe^{III}, a 3d⁵ system. The high-spin and low-spin form differ in electronic population of the 3d orbitals with an associated alteration of the magnetic and structural characteristics.

Spin-crossover is observed in Fe^{III} systems (3d⁵), whereby the significant difference is the spin of the high and low-spin states. For octahedral Fe^{III} the ground state terms for $S = 5/2$ (high-spin) and $S = 1/2$ (low-spin) configuration of the 3d⁵ electronic system are described as being the sextet ⁶A₁ and the doublet ²T₂, respectively. (The theoretical treatment of the crystal field of the present Fe^{III} system is similar to that of the Fe^{II} system which is described in detail by Hauser [2].) It is widely recognised that the splitting by the octahedral crystal field is both sensitive to the nature of the ligand and the metal-donor atom bond distances. The latter causes a relative displacement of potentials wells for the low-spin (²T₂ doublet) and high-spin (⁶A₁ sextet) configurations along the symmetric stretch vibration, as represented in Figure 1.4 [2].

The horizontal displacement of the potential wells corresponds to the population of the anti-bonding e_g orbitals in the high-spin state, which gives rise to the lengthening of the metal-donor atom distances when switching from the low-spin to the high-spin state. Furthermore, the vertical displacement corresponds to the difference of the zero-point energies of the high-spin and low-spin configurations; this is defined as ΔE^o(HL). It is realised that for the possibility for the thermal spin transition to occur ΔE^o(HL) has to be of the order of k_BT (thermal energy). For spin-crossover active metal complexes with the electronic configuration of 3d⁵, at low temperatures, the spin-crossover centre is usually found to be in the low-spin state ($S = 1/2$), and upon increasing the temperature the metal ion transitions into the high-spin state ($S = 5/2$).

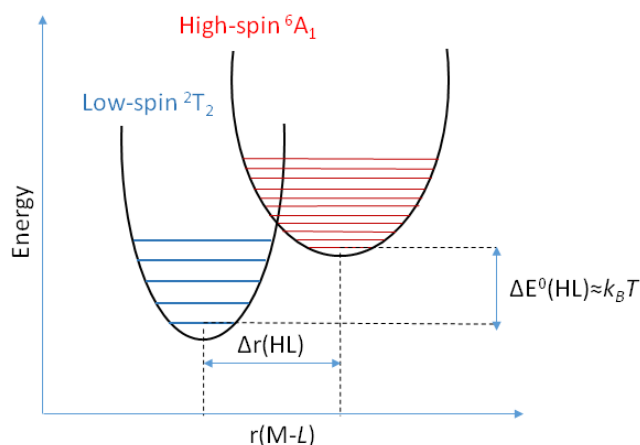


Figure 1.4 The potential wells for the high-spin (6A_1) and the low-spin (2T_2) states as a function of the Fe^{III} -donor atom distance, along the symmetric metal-ligand stretching vibration ($r(M-L)$ where M = metal cation and L = ligand). The change in metal-ligand bond distance (*i.e.* the horizontal displacement of the wells) is represented by $\Delta r(\text{HL})$, and $\Delta E^\circ(\text{HL})$ represents the zero point energy difference between the two spin states. (Adapted from reference [2]).

Spin transitions can occur both in solution and in the solid state, and for the basis of this thesis only spin transitions of solids will be discussed. Spin-crossover of Fe^{III} ions can be represented by their high-spin fraction (γ_{HS}) vs. a dependent variable, such as temperature. The most common types of spin transition curves are illustrated in Figure 1.5. [1]; these are:

- (i) A gradual smooth and continuous change of γ_{HS} over the temperature range;
- (ii) The transition is abrupt, whereby the transition can occur in a very narrow temperature range;
- (iii) An abrupt transition with hysteresis;
- (iv) Spin transition with steps;
- (v) Spin transition is incomplete.

If the spin transition curve shows the presence of hysteresis the complex may undergo a structural phase change accompanied by the transition in the spin, from the low-spin to the high-spin state, giving rise to the named discontinuous transition.

The manifestation of a spin transition in a solid state system is subject to the operation of lattice forces. So, it is known that the nature of the spin transition curve $\gamma_{\text{HS}}(T)$ can be strongly influenced by chemical contributions which affect the lattice interactions. These include:

- (i) The nature of the anion or cation associated with the complex cation or complex anion;
- (ii) The extent and nature of solvation of the complex;

- (iii) Variations in the ligand substituents;
- (iv) Actual ligand replacement.

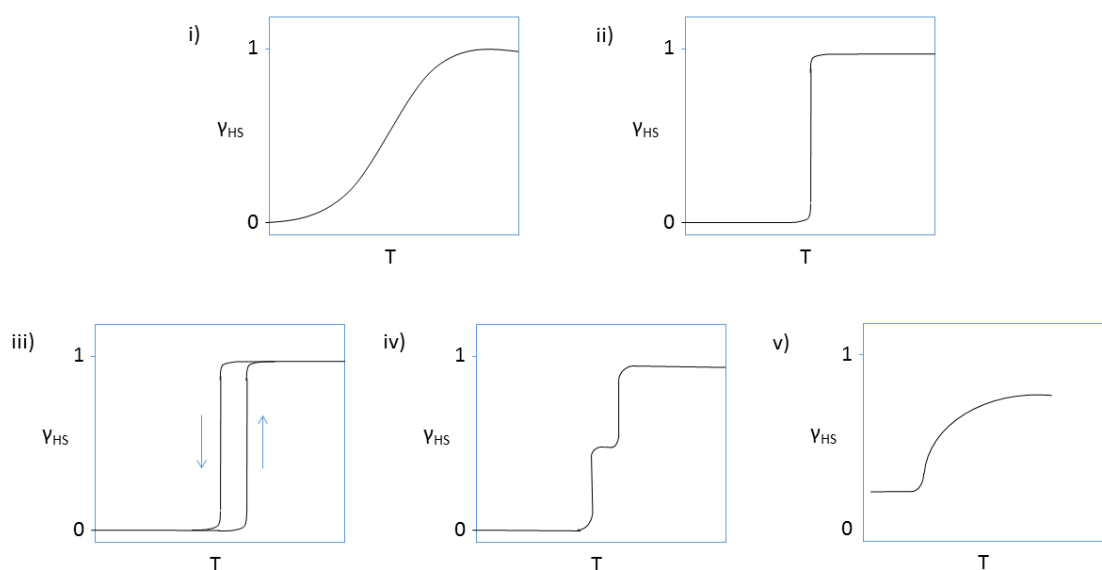


Figure 1.5 $\gamma_{\text{HS}}(T)$ plots of the possible different types of thermal spin transition curve i) smooth and continuous, ii) abrupt, iii) with hysteresis, iv) with steps and v) incomplete.

1.2 Iron(III) spin-crossover

Since the discovery of the spin-crossover phenomenon was first described, its development has offered an insight into the unique process with Fe^{III} coordination compounds. The spin-crossover effect was first reported by Cambi and Szegő who in 1931, conveyed the unusual temperature dependence of the magnetic susceptibility of various tris(*N,N*-dialkyl-dithiocarbamato)iron(III) compounds [3, 4]. Over the past 80 years spin-crossover coordination compounds have been of major interest to many researchers; and to date spin-crossover has been reported for some of the first row metal ions *i.e.* $3d^4$ - d^7 configurations.

Major interest and significance of the thiosemicarbazones and their metal complexes is due to their diverse chemical and structural characteristics including their biological and chemical applications [5-8]. Particular interest has been developed in the area concerning the thiosemicarbazone being condensed with a suitable aldehyde to yield Schiff base-type ligands. This allows for predetermined, specific modifications of the ligands making them ideal candidates for generating spin-crossover in the Fe^{III} compounds.

1.2.1 R-salicylaldehyde 4R'-thiosemicarbazone ligand system

In solution, the free R-salicylaldehyde 4R'-thiosemicarbazone (H_2L) exists in two tautomeric forms, *i.e.* the thione and thiol forms, as illustrated in Figure 1.6. Consequently, in Fe^{III} compounds, the ligand may be present in either of the possible tautomers, and may be neutral, anionic or dianionic. Referring to the thiol tautomer, neutral H_2L has H atoms located on the phenol O atom and the thiol S atom. The first deprotonation step involving the phenol group results in the formation of R-salicylaldehyde 4R'-thiosemicarbazone(1-) (abbreviated as HL^-). Subsequent deprotonation yields R-salicylaldehyde 4R'-thiosemicarbazone(2-) (abbreviated as L^{2-}).

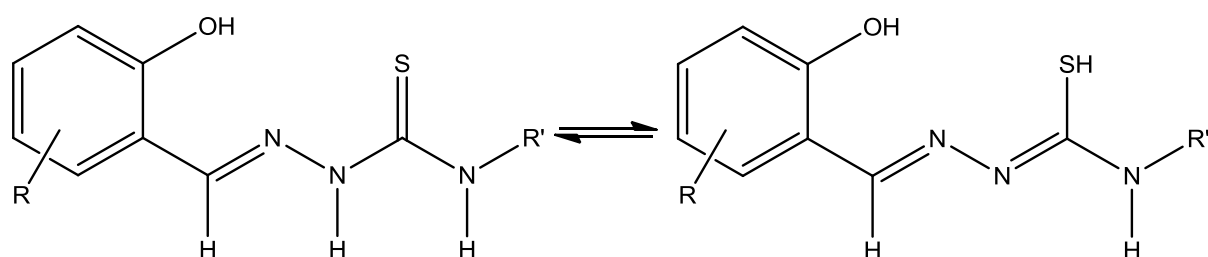


Figure 1.6 The two tautomeric forms of R-salicylaldehyde 4R'-thiosemicarbazone, the thione (left) and the thiol (right).

It has been observed that in solution thiosemicarbazones may consist of an equilibrium mixture of thione and thiol tautomers, as illustrated in Figure 1.6 [6-8]. This class of chelating tridentate R-salicylaldehyde 4R'-thiosemicarbazone ligands generally coordinates in the anionic thiolate form (illustrated in Figure 1.7) [9]. The salts of the anionic bis(ligand) Fe^{III} complexes of this class of Schiff base dianion frequently show spin-crossover behaviour. Typically, these Fe^{III} compounds contain two doubly deprotonated ligands, and the crystal lattice comprises an associated cation and may contain solvent molecules as well. However, Fe^{III} compounds with one-fold deprotonated or neutral ligands may also be obtained, and sometimes ligands of different degrees of deprotonation may be present in the same Fe^{III} compound.

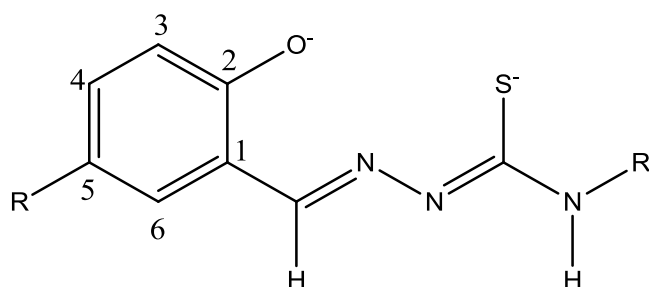


Figure 1.7 The dianion of R-salicylaldehyde 4R'-thiosemicarbazone, together with the atom labelling of the R-salicylaldehyde unit.

This particular class of ferric complex, Fe^{III} bis(R-salicylaldehyde 4R'-thiosemicarbazonato) systems, is the main focus of the thesis, therefore, in the following sections of this chapter selected R-substituted salicylaldehyde 4R'-thiosemicarbazone ferric complex systems are discussed in order to describe the factors affecting spin-crossover *i.e.* the chemical and physical influences. Experimental techniques to detect a spin transition are presented together with their application. An overview of the progress made in the research field of selected R-substituted salicylaldehyde 4R'-substituted thiosemicarbazone ferric spin-crossover systems is herein discussed.

1.3 Factors affecting spin-crossover

The potential of a compound to exhibit a spin transition can be affected by chemical or physical influences which consequently can change the characteristics of the material. The conversion from the low-spin to the high-spin state gives rise to the increase in the ionic radius of the metal ion associated with the increased occupation of the anti-bonding e_g orbitals and greater distance of the ligand donor atoms from the metal ion. This corresponds to an increase in the metal – ligand donor atom bond lengths. It is important to note the important consequences of a spin transition; these include the following:

- (i) The size increase of the ionic radius of the metal ion;
- (ii) The change in magnetic properties;
- (iii) The change in the d-d transitions (colour change).

The main factors affecting the spin transition of a particular compound can be categorised into two factors: firstly, the chemical influences and secondly, the physical influences. Chemical modifications of spin-crossover systems include:

- (i) The nature of the anion or cation associated with the complex cation or complex anion;
- (ii) The extent and nature of solvation of the complex;
- (iii) Variations in the ligand substituents;
- (iv) Actual ligand replacement.

Furthermore, the physical influences that affect the spin transition of this type of systems include:

- (i) Sample condition;
- (ii) Effect of temperature;
- (iii) Effect of pressure;
- (iv) Effect of light irradiation;
- (v) Effect of a magnetic field.

For the purpose of this thesis, anion/cation and solvent effect of the chemical influences will be discussed, as well as the effect of temperature, effect of pressure, and light irradiation on the spin transition of R-salicylaldehyde 4R'-thiosemicarbazone Fe^{III} type compounds.

1.3.1 Chemical Influences

Anion/Cation and solvent effects

It has been recognised that for R-salicylaldehyde 4R'-thiosemicarbazone Fe^{III} compounds the spin-state may be sensitive to changes in the counter-ion, whether that is an anion with respect to an [Fe^{III}(HL)₂]⁺ type compound or a cation with respect to an [Fe^{III}(L)₂]⁻ type compound [9-10]. The variation of the associated cation has been investigated for various Fe^{III} compounds of R-salicylaldehyde 4R'-thiosemicarbazones. In particular, the ferric complexes with the unsubstituted dianionic salicylaldehyde thiosemicarbazone (thsa²⁻) have been extensively researched, whereby the outersphere cation has been varied, to give rise to the compounds NH₄[Fe(thsa)₂] [11], Cs[Fe(thsa)₂] [12], Li[Fe(thsa)₂].2H₂O [13], Na[Fe(thsa)₂].3H₂O [13] and (C₅H₅NH)[Fe(thsa)₂].H₂O [14].

The attempts made to correlate the structural features of these types of systems concluded that significant changes in the magnetic behaviour may be due to:

- (i) The replacement of the associated outer-sphere cation in the ferric complex;
- (ii) The introduction of R-substituents into the salicylaldehyde moiety of the salicylaldehyde thiosemicarbazone type ligands;
- (iii) The incorporation of the substituents on the terminal amido group of the thiosemicarbazone residue;
- (iv) The degree of hydration of the complex system.

The compound NH₄[Fe(thsa)₂] [11] was found to be in the low-spin state at 300 K. Replacing the NH₄⁺ cation with Cs⁺, creating the compound Cs[Fe(thsa)₂] [12] gave rise to a compound in the high-spin state at 298 and 103 K. The ferric complex Li[Fe(thsa)₂].2H₂O is in the low-spin state (at both measurement temperatures 80 and 300 K), whereas Na[Fe(thsa)₂].3H₂O was found to exhibit a spin transition between the low- and high-spin state over the temperature range 80-300 K [13]. Furthermore, (C₅H₅NH)[Fe(thsa)₂].H₂O (C₅H₅NH = pyridine) was found to exhibit spin-crossover behaviour using ⁵⁷Fe Mössbauer spectroscopy in the temperature range 80 – 280 K [14]. It may be considered that the variation of the cation has an indirect influence on the spin state of the Fe^{III} ion, with respect to the crystal packing of the ferric complexes and the degree of hydration of the system. In addition, the R-substituted ligands 5-bromosalicylaldehyde and 5-chlorosalicylaldehyde thiosemicarbazone ferric complexes have also been investigated for the variation of the associated cation. The crystal structures determined for NH₄[Fe(5-Br-thsa)₂] (at 298 K) [15] and NH₄[Fe(5-Cl-

thsa)₂] (at 135 and 298 K) [16] show that all three crystal structures contain an Fe^{III} cation in the low-spin state.

1.3.2 Physical Influences

Effects of Temperature

Thermally induced spin transitions are the most widely recognised form of spin-crossover for Fe^{III} compounds. Thermally induced discontinuous spin-crossover conversions exist for those systems of which the high-spin to low-spin transition occurs abruptly over a minute temperature interval. The temperature at which the thermal spin transition is usually described as T_{1/2}, which is considered as the temperature at which half of the low-spin (S = 1/2) Fe^{III} cations have transitioned to the high-spin state (S = 5/2). Furthermore, for those systems which exhibit hysteresis two T_{1/2} values will be observed, one for the transition when measured in the heating mode and the other when decreasing the temperature.

Effects of Light Irradiation

Decurtins *et al.*, discovered for Fe^{II} that by irradiating a low-spin solid-state sample with green light ($\lambda = 514$ nm), the low-spin compound could be promoted to a metastable high-spin state [17]. This phenomenon is known as the LIESST effect (Light Induced Excited Spin State Trapping) [17]. The LIESST effect has been demonstrated for Fe^{II} spin-crossover systems and even though the phenomenon appears to be unfavourable for Fe^{III} spin-crossover systems, it has been observed that systems which exhibit strong intermolecular interactions such as π - π stacking and hydrogen bonds afford cooperative spin transitions with large thermal hysteresis and LIESST effects [18, 19]. In particular, this type of behaviour is of great interest as it creates the bistability required for essential applications such as optical switches in memory devices.

At this stage, the process has been described for Fe^{II}, however the exact mechanism for Fe^{III} has not been entirely clarified thus far, therefore, the mechanism for Fe^{II} will now be discussed in detail. The LIESST effect is depicted in a schematic mechanism in Figure 1.8 [20]. The process for Fe^{II} typically allows for the irradiation of a low-spin sample using an Ar⁺ laser with a wavelength of approximately $\lambda = 514$ nm (green) and at temperature below 50 K. This causes the sample to become bleached, hence results in a colour change. The LIESST effect was first observed for the compound [Fe^{II}(1-propyltetrazole)₆](BF₄)₂, which resulted in the low-spin purple sample becoming colourless (high-spin). Stimulation due to exposure to the green light causes the complex to be in an excited state when undergoing a spin allowed transition from the low-spin, ¹A₁ state to the ¹T₁ state. The

metastable high-spin state, 5T_2 , is reached due to a small probability that the excited 1T_1 state decays by a two stage intersystem crossing process via the intermediate 3T_1 spin state. The trapped excited spin state, 5T_2 , has a long lifetime at low temperatures (usually below 50 K).

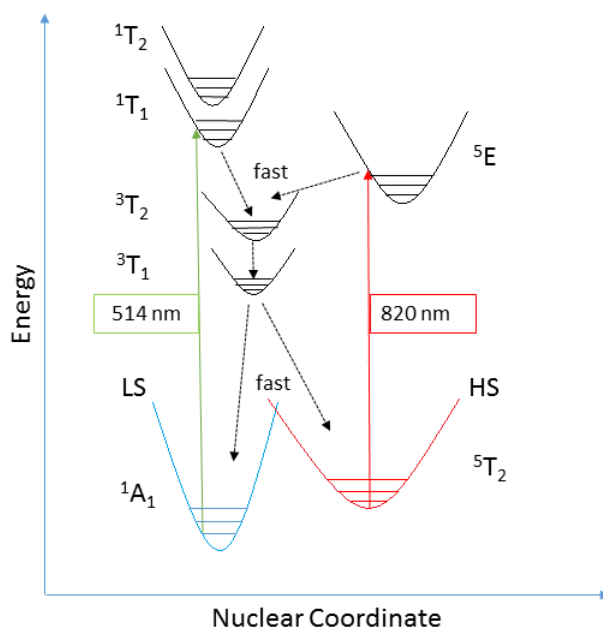


Figure 1.8 Schematic representation of the mechanism for LIESST (green arrow) and reverse-LIESST (red arrow) for Fe^{II} systems. The solid lines indicate excitation by irradiation while dotted lines represent relaxation pathways. (Adapted from reference [20]).

In 1986 Hauser discovered the existence of the reverse process termed reverse-LIESST [21], for which the excitation results from using a longer wavelength of light (red light, $\lambda = 980$ nm) [22]. The metastable high-spin state is converted back to the low-spin state, 1A_1 , via an intersystem crossing resulting in the transformation from ${}^5T_2 \rightarrow {}^3T_1 \rightarrow {}^1A_1$. However, the metastable high-spin state can also be converted back to the low-spin state by increasing the temperature above 50 K *i.e.* thermal relaxation.

The manifestation of the possible photo-control of the spin-state of spin-crossover systems meant these type of compounds could be used as optical switches, storage and memory devices [1]. Due to the low temperatures required to keep the systems in the photo-induced metastable high-spin state, further research was conducted to develop an array of new phenomena.

Since the discovery of the LIESST effect, many other light-induced spin-crossover techniques have been identified. This has mainly been driven by the limitations of the LIESST effect, as this occurs at low-temperatures and is incompatible with room temperature applications. The list of discovered light induced stimuli for spin-crossover materials is as follows:

- (i) NIESST – Nuclear induced excited spin state trapping [23-26]
- (ii) LIESST – Light induced excited spin state trapping
- (iii) LD-LISC – Ligand driven light induced spin change [27]
- (iv) LD-CISSS – Light driven coordination induced spin state switching [28]
- (v) SOXIESST – Soft X-ray induced excited spin state trapping [29]
- (vi) SF-LIESST – Strong field light induced excited spin state trapping [30]
- (vii) HAXIESST – Hard X-ray induced excited spin state trapping [31]
- (viii) VUVIESST – Vacuum UV induced excited spin state trapping [32]
- (ix) LITH – Light induced thermal hysteresis [33, 34]
- (x) LIOH – Light induced optical hysteresis [33]
- (xi) LiPTH – Light induced perturbed thermal hysteresis [35]
- (xii) LiPOH – Light induced perturbed optical hysteresis [35, 36]
- (xiii) HAXITH – Hard X-ray induced thermal hysteresis [37]

LIESST and NIESST are initiated at cryogenic temperatures, this leads to the decay of the meta-stable states at higher temperatures, thus preventing potential room temperature photo-induced spin state switching and their use in molecular switching applications.

Ligand Driven – Light Induced Spin Changes (LD – LISC) have been reported by Zarembowitch *et al.*, [38]. This phenomenon occurs when light irradiation promotes a change in the ligand, *e.g.* *cis-trans* isomerism in the ligand creating a change in the ligand field strength, which triggers a spin transition at the metal centre [38]. This may allow for a longer life time of the photo-induced spin conversions between spin-states at higher temperatures. An example of the LD – LISC phenomenon has been reported for the compound $[\text{Fe}(\textit{trans}\text{-stpy})_4(\text{NCS})_2]$ (where stpy = 4-styrylpyridine) [38]. The 4-styrylpyridine was used as the photo-switchable ligand, giving rise to *cis*- and *trans*-4-styrylpyridine (Figure 1.9). $[\text{Fe}(\textit{trans}\text{-stpy})_4(\text{NCS})_2]$ exhibits a thermally induced spin transition at around 108 K, whereas $[\text{Fe}(\textit{cis}\text{-stpy})_4(\text{NCS})_2]$ is found to be in the high-spin state at any temperature [38]. In general, by irradiating the sample with light of an appropriate wavelength, one should be able to induce a spin transition in the system resultant from the photo-conversion of the ligand.

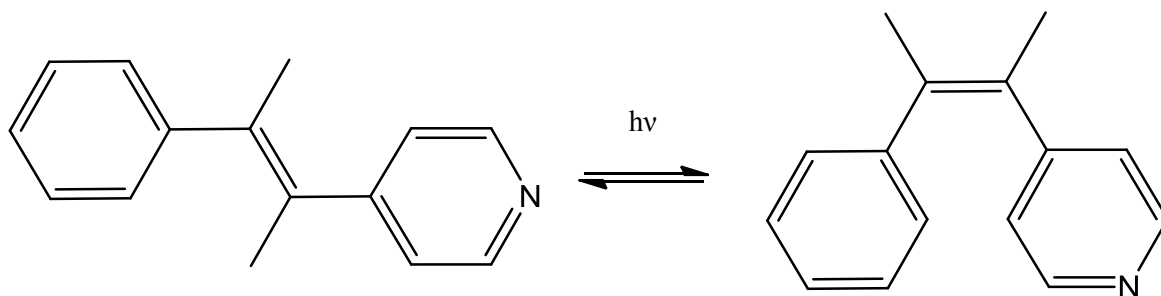


Figure 1.9 *Trans* (left)/*cis* (right) isomerisation in 4-styrylpyridine (stpy).

The many mechanisms induced by visible light discovered in recent decades show the differentiation between using light irradiation as a single excitation pulse and that of continuous exposure of visible light. Most of the aforementioned mechanisms are based on the LIESST phenomena, using continuous light irradiation. However, the mechanisms labelled LITH and LIOH are induced at cryogenic temperatures, whereas, LiPTH and LiPOH may occur at much higher temperatures [35, 36]. The LiPTH and LiPOH mechanisms that stimulate spin-state switching are therefore eligible candidates for potential applications.

Létard *et al.*, and Varret *et al.*, both identified hysteretic switchable materials, an Fe^{II} mononuclear complex [34] and a coordination polymer [33] by the LITH phenomena. After the population of the meta-stable high-spin state at low temperature (via the LIESST effect), the LITH effect maintains the green light irradiation both in the warming and heating modes. Varret *et al.*, [33] observed a similar behaviour to that of the LITH effect, by varying the intensity of the light irradiation at a constant temperature, this hysteresis effect is known as LIOH. LIESST, LITH, and LIOH mechanisms demonstrate hysteresis effects at cryogenic temperatures, whereas the LiPTH [35] and LiPOH [35,36] are spin transition stimuli at higher temperatures. Both the LiPTH and LiPOH mechanisms are based on the high-spin state excitation by light and thermal decay, whereby the hysteresis behaviour may be manipulated [35,36]. Renz *et al.*, [35] reported the coordination compound $[\text{Fe}(\text{phy})_2](\text{BF}_4)_2$ (phy = 1,10 phenanthroline-2-carbaldehyde-phenylhydrazone) demonstrated a thermal hysteresis between 270 K and 280 K, by exposure to continuous irradiation with green light the thermal hysteresis shifted to lower temperatures and with exposure to red light shifted to higher temperatures [35].

The previously mentioned effects LITH, LIOH, LiPTH and LIPOH stimulate a spin-crossover by visible light, however, spin-crossover can be induced by X-ray excitation. This fairly new stimulus was first observed by Collison *et al.*, [29] which discusses the first excitation effects induced by X-rays, though it should be noted that XPS and XAFS were used to monitor spin-crossover in coordination compounds [39,40]. Collison *et al.*, have evidenced that X-rays with low energy may stimulate a spin-crossover at low temperatures, this effect is known as SOXIESST – Soft X-ray Induced Excited Spin State Trapping. Similar to the LIESST effect, the SOXIESST effect also traps the high-spin state below a certain temperature by irradiation with soft X-rays (instead on light). The SOXIESST effect has been observed for the mononuclear complex $[\text{Fe}(\text{bpz})_2(\text{phen})]$ (where bpz = dihydrobis(pyrazolyl)borate) whereby the named complex was in direct contact with a highly oriented pyrolytic graphite surface [41] or absorbed on Au(111) [42]. Moreover, the HAXIESST effect (Hard X-ray Induced Spin State Trapping) was also discovered in the mononuclear complex $[\text{Fe}(\text{bpz})_2(\text{phen})]$ (where bpz = dihydrobis(pyrazolyl)borate) at low temperatures.

This array of mechanisms induced by light irradiation or X-rays, opens the door for potential a new array of mononuclear and multinuclear switchable coordination compounds, which could indeed stimulate progression in the field owing to the applications of the materials in nanoscience to customize future spintronic devices.

Effects of Pressure

Physical perturbations can either initiate or modify a spin transition. The occurrence of a spin transition in a metal complex results in a considerable change in the metal-ligand bond lengths and therefore a change in volume of the crystallographic unit cell, provided that the symmetry and hence the space group of the unit cell remains unchanged. Due to this feature, the spin-crossover materials are sensitive to the application of pressure; this is particularly so for Fe^{II} spin-crossover materials. It is known that the compound in the high-spin state has a larger volume than that of the respective low-spin form of a compound, thus the application of an increased external perturbation, in this case pressure to a spin-crossover system in the high-spin state at ambient pressure can result in the formation of the low-spin form. Referring to the energy diagram of Fe^{II} systems (displayed in Figure 1.10) the applied (higher) pressure raises the energy of the ⁵T₂ high-spin state potential well [43]. This rise in energy results in a decrease in activation energy (ΔW_{HL}) and an increase in the difference in zero point energy (ΔE_{HL}), therefore favouring the low-spin state of Fe^{II}, ¹A₁.

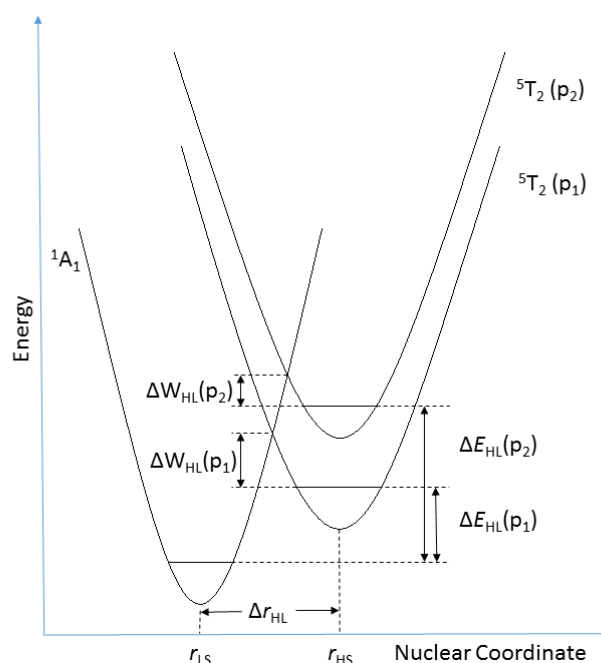


Figure 1.10 Schematic representation of the effect of pressure (p) on Fe^{II} spin-crossover systems. (Adapted from reference [43]).

The effect of an applied external pressure on Fe^{III} spin-crossover materials has not been extensively studied. The first studies using high-pressure to initiate a spin transition of spin-crossover materials were carried out in the 1960s and primarily focused upon a series of Fe^{III} complexes [44]. In 1969 Ewald *et al.*, showed that for tris(N,N-disubstituted-dithiocarbamato)iron(III) compounds spin transitions may be induced when the pressure on the ferric complexes in solution is increased at constant temperature [44]. Butcher *et al.*, studied the effect of an applied external pressure by analysing the infrared spectra of these Fe^{III} spin-crossover materials by studying the metal-ligand stretching region as a function of pressure (up to 35 kbar) [45]. For the spin-crossover compound tris(N-ethyl-N-phenyl-dithiocarbamato)iron(III) it was deduced that the intensity of the metal-sulfur band assigned to the low-spin state increases relative to the high-spin state band with increasing pressure [45].

Effects of an applied Magnetic Field

The spin transition alters the magnetic properties of the metal system. It is anticipated that perturbation of a spin transition material by an external magnetic field could therefore affect the transition. This effect may be predicted by theoretical calculations, in particular based on the thermodynamics and the magnitude of the change in transition temperature [1]. In an applied magnetic field, B, a decrease in the transition temperature is anticipated, this is caused by the decrease in the energy of the molecules in the high-spin state by their magnetic moment $\mu_{HS} = \chi B$ [1, 46]. The theoretical calculations for an Fe^{II} system have predicted that the effect of the applied magnetic field would be minute whereby a change in the critical temperature of only -0.1 K is calculated for a field of 5 Tesla. Applied magnetic field studies carried out by Qi *et al.*, measured the shift in the transition curve for the compound $[\text{Fe}^{\text{II}}(\text{phen})_2(\text{NCS})_2]$, the results (-0.11 ± 0.04 K when exposed to fields of between 1 and 5 Tesla) agreed with the predicted values [47]. It was concluded from these studies that the effect of the magnetic field on the spin transition temperature was weak. More recently, the applied magnetic field studies of the same Fe^{II} compound have advanced somewhat to yield the spin-crossover transition temperature a change in the critical temperature of -1.8 K in a pulsed magnetic field of 30 Tesla [48-50].

1.3.3 Detection of spin-crossover

A spin-crossover in a material can be measured by a variety of techniques due to three key consequences of a spin transition: (i) the changes in the metal-donor atom distances, resultant from the change in relative occupancies of the t_{2g} and e_g orbitals, (ii) changes in d-d transitions give rise to different optical properties and (iii) the changes of the magnetic properties. The principal

techniques employed in this thesis for detecting a spin transition of 3d⁴-3d⁷ metal complexes are herein briefly described.

1.3.3.1 Experimental techniques

Magnetic Measurements

The principal technique to characterise the spin transition of a 3d⁴-3d⁷ metal complex is the measurement of the molar magnetic susceptibility as a function of temperature, $\chi_M(T)$. A spin-crossover transition involves a change in the number of unpaired electrons on the metal ion which is evidenced by the magnetic behaviour of the spin-crossover material. The magnetic susceptibility of the sample is proportional to the amount of material being in the high-spin and low-spin state; this data is used to express a spin transition curve (*vide supra*). Notably, the magnetism is a property of the bulk material whereas the spin transition of these types of compounds is defined by individual molecules and so hence the change in magnetism is not sufficient to verify the existence of the spin transition [1, 51].

In order to study the magnetic properties of these type of materials, solid-state measurement techniques such as a Faraday balance, a SQUID (Superconducting Quantum Interference Device) or a Foner-type magnetometer can be used, whereas for liquids, the Evans NMR method can be employed. In recent years, primarily the SQUID measurement technique has been at the fore front for measuring the magnetic properties of these materials [1].

When measuring the magnetic susceptibility of a material as a function of temperature, the material is exposed to a homogeneous external magnetic field and a magnetisation is induced in the sample material. This degree of magnetisation can be expressed in terms of molar magnetic susceptibility (χ_M), which is comprised of two components (i) the paramagnetic component originating from a permanent magnetic dipole moment, which acts in the direction of the applied field and (ii) the diamagnetic component which is a distortion causing a small magnetic moment against the applied field [52]. For a spin-crossover material, the product of the molar magnetic susceptibility and temperature (T) as a function of temperature, $\chi_M T(T)$, can be obtained through Equation 1.1, where M is the magnetisation of the sample, H is the applied magnetic field, m is the mass of the sample, M_r is the molar mass of the compound and T is the temperature.

$$\chi_M T = \left[\frac{M}{H \times \left(\frac{m}{M_r}\right)} \right] T \quad (1.1)$$

Expected values for $\chi_M T$ for octahedral Fe^{III} spin-crossover compounds are as follows:

- (i) $\chi_M T = 0.375 \text{ cm}^3 \text{ mol}^{-1} \text{ K}$ (for $g = 2.0023$) for the low-spin state ($S = 1/2$) material,

- (ii) $\chi_M T = 4.37 \text{ cm}^3 \text{ mol}^{-1} \text{ K}$ (for $g = 2.0023$) for the high-spin state ($S = 5/2$) material.

Crystallographic Studies

Single crystal X-ray diffraction is used extensively in the study of spin-crossover compounds. The existence of a spin transition of a transition metal complex can be confirmed through the determination of the difference of the bond distances between the structures of compounds in the two spin states, detected both above and below the transition temperature. These variable temperature measurements of the structural features of these types of compounds indicate whether the spin transition, if present, is associated with a change in the crystallographic space group. It is noteworthy, that continuous spin transitions generally only reveal changes in both the metal – ligand bond distances and angles, whereas a discontinuous spin transition exhibiting hysteresis in a thermally induced spin transition often occurs with a change in the crystallographic space group [1, 53]. Thus, it can be suggested that the variable temperature structural investigations can be used to interpret the effect of intermolecular interactions on the spin-transition and therefore the cooperativity property of the sample. The cooperativity displayed by a spin-crossover material is a type of behaviour whereby a number of seemingly independent components of the system act collectively. The relationship between the structural features and the spin transition of spin-crossover compounds allows the directed design and synthesis of these materials to give rise to specific physical properties, such as an abrupt spin transition near ambient temperature. Therefore, the determination of the crystal structure of these spin-crossover materials is critical, specifically at variable temperatures around the spin-transition temperature. Structural investigations of spin-crossover materials have revealed that in all cases it is expected that the metal-ligand bond distance is shorter in the low-spin state than that of the high-spin state, due to the change from $S = 1/2$ to $S = 5/2$; therefore, a restructuring of charge occurs in the system.

Spectroscopic Methods

Variable temperature near- and far-infrared spectroscopy and UV-Vis spectroscopy can be used to detect a spin-transition of a material, as well as obtaining information on the structure of the compound. The thermally induced spin transition from the high-spin to low-spin states of Fe^{III} spin-crossover compounds is accompanied by a depletion of the charge in the antibonding e_g orbitals and simultaneous increase of charge in the bonding t_{2g} orbitals. As a consequence, a change in the metal-ligand bond distances on going through the transition makes the vibrational spectroscopies extremely useful. As a detection tool UV-Vis spectroscopy can also be used to detect the electronic changes of a spin-crossover system. In some cases, one may follow the d-d transitions of the low-spin and the

high-spin species individually. For Fe^{III} spin-crossover systems, the ${}^5T_2 \rightarrow {}^5E$ transition of the high-spin species appears as a weak band in the near infrared, while for the low-spin species two bands occur, corresponding to the two ligand field transitions ${}^1A_1 \rightarrow {}^1T_1$ and ${}^1A_1 \rightarrow {}^1T_2$, both in the visible region. In the occurrence of ligands with low-lying π^* orbitals, the metal to ligand charge-transfer transitions for both spin states appear in the visible region and mask the d-d transitions for the low-spin state, but for the high-spin state they are generally displaced to higher frequencies and are much weaker, so the spin transition can still be followed by the appearance and disappearance of the metal to ligand charge-transfer band of the low-spin state.

Mössbauer Spectroscopy

Mössbauer spectroscopy is a technique that probes the hyperfine interactions between the nuclei and its surrounding electrons to measure information on the magnetic, electronic and structural properties within a material. The most common isotope to Mössbauer spectroscopy is the ${}^{57}\text{Fe}$ isotope and hence Fe^{II} and Fe^{III} containing spin-crossover materials are widely investigated [1, 53]. ${}^{57}\text{Fe}$ Mössbauer spectroscopy has proved a useful application in the characterisation of a spin transition curve influenced by a variety of conditions such as; variable temperature, pressure and concentration.

The most significant Mössbauer spectral parameters are the isomer shift, δ , and the quadrupole splitting, ΔE_Q , which are derived from an Mössbauer spectrum [1, 53-55]. The hyperfine interactions are probed by oscillating gamma rays, when the energy of the gamma ray is equivalent to that of a nuclear transition in the ${}^{57}\text{Fe}$ Mössbauer nucleus, the gamma ray is resonantly absorbed, and a peak is observed on the Mössbauer spectrum [53]. The isomer shift (position of the peak), δ , is reported relative to a known absorber. The isomer shift is dependent on the screening effect of d-electrons on the nucleus *i.e.* more d-electrons increases the screening effect which results in a large positive isomer shift [53]. The isomer shift is proportional to the s-electron density at the nucleus, and hence is directly influenced by the s-electron population and indirectly (via shielding effects) by the d-electron population in the valence shell, *i.e.* the area of each peak is proportional to the amount of species present [54,55]. As a result, when there are multiple peaks the ratio of species present in a sample can be determined *i.e.* the ratio of Fe^{II} to Fe^{III} or high-spin to the low-spin state. Therefore, variable temperature Mössbauer spectroscopy is a very useful technique for observing spin-crossover, and to examine the proportion of the low-spin to the high-spin states during the spin-transition [1]. Furthermore, a Mössbauer spectrum includes the quadrupole splitting, ΔE_Q , which is observed as a doublet peak on the spectrum. The quadrupole splitting is observed when an inhomogeneous electric field at the Mössbauer nucleus is present, a nuclear quadrupole moment is produced when nuclei have an asymmetrical charge distribution, which interacts with the electric field gradient and results in the splitting of the nuclear energy levels [1,54,55]. The quadrupole

splitting is the distance between the two peak observed on a spectrum. The data collected from the quadrupole splitting gives rise to information on the molecular structure of the materials, as well as, together with the isomer shift, can be used to distinguish between different oxidation and spin states [1].

Differential Scanning Calorimetry

Differential Scanning Calorimetry (DSC) can be used to determine the transition temperature of the spin transition in addition to the enthalpy (ΔH) and entropy (ΔS) of the spin transition [56].

1.4 Iron(III) spin-crossover systems with bis(R-salicylaldehyde 4R'-thiosemicarbazone) ligands

Iron(III) occupies a unique position in the development of the spin-crossover area since it was for derivatives of this ion that the phenomenon was first discovered. The aim of this section is to introduce the class of spin-crossover compounds, iron(III) bis(R-salicylaldehyde 4R'-thiosemicarbazone), as this type of compound will be the main focus in this thesis.

1.4.1 Structural aspects

The structures of Fe^{III} bis(ligand) systems consist of a distorted $\text{FeO}_2\text{N}_2\text{S}_2$ octahedral core, in which the two tridentate ligands coordinate meridionally around the Fe^{III} cation [57]. The coordination core contains two nitrogen atoms (imine) in *trans* disposition, two oxygen atoms (phenolate) and two sulfur atoms, whereby the S and O atoms are located in *cis* positions [57]. The crystal structures of several R-substituted salicylaldehyde 4R'-thiosemicarbazone Fe^{III} compounds have been determined at various temperatures and the iron-donor atom distances are recorded in Table 1.1.

The details of the Fe^{III} bis(ligand) compounds as displayed in Table 1.1 indicate that it is possible for the R-salicylaldehyde 4R'-thiosemicarbazone ligands to coordinate to the Fe^{III} ion in manner of different forms. Up to now the following forms have been reported: the Fe^{III} bis(ligand) compounds can be comprised of their constituents in one of three ways: (cation⁺)[$\text{Fe}(\text{L}^{2-})_2$] \cdot solvent, [$\text{Fe}(\text{HL}^-)(\text{L}^{2-})$] \cdot solvent or [$\text{Fe}(\text{HL}^-)_2$] \cdot (anion⁻) \cdot solvent. The abbreviated term HL^- represents the singly deprotonated R-salicylaldehyde 4R'-thiosemicarbazone(1-) ligand (involving the phenolate group) and the abbreviated L^{2-} term denotes the doubly deprotonated R-salicylaldehyde 4R'-thiosemicarbazone(2-) ligand.

Table 1.1 Crystallographic data of R-salicylaldehyde 4R'-thiosemicarbazone Fe^{III} bis(ligand) compounds.

Compound ⁱ	T (K)	Space group	Fe-S (Å)	Fe-N (Å)	Fe-O (Å)	Spin State ⁱⁱ	Ref
Cs[Fe(thsa) ₂]	298	<i>Pna2₁</i>	2.44	2.12	1.96	HS	[12]
	103	<i>Pna2₁</i>	2.44	2.15	1.96	HS	
NH ₄ [Fe(5-Br-thsa) ₂] ⁱⁱⁱ	298	<i>Pnca</i>	2.23	1.93	1.95	LS	[15]
NH ₄ [Fe(5-Cl-thsa) ₂]	298	<i>Pnca</i>	2.24	1.95	1.93	LS	[16]
	135	<i>Pnca</i>	2.23	1.96	1.94	LS	
NH ₄ [Fe(3,5-Cl-thsa) ₂]·1.5H ₂ O	298	<i>P2₁/a</i>					[58]
		<i>Site A</i>	2.26	1.95	1.93	LS	
		<i>Site B</i>	2.40	2.06	1.97	HS-sco	
	103	<i>P2₁/a</i>					
		<i>Site A</i>	2.25	1.95	1.93	LS	
		<i>Site B</i>	2.31	1.95	1.94	LS-sco	
Li[Fe(5-Br-thsa) ₂]·H ₂ O	373	<i>P2₁/c</i>	2.35	2.17	1.95	HS	[59]
	150	<i>P2₁/c</i>	2.25	1.98	1.93	LS	
[Fe(H-thsa)(thsa)]·H ₂ O	295	<i>P2₁/n</i>	2.406	2.139	1.911	HS	[18]

Table 1.1 Crystallographic data of R-salicylaldehyde 4R'-thiosemicarbazone Fe^{III} bis(ligand) compounds (continued).

Compound ⁱ	T (K)	Space group	Fe-S (Å)	Fe-N (Å)	Fe-O (Å)	Spin State ⁱⁱ	Ref
[Fe(H-5-Cl-thsa)(5-Cl-thsa)]·H ₂ O	295	<i>P2₁/n</i>	2.367	2.164	1.911	HS	[18]
[Fe(H-5-Br-thsa)(5-Br-thsa)]·H ₂ O	303	<i>P2₁/n</i>	2.445	2.14	1.945	HS	[60]
	123	<i>P2₁/n</i>	2.259	1.95	1.96	LS	
[Fe(H-5-Cl-thsa-Me)(5-Cl-thsa-Me)]·H ₂ O	293	<i>Cc</i>	2.422	2.11	1.92	HS	[19]
	260	<i>Cc</i>	2.32	2.00	1.925	IS	
	110	<i>Cc</i>	2.24	1.94	1.936	LS	

ⁱ The ligands are defined as follows: salicylaldehyde thiosemicarbazone = H₂thsa (H₂L form), 5-bromosalicylaldehyde thiosemicarbazone = H₂-5-Br-thsa (H₂L form), 5-chlorosalicylaldehyde thiosemicarbazone = H₂-5-Cl-thsa (H₂L form), and 5-chlorosalicylaldehyde 4-methylthiosemicarbazone = H₂-5-Cl-thsa-Me (H₂L form).

ⁱⁱ The spin states are defined as low-spin (LS) and high-spin (HS); sco indicates the occurrence of spin-crossover.

ⁱⁱⁱ Determined for crystals of tabular form.

Several compounds reported by Ryabova *et al.*, [12, 15, 16, 58] display coordination of the R-salicylaldehyde 4R-thiosemicarbazone ligands to the Fe^{III} cation in the dianionic thiol form, giving rise to an anionic metal fragment. These systems are usually composed of a cation, an anionic [Fe^{III}(L²⁻)₂]⁻ fragment and in the case of the compound NH₄[Fe(3,5-Cl-thsa)₂].1.5H₂O [58], water solvent molecules. Similarly, Floquet *et al.*, reported the (cation⁺)[Fe(L²⁻)₂]:solvent compound Li[Fe(5-Br-thsa)₂].H₂O [59].

Furthermore, the complexes consistent with the [Fe(HL⁻)(L²⁻)]·solvent composition have only been reported in the literature for Fe(III) over the past decade [18, 19, 60]. The compounds containing both the anionic and dianionic form of the ligand, so in the thione and thiol form of the tautomer,

appear more likely to exhibit the spin-crossover phenomenon than the more common (cation⁺)[Fe(L²⁻)₂]·solvent compounds.

The spin state of the metal ion of these Fe^{III} bis(ligand) compounds can be inferred from the metal-donor atom bond distances. X-ray structural data of this class of Fe^{III} bis(ligand) compounds containing Fe^{III}O₂N₂S₂ geometry, show that the Fe–S, Fe–N and Fe–O bond distances are in the ranges 2.23-2.31, 1.93-1.95 and 1.88-1.96 Å, respectively, for low-spin Fe^{III} compounds, and 2.40-2.44, 1.96-1.99 and 2.05-2.15 Å, respectively, for corresponding high-spin Fe^{III} compounds [9].

The non-solvated Fe^{III} bis(ligand) compounds reported by Ryabova *et al.*, [12, 15, 16] (Table 1.1) do not exhibit a transition from low-spin to high-spin Fe^{III}, however, similar materials have been found to exhibit the spin-crossover phenomenon with increasing temperature, but crystallographic data are not available for these non-solvated materials. The Fe^{III} cation in the compound Cs[Fe(thsa)₂] is in the high-spin state at both 103 and 298 K [12], whereas the Fe^{III} cation in NH₄[Fe(5-Cl-thsa)₂] is in the low-spin state at both 135 and 298 K [16]. Furthermore, in NH₄[Fe(5-Br-thsa)₂], the Fe^{III} cation is in the low-spin state at 298 K [15]. For the compounds NH₄[Fe(3,5-Cl-thsa)₂]·1.5H₂O [58] and Li[Fe(5-Br-thsa)₂]·H₂O [59], with increasing temperature the Fe^{III} cation undergoes a spin transition from low-spin (S = 1/2) to high-spin (S = 5/2) state. Furthermore, the crystallographic data of NH₄[Fe(3,5-Cl-thsa)₂]·1.5H₂O indicated that within the unit cell there are two different Fe^{III} centres, labelled *Site A* and *Site B* (Table 1.1). Only *Site B* undergoes a spin transition upon increasing temperature, whereas *Site A* remains in the low-spin state [58].

The structure of Li[Fe(5-Br-thsa)₂]·H₂O has been determined at 373 and 103 K [59]. Both the high-spin and low-spin form of the complex crystallise in the monoclinic system *P2₁/c*; this despite the occurrence of the crystallographic phase transition at 150 K in the low-spin form where the crystal structure preferentially favours the pseudo-orthorhombic system [59]. The structure determined for the high-spin form of the [Fe(5-Br-thsa)₂]⁻ fragment at 373 K shows a distortion from the ideal octahedral symmetry with bond angles involving the Fe^{III} ion and the ligand donor atoms deviating from the expected 90° [59]. The distortion of the octahedron is due to the strain caused by the interconnected five- and six-membered chelate rings. Floquet *et al.*, cited that the determined bond angles of the high-spin ferric complex [Fe(5-Br-thsa)₂]⁻ at 373 K are very similar to those reported by Ryabova *et al.*, for the high-spin ferric complex Cs[Fe(thsa)₂] [12]. Moreover, van Koningsbruggen *et al.*, [9] reported that the FeO₂N₂S₂ geometry of the Fe^{III} atom in the Cs[Fe(thsa)₂] complex is very close to that reported for the *Site B* of the NH₄[Fe(3,5-Cl-thsa)₂]·1.5H₂O. The low-spin form at 150 K of the compound Li[Fe(5-Br-thsa)₂]·H₂O is quite different to the reported high-spin state compound at 373 K [59]. The crystal structure of the low-spin form gives rise to a distorted Fe^{III}O₂N₂S₂ orthorhombic system which is similar to the Fe^{III} bis(ligand) compound reported by Ryabova *et al.*, for the low-spin ferric complexes NH₄[Fe(5-Br-thsa)₂] [15] and NH₄[Fe(5-Cl-thsa)₂]

[16]. Considering both the $\text{Fe}^{\text{III}}\text{O}_2\text{N}_2\text{S}_2$ geometry and crystal structure of the low-spin $[\text{Fe}(5\text{-Br-}t\text{hsa})_2]^-$ (at 150 K), both infer that the unit cell parameters and moreover the molecular packing display a dramatic change upon temperature decrease [59]. The molecular characteristics determine the packing and intermolecular interactions of both the high-spin (373 K) and low-spin (150 K) form of $[\text{Fe}(5\text{-Br-}t\text{hsa})_2]^-$, illustrated in Figure 1.11 [59]. Generally, the crystal packing and intra/intermolecular interactions involve hydrogen bonding and π - π interactions. In particular, attention can be focused on the nature of the interactions and how the crystallographic phase transition is modified as a consequence of the strength of these interactions. The comparison of these interactions from both the high-spin and low-spin forms leads to the indication that the molecular packing of the ferric complexes occurs in layers [59]. The low-spin form strongly suggests close packing occurring due to hydrogen bonding. The anionic compound in both the low-spin and high-spin state have been continuously influenced by the intermolecular interactions involving both the N-atoms and O-atoms of the dianionic tridentate ligand, but also the interactions formed with the Br-substituent of the salicylaldehyde moiety [59]. The high-spin form displayed no π - π stacking interactions, though it was identified that the hydrophobic component of the dianionic ligand, *i.e.* the bromo-substituted aromatic ring, separated the parallel layers of the ferric complex molecular packing [59].

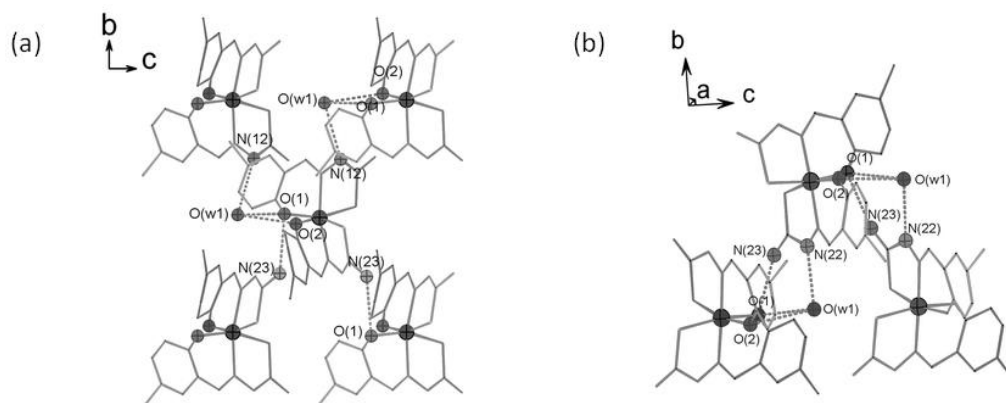


Figure 1.11 The strongest intermolecular contacts between $[\text{Fe}(5\text{-Br-}t\text{hsa})_2]^-$ complexes at (a) 150 K and (b) 373 K, adapted from reference [59].

The Fe^{III} compounds with the $[\text{Fe}(\text{HL})(\text{L})]\text{-solvent}$ configuration listed in Table 1.1 show that the chelated ligands are bound to the central Fe^{III} atom in two differently charged tautomeric forms, *i.e.* the thione and thiol tautomers. The thione form is the anionic tridentate ligand and bears a proton on the hydrazinic nitrogen atom, whereas the dianionic thiol form, does not possess a proton on the hydrazinic nitrogen atom. Typically, the compounds of this configuration as displayed in Table 1.1

exhibit a distorted octahedral geometry as the Fe-donor atom bond angles deviate from the ideal 90° [18, 19, 60].

Yemeli Tido reported the crystal structures of the isostructural compounds $[\text{Fe}(\text{H-thsa})(\text{thsa})]\cdot\text{H}_2\text{O}$ and $[\text{Fe}(\text{H-5-Cl-thsa})(5\text{-Cl-thsa})]\cdot\text{H}_2\text{O}$ at 295 K [18]. Both compounds crystallise in the monoclinic $P2_1/n$ system. The Fe^{III} cation in both compounds was found to be in the high-spin state at 295 K. The packing arrangements of $[\text{Fe}(\text{H-thsa})(\text{thsa})]\cdot\text{H}_2\text{O}$ and $[\text{Fe}(\text{H-5-Cl-thsa})(5\text{-Cl-thsa})]\cdot\text{H}_2\text{O}$ (displayed in Figure 1.12) are such that 2D sheets are formed, whereby the Fe^{III} entities are packed closely together forming a parallel π - π stacking interaction with the water solvent molecules inserted within each sheet [18].

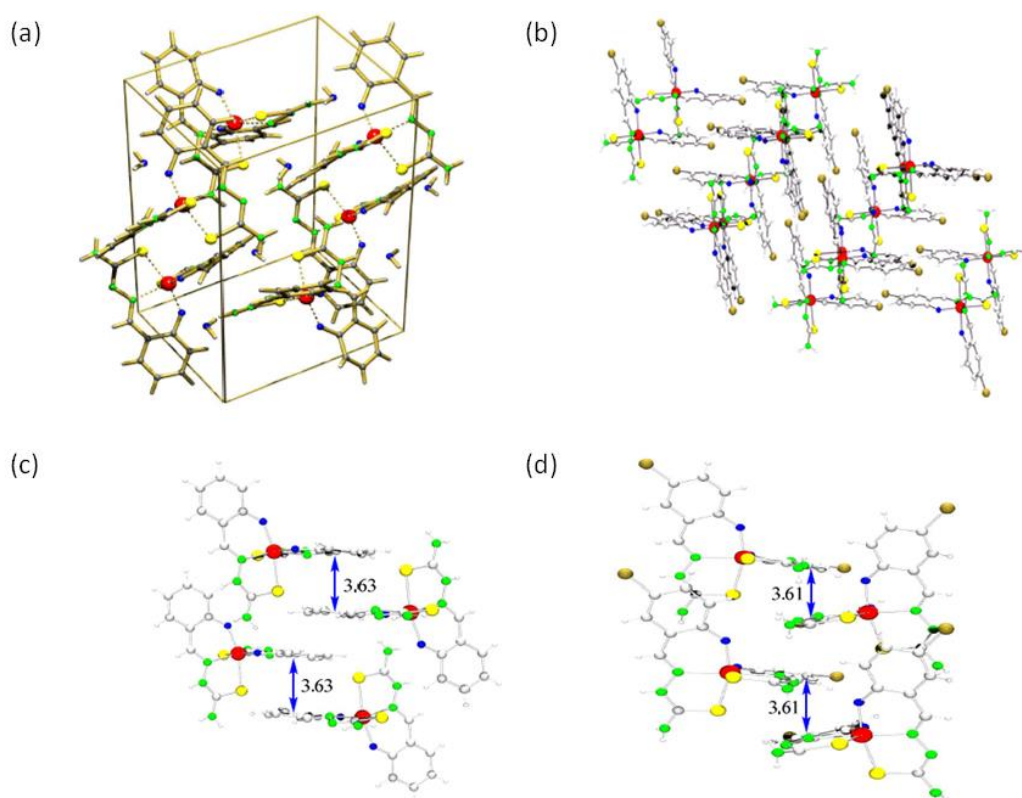


Figure 1.12 (a) The molecular packing arrange of $[\text{Fe}(\text{H-thsa})(\text{thsa})]\cdot\text{H}_2\text{O}$ and (b) illustrates the 2D networks of $[\text{Fe}(\text{H-5-Cl-thsa})(5\text{-Cl-thsa})]\cdot\text{H}_2\text{O}$. (c) and (d) illustrate the π - π stacking interactions of $[\text{Fe}(\text{H-thsa})(\text{thsa})]\cdot\text{H}_2\text{O}$ and $[\text{Fe}(\text{H-5-Cl-thsa})(5\text{-Cl-thsa})]\cdot\text{H}_2\text{O}$ at 295 K, respectively. (Adapted from reference [18]).

Furthermore, the crystal structure of $[\text{Fe}(\text{H-5-Br-thsa})(5\text{-Br-thsa})]\cdot\text{H}_2\text{O}$ reported by Li *et al.*, [60] at 303 and 123 K was found to be isostructural to the compounds $[\text{Fe}(\text{H-thsa})(\text{thsa})]\cdot\text{H}_2\text{O}$ [18] and $[\text{Fe}(\text{H-5-Cl-thsa})(5\text{-Cl-thsa})]\cdot\text{H}_2\text{O}$ [18]. The Fe^{III} atom of $[\text{Fe}(\text{H-5-Br-thsa})(5\text{-Br-thsa})]\cdot\text{H}_2\text{O}$ was found to be in the high-spin state at 303 K, and in the low-spin state at 123 K [60]. Interestingly, Li

et al., observed upon decreasing the temperature from room temperature the crystallographic data revealed a symmetry closer to the triclinic space group $P1$ ($Z = 4$), where there were found to be four crystallographically independent Fe^{III} complexes in the unit cell, *i.e.* three in the high-spin state and one Fe^{III} complex in the low-spin state [60]. Moreover, Li and co-workers reported the polar space group Pn ($Z = 4$) was more suitable to the crystallographic data recorded due to the lower R_1 value [60]. At 223 K, it was observed that the two crystallographically independent Fe^{III} complexes exhibited different spin states; one in the high-spin state and the other Fe^{III} complex in the low-spin state [60]. It was determined that the Pn space group was maintained until the temperature reached 163 K, by 123 K the $P2_1/n$ space group is observed where one independent Fe^{III} complex exists in the unit cell [60]. The comparison of the high-spin to low-spin state packing arrangements of the present Fe^{III} complex reveals that both spin state forms give rise to a two-dimensional supramolecular structure (illustrated in Figure 1.13) in which the Fe^{III} entities are linked through hydrogen bonding [60]. However, the low-spin Fe^{III} compound showed strong hydrogen bonding interactions between the terminal N atoms and the O atom of the phenolate group whereas, in the high-spin form only moderate interactions were observed.

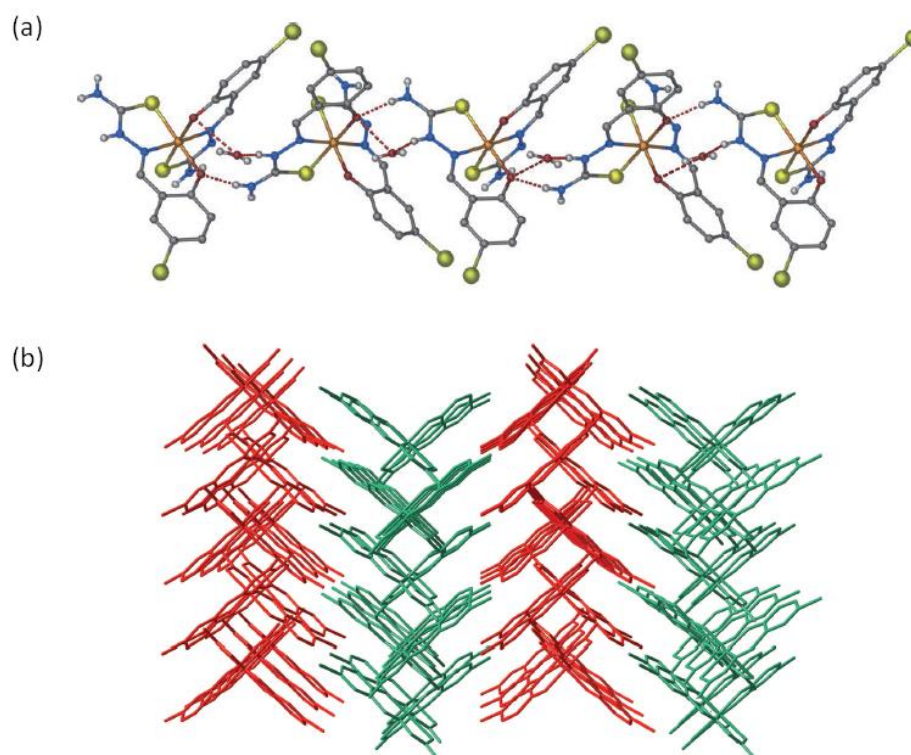


Figure 1.13 (a) 1D supramolecular chain connected by the hydrogen bonds $\text{N}(\text{azomethine})\text{-H}\cdots\text{Ow}$ and $\text{N}(\text{amide})\text{-H}\cdots\text{O}$ at 123 K. (b) 2D supramolecular packing structure of $[\text{Fe}(\text{H-5-Br-thsa})(\text{5-Br-thsa})]\cdot\text{H}_2\text{O}$ along the c axis at 183 K. (Adapted from reference [60]).

Li *et al.*, reported the neutral $\text{Fe}^{\text{III}}\text{O}_2\text{N}_2\text{S}_2$ compound $[\text{Fe}(\text{H-5-Cl-thsa-Me})(5\text{-Cl-thsa-Me})]\cdot\text{H}_2\text{O}$, where the crystallographic data were collected at 110, 260 and 293 K [19]. The space group for the Fe^{III} atom at measurement temperatures 110, 260 and 293 K, was determined to be *Cc*. The Fe^{III} atom was found to be in the high-spin state at 293 K, and in the low-spin state at 110 K, however, at the measurement temperature 260 K, the averaged Fe-donor atom bond distances are indicative for the Fe^{III} atom being in the process of converting from the low-spin to the high-spin state [19]. The packing arrangements (Figure 1.14) of the Fe^{III} entities in the unit cell show hydrogen bonding interactions which link the Fe^{III} entities in a chain by an amide nitrogen atom and the phenolate oxygen atom of the salicylaldehyde moiety of the ligand [19].

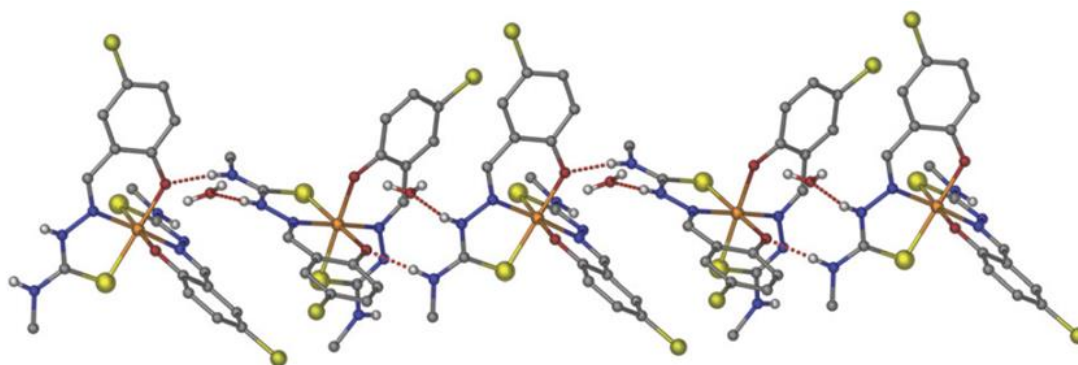


Figure 1.14 Supramolecular hydrogen bonding packing arrangement of $[\text{Fe}(\text{H-5-Cl-thsa-Me})(5\text{-Cl-thsa-Me})]\cdot\text{H}_2\text{O}$. (Adapted from reference [19]).

Interestingly, a feature that has been recognised throughout the series of $[\text{Fe}(\text{HL})(\text{L})]\cdot\text{H}_2\text{O}$ type compounds is that the coordinated singly deprotonated and doubly deprotonated ligands' bond distances change significantly when the spin state of the Fe^{III} atom changes from the high-spin to the low-spin state. Specifically, the spin transition mainly affects the C–S and C–N bond distances that involve the electron delocalisation of the Fe^{III} -nitrogen donor atom. This feature causes a change in the ligand field strength during the process of the thermally induced spin transition. Furthermore, the close packing arrangements and the hydrogen bonding interactions between the Fe^{III} entities of this family of compounds reveal that the coordination sphere of the $\text{Fe}^{\text{III}}\text{O}_2\text{N}_2\text{S}_2$ entities is restricted, which causes the Fe^{III} complex to rearrange within the unit cell when undergoing a thermal induced spin transition. When the thermally induced spin-crossover occurs the Fe^{III} -donor atom bond distances change significantly between the low-spin and high-spin forms.

1.4.2 Characterisation by Spectroscopic Techniques

A wide variety of spectroscopic techniques can be used to characterise the spin-state and therefore the occurrence of a spin transition of Fe^{III} bis(ligand) type compounds. The most extensively applied spectroscopic technique is ⁵⁷Fe Mössbauer Spectroscopy, where variable temperature ⁵⁷Fe Mössbauer spectral studies of various coordination compounds have revealed the compounds to exhibit a spin transition. Floquet *et al.* [59, 61], Li *et al.* [19, 60], and Yemeli Tido *et al.* [18], have reported various R-salicylaldehyde 4R'-thiosemicarbazone Fe^{III} bis(ligand) compounds. ⁵⁷Fe Mössbauer spectral measurements showed that the solvated Fe^{III} compounds Li[Fe(5-Br-thsa)₂].1.5H₂O [59], [Fe(H-thsa)(thsa)].H₂O [18], [Fe(H-5-Cl-thsa)(5-Cl-thsa)].H₂O [18] and [Fe(H-5-Cl-thsa-Me)(5-Cl-thsa-Me)].H₂O [19] display spin-crossover behaviour. Typical values of the quadrupole splitting (ΔE_Q) and isomer shift (δ) parameters for both the high-spin and low-spin state observed for complexes with Fe^{III}O₂N₂S₂ coordination core are $\Delta E_Q = 0.4\text{-}0.8\text{ mm s}^{-1}$; $\delta = 0.34\text{-}0.54\text{ mm s}^{-1}$ and $\Delta E_Q = 2.7\text{-}3.1\text{ mm s}^{-1}$; $\delta = 0.14\text{-}0.34\text{ mm s}^{-1}$, respectively [62-66].

The ⁵⁷Fe Mössbauer spectra recorded between 300 – 77 K of the compounds [Fe(H-5-Cl-thsa)(5-Cl-thsa)].H₂O and [Fe(H-thsa)(thsa)].H₂O both show very similar behaviour in which they reveal quadrupole-split absorption lines devoid of magnetic splitting at all measurement temperatures [18]. Typically at room temperature the ⁵⁷Fe Mössbauer spectra of the present compounds exhibit an asymmetric doublet, and as the temperature decreases to *ca.* 270 K and *ca.* 230 K for [Fe(H-thsa)(thsa)].H₂O and [Fe(H-5-Cl-thsa)(5-Cl-thsa)].H₂O, respectively, there are two distinct quadrupole split doublets. The two doublets are indicative for the existence of two different Fe^{III} environments, such that one doublet corresponds to the low-spin fraction and the contribution of the other doublet is ascribed to the high-spin fraction of Fe^{III}. At 77 K, the corresponding values of the isomer shift and quadrupole splitting for [Fe(H-thsa)(thsa)].H₂O and [Fe(H-5-Cl-thsa)(5-Cl-thsa)].H₂O ($\delta = 0.22\text{-}0.53\text{ mm s}^{-1}$; $\Delta E_Q = 1.37\text{-}2.78\text{ mm s}^{-1}$ and $\delta = 0.22\text{-}0.54\text{ mm s}^{-1}$; $\Delta E_Q = 0.84\text{-}2.79\text{ mm s}^{-1}$, respectively) suggest that the Fe^{III}O₂N₂S₂ core of the two compounds have exhibited a spin transition from the high-spin ($S = 5/2$) to the low-spin ($S = 1/2$) state. The ⁵⁷Fe Mössbauer isomer shift and quadrupole splitting parameters indicate that the Fe^{III}O₂N₂S₂ core undergoes a spin transition from the high-spin to the low-spin state between 300 and 77 K [18].

The ⁵⁷Fe Mössbauer spectrum of the compound Li[Fe(5-Br-thsa)₂].1.5H₂O at 360 K is characterised by the isomer shift and quadrupole splitting values of $\delta = 0.294\text{ mm s}^{-1}$ and $\Delta E_Q = 0.338\text{ mm s}^{-1}$, which are attributed to the high-spin state of Fe^{III} [61]. Between 160 K and 360 K two distinct quadrupole doublets are observed, one being attributed to the fraction of low-spin and the other assigned to the contribution of the high-spin fraction of Fe^{III}. With decreasing the temperature to 77 K, the ⁵⁷Fe Mössbauer spectrum is characterised by a quadrupole splitting of $\Delta E_Q = 2.584\text{ mm s}^{-1}$ and an isomer shift of $\delta = 0.262\text{ mm s}^{-1}$; these values are consistent with the low-spin state of Fe^{III}.

This indicates that the compound converts from the high-spin to low-spin state over the temperature range 360 – 77 K [61].

The recorded ^{57}Fe Mössbauer spectra of the Fe^{III} compound $[\text{Fe}(\text{H-5-Cl-thsa-Me})(\text{5-Cl-thsa-Me})]\cdot\text{H}_2\text{O}$ corroborate the observed two-step spin transition as supported by the magnetic and the crystallographic studies [19]. A quadrupole doublet is observed at 300 K, which is characterised by an isomer shift $\delta = 0.297 \text{ mm s}^{-1}$ and quadrupole splitting $\Delta E_{\text{Q}} = 0.592 \text{ mm s}^{-1}$ [19]. These values are consistent with high-spin ($S = 5/2$) Fe^{III} . At 260 K the isomer shift is equal to $\delta = 0.091 \text{ mm s}^{-1}$ and the quadrupole splitting equals $\Delta E_{\text{Q}} = 2.692 \text{ mm s}^{-1}$ for the low-spin fraction, moreover, for the high-spin fraction, the isomer shift is equal to $\delta = 0.326 \text{ mm s}^{-1}$ and the quadrupole splitting, $\Delta E_{\text{Q}} = 0.823 \text{ mm s}^{-1}$ [19]. The spectrum at the decreased temperature of 110 K reveals the compound has converted completely to the low-spin state, with isomer shift and quadrupole splitting values of 0.148 mm s^{-1} and 2.735 mm s^{-1} , respectively [19].

1.4.3 Magnetic Studies

Iron(III) thiosemicarbazone complexes belong to a unique family that potentially exhibit cooperative thermal spin-crossover from low-spin, $S = 1/2 \leftrightarrow S = 5/2$, high-spin. The reported ferric complexes' thermal spin-crossover behaviour from high-spin to low-spin state is characterised by minute changes in both molecular structure and molecular volume [12, 15, 16, 18, 19, 59-61]. Discontinuous and continuous transitions of spin-crossover have been identified as well as the rare two-step transition observed by Zelentsov *et al.*, and the multi-step transition reported by Li *et al.*, [19, 60]. In particular, this class of ferric bis(R-salicylaldehyde 4R'-thiosemicarbazone) spin-crossover compounds may also exhibit a spin-crossover with a thermal hysteresis loop, similar to those reported with ferric complexes with protonated forms of pyruvic acid thiosemicarbazones and pyridoxal thiosemicarbazones [18]. Variable temperature magnetic measurements are used to study the potential of a solid compound to exhibit a thermally induced spin-crossover.

The compound $\text{NH}_4[\text{Fe}(\text{5-Cl-thsa})_2]$ does not exhibit a thermally induced spin transition, however the compound $\text{NH}_4[\text{Fe}(\text{5-Br-thsa})_2]$ in both the tabular and mica-like crystal forms exhibits a thermally induced spin transition, although each crystal form undergoes a spin transition in a different temperature region [15, 16]. The mica-like crystal form shows spin-crossover in the region around 200 K. The tabular crystalline form of $\text{NH}_4[\text{Fe}(\text{5-Br-thsa})_2]$ is in the low-spin state at room temperature with a magnetic moment of $\mu_{\text{eff}} = 2.16 \text{ B.M.}$, however, upon increasing the temperature to 400 K the effective magnetic moment increases to reach a value for high-spin Fe^{III} ($\mu_{\text{eff}} = 5.84 \text{ B.M.}$) [15].

The ferric complex $\text{Li}[\text{Fe}(\text{5-Br-thsa})_2]\cdot\text{H}_2\text{O}$ showed that the temperature dependence of the χ_{MT} product indicates a discontinuous $S=1/2 \leftrightarrow S=5/2$ transition with a broad asymmetric hysteresis loop

[59], illustrated in Figure 1.15. The associated hysteresis loop is centred at $T_{1/2\downarrow} = 292$ K and $T_{1/2\uparrow} = 329$ K [59].

For the ferric complex, $\text{Li}[\text{Fe}(\text{5-Br-thsa})_2] \cdot \text{H}_2\text{O}$ reported by Floquet *et al.*, [61] the hysteresis loop is centred at $T_{1/2\downarrow} = 294$ K and $T_{1/2\uparrow} = 333$ K. The $\chi_M T$ values $0.63 \text{ cm}^3 \text{ mol}^{-1} \text{ K}$ at 50 K and $0.46 \text{ cm}^3 \text{ mol}^{-1} \text{ K}$ at 10 K correspond to the low-spin form of the ferric complex whereas the $\chi_M T$ values for the high-spin form are $3.91 \text{ cm}^3 \text{ mol}^{-1} \text{ K}$ at 383 K and $3.74 \text{ cm}^3 \text{ mol}^{-1} \text{ K}$ at 380 K [59]. These reported products of temperature dependent magnetic susceptibility values are indicative of a near complete spin transition. Floquet *et al.*, detected the spin-crossover by DSC and X-ray powder diffraction measurements. Both techniques allowed for the analysis of hysteretic behaviour. It was found that the observation of the hysteresis of the $\chi_M T$ product was caused to the first order crystallographic phase transition association with spin-crossover [59, 61]. The $\text{Li}[\text{Fe}(\text{5-Br-thsa})_2] \cdot \text{H}_2\text{O}$ compound displayed a discontinuous spin transition; and the magnetic behaviour is influenced by the solvent water molecule [59, 61]. The water molecule sets up a hydrogen bonding network resulting in cooperative spin-crossover behaviour [59].

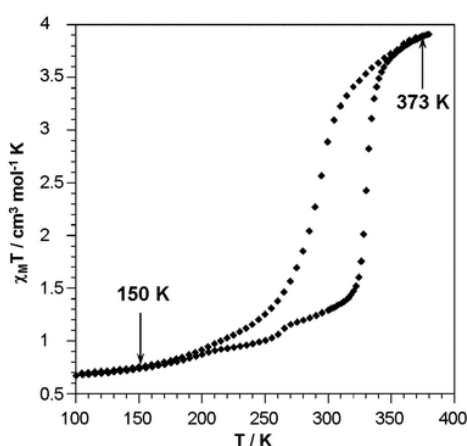


Figure 1.15 Temperature dependence of the $\chi_M T$ product for $\text{Li}[\text{Fe}(\text{5-Br-thsa})_2] \cdot \text{H}_2\text{O}$. (Adapted from reference [59]).

Yemeli Tido reported the two isostructural compounds $[\text{Fe}(\text{H-thsa})(\text{thsa})] \cdot \text{H}_2\text{O}$ and $[\text{Fe}(\text{H-5-Cl-thsa})(\text{5-Cl-thsa})] \cdot \text{H}_2\text{O}$. Both compounds exhibited a thermally induced spin transition over the temperature range 50 – 340 K [18]. The temperature dependence of the $\chi_M T$ product for the compound $[\text{Fe}(\text{H-5-Cl-thsa})(\text{5-Cl-thsa})] \cdot \text{H}_2\text{O}$ (Figure 1.16) reveals an abrupt transition in the warming mode which is observed around $T_{1/2\uparrow} = 231$ K [18]. Upon cooling the sample the $\chi_M T$ value decreases abruptly around $T_{1/2\downarrow} = 230$ K. The magnetic properties of $[\text{Fe}(\text{H-thsa})(\text{thsa})] \cdot \text{H}_2\text{O}$ (Figure 1.16) reveal the $\chi_M T$ value at 340 K is equal to $3.80 \text{ cm}^3 \text{ K mol}^{-1}$, which lies in the range expected for Fe^{III} in the high-spin state ($S = 5/2$), with an abrupt transition occurring at $T_{1/2\uparrow} = 274$ K, indicating a thermally induced spin-crossover from the low-spin to high-spin state [18].

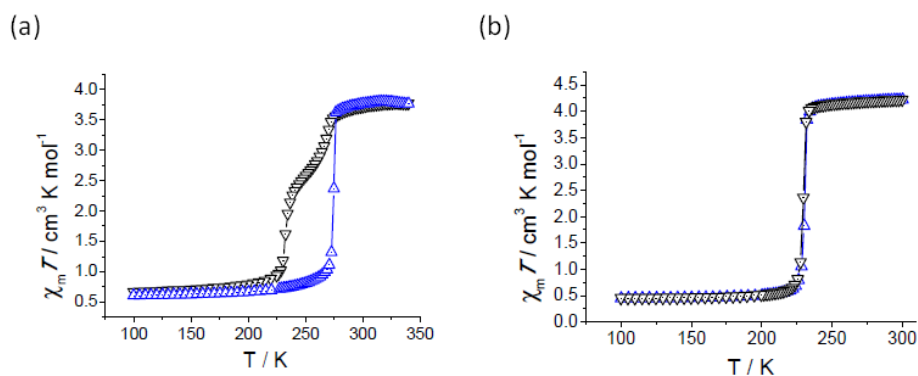


Figure 1.16 Temperature dependence of the $\chi_M T$ product for (a) $[\text{Fe}(\text{H-thsa})(\text{thsa})]\cdot\text{H}_2\text{O}$ and (b) $[\text{Fe}(\text{H-5-Cl-thsa})(\text{5-Cl-thsa})]\cdot\text{H}_2\text{O}$. (Adapted from reference [18]).

Interestingly, the magnetic measurements upon cooling of the compound $[\text{Fe}(\text{H-thsa})(\text{thsa})]\cdot\text{H}_2\text{O}$, showed that the Fe^{III} ion exhibits a rare two step hysteresis; the first and second transition steps are centered at temperatures of $T_{1/2\downarrow} = 262 \text{ K}$ and $T_{1/2\downarrow} = 232 \text{ K}$, respectively, whereas upon heating the sample the Fe^{III} ion undergoes a one-step transition at $T_{1/2\uparrow} = 274 \text{ K}$ [18]. Furthermore, the Fe^{III} compound $[\text{Fe}(\text{H-5-Br-thsa})(\text{5-Br-thsa})]\cdot\text{H}_2\text{O}$ reported by Li *et al.*, shows that the magnetic properties reveal a multi-step spin-crossover during both the heating and cooling measurements (5 – 300 K), illustrated in Figure 1.17 [60].

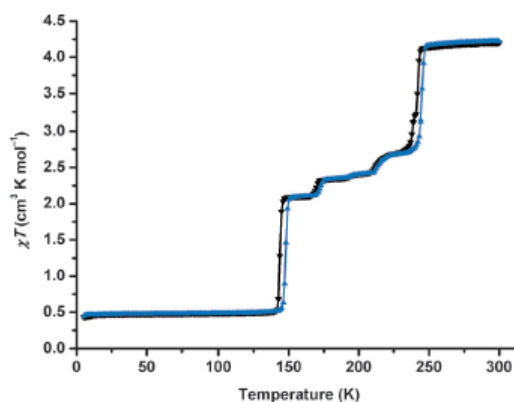


Figure 1.17 Temperature dependence of the $\chi_M T$ product for $[\text{Fe}(\text{H-5-Br-thsa})(\text{5-Br-thsa})]\cdot\text{H}_2\text{O}$. (Adapted from reference [60]).

The conversion of the Fe^{III} spin state from high-spin to low-spin over the temperature range 300 to 5 K is verified by the $\chi_M T$ values of $4.20 \text{ cm}^3 \text{ K mol}^{-1}$ at 300 K and $0.44 \text{ cm}^3 \text{ K mol}^{-1}$ at 5 K, respectively [60]. The first and sixth transition step are centered at temperatures of $T_{1/2\downarrow} = 242 \text{ K}$ and $T_{1/2\downarrow} = 144 \text{ K}$, respectively, with $\chi_M T$ values of $3.50 \text{ cm}^3 \text{ K mol}^{-1}$ and $0.44 \text{ cm}^3 \text{ K mol}^{-1}$, respectively [60]. The second, third, fourth and fifth transition steps are centered at 238 K, 211 K, 194 K and 170 K, severally. Li *et al.*, determined that upon heating, the spin-crossover is observed with hysteresis of about 7 K at the first and sixth step [60].

The magnetic behaviour of the neutral compound $[\text{Fe}(\text{H}-5\text{-Cl-thsa-Me})(5\text{-Cl-thsa-Me})]\cdot\text{H}_2\text{O}$ revealed a two-step spin transition with hysteresis (Figure 1.18) [19]. At 300 K the $\chi_{\text{M}}T$ value is equal to $3.89 \text{ cm}^3 \text{ K mol}^{-1}$, which lies in the range expected for high-spin Fe^{III} [19]. On cooling the sample, the first transition step is centered at $T_{1/2\downarrow} = 270 \text{ K}$, while decreasing the temperature revealed the second transition step centered at $T_{1/2\downarrow} = 245 \text{ K}$ [19]. In the warming mode the second and first transition steps are centered at the temperatures of $T_{1/2\uparrow} = 249 \text{ K}$ and 278 K , respectively, creating a hysteresis of 4 K and 8 K for the first and second spin transitions [19].

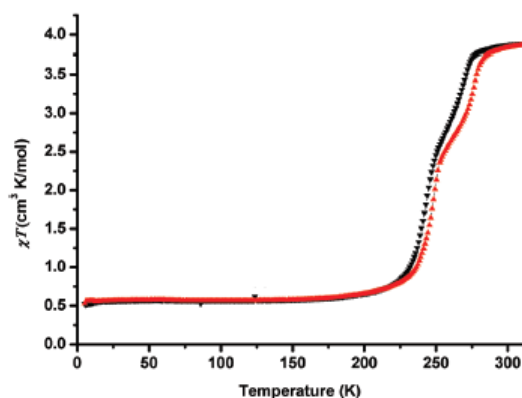


Figure 1.18 Temperature dependence of the $\chi_{\text{M}}T$ product for $[\text{Fe}(\text{H}-5\text{-Cl-thsa})(5\text{-Cl-thsa})]\cdot\text{H}_2\text{O}$. (Adapted from reference [19]).

1.5 Applications of Spin Crossover Materials

In the last 50 years there has been growing interest in spin crossover materials and their possible technological applications, which has been reflected through the current advances occurring in this field. As molecular-based switchable materials can be tailor made, they provide a unique tool for fine-tuning the physical properties, as well as their sensitivity to the external environment in combination with measurable effects to the bulk properties [67,68]. This provides a wide range of potential applications, which include:

- (i) Data storage devices;
- (ii) Molecular switches;
- (iii) Display devices;
- (iv) Sensors.

The field of potential applications is influenced by the constant pressures of advancing technology, mainly caused by the demand for miniaturisation in current technology which therefore increases the interest in molecular materials. Among these materials, molecular switches are transition metal complexes (having a d^n , where $n = 4-7$) exhibiting spin-crossover. These materials exhibit reversible switching behaviour, *i.e.* the conversion between two spin states, the low-spin and high-spin

electronic configurations. These so-called spin transitions can be caused by various external stimuli such as temperature, pressure, light or X-ray irradiation, an intense magnetic field or the inclusion of a guest molecule [68]. As discussed in previous sections of this chapter, the low-spin and high-spin states can be determined by their different magnetic, optical, mechanical, spectroscopic and structural properties [68]. The ability of spin-crossover materials to switch between spin-states can produce hysteresis phenomena. This aspect of the spin-crossover materials is of interest from a technological point of view, as the materials provide molecular bistability; and thus provide a promising area of research that spin-crossover materials can potentially be useful molecular switches, as well as components in displays [67], data storage [69], sensors [70,71], nano-thermometers [72], optoelectronic devices [73] and actuators [74].

Létard *et al.*, [67] reviewed in 2004 the possible applications of spin-crossover materials in molecular electronics, data storage, display devices, non-linear optics, and photomagnetism, with emphasis towards the design of molecular switches and their shortfalls for possible practical application. Switchable molecular materials have been considered since the miniaturisation of silicon based devices and magnetic storage devices, together with the technological and physical limitations these switches impose on the application phase [68,75-77]. This leads to the question of whether single crystals or powder spin-crossover materials are compatible with technological requirements, for the construction of possible technological devices. Kahn *et al.* in the 1990s proposed that spin-crossover materials could be incorporated into polymer systems for applications towards spin transition polymers for memory devices [69,78]. More recently, Bousseksou *et al.*, have made key contributions towards research focused on nano-scale spin-crossover materials, and attempting to emphasise the important aspects required to understand before the construction of the applications. These aspects include: (i) spin-crossover nano-particles and thin films, (ii) nano-patterning and nano-scale organisation and (iii) future possibilities of addressable nano-structures for gas sensors, displays and switchable photonic devices [79-91].

The latest review (2016) by Bousseksou *et al.*, [68] gives an overview of several research groups' efforts concerning the studies of electrical properties of spin-crossover materials, including the possibilities of utilising the electrical field and/or current. Instead of using temperature, pressure or light irradiation as the stimulus or 'input', the use of electrical stimuli to activate the spin-state interconversion would be more advantageous, not only due to faster dynamics, but for the compatibility with current technology and the ability of size reduction [68]. Bousseksou *et al.*, reviewed the present studies of electrical properties of spin-crossover materials, this including (i) bulk powders and crystals, (ii) reduction of scale to thin films and nano-particles and (iii) single molecules.

The following sections will discuss the properties required for the application of spin-crossover materials in technology and emphasise important aspects required so these materials can become functional components of these applications.

Molecular switches

A molecular switch is defined as possessing two states, the 'on' state and 'off' state; materials exhibiting spin-crossover act as molecular switches, whereby the interconversion between the low-spin and high-spin states differentiates between the 'on' and 'off' states. The ability of a material to act as a molecular switch is defined as possessing molecular bistability. This can be interpreted as binary code *i.e.* the strings of 0s and 1s that are used for encoding of information in digital computing and communication systems. The 'on' and 'off' states of a molecular switch are corroborative of the low-spin and high-spin states. Although, for these systems to be useful in current technology, the interconversion between on and off states must be repeatable without deterioration and occur at a rapid pace, as well as the individual states being accessible with simple input and readable output functions. As previously stated, the simplest stimuli or 'input' are temperature, pressure and light irradiation. An abrupt spin-crossover is required in response to the input, in order to produce a detectable output functions which can be identified by the magnetic moment or the colour absorption between the low-spin and high-spin states. Due to the requirement of an abrupt transition for the molecular switch to be useful, it has been determined that these materials cannot act as operators in logic operations *i.e.* where one input produces one output.

There is potential use for multinuclear spin-crossover systems, which would provide a more complex molecular switch, whereby more than two states are accessible and therefore more complex uses are possible [92]. Another potential use for these materials as reviewed by Bousseksou *et al.*, is using their potential as an electrical conductor, hence the spin-transition is measured by passing a current through the material and measuring the resistance [68]. This would be more advantageous as electrical conductivity is easy to measure and compatible with the current technology [68].

Data storage devices

Similar to molecular switches, systems with molecular-based memory must have two states, the so-called 'on' and 'off' states. Molecular based memory systems also require materials with bistability, such as hysteretic spin-crossover compounds exist in two states at a given temperature, hence provides potential applications in memory storage devices. For these systems to be utilised in data storage, they must remain in a chosen state after the input (stimuli) function has been removed up until that information is required [67]. At present, data is stored in a binary format [67].

Both the LIESST and reverse-LIESST phenomena in spin-crossover materials, where switching between the low-spin and excited high-spin state occurs from the input of light irradiation, has shown they are possible candidates for memory storage devices. However, as the excited high-spin state lifetime is only seen at cryogenic temperatures, these materials are not ideal in data storage for current technologies. Materials with an easily-triggered abrupt hysteretic spin-transition at room temperature are ideal systems for memory storage devices. The hysteretic system is resultant from cooperative interactions between a series of molecules, hence spin-crossover materials designed for data storage devices consist of a range of spin-crossover centres instead of individual sites, as used in molecular switches [67]. Interestingly, multifunctional materials which exhibit spin-crossover together with electrical conductivity represents another step toward the application of these materials in future technologies [68].

Display Devices

Spin-crossover materials have the potentials to be used in display devices if a number of general requirements are fulfilled; the material should have a strong thermochromic response to the spin-state change, the material must be chemically stable and not be subject to deterioration and the spin-transitions must be abrupt, exhibiting a wide hysteresis centred at room temperature. This list of criteria is not always easily executed due to particular intermolecular interactions which can occur, such as π - π stacking interactions, which is frequently a requirement for hysteresis, however this often leads to charge transfer transitions which mask any visible colour change upon transition [67].

Létard *et al.*, created a functioning display device using triazole derivatives [67]. This approach used the spin-crossover materials suspended in ink which was printed onto a screen, to which a heating element is placed below the screen in combination with a mask incorporating the design of visual display and when the temperature is increased the design is revealed [67]. However, display devices as created by Létard *et al.*, or presented by Kahn *et al.*, rely on thermal transition and heating, which is not a practical method suitable for current display devices [67].

Sensors

Developments of temperature or pressure sensors are of interest in the field of spin-crossover materials due to the temperature and pressure dependence of a spin transitions. The spin-crossover behaviour exhibited by a change in pressure has applications as pressure sensors, and thermally induced spin-crossover materials can be utilised as temperature sensors [67]. Preferably these spin-crossover systems would exhibit a visibly pronounced colour change upon interconversion between spin-states, hence easily detected. Moreover, it would be highly advantageous to create a sensor

which could detect both temperature and pressure, as this would enable materials which have well-defined phase diagrams to be used to detect temperature changes at a constant pressure, as well as pressure changes at a constant temperature [70].

1.6 Objectives and Scope of Research

The initial stage of the project was to synthesise a variety of functionalised R-salicylaldehyde 4R'-thiosemicarbazone ligands. Once obtained, the aim was to design new mononuclear Fe^{III} compounds with a view of studying their structural and magnetic properties. The focus of the investigation was to design three types of structural configurations of Fe^{III}-bis(ligand) complexes, these include: (i) (cation⁺)[Fe^{III}(L²⁻)₂].x(solvent), (ii) [Fe^{III}(HL⁻)(L²⁻)].x(solvent) and (iii) [Fe^{III}(HL⁻)₂](anion⁻).x(solvent). Dependent upon the structural data interpreted, an attempt would then be made to outline correlations between the observed magnetic behaviours of the obtained ferric complexes and the structure of the Fe^{III} entities and the packing of the Fe^{III} entities within the crystal lattice, both spin-active and in-active. An in-depth study of these observations and relationships would then be compared to similar types of ferric complexes published in this research field. The results of this project are detailed in this thesis.

Chapter II details the synthetic procedures of the obtained ferric complexes and their corresponding ligands, in addition to the experimental details for the physical characterisation of the obtained ferric complexes. Chapter III describes the research of (cation⁺)[Fe^{III}(L²⁻)₂].xsolvent type complexes containing two dianionic R-salicylaldehyde 4R'-thiosemicarbazonate(2-) ligands, with a focus of investigating the effect of varying R- and R'-substituents, cations and solvent molecules within the lattice on the magnetic properties and crystal packing. Chapter IV provides a study of three mononuclear [Fe^{III}(HL⁻)(L²⁻)].H₂O type complexes, containing one anionic and one dianionic R-salicylaldehyde 4R'-thiosemicarbazone ligand. Correlations between the steric and electronic effects imposed by the R- and R'-substituents of the ligands bound to the Fe^{III} ions and the magnetic properties observed will then be discussed. Chapter V investigates [Fe^{III}(HL⁻)₂](anion⁻).xH₂O type complexes, with focus upon the effect of varying the anions and the R- and R'-substituents of the coordinated one-fold deprotonated ligands within the crystal lattice on the magnetic properties and crystal packing of [Fe^{III}(HL⁻)₂](anion⁻).xH₂O type complexes. Chapter VI offers the final conclusions and suggested future work based on the results obtained in this thesis.

1.7 References

1. Gütlich, P. and Goodwin, H. A. (2004). Editors. *Spin Crossover in Transition Metal Compounds I*, edited by Gütlich, P. and Goodwin, H. A., *Top. Curr. Chem.* Berlin: Springer, **233**, pp. 1-47.
2. Hauser, A. (2004). *Spin Crossover in Transition Metal Compounds I*, edited by Gütlich, P. and Goodwin, H. A., *Top. Curr. Chem.* Berlin: Springer, **233**, pp. 49-58.
3. Cambi, L. and Szegö, L. (1931). *Ber. dtsh. Chem. Ges A/B*, **64**, pp. 2591-2598.
4. Cambi, L. and Szegö, L. (1933). *Ber. dtsh. Chem. Ges A/B*, **66**, pp. 656-661.
5. Campbell, M. J. M. (1975). *Coord. Chem. Rev.* **15**, pp. 279-319.
6. Padhyé, S. and Kauffman, G. B. (1985). *Coord. Chem. Rev.* **63** (4), pp. 127-160.
7. West, D. X., Padhyé, S. B. and Sonawane, P. B. (1991). *Structure Bonding.* **76**, pp.1-50.
8. West, D. X., Liberta, A. E., Padhyé, S. B., Chikate, R. C., Sonawane, P. B., Kumbhar, A. S. and Yerande, R. G. (1993). *Coord. Chem. Rev.* **123** (2), pp. 49-71.
9. Koningsbruggen, P. J. van, Maeda, Y. and Oshio, H. (2004). *Spin Crossover in Transition Metal Compounds I*, edited by Gütlich, P. and Goodwin, H. A., *Top. Curr. Chem.* **233**, pp. 259-324.
10. Zelentsov, V. V., Bogdanova, L. G., Ablov, A. V., Gerbeleu, N. V. and Dyatlova, Ch. V. (1973). *Russ. J. Inorg. Chem.* **18**(10), pp. 1410-1412.
11. Ivanov, E. V., Zelentsov, V. V., Gerbeleu, N. V. and Ablov, A. V. (1970). *Dokl. Akad. Nauk SSSR.* **191**, pp. 827.
12. Ryabova, N. A., Ponomarev, V. I., Zelentsov, V. V. and Atovmyan, L. O. (1981). *Kristallografiya.* **26**, pp. 101-108.
13. Zelentsov, V. V., Ablov, A. V., Turta, K. I., Stukan, R. A., Gerbeleu, N. V., Ivanov, E. V., Bogdanov, A. P., Barba, N. A. and Bodyu, V. G. (1972). *Russ. J. Inorg. Chem.* **17**(7), pp. 1000-1003.
14. Ablov, A. V., Goldanskii, V. I., Turka, K. I., Stukan, R. A., Zelentsov, V. V., Ivanov, E. V. and Gerbeleu, N. V. (1971). *Dokl. Akad. Nauk. SSSR.* **196**, pp. 1101.
15. Ryabova, N. A., Ponomarev, V. I., Zelentsov, V. V., Shipilov, V. I. and Atovmyan, L. O. (1981). *J. Struct. Chem.* **22**, pp. 111-115.
16. Ryabova, N. A., Ponomarev, V. I., Atovmyan, L. O., Zelentsov, V. V. and Shipilov, V. I. (1978). *Koord Khim.* **4**, pp. 119-126.
17. Decurtins, S., Gütlich, P., Hasselbach, M., Spiering, H. and Hauser, A. (1985). *Inorg. Chem.* **24**, pp.2174-2178.
18. Yemeli Tido, E. W. (2010). PhD Thesis, University of Groningen, The Netherlands.
19. Li, Z.-Y., Dai, J.-W., Gagnon, K. J., Cai, H.-L., Yamamoto, T., Einaga, Y., Zhao, H.-H., Kanegawa, S., Sato, O., Dunbar, K. R. and Xiong, R.-R. (2013). *Dalton. Trans.* **42**, pp. 14685-14688.

20. Hauser, A. (2004). *Spin Crossover in Transition Metal Compounds II*, edited by Gütlich, P. and Goodwin, H. A., *Top. Curr. Chem.* Berlin: Springer, **234**, pp. 155-198.
21. Hauser, A. (1986). *Chem. Phys. Lett.* **124**, pp. 543-548.
22. Hauser, A. (1991). *J. Chem. Phys.* **94**(4), pp. 2741-2748.
23. Szilard, L. and Chalmers, T. A. (1934). *Nature.* **134**, pp. 462.
24. Tominaga, T. and Tachikawa, E. (1981). *Modern Hot-atom Chemistry and its Applications.* Berlin Heidelberg New York: Springer.
25. Matsuura, T. (1984). *Hot-Atom Chemistry.* Kodanski, Tokyo.
26. Gütlich, P. (2004). *Spin-crossover in Transition Metal Compounds II*, edited by Gütlich, P. and Goodwin, H. A., *Top. Curr. Chem.* Berlin: Springer, **234**, pp. 231-260.
27. Boillot, M. -L., Zarembowitch, J. and Sour, A. (2004). *Spin-crossover in Transition Metal Compounds II*, edited by Gütlich, P. and Goodwin, H. A., *Top. Curr. Chem.* Berlin: Springer, **234**, pp. 261-276.
28. Venkataramani, S., Jana, U., Dommaschk, M., Sönnichsen, F. D., Tuzcek, F. and Herges, R. (2011). *Science.* **331**, pp. 445-448.
29. Collison, D., Garner, C. D., McGarth, C. M., Mosselmans, J. F. W., Roper, M. D., Seddon, J. M. W., Sinn, E. and Young, N. A. (1997). *J. Chem. Soc., Dalton Trans.*, pp. 4371-4376.
30. Renz, F., Oshio, H., Ksenofontov, V., Waldeck, M. Spiering, H. and Gütlich, P. (2000). *Angew. Chem., Int. Ed.* **112**, pp. 3832-3834.
31. Vankó, G., Renz, F., Molnar, G., Neisius, T. and Karpati, S. (2007). *Angew. Chem., Int. Ed.* **46**, pp. 5306-5309.
32. Ludwig, E., Naggert, H., Kalläne, M., Rohlf, S., Kröger, E., Bannwarth, A., Quer, A., Rosnagel, K., Kipp, L. and Tuzcek, F. (2014). *Angew. Chem., Int. Ed.* **53**, pp. 3019-3023.
33. Desaix, A., Roubeau, O., Jetic, J., Haasnoot, J. G., Boukheddaden, K., Codjovi, E., Linares, L., Nogues, M. and Varret, F. (1998). *Eur. Phys. J. B.* **6**, pp. 183-193.
34. Létard, J. F., Guionneau, P., Rabardel, L., Howard, J. A. K., Goeta, A. E., Chasseau, D. and Kahn, O. (1998). *Inorg. Chem.* **37**, pp. 4432-4441.
35. Renz, F., Spiering, H., Goodwin, H. A. and Gütlich, P. (2000). *Hyperfine Interact.* **126**, pp. 155-158.
36. Renz, F., Spiering, H., Gütlich, P., Sugiyarto, K. H. and Goodwin, H. A. (2002). *TOSS-Meeting*, Seeheim, Germany.
37. Renz, F., Vankó, G., Homenya, P., Saadat, R., Németh, Z. and Huotari, S. (2012). *Eur. J. Inorg. Chem.*, pp. 2653-2655.
38. Roux, C., Zarembowitch, J., Gallois, B., Granier, T. and Claude, R. (1994). *Inorg. Chem.* **33**, pp. 2273-2279.
39. Vesudevan, S., Vasani, H. N. and Rao, C. N. R. (1979). *Chem. Phys. Lett.* **65**, pp. 444-451.

40. Cartier, C., Thuéry, P., Verdaguer, M., Zarembowitch, J. and Michalowicz, A. (1986). *J. Phys. Colloq.* **47-C8**, pp. 563-569.
41. Bernien, M., Naggert, H., Arruda, L. M., Kipgen, L., Nickel, F., Miguel, J., Hermanns, C. F., Krüger, A., Krüger, D., Schierle, E., Weschke, E., Tuczek, F. and Kuch, W. (2015). *ACS Nano.* **9**, pp. 8960-8966.
42. Gopakumar, T. G., Bernien, M., Naggert, H., Matino, F., Hermanns, C. F., Bannwarth, A., Mühlenberend, S., Krüger, A., Krüger, D., Nickel, F., Walter, W., Berndt, R., Kuch, W. and Tuczek, F. (2013). *Chem. -Eur. J.* **19**, pp.15702-175709.
43. Ksenofontov, V., Gaspar, A. B. and Gülich, P. (2004). *Spin Crossover in Transition Metal Compounds III*, edited by Gülich, P. and Goodwin, H. A., *Top. Curr. Chem.* Berlin: Springer, **235**, pp. 23-64.
44. Ewald, A. H., Martin, R. L., Sinn, E. and White, A. H. (1969). *Inorg. Chem.* **8**(9), pp. 1837.
45. Butcher, R. J., Ferraro, J. R. and Sinn, E. (1976). *Inorg. Chem.* **15**(9), pp. 2077-2079.
46. Bousseksou, A., Varret, F., Goiran, M., Boukheddaden, K. and Tuchagues, J.-P. (2004). *Spin Crossover in Transition Metal Compounds III*, edited by Gülich, P. and Goodwin, H. A., *Top. Curr. Chem.* Berlin: Springer, **235**, pp. 65-84.
47. Qi, E., Müller, E. W., Spiering, H. and Gülich, P. (1983). *Chem. Phys. Lett.* **101**, pp. 503-505.
48. Bousseksou, A., Nègre, N., Goiran, M., Salmon, L., Tuchagues, J.-P., Boillot, M.-L., Boukheddaden, K. and Varret, F. (2000). *Eur. Phys. J. B.* **13**, pp. 451-456.
49. Bousseksou, A., Molnár, G., Tuchagues, J.-P., Menéndez, N., Codjovi, E. and Varret, F. (2003). *C. R. Chim.* **6**, pp. 329.
50. Mabbs, F. E. and Machin, D. J. (1973). *Magnetism and Transition Metal Complexes*. Dover Publications.
51. Orchard, A. F. (2003). *Magnetochemistry*. Oxford University Press.
52. Gülich, P., Gaspar, A. B. and Garcia, Y. (2013). *Beilstein J. Org. Chem.* **9**, pp. 342-391.
53. Fultz, B. (1993). *Mössbauer Spectroscopy Applied to Magnetism and Materials Science Chapter 1*, edited by Long, G. J. and Grandjean, F., *Modern Inorganic Chemistry*. New York: Springer, **1**, pp. 1-31.
54. Greenwood, N. N. and Gibb, T. B., (1971) *Mössbauer spectroscopy*. Chapman and Hall Ltd: London.
55. Gülich, P., Link R. and Trautwein, A. X., (1978). *Mössbauer Spectroscopy and Transition Metal Chemistry. Inorganic chemistry concepts series No 3*. Springer: Berlin Heidelberg New York.
56. Höhne, G., Flemminger, W. F. and Flammersheim, H.-J. (2003). *Differential Scanning Calorimetry*. 2nd Ed. Berlin: Springer.
57. Zelentsov, V. V. (1983). *Advances in Inorganic Chemistry*. 6th Ed. MIR Publishers.

58. Ryabova, N. A., Ponomarev V. I., Zelentsov, V. V. and Atovmyan L. O. (1982). *Sov. Phys. Crystallogr.* **27**, pp. 46.
59. Floquet, S., Guillou, N., Négrier, P., Rivière, E. and Boillot M.-L. (2006). *New. J. Chem.* **30**, pp. 1621-1627.
60. Li, Z.-Y., Dai, J.-W., Shiota, Y., Yoshizawa, K., Kanegawa, S. and Sato, O. (2013). *Chem. Eur. J.* **19**, pp. 12948-12952.
61. Floquet, S., Boillot M.-L., Rivière, E., Varret, F., Boukheddaden, K., Morineau, D. and Négrier, P. (2003). *New. J. Chem.* **27**, pp. 341-348.
62. Zelentsov, V. V. (1987). *Sov. Sci. Rev. B, Chem.* **10**, pp. 485
63. Zelentsov, V. V. (1992). *Koord. Khim.* **18**, pp. 787.
64. Turta, K. I., Ablov, A. V., Gerbelev, N. V., Stukan, R. A. and Dyatlova, C. V. (1975). *Russ. J. Inorg. Chem.* **20**, pp. 82.
65. Turta, K. I., Ablov, A. V., Gerbelev, N. V., Dyatlova, C. V. and Stukan, R. A. (1976). *Russ. J. Inorg. Chem.* **21**, pp. 266.
66. Ablov, A. V., Stukan, R. A., Turta, K. I., Gerbelev, N. V., Dyatlova, C. V. and Barba, N. A. (1974). *Russ. J. Inorg. Chem.* **19**, pp. 59.
67. Létard, J. -F., Guionneau, P. and Goux-Capes, L. (2004). *Spin Crossover in Transition Metal Compounds III*, edited by Gülich, P. and Goodwin, H. A., *Top. Curr. Chem.* Berlin: Springer, **235**, pp. 221-249.
68. Lefter, C., Vincent Davesne, V., Salmon, L., Molnár, G., Demont, P., Rotaru, A. and Bousseksou, A. (2016). *Magnetochemistry.* **2**, pp.18.
69. Kahn, O. and Jay-Martinez, C. (1998). *Science.* **279**, pp.44-48.
70. Linares, J., Codjovi, E. and Garcia, Y. (2012). *Sensors.* **12**, pp.4479–4492.
71. Bartual-Murgui, C., Akou, A., Thibault, C., Molnár, G., Vieu, C., Salmon, L. and Bousseksou, A. (2015). *J. Mater. Chem. C.* **3**, pp.1277–1285.
72. Salmon, L., Molnár, G., Zitouni, D., Quintero, C., Bergaud, C., Micheau, J.C. and Bousseksou, A. (2010). *J. Mater. Chem.* **20**, pp.5499–5503.
73. Matsuda, M., Kiyoshima, K., Uchida, R., Kinoshita, N. and Tajima, H. (2013). *Thin Solid Films.* **531**, pp.451–453.
74. Shepherd, H. J., Gural'skiy, I. A., Quintero, C. M., Tricard, S., Salmon, L., Molnár, G. and Bousseksou, A. (2013). *Nat. Commun.* , **4**.
75. Rohrer, H. (1993). *Jpn. J. Appl. Phys.* **32**, pp.1335.
76. Peercy, P.S. (2000). *Nature.* **406**, pp.1023–1026.
77. Keyes, R.W. (2001). *Proc. IEEE.* **89**, pp.227–239.
78. Kahn, O., Kröer, J. and Jay, C. (1992). *Adv. Mater.* **4**, pp.718-728.
79. Bousseksou, A., Molnár, G., Salmon, L. and Nicolazzi, W. (2011). *Chem. Soc. Rev.* **40**, pp.3313–3335.

80. Murray, K. S. (2013). *Spin-Crossover Materials: Properties and Applications*, edited by Halcrow, M. A., John Wiley & Sons Ltd, Oxford, UK.
81. Muñoz, M. C. and Real, J. A. (2011). *Coord. Chem. Rev.* **255**, pp.2068–2093.
82. Cobo, S., Molnár, G., Real, J. A. and Bousseksou, A. (2006). *Angew. Chem. Int. Ed.* **45**, pp. 5786–5789.
83. Bartual-Murgui, C., Akou, A., Salmon, L., Molnár, G., Thibault, C., Real, J. A. and Bousseksou, A. (2011). *Small.* **7**, pp.3385–3391.
84. Forestier, T., Mornet, S., Daro, N., Nishihara, T., Mouri, S., Tanaka, K., Fouché, O., Freysz, E., Létard, J.-F. (2008). *Chem. Commun.* **36**, pp. 4327–4329.
85. Volatron, F., Catala, L., Rivière, E., Gloter, A., Stéphan, O. and Mallah, T. (2008). *Inorg. Chem.* **47**, pp. 6584–6586.
86. Prins, F., Monrabal-Capilla, M., Osorio, E. A., Coronado, E. and van der Zant, H. S. J. (2011). *Adv. Mater.* **23**, pp.1545–1549.
87. Tissot, A., Bardeau, J.-F., Rivière, E., Brisset, F. and Boillot, M.-L. (2010). *Dalton Trans.* **39**, pp. 7806–7812.
88. Cavallini, M., Bergenti, I., Milita, S., Ruani, G., Salitros, I., Qu, Z.-R., Chandrasekar, R. and Ruben, M. (2008). *Angew. Chem. Int. Ed.*, **47**, pp. 8596–8600.
89. Cavallini, M., Bergenti, I., Milita, S., Kengne, J. C., Gentili, D., Ruani, G., Salitros, I., Meded, V. and Ruben, M. (2011). *Langmuir.* **27**, pp. 4076–4081.
90. Meded, V., Bagrets, A., Fink, K., Chandrasekar, R., Ruben, M., Evers, F., Bernard-Mantel, A., Seldenthuis, J., Beukman, A. and van der Zant, H. (2011). *Phys. Rev. B.* **83**, pp. 245415.
91. Cavallini, M. (2012). *Phys. Chem. Chem. Phys.* **14**, pp. 11867–11876.
92. Gaspar, A. B., Muñoz, M. C. and Real, J. A. (2006). *J. Mater. Chem.*, **16**, pp. 2522.

Chapter II

Materials and Methods

2.0 Materials and Methods

2.1 Introduction

This chapter details the materials, techniques and methods used for the synthesis, characterisation and determination of the physical properties of the ferric complexes and their corresponding ligands. Firstly, the materials used are provided, which is followed by a description of the synthesis of both the ligands and ferric complexes presented in this thesis, the syntheses not presented in the thesis are displayed in the appendix. Secondly, the standard techniques used to characterise the ligand and ferric complexes are herein described. A more detailed description of the single crystal X-ray structure solution and refinement can be found in the corresponding chapters. Finally, is followed by a brief description of the physical techniques used to determine the magnetic properties of the ferric complexes.

2.2 Materials

The R-salicylaldehyde derivatives, 4R'-thiosemicarbazone derivatives, iron(III) salts and bases used in the synthesis of the ferric complexes and their corresponding ligands are displayed in Tables 2.1, 2.2, 2.3 and 2.4, severally.

The iron(III) salts were all purchased from Sigma-Aldrich and used without further purification. Derivatives of both the R-salicylaldehyde and 4R'-thiosemicarbazide compounds purchased from either Sigma-Aldrich or Alfa Aesar were also used without further purification in the R-salicylaldehyde 4R'-thiosemicarbazone ligand syntheses presented in Section 2.3. Solvents used in the synthesis of the ligands and ferric complexes were all purchased from Fisher-Scientific.

Table 2.1 Salicylaldehyde derivatives utilised in the synthesis of the various R-salicylaldehyde 4R'-thiosemicarbazone ligands.

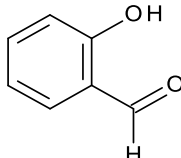
Name	Structure	Supplier
Salicylaldehyde, 98%		Sigma-Aldrich

Table 2.1 Salicylaldehyde derivatives utilised in the synthesis of the various R-salicylaldehyde 4R'-thiosemicarbazone ligands (continued)

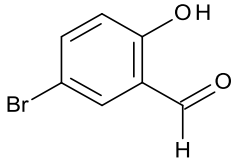
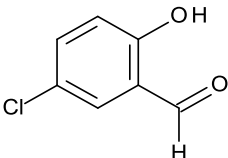
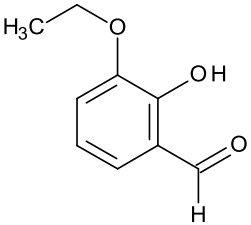
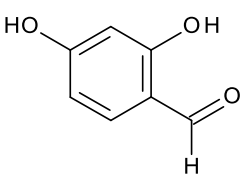
Name	Structure	Supplier
5-bromosalicylaldehyde, 98%		Sigma-Aldrich
5-chlorosalicylaldehyde, 98%		Alfa Aesar
3-ethoxysalicylaldehyde, 97%		Alfa Aesar
2,4-dihydroxybenzaldehyde, 98%		Alfa Aesar

Table 2.2 Thiosemicarbazone derivatives utilised in the synthesis of the various R-salicylaldehyde 4R'-thiosemicarbazone ligands

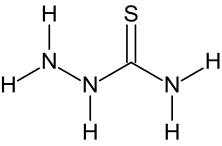
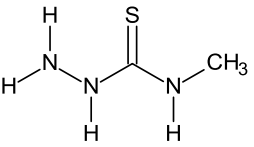
Name	Structure	Supplier
Thiosemicarbazide, 99%		Alfa Aesar
4-Methyl-3-thiosemicarbazide, 97%		Alfa Aesar

Table 2.2 Thiosemicarbazone derivatives utilised in the synthesis of the various R-salicylaldehyde 4R'-thiosemicarbazone ligands (continued)

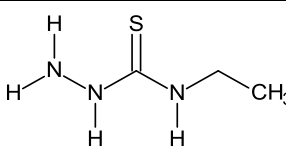
Name	Structure	Supplier
4-Ethyl-3-thiosemicarbazide, 97%		Sigma-Aldrich

Table 2.3 Various Fe^{III} salts used in the synthesis of the Fe^{III} bis(ligand) compounds

Name	Composition	Supplier
Iron(III) chloride hexahydrate, >98%	[FeCl ₃].6H ₂ O	Sigma-Aldrich
Iron(III) nitrate nonahydrate, >98%	[Fe(NO ₃) ₃].9H ₂ O	Sigma-Aldrich
Iron(III) sulfate hydrate, 97%	[Fe ₂ (SO ₄) ₃].H ₂ O	Sigma-Aldrich
Iron(III) <i>p</i>-toluenesulfonate hexahydrate	[Fe(CH ₃ C ₆ H ₄ SO ₃) ₃].6H ₂ O	Sigma-Aldrich

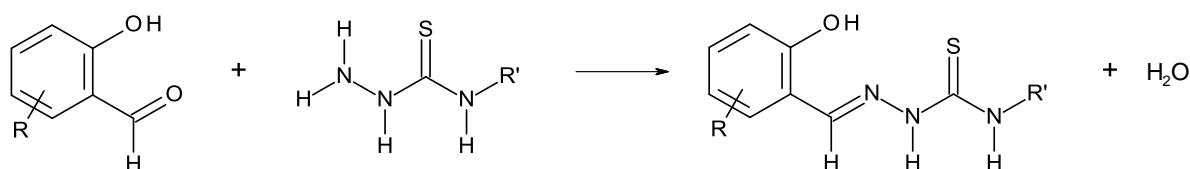
Table 2.4 Different bases used in the synthesis of the Fe^{III} bis(ligand) complexes

Name	Composition	Supplier
Caesium hydroxide monohydrate, >95%	CsOH	Alfa Aesar
Ammonium hydroxide solution, 35% in water	NH ₄ OH	Fisher Scientific
Dimethylamine, 40% wt in water	NH(CH ₃) ₂	ACROS Organics
Triethylamine, >98%	N(C ₂ H ₅) ₃	Sigma-Aldrich

2.3 Ligand Synthesis

2.3.1 Synthesis of R-salicylaldehyde 4R'-thiosemicarbazone (H₂L) based ligands

The preparation of the desired R-salicylaldehyde 4R'-thiosemicarbazone ligands incorporated the synthesis between thiosemicarbazide and an R-substituted salicylaldehyde in ethanolic solution. The general reaction scheme is illustrated in Scheme 2.1.



R = -H, 5-Br, 5-Cl, 3-OCH₂CH₃, 4-OH

R' = -H, -CH₃, -CH₂CH₃

Scheme 2.1

49 mmol of R-substituted salicylaldehyde was dissolved in 80 mL of ethanol with constant stirring, and was added to 49 mmol of the 4R'-thiosemicarbazide dissolved in 40 mL of ethanol. The corresponding mixture was refluxed for 120 minutes. The resulting solution was cooled to room temperature, the solid isolated by filtration, washed with ether and dried in a vacuum for two days.

Salicylaldehyde thiosemicarbazone (H₂thsa)

The synthesis of H₂thsa has been carried out by the general procedure described *vide supra*. Yield: 7.75 g (39.70 mmol, 81.0%). Mp: 218°C. H₂thsa is soluble in methanol, acetone and DMSO. ¹H NMR (300 MHz, DMSO-d₆) δ (ppm): 11.40 (1H, s, OH), 9.90 (1H, s, S=C-NH), 8.37 (1H, s, N=C-H), 7.91–8.12 (2H, m, S=C-NH₂), 6.78–7.24 (aromatic 4H, m, C-H). ¹³C NMR (300 MHz, DMSO-d₆) δ (ppm): 178.1 (C=S), 156.8 (C-O), 140.0 (C=N), 131.5, 127.2, 120.8, 119.7, 116.5, 108.2 (C aromatic), 52.9 (C-N). IR (cm⁻¹, KBr): 3444.83 (νOH), 3174.51 (νNH), 3319.44 (νNH₂), 1616.29 (νC=N), 1539.61–1602.70 (νC=C), 1265.82 (νC-N), 1110.84 (νC=S).

Salicylaldehyde 4-methylthiosemicarbazone (H₂thsa-Me)

The synthesis of H₂thsa-Me has been carried out by the general procedure described *vide supra*. Yield: 11.79 g (49.38 mmol, 98.7%). Mp: 208°C. H₂-thsa-Me is soluble in methanol, ethanol, acetone and DMSO. ¹H NMR (300 MHz, DMSO-d₆) δ (ppm): 11.40 (1H, s, OH), 9.90 (1H, s, S=C-NH), 8.37 (1H, s, N=CH), 8.42-8.44 (1H, m, S=C-NH(CH₃)), 6.79-7.97 (aromatic 3H, m, C-H), 3.00 (3H, d, NH(CH₃)). ¹³C NMR (300 MHz, DMSO-d₆) δ (ppm): 177.4 (C=S), 156.3 (C-O),

138.9 (C=N), 131.0, 126.6, 120.4, 119.2, 116.1 (C-C aromatic), 31.1 (CH₃). IR (cm⁻¹, KBr): 3362.01 (νOH), 3256.21 (νNH), 2965.70 (νCH₃), 1618.15 (νC=N), 1605.92, 1554.21 (νC=C), 1254.37 (νC-N), 1100.03 (νC=S).

5-Bromosalicylaldehyde thiosemicarbazone (H₂-5-Br-thsa)

The synthesis of H₂-5-Br-thsa has been carried out by the general procedure described *vide supra*. Yield: 11.58 g (42.24 mmol, 86.2%). Mp: 262°C. H₂-5-Br-thsa is soluble in methanol, ethanol, acetone and DMSO. ¹H NMR (300 MHz, DMSO-d₆) δ (ppm): 11.42 (1H, s, OH), 10.25 (1H, s, S=C-NH), 8.28 (1H, s, N=C-H), 8.15–8.23 (2H, m, C-NH₂), 6.82–7.33 (aromatic 3H, m, C-H). ¹³C NMR (300 MHz, DMSO-d₆) δ (ppm): 177.7 (C=S), 155.6 (C-O), 137.3 (C=N), 133.29, 128.4, 122.8 (C-C aromatic) 11.0 (C-Br). IR (cm⁻¹, KBr): 3456.13 (νOH), 3161.84 (νNH), 3248.73 (νNH₂), 1610.08 (νC=N), 1545.34–1602.00 (νC=C), 1264.20 (νC-N), 1191.52 (νC=S).

5-Bromosalicylaldehyde 4-ethylthiosemicarbazone (H₂-5-Br-thsa-Et)

The synthesis of H₂-5-Br-thsa-Et has been carried out by the general procedure described *vide supra*. Yield: 14.32 g (47.55 mmol, 97.0%). Mp: 186°C. H₂-5-Br-thsa-Et is soluble in methanol, acetone and DMSO. ¹H NMR (300 MHz, DMSO-d₆) δ (ppm): 11.42 (1H, s, OH), 10.28 (1H, s, S=C-NH), 8.32 (1H, m, N=CH), 8.66 (1H, t, S=C-NH(CH₂CH₃)), 6.80-7.38 (aromatic 3H, m, C-H), 3.60 (2H, p, NH-CH₂), 1.15 (3H t, NHCH₂-CH₃). ¹³C NMR (300 MHz, DMSO-d₆) δ (ppm): 176.5 (C=S), 155.5 (C-O), 137.0 (C=N), 133.2, 128.1, 122.9, 118.2 (C-C aromatic), 110.9 (C-Br), 38.2 (CH₂), 14.8 (CH₃). IR (cm⁻¹, KBr): 3299.28 (νOH), 3146.02 (νNH), 2990.34 (νCH₃), 2936.0 (νCH₂), 1613.36 (νC=N), 1601.19, 1549.90 (νC=C), 1236.91 (νC-N), 1046.78 (νC=S).

5-Chlorosalicylaldehyde 4-methylthiosemicarbazone (H₂-5-Cl-thsa-Me)

The synthesis of H₂-5-Cl-thsa-Me has been carried out by the general procedure described *vide supra*. Yield: 11.79 g (49.38 mmol, 98.7%). Mp: 224°C. H₂-5-Cl-thsa-Me is soluble in methanol, acetone and DMSO. ¹H NMR (300 MHz, DMSO-d₆) δ (ppm): 11.49 (1H, s, OH), 10.24 (1H, s, S=C-NH), 8.29 (1H, s, N=CH), 8.58-8.59 (2H, m, S=C-NH(CH₃)), 6.85-7.23 (aromatic 3H, m, C-H), 3.01 (3H, d, NH(CH₃)). ¹³C NMR (300 MHz, DMSO-d₆) δ (ppm): 177.8 (C=S), 155.1 (C-O), 137.3 (C=N), 130.5, 125.5, 122.3, 117.7 (C-C aromatic), 123.4 (C-Cl), 31.1 (CH₃). IR (cm⁻¹, KBr): 3397.86 (νOH), 3254.90, 3124.07 (νNH), 2983.97 (νCH₃), 1600.69 (νC=N), 1552.98, 1527.96 (νC=C), 1270.10 (νC-N), 1182.31 (νC=S).

3-Ethoxysalicylaldehyde thiosemicarbazone (H₂-3-OEt-thsa)

The synthesis of H₂-3-OEt-thsa has been carried out by the general procedure described *vide supra*. Yield: 11.14 g (46.55 mmol, 95.0%). Mp: 224°C. H₂-3-OEt-thsa is soluble in methanol, ethanol, acetone and DMSO. ¹H NMR (300 MHz, DMSO-d₆) δ (ppm): 11.39 (1H, s, OH), 9.02 (1H, s,

S=C-NH), 8.40 (1H, s, N=C-H), 7.90–8.13 (2H, m, S=C-NH₂), 6.72–7.50 (aromatic 3H, m, C-H), 4.05 (2H, q, O-CH₂), 1.35 (3H, t, O-C-CH₃). ¹³C NMR (300 MHz, DMSO-d₆) δ (ppm): 182.8 (C=S), 147.4, 146.7 (C-O), 140.1 (C=N), 119.5, 118.7, 114.5 (C aromatic), 64.6 (C-N), 74.0 (O-CH₂), 15.1 (O-C-CH₃). IR (cm⁻¹, KBr): 3400.03 (νOH), 3169.30 (νNH), 3248.73 (νNH₂), 2934.86 (νCH₃), 2895.68 (νCH₂), 1617.76 (νC=N), 1534.53-1599.81 (νC=C), 1270.18 (νC-N), 1166.98 (νC=S).

3-Ethoxysalicylaldehyde 4-methylthiosemicarbazone (H₂-3-OEt-thsa-Me)

The synthesis of H₂-3-OEt-thsa-Me has been carried out by the general procedure described *vide supra*. Yield: 11.80 g (46.58 mmol, 95.1%). Mp: 228°C. H₂-3-OEt-thsa-Me is soluble in methanol, ethanol, acetone and DMSO. ¹H NMR (300 MHz, DMSO-d₆) δ (ppm): 11.42 (1H, s, OH), 9.02 (1H, s, S=C-NH), 8.42 (1H, s, N=CH), 8.39 (2H, m, S=C-NH(CH₃)), 6.78–7.54 (aromatic 3H, m, C-H), 4.10 (2H, q, O-CH₂), 1.35 (3H, t, O-C-CH₃). ¹³C NMR (300 MHz, DMSO-d₆) δ (ppm): 177.6 (C=S), 147.0, 146.1 (C-O), 139.0 (C=N), 120.8, 118.9, 118.01 113.8 (C aromatic), 64.3 (O-CH₂), 30.8 (N-CH₃), 14.6 (O-C-CH₃). IR (cm⁻¹, KBr): 3350.03 (νOH), 3307.61 (νNH), 2977.95, 2926.71 (νCH₃), 2895.74 (νCH₂), 1606.79 (νC=N), 1531.75-1581.09 (νC=C), 1221.49 (νC-N), 1107.16 (νC=S).

2, 4-Dihydroxybenzaldehyde thiosemicarbazone (H₂-4-OH-thsa)

The synthesis of H₂-4-OH-thsa has been carried out by the general procedure described *vide supra*. Yield 9.51 g (45.07 mmol, 92.0%). Mp: 226°C. H₂-4-OH-thsa is soluble in ethanol, methanol, DMSO and acetone. ¹H NMR (300 MHz, DMSO-d₆) δ (ppm): 11.19 (1H, s, S=C-NH), 9.76 (2H, s, OH), 8.24 (1H, s, N=C-H), 7.66 – 7.97 (2H, m, S=C-NH₂), 6.23 – 6.29 (aromatic 3H, m, C-H). ¹³C NMR (300 MHz, DMSO-d₆) δ (ppm): 176.9 (C=S), 160.4, 157.9 (C-O), 140.9 (C=N), 128.4, 11.7, 107.8, 102.2 (C aromatic). IR (cm⁻¹, KBr): 3478.60 (νOH), 3167.12 (νNH), 3338.21 (νNH₂), 1631.49 (νC=N), 1553.56-1578.28 (νC=C ring), 1230.44 (νC-N), 1121.49 (νC=S).

2.4 Synthesis of Iron(III) Coordination Compounds

2.4.1 (Cation)[Fe^{III}(L)₂]-solvent Complexes

Cs[Fe(3-OEt-thsa-Me)₂]-CH₃OH

FeCl₃·6H₂O (1.0 mmol, 0.27 g) was dissolved in 5 mL of methanol. The ligand H₂-3-OEt-thsa-Me (1.0 mmol, 0.25 g) was dissolved in 30 mL of methanol with the addition of CsOH·H₂O (4.0 mmol, 0.67 g). To this mixture, the methanolic Fe(III) salt solution was added drop wise on constant stirring. The resulting dark green solution was stirred and heated to 80°C for approximately 10 minutes. The solution was then allowed to stand at room temperature until crystals were formed. The dark green

microcrystals were isolated by filtration and dried. Yield: 0.29 g (0.4 mmol, 40.1%). IR (cm⁻¹, KBr) 3401.50 (νOH), 3319.35 (νNH), 2967.94, 2931.51 (νCH₃), 2885.50 (νCH₂), 1636.73, 1593.97 (νC=N), 1545.79-1509.33 (νC=C ring), 1218.78 (νC-O), 1163.95 (νN-N), 1021.92 (νC-N), 738.02 (νC-S).

Cs[Fe(5-Br-thsa)₂]

FeCl₃·6H₂O (1.0 mmol, 0.27 g) was dissolved in 10 mL of methanol. The ligand H₂-5-Br-thsa (2.0 mmol, 0.54 g) was dissolved in 60 mL of methanol with the addition of CsOH·H₂O (4.0 mmol, 0.67 g). To this mixture, the methanolic Fe(III) salt solution was added drop wise on constant stirring. The resulting dark green solution was stirred and heated to 80°C for approximately 10 minutes. The solution was then allowed to stand at room temperature until crystals were formed. The dark green microcrystals were isolated by filtration and dried. Yield: 0.43 g (0.57 mmol, 58.7%). IR (cm⁻¹, ATR): 3464.82, 3251.42 (νNH), 3075.11 (νNH₂), 1611.31, 1590.53 (νC=N), 1538.98-1497.13 (νC=C ring), 1273.72 (νC-O), 1199.90 (νN-N), 1030.60 (νC-N), 817.71 (νC-S).

NH₄[Fe(thsa)₂]

Fe(*p*-CH₃C₆H₄SO₃)₃·6H₂O (1.0 mmol, 0.68 g) was dissolved in 5 mL of methanol. The ligand H₂thsa (1.0 mmol, 0.20 g) was dissolved in 25 mL of methanol with the addition of 20 mL of NH₄OH (35 wt% in water). To this mixture, the methanolic Fe(III) salt solution was added drop wise on constant stirring. The resulting dark green solution was stirred and heated to 80°C for approximately 10 minutes. The solution was then allowed to stand at room temperature until crystals were formed. The dark green microcrystals were isolated by filtration and dried. Yield: 0.10 g (0.22 mmol, 21.7%). IR (cm⁻¹, KBr): 3472.47, 3239.56 (νNH), 3015.68 (νNH₂), 1595.06 (νC=N), 1546.07-1508.53 (νC=C ring), 1277.90 (νC-O), 1203.23 (νN-N), 1027.15 (νC-N), 756.07 (νC-S).

NH₄[Fe(5-Br-thsa)₂]

FeCl₃·6H₂O (1.0 mmol, 0.27 g) was dissolved in 5 mL of methanol. The ligand H₂-5-Br-thsa (1.0 mmol, 0.27 g) was dissolved in 30 mL of methanol with the addition of 20 mL of NH₄OH (35 wt% in water). To this mixture, the methanolic Fe(III) salt solution was added drop wise on constant stirring. The resulting dark green solution was stirred and heated to 80°C for approximately 10 minutes. The solution was then allowed to stand at room temperature until crystals were formed. The dark green microcrystals were isolated by filtration and dried. Yield: 0.24 g (0.39 mmol, 38.8%). IR (cm⁻¹, ATR): 3461.85 (νNH), 3247.45, 3098.95 (νNH₂), 1609.77 (νC=N), 1535.21-1505.30 (νC=C ring), 1276.15 (νC-O), 1198.10 (νN-N), 1031.48 (νC-N), 816.65 (νC-S).

(CH₃)₂NH₂[Fe(3-OEt-thsa)₂]

Fe(NO₃)₃·9H₂O (1.0 mmol, 0.40 g) was dissolved in 10 mL of water. The ligand H₂-3-OEt-thsa (2.0 mmol, 0.46 g) was dissolved in 60 mL of methanol with the addition of addition of dimethylamine, 40wt% in water (10 mmol, 0.51 mL). To this mixture, the Fe(III) salt solution was added drop wise on constant stirring. The resulting dark green solution was stirred and heated to 80°C for approximately 10 minutes. The solution was then allowed to stand at room temperature until crystals were formed. The dark green microcrystals were isolated by filtration and dried. Yield: 0.30 g (0.52 mmol, 52.0%). IR (cm⁻¹, ATR): 3436, 3413.5 (νNH), 3264.7, 3097.7 (νNH₂), 3012 (νCH₃), 2971.4 (νCH₂), 1613.5, 1586.1 (νC=N), 1570.2-1541.4 (νC=C ring), 1237.7 (νC-O), 1215.3 (νN-N), 1077.8 (νC-N), 735.7 (νC-S).

2.4.2 [Fe^{III}(HL)(L)]·solvent Complexes

[Fe(Hthsa-Me)(thsa-Me)]·H₂O

Fe(NO₃)₃·9H₂O (1.0 mmol, 0.40 g) was dissolved in 5 mL of water. The ligand H₂thsa-Me (2.0 mmol, 0.42 g) was dissolved in an ethanol/methanol/water mixture (v: v: v, 5: 5: 1) with the addition of dimethylamine, 40wt% in water (10 mmol, 0.51 mL). To this mixture, the Fe(III) salt solution was added drop wise on constant stirring. The resulting dark green solution was stirred and heated to 80°C for approximately 10 minutes. The solution was then allowed to stand at room temperature until crystals were formed. The dark green microcrystals were isolated by filtration and dried. Yield: 0.12 g (0.25 mmol, 24.5%). IR (cm⁻¹, ATR) 3558.1, 3481.4, 3149 (νNH), 3017.6 (νCH₃), 2973.8, 2937.3, 2897, 2849.6 (νC-H aromatic), 1604.3 (νC=N), 1589.7, 1542.2 (νC=C ring), 1279.3 (νC-O), 1323 (νN-N), 749.73 (νC-S).

[Fe(H-3-OEt-thsa-Me)(3-OEt-thsa-Me)]·H₂O

Fe(NO₃)₃·9H₂O (1.0 mmol, 0.40 g) was dissolved in 10 mL of water. The ligand H₂-3-OEt-thsa-Me (2.0 mmol, 0.50 g) was dissolved in 60 mL of methanol with the addition of dimethylamine, 40wt% in water (10 mmol, 0.51 mL). To this mixture, the Fe(III) salt solution was added drop wise on constant stirring. The resulting dark green solution was stirred and heated to 80°C for approximately 10 minutes. The solution was then allowed to stand at room temperature until crystals were formed. The dark green microcrystals were isolated by filtration and dried. Yield: 0.60g (0.53 mmol, 53.1%). IR (cm⁻¹, ATR) 3423, 3317, 3211.2 (νNH), 3010.3 (νCH₃), 2973.8 (νCH₂), 2926.3, 2889.8, 2875.2 (νC-H aromatic), 1597 (νC=N), 1582.4, 1542.2 (νC=C ring), 1213.5 (νC-O), 1239 (νN-N), 1077.8 (νC-N), 727.82 (νC-S).

[Fe(H-5-Cl-thsa-Me)(5-Cl-thsa-Me)]·H₂O

Fe(NO₃)₃·9H₂O (1.0 mmol, 0.40 g) was dissolved in 5 mL of methanol. The ligand H₂-5-Cl-thsa-Me (1.0 mmol, 0.24 g) was dissolved in 25 mL of methanol with the addition of 20 mL of NH₄OH (35 wt% in water). To this mixture, the methanolic Fe(III) salt solution was added drop wise on constant stirring. The resulting dark green solution was stirred and heated to 80°C for approximately 10 minutes. The solution was then allowed to stand at room temperature until crystals were formed. The dark green microcrystals were isolated by filtration and dried. Yield: 0.35 g (0.63 mmol, 62.7%). IR (cm⁻¹, ATR): 3525.8, 3217.5, 3172.5 (νNH), 3028.6 (νCH₃), 2965.6, 2934.1, 2889.2, 2848.7 (νCH aromatic), 1604.3 (νC=N), 1586, 1567.8 (νC=C ring), 1315.8 (νC-O), 1286.6, 1188 (νN-N) 815.47 (νC-S).

2.4.3 [Fe^{III}(HL)₂]·anion·solvent Complexes

[Fe(H-5-Br-thsa-Et)₂]NO₃·H₂O

Fe(NO₃)₃·9H₂O (1.0 mmol, 0.40 g) was dissolved in 5 mL of distilled water. The ligand H₂-5-Br-thsa-Et (2.0 mmol, 0.60 g) was dissolved in an ethanol/methanol/water mixture (v: v: v, 5: 5: 1) with the addition of dimethylamine, 40wt% in water (10 mmol, 0.51 mL). To this mixture, the Fe(III) salt solution was added drop wise on constant stirring. The resulting dark green solution was stirred and heated to 120°C for approximately 10 minutes. The solution was then allowed to stand at room temperature until crystals were formed. The dark green microcrystals were isolated by filtration and dried. Yield: 0.54 g (0.73 mmol, 73.2%). IR (cm⁻¹, ATR): 3313.4, 3225.8 (νNH), 3046.8 (νCH₃), 2997.4 (νCH₂), 1600.6 (νC=N), 1582.4, 1542.2 (νC=C ring), 1293.9 (νC-O), 1312.1 (νN-N), 819.12 (νC-S), 866.6, 1352.3 (νNO).

[Fe(H-4-OH-thsa)₂]₄·(SO₄)₂·9H₂O

Fe₂(SO₄)₄·H₂O (0.5 mmol, 0.21 g) was dissolved in 5 mL of distilled water. The ligand H₂-4-OH-thsa (1.0 mmol, 0.21 g) was dissolved in 25 mL of methanol with the addition of dimethylamine, 40wt% in water (0.1 mmol, 0.051 mL). To this mixture, the Fe(III) salt solution was added drop wise on constant stirring. The resulting dark green solution was stirred and heated to 80°C for approximately 10 minutes. The solution was then allowed to stand at room temperature until crystals were formed. The dark green microcrystals were isolated by filtration and dried. Yield: 0.43g (0.38 mmol, 38.1%). IR (cm⁻¹, ATR): 3291.5 (νOH), 3174.7 (νNH), 3068.7 (νNH₂), 1597 (νC=N), 1578.7, 1542.2 (νC=C ring), 1224.5 (νC-O), 1341.4 (νN-N), 1031 (νC-S), 1432.7 (νSO).

2.5 Analytical Techniques

2.5.1 Fourier Transform Infrared Spectroscopy

Room temperature IR spectra for all ligands and ferric complexes were recorded on a Perkin Elmer FT-IR spectrometer Spectrum RXI by using KBr pellets within the range 4000-400 cm^{-1} . Some additional IR spectroscopic measurements of the R-salicylaldehyde 4R'-thiosemicarbazone ligands were carried out (at room temperature) using an ATR (Attenuated Total Reflectance) Perkin Elmer FT-IR spectrometer Frontier within the range 4000-600 cm^{-1} .

2.5.2 Nuclear Magnetic Resonance Spectroscopy

^1H and ^{13}C NMR spectra were recorded in DMSO- d_6 for the R-salicylaldehyde 4R'-thiosemicarbazone ligands using a BRUKER cyromagnet BZH 300/52 spectrometer (300 MHz) with the recorded chemical shifts in δ (parts per million) relative to an internal standard of TMS (tetramethylsilane).

2.5.3 Single Crystal X-ray Diffraction Measurements

Crystallographic data details on data collection and refinement for all ferric complexes can be found in the corresponding chapters of this thesis. The data collection for the compounds $\text{Cs}[\text{Fe}(\text{3-OEt-thsa-Me})_2]\cdot\text{CH}_3\text{OH}$, $\text{Cs}[\text{Fe}(\text{5-Br-thsa})_2]$, $(\text{CH}_3)_2\text{NH}_2[\text{Fe}(\text{3-OEt-thsa})_2]$, $[\text{Fe}(\text{H-thsa-Me})(\text{thsa-Me})]\cdot\text{H}_2\text{O}$, $[\text{Fe}(\text{H-5-Cl-thsa-Me})(\text{5-Cl-thsa-Me})]\cdot\text{H}_2\text{O}$, $[\text{Fe}(\text{H-5-Br-thsa-Et})_2](\text{NO}_3)\cdot\text{H}_2\text{O}$ and $[\text{Fe}(\text{H-4-OH-thsa})_2]_4(\text{SO}_4)_2\cdot 9\text{H}_2\text{O}$ were performed on *Rigaku AFC12* four-circle κ diffractometer, equipped with an enhanced sensitivity (HG) *Saturn724+* detector mounted at the window of an *FR-E+ SuperBright* molybdenum rotating anode generator with VHF *Varimax* optics (70 μm focus/100 μm focus). The data were collected at 100 K for the ferric complexes (*vide supra*) apart from $\text{Cs}[\text{Fe}(\text{5-Br-thsa})_2]$, of which the data was collected at 293 K, all with a Mo $K\alpha$ radiation, $\lambda = 0.71075 \text{ \AA}$. Data collection was performed using the commercially designed software, *CrystalClear-SM Expert* [1, 2]. Data reduction, cell refinement and absorption correction were performed using *CrystalClear-SM Expert* [1, 2] and *CrysAlisPro* [3] packages. The structure solution and structure refinement of the ferric complexes data were carried out using *SUPERFLIP* [4] and *SHELX* programmes [5, 6]. The data collection of the compounds $\text{Cs}[\text{Fe}(\text{3-OEt-thsa-Me})_2]\cdot\text{CH}_3\text{OH}$, $\text{Cs}[\text{Fe}(\text{5-Br-thsa})_2]$, $(\text{CH}_3)_2\text{NH}_2[\text{Fe}(\text{3-OEt-thsa})_2]$, $[\text{Fe}(\text{H-thsa-Me})(\text{thsa-Me})]\cdot\text{H}_2\text{O}$, $[\text{Fe}(\text{H-5-Cl-thsa-Me})(\text{5-Cl-thsa-Me})]\cdot\text{H}_2\text{O}$, $[\text{Fe}(\text{H-5-Br-thsa-Et})_2](\text{NO}_3)\cdot\text{H}_2\text{O}$ and $[\text{Fe}(\text{H-4-OH-thsa})_2]_4(\text{SO}_4)_2\cdot 9\text{H}_2\text{O}$ were carried out at the ESRP National Crystallography Service, at the University of Southampton.

The data collection for the compound $[\text{Fe}(\text{H}-3\text{-OEt-thsa-Me})(3\text{-OEt-thsa-Me})]\cdot\text{H}_2\text{O}$ was conducted at the synchrotron-based facility at the Diamond Light Source, UK national synchrotron science facility located at the Harwell Science and Innovation Campus Oxfordshire. The data collection was performed on beamline I19 situated on an undulator insertion device with a combination of double crystal monochromator, vertical and horizontal focussing mirrors and a series of beam splits (primary white beam and either side of the focussing mirrors). The experimental hutch (EH1) is equipped with a Crystal Logic four-circle κ geometry goniometer with a Rigaku Saturn 724 CCD detector and an Oxford Cryosystems Cryostream plus cryostat (80-500 K). The crystal data was collected at 100 K, with an energy of the X-ray beam of 18 keV ($\lambda = 0.6889 \text{ \AA}$). Cell determination and data collection were performed using the program *CrystalClear-SM Expert 2.0 r5* [7]. Moreover, the data reduction, cell refinement and absorption correction were performed using the program *CrystalClear-SM Expert 2.0 r5* [7]. The structure solution of $[\text{Fe}(3\text{-OEt-thsa-Me})(\text{H}-3\text{-OEt-thsa-Me})]\cdot\text{H}_2\text{O}$ was determined using the program *SUPERFLIP* [4].

Furthermore, the crystal data collection for the ferric complexes $\text{NH}_4[\text{Fe}(\text{thsa})_2]$ and $\text{NH}_4[\text{Fe}(5\text{-Br-thsa})_2]$, were carried out after attaching a single crystal to a glass fibre by using perfluorinated oil and mounted on a Bruker KAPPA APEX II diffractometer equipped with a CCD detector. Data were collected at 100 K in a dry stream of nitrogen with $\text{MoK}\alpha$ radiation ($\lambda=0.71073 \text{ \AA}$). Data were reduced to intensity values using *SAINTE-Plus* [8] and absorption correction was applied using the multi-scan method implemented by *SADABS* [8]. The structures were solved using charge-flipping implemented by *SUPERFLIP* [4] and refined against F-values with *JANA2006* [9].

2.6 Physical Measurements

2.6.1 Differential Scanning Calorimetry

DSC experiments were performed with a differential scanning calorimeter Mettler Toledo DSC1 STAR^c System. The temperature and enthalpy scales were calibrated with a standard sample of indium, using its melting transition (156.6°C , 3296 Jmol^{-1}). The calorimetric measurements were carried out in 40 μL aluminium pans, containing $\sim 5\text{-}15 \text{ mg}$ of the ferric complex sample, which was sealed with an aluminium lid and crimped. An empty sealed 40 μL aluminium pan and lid was used as the reference. The measurements were carried out at a heating rate of 5 K/min under N_2 atmosphere in the temperature range of 123 – 353 K.

2.6.2 Magnetic Measurements

Variable temperature magnetic susceptibility data for the coordination compounds Cs[Fe(3-OEt-thsa-Me)₂] \cdot CH₃OH and Cs[Fe(5-Br-thsa)₂] were obtained with a cryogenic vibrating-sample magnetometer (VSM) at the Institute of Applied Synthetic Chemistry, Vienna University of Technology. The rate of temperature change was at 5 K/min. The magnetometer was calibrated using Gd₂(SO₄)₃ and a certified Pd-sample. The data collected from the vibrating sample magnetometer (VSM) in the temperature range 10 – 300 K was converted to $\chi_M T$ by equation 1 (Eq 1):

$$\chi_M T = [M / (\text{magnetic field} * (\text{sample amount} / \text{MW}))] * T \quad (\text{Eq 1})$$

The different terms displayed in equation 1 and their respective units are defined as:

Magnetisation (M)	emu
Magnetic field	Oe
Sample amount	g
Sample molecular weight (MW)	g/mol
Temperature (T)	K

Data were corrected for diamagnetic contributions, which were estimated from Pascal's constants.

Temperature dependent magnetic measurements of the ferric complexes presented in this thesis were carried out at the Physics Department of the University of Warwick, using a Quantum Design MPMS-5S SQUID (Superconducting Quantum Interference Device) magnetometer. The magnetic measurements were conducted with scan temperatures between 5-320 K with a rate of 2 K/min and an applied field of 1 T. The SQUID magnetometer was calibrated against the standard palladium sample. Data collected from the SQUID magnetometer was converted to $\chi_M T$ (χ_M is the molar magnetic susceptibility and T the temperature) via equation 1 (*vide supra*).

2.7 References

1. Rigaku (2013). *CrystalClear-SM Expert 2.1 b29*. Rigaku Corporation, The Woodlands, Texas, USA.
2. Rigaku (2014) *CrystalClear-SM Expert 3.1 b27*. Rigaku Corporation, The Woodlands, Texas, USA.
3. Agilent (2014). *CrysAlisPro*. Agilent Technologies UK Ltd, Yarnton, England.

4. Palatinus, L. and Chapuis, G. (2007). *J. Appl. Cryst.* **40**, pp. 786-790.
5. Sheldrick, G.M. (2008). *Acta Cryst.* **A64**, pp. 112-122.
6. Sheldrick, G.M. (2015). *Acta Cryst.* **A71**, pp. 3-8.
7. Rigaku (2010). *CrystalClear-SM Expert 2.0 r5*. Rigaku Corporation, The Woodlands, Texas, USA.
8. Bruker (2012). *SAINT-Plus*. Bruker AXS Inc., Madison, Wisconsin, USA.
9. Petricek, V. and Dusek, M. (2006). *JANA2006*. Institute of Physics, Czech Academy of Sciences, Prague, Czech Republic.

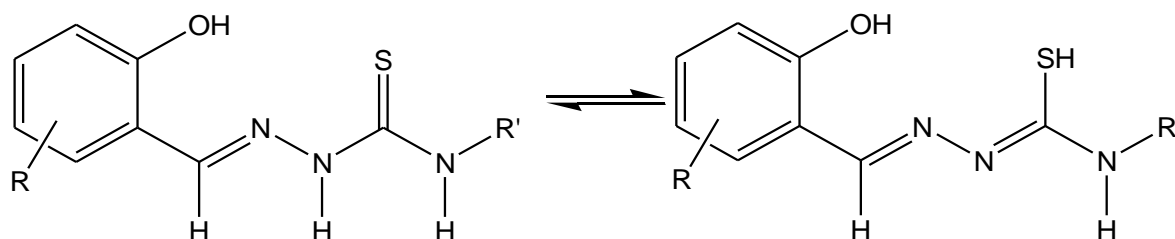
Chapter III
Anionic Fe(III) Complexes of
R-salicylaldehyde 4-R'-thiosemicarbazones

3.0 Anionic Fe(III) Complexes of R-salicylaldehyde 4R'-thiosemicarbazones

3.1 Introduction

It is recognised that octahedral metal complexes with $3d^4 - 3d^7$ electronic configurations with specific ligands can exhibit spin-crossover behaviour, the magnetic interconversion between low-spin and high-spin state, dependent upon external perturbations of temperature, pressure or light irradiation [1]. In recent years, particular interest has focused on Fe^{III} ($3d^5$) complexes of substituted derivatives of R-salicylaldehyde 4R'-thiosemicarbazone [2-7] for generating Fe^{III} spin-crossover. The spin-crossover properties of this class of Fe^{III} bis(ligand) complexes have been found to be sensitive to the presence of a particular counter-ion, the degree of solvation and the nature of the R,R'-substituted ligands [7, 8]. Furthermore, it has been established that varying the pH during the synthesis of the Fe^{III} bis(ligand) entities leads to the formation of Fe^{III} compounds differing in the degree of deprotonation of the ligand, whereby the complex unit can be neutral, monocationic or monoanionic [4, 6, 9].

In Fe^{III} compounds, it is possible for the tridentate R-salicylaldehyde 4R'-thiosemicarbazone ligand (H_2L) to exist in tautomeric forms; moreover, the ligand may also be present in its neutral, anionic or dianionic form. The free R-salicylaldehyde 4R'-thiosemicarbazone ligand (H_2L) in solution exists in two tautomeric forms *i.e.* the thione and thiol forms, as illustrated in Scheme 3.1.1.



Scheme 3.1.1

In this chapter, the synthesis and crystallographic studies of five anionic Fe^{III} compounds of R-salicylaldehyde 4R'-thiosemicarbazonato(2-) are reported: $\text{Cs}[\text{Fe}(\text{3-OEt-thsa-Me})_2] \cdot \text{CH}_3\text{OH}$, $\text{Cs}[\text{Fe}(\text{5-Br-thsa})_2]$, $\text{NH}_4[\text{Fe}(\text{thsa})_2]$, $\text{NH}_4[\text{Fe}(\text{5-Br-thsa})_2]$ and $(\text{CH}_3)_2\text{NH}_2[\text{Fe}(\text{3-OEt-thsa})_2]$; the ligands are depicted in Figure 3.1.1. Furthermore, the electronic properties of the Fe^{III} coordination compounds are herein investigated, with focus upon the effect of the varied R and R'-substituted salicylaldehyde thiosemicarbazone ligands and the effect of the variation of the non-coordinating cation.

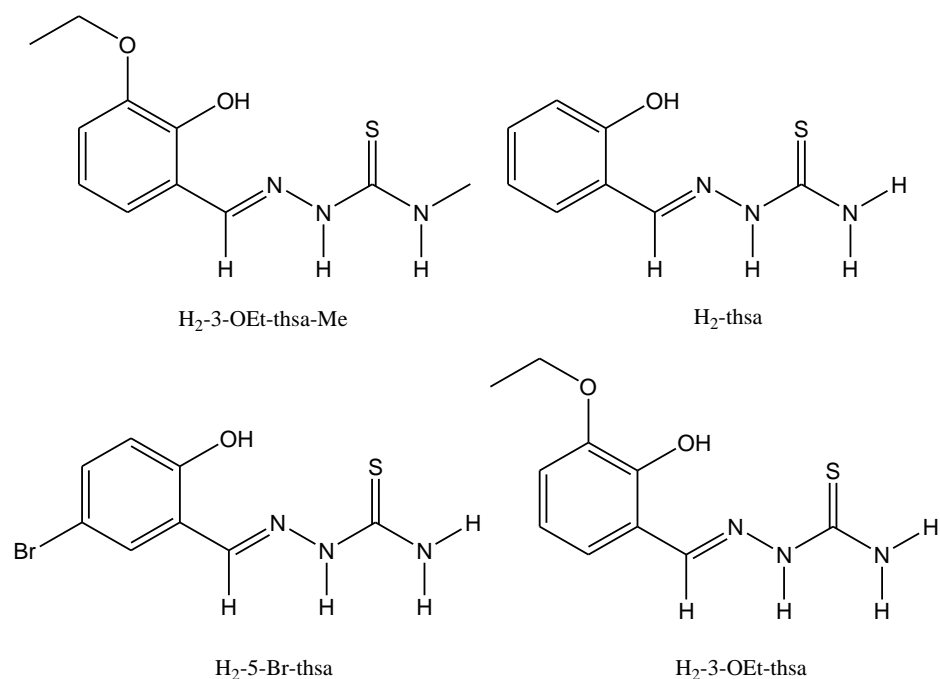
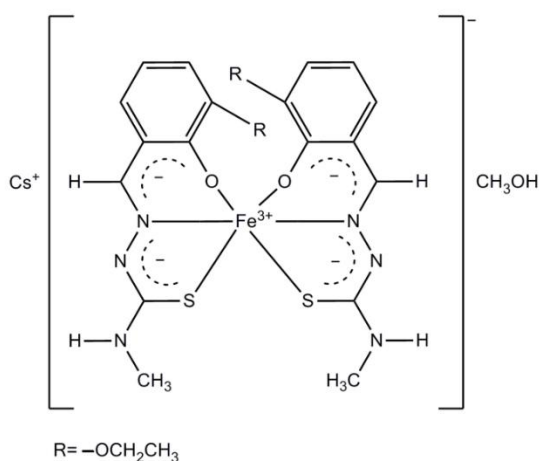


Figure 3.1.1 Structure of H₂L R-salicylaldehyde 4R'-thiosemicarbazone ligands

3.2 The crystal structure and magnetic properties of caesium bis(3-ethoxysalicylaldehyde 4-methylthiosemicarbazonato(2-)- κ^3 -O²,N¹,S)ferrate(III) methanol monosolvate

The magnetic properties are herein reported of the novel Fe^{III} compound Cs[Fe(3-OEt-thsa-Me)₂]·CH₃OH containing two dianionic tridentate 3-ethoxysalicylaldehyde 4-methylthiosemicarbazonato(2-) (L²⁻) ligands (Scheme 3.2.1) and the determination and description of its structure at 100 K.

The experimental data are reported in Chapter II for the synthesis of Cs[Fe(3-OEt-thsa-Me)₂]·CH₃OH and corresponding ligand, 3-ethoxysalicylaldehyde 4-methylthiosemicarbazone.



Scheme 3.2.1

3.2.1 Crystal Data and Structure Refinement Details of Cs[Fe(3-OEt-thsa-Me)₂] \cdot CH₃OH

Crystal data, data collection and structure refinement details are summarised in Table 3.2.1. The hydrogen atoms on the secondary amine atoms N13 and N23 were located in difference Fourier maps and refined with restrained N–H distances of 0.88(2) Å and with $U_{\text{iso}}(\text{H}) = 1.2U_{\text{eq}}(\text{N})$. The hydrogen atom attached to atom O3 of the methanol molecule was located in a difference Fourier map and refined with an O–H distance restraint of 0.84(2) Å and $U_{\text{iso}}(\text{H}) = 1.5U_{\text{eq}}(\text{O})$. The remaining hydrogen atoms were included in the refinement in calculated positions and treated as riding on their parent atoms, with C–H = 0.95 Å and $U_{\text{iso}}(\text{H}) = 1.2U_{\text{eq}}(\text{C})$ for aryl (–CH=) hydrogen atoms, C–H = 0.99 Å and $U_{\text{iso}}(\text{H}) = 1.2U_{\text{eq}}(\text{C})$ for methylene (–CH₂–) hydrogen atoms, C–H = 0.98 Å and $U_{\text{iso}}(\text{H}) = 1.5U_{\text{eq}}(\text{C})$ for methyl (–CH₃) hydrogen atoms. The ethoxy group of one of the ligands shows positional disorder. Two different sets of positions for the methyl and methylene carbon atoms were identified in the difference Fourier synthesis, *i.e.* C111 and C110; and C113 and C112, respectively, which were refined with inversely proportional occupancy factors [0.552(17) and 0.448(17)]. Similarity restraints were applied to the chemically equivalent bonds within the two disordered conformations. The residual density on a difference Fourier map included a quadrilateral of peaks near Cs of height 1.21–1.84 e Å⁻³. Unreasonably close contacts to some ligand atoms, which persisted after refinement, ruled out an attribution of these peaks to disorder of the Cs site. Twinning was also considered and rejected; three possible twin laws were provided by ROTAX [10], but refinement in SHELXL97 [11] led to a negligible scale factor for each such twin component. Therefore, the peaks, which represent a small fraction of the 54 electrons in the Cs⁺ ion, are assumed to arise from limitations of the data.

Table 3.2.1 Crystal data and structure refinement details of Cs[Fe(3-OEt-thsa-Me)₂] \cdot CH₃OH

Crystal data	
Chemical formula	Cs[Fe(C ₁₁ H ₁₃ O ₂ N ₃ S) ₂] \cdot CH ₃ OH
M_r	723.40
Crystal system, space group	Triclinic, <i>P</i> -1
Temperature (K)	100
a, b, c (Å)	8.486 (3), 9.078 (3), 19.875 (7)
α, β, γ (°)	100.629 (5), 91.549 (5), 113.674 (5)
V (Å ³)	1369.5 (8)
Z	2
Radiation type	Mo $K\alpha$
μ (mm ⁻¹)	2.06
Crystal size (mm)	0.04 \times 0.02 \times 0.01

Table 3.2.1 Crystal data and structure refinement details of Cs[Fe(3-OEt-thsa-Me)₂] \cdot CH₃OH (continued)

Colour	Green (plate)
Data collection	
Diffractometer	Rigaku AFC12 four-circle Kappa diffractometer
Absorption correction	Multi-scan (<i>CrystalClear-SM Expert</i> [12])
T_{\min} , T_{\max}	0.711, 1.000
No. of measured, independent and observed [$I > 2\sigma(I)$] reflections	15188, 4844, 3414
R_{int}	0.082
Refinement	
$R[F^2 > 2\sigma(F^2)]$, $wR(F^2)$, S	0.052, 0.122, 0.92
No. of reflections	4844
No. of parameters	377
No. of restraints	5
H-atom treatment	H atoms treated by a mixture of independent and constrained refinement
$\Delta\rho_{\text{max}}$, $\Delta\rho_{\text{min}}$ (e \AA^{-3})	1.84, -0.62

The program used for data collection, cell refinement and data reduction: *CrystalClear-SM Expert* [12]. The program used for the structure solution: *SUPERFLIP* [13-15]; the structure refinement used the program *SHELXL97* [11]. The *ORTEP-3* for Windows [16] and *OLEX2* [17] programs were used to produce the molecular graphics.

3.2.2 Crystallographic study of Cs[Fe(3-OEt-thsa-Me)₂] \cdot CH₃OH

The structure of caesium bis(3-ethoxy-salicylaldehyde-methylthiosemicarbazonato(2-)- κ^3O^2, N^1S)ferrate(III) methanol (Cs[Fe(3-OEt-thsa-Me)₂] \cdot CH₃OH) (Figure 3.2.1) was determined at 100 K. Cs[Fe(3-OEt-thsa-Me)₂] \cdot CH₃OH was found to crystallise in a triclinic system and in the space group *P*-1. The asymmetric unit consists of one formula unit, Cs[Fe(L)₂] \cdot CH₃OH, with no atom at a special position. The structure of Cs[Fe(3-OEt-thsa-Me)₂] \cdot CH₃OH shows that the Fe^{III} ion is coordinated by two dianionic tridentate thiosemicarbazonato-O,N,S ligands, displaying an distorted octahedral Fe^{III}O₂N₂S₂ geometry. Selected geometric parameters are listed in Table 3.2.2. The donor atoms of the ligands are situated in two perpendicular planes with O and S atoms in *cis* positions,

whereas the N atoms are in *trans* positions. These features are corroborated by the bond angles involving the Fe atom and the donor atoms (Table 3.2.2).

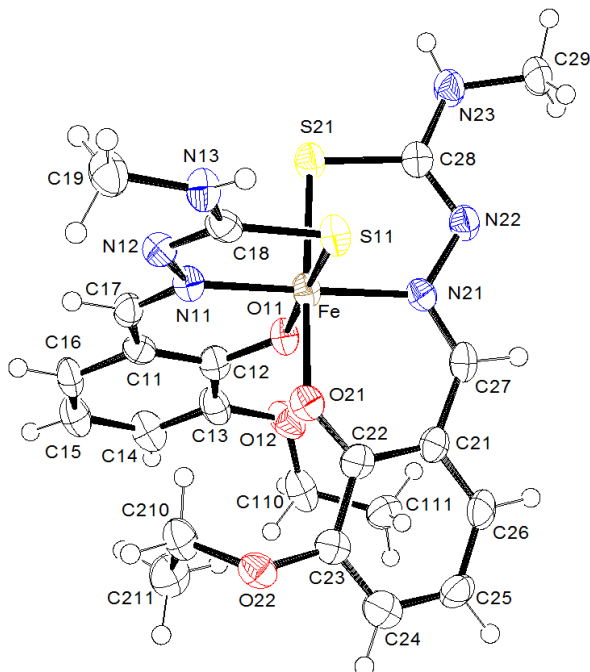


Figure 3.2.1 The molecular structure and atom-numbering scheme for Cs[Fe(3-OEt-thsa-Me)₂]·CH₃OH. The Cs⁺, CH₃OH and an alternative orientation for C110-C111 have been omitted for clarity. Displacement ellipsoids are drawn at the 50% probability level.

The bond distances involving the Fe atom and the donor atoms (Table 3.2.2) suggest that the present compound contains low-spin Fe^{III} at 100 K. Typical distances for Fe–S, Fe–O and Fe–N bonds are 2.23–2.31 Å, 1.93–1.95 Å and 1.88–1.96 Å, respectively, for low-spin Fe^{III} compounds of this family, and 2.40–2.44 Å, 1.96–1.99 Å and 2.05–2.15 Å, respectively, for the corresponding high-spin Fe^{III} compounds [8]. It is noteworthy that the Fe–O distances in Cs[Fe(3-OEt-thsa-Me)₂]·CH₃OH are both shorter than the typical values quoted for low-spin Fe^{III}. One reason may be invoked for this occurrence; the low-spin Fe–O reference values are mainly taken from X-ray crystal structures determined at temperatures higher than that at which the structure of the present compound was determined (100 K), hence it may be anticipated that the range of actual low-spin Fe–O distances at 100 K will be slightly shorter than the cited values. Furthermore, it is significant to note that the Fe–O distances seem to be less sensitive to a change in Fe^{III} spin state than the Fe–N and Fe–S distances, which may be related to the π -acceptor capability of the N- and S-donor atoms opposed to the π -donor capability of the O-donor atoms. This is of particular significance when Fe^{III} is in the low-spin state as increased back-bonding will lead to comparatively more pronounced shortening of the Fe–N and Fe–S bonds than of the Fe–O bonds.

Table 3.2.2 Selected geometric parameters of Cs[Fe(3-OEt-thsa-Me)₂] \cdot CH₃OH (Å, °)

Fe1–S11	2.2686(19)	Fe1–S21	2.265(2)
Fe1–O11	1.904(4)	Fe1–O21	1.918(4)
Fe1–N11	1.933(5)	Fe1–N21	1.939(5)
S11–Fe1–S21	89.61(7)	O11–C12–C11	124.2(6)
S11–Fe1–N11	85.55(15)	C12–C11–C17	123.6(5)
S11–Fe1–O11	177.83(14)	C11–C17–N11	125.3(6)
S11–Fe1–O21	89.34(13)	C17–N11–Fe1	125.4(4)
S11–Fe1–N21	94.57(15)	Fe1–O21–C22	122.8(4)
S21–Fe1–O11	92.56(14)	O21–C22–C21	124.3(3)
S21–Fe1–O21	178.01(13)	C22–C21–C27	122.1(6)
S21–Fe1–N11	94.17(16)	C21–C27–N21	126.2(6)
S21–Fe1–N21	84.71(16)	C27–N21–Fe1	123.8(4)
O11–Fe1–O21	88.49(18)	C18–S11–Fe1	94.6(2)
O11–Fe1–N11	94.37(19)	N11–N12–C18	113.3(5)
O11–Fe1–N21	85.55(18)	N12–C18–S11	124.8(5)
O21–Fe1–N11	87.4(2)	C28–S21–Fe1	94.3(2)
O21–Fe1–N21	93.7(2)	N21–N22–C28	113.1(5)
N11–Fe1–N21	178.9(2)	N22–C28–S21	124.3(5)
Fe1–N11–C12	126.14(4)		

The tridentate ligands in the present compound coordinate to the Fe^{III} cation by the thiolate-S, phenolate-O and the imine-N, forming six- and five-membered chelate rings. As might be expected, the six-membered chelate ring involves a significantly less restricted bite angle [O11–Fe–N11 = 94.37(19)° and O21–Fe–N21 = 93.7(2)°] than the five-membered chelate ring [S11–Fe–N11 = 85.55(15)° and S21–Fe–N21 = 84.71(16)°]. The conformation of the 5- and 6-membered chelate rings of Cs[Fe(3-OEt-thsa-Me)₂] \cdot CH₃OH illustrate there is no major strain relief through puckering. At 100 K, the root-mean-square deviations from their least-squares plane of atoms comprising the 6-membered [Fe1 N11 C17 C11 C12 O11] and [Fe1 N21 C27 C21 C22 O21] chelate rings are 0.038 and 0.123 Å, respectively; corresponding values for the 5-membered [Fe1 N11 N12 C18 S11] and [Fe1 N21 N22 C28 S21] chelate rings are 0.012 and 0.083 Å, respectively. The O–Fe–N bite angle of the 6-membered chelate rings is deficient by *ca.* 26° from the ideal 120° angles in a regular hexagon. The remaining bite angles (listed in Table 3.2.2) of the 6-membered chelate rings are within

3° of 125°. In comparison to the 108° angles of a regular pentagon, the S–Fe–N bite angles are deficient by 23°. The C–S–Fe angles are 94.6(2)° and 94.3(2)°, respectively, creating an additional deficiency of *ca.* 14°. The deficiencies of the bite angles can be offset by an increase in the other bite angles of the 5-membered chelate ring to *ca.* 120°. In fact, the N–N–C angles are 113.3(5)° and 113.1(5)°, respectively, and the N–C–S bite angles are 124.8(5)° and 124.3(5)°, respectively. The C and N atoms form bonds which display sp² hybridisation which is contaminant of the 120° angles. Further stabilisation arises from the near alternation of single and double bonds in the different electronic forms allowing a high degree of π-electron delocalisation throughout both of the chelate rings. Hydrogen atoms could not be located on the phenolate-O and the thiolate-S atoms, which implies that both ligands are in the dianionic form. This is concomitant with the presence of a trivalent iron ion together with a monovalent caesium cation. Ryabova *et al.* [18] reported on the related compound Cs[Fe(L)₂] [where L²⁻ = salicylaldehyde thiosemicarbazonato(2-)], although this material contains high-spin Fe^{III}.

The binding of the twofold deprotonated ligand of Cs[Fe(3-OEt-thsa-Me)₂]·CH₃OH to the Fe^{III} cation involves electron delocalisation within the chelate ring, which is evident from geometric parameters. The C18–S11 bond distance of 1.742(7) Å and C28–S21 bond distance of 1.759(6) Å suggest a partial electron delocalisation of these bonds. This corresponds well with the C–S bond distance of 1.750(6) Å for the low-spin Fe^{III} compound NH₄[Fe(L)₂] (where L²⁻ = 5-chlorosalicylaldehyde thiosemicarbazonato(2-)) at 135 K [19]. Similarly, a bond order larger than one can be inferred for the C–N bond involving the deprotonated hydrazinic nitrogen atom. The bond distances for the C17–N11 and C27–N21 bonds in the present Fe^{III} complex are 1.302(7) Å and 1.291(8) Å, respectively, which correlates with the value reported by Ryabova *et al.* [19], *i.e.* a C–N bond distance of 1.265(8) Å for NH₄[Fe(L)₂] at 135 K. Moreover, for Cs[Fe(3-OEt-thsa-Me)₂]·CH₃OH, the N11–N12 and N21–N22 bond lengths are 1.398(7) Å and 1.406(7) Å, respectively, indicating some electron delocalisation.

The hydrogen bonding interactions of Cs[Fe(3-OEt-thsa-Me)₂]·CH₃OH are listed in Table 3.2.3 and displayed in Figure 3.2.2. N13–H13⋯S11 (–x + 1, –y + 1, –z + 1) interactions paired about the inversion centre at (0.5, 0.5, 0.5) create R₂² (8) rings [20], as do N23–H23⋯S21 (–x, –y + 1, –z + 1) contacts about (0, 0.5, 0.5). In this manner, successive Fe^{III} entities are linked in the *a* direction. The CH₃OH solvent oxygen atom O3 forms an O3–H3⋯N12 contact involving the hydrazinic nitrogen atom N12. In turn, the hydrazinic atom N12 is bonded to the imine atom N11, which is coordinated to the Fe^{III} cation centre. However, the Fe–N11 bond length [1.933(5) Å] is virtually identical to the Fe–N21 bond length [1.939(5) Å] involving the other ligand, which is devoid of hydrogen bonding interactions. The Cs⁺ cations link the anions into chains along [100].

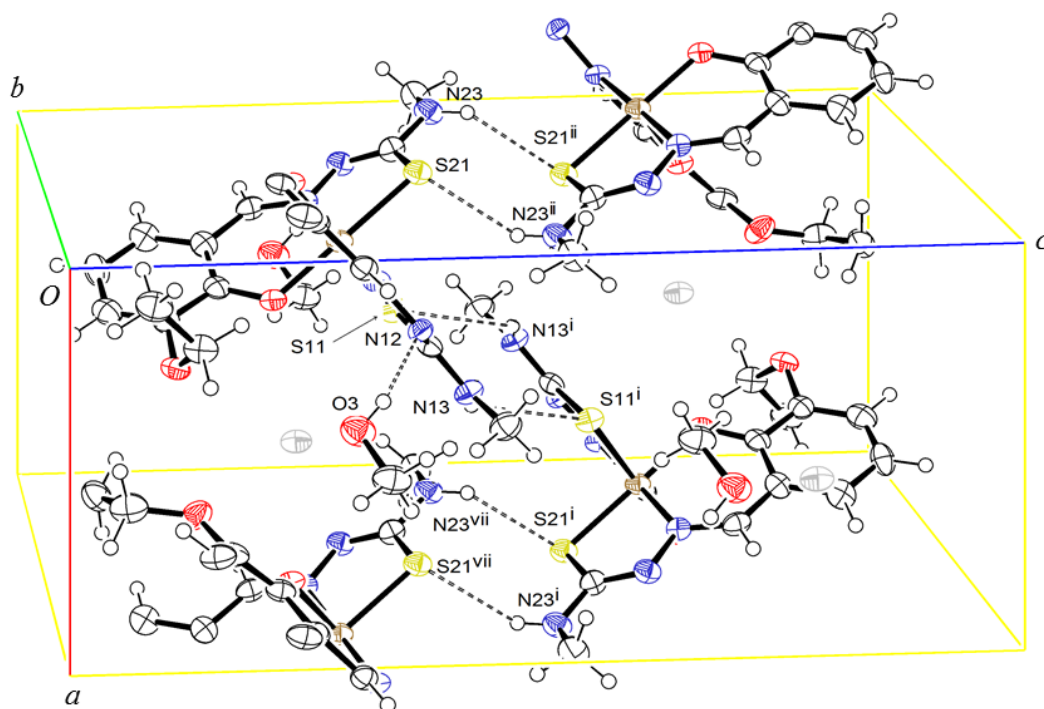


Figure 3.2.2 A projection showing the unit cell of Cs[Fe(3-OEt-thsa-Me)₂] \cdot CH₃OH. An alternative orientation for C110–C111 has been omitted for clarity. Displacement ellipsoids are drawn at the 50% probability level. [Symmetry codes: (i) $-x + 1, -y + 1, -z + 1$; (ii) $-x, -y + 1, -z + 1$.]

Table 3.2.3 Hydrogen bond geometry of Cs[Fe(3-OEt-thsa-Me)₂] \cdot CH₃OH (Å, °)

<i>D</i> –H \cdots <i>A</i>	<i>D</i> –H	H \cdots <i>A</i>	<i>D</i> \cdots <i>A</i>	<i>D</i> –H \cdots <i>A</i>
N13–H13 \cdots S11 ⁱ	0.87(2)	2.97(6)	3.505(6)	122(5)
N23–H23 \cdots S21 ⁱⁱ	0.87(2)	2.70(5)	3.416(6)	141(6)
O3–H3 \cdots N12	0.85(2)	2.04(4)	2.852(7)	160(8)

Symmetry codes: (i) $-x + 1, -y + 1, -z + 1$; (ii) $-x, -y + 1, -z + 1$.

3.2.3 Magnetic Studies of Cs[Fe(3-OEt-thsa-Me)₂] \cdot CH₃OH

The temperature dependence of the $\chi_M T$ product (χ_M being the molar magnetic susceptibility and T, temperature) for the compound Cs[Fe(3-OEt-thsa-Me)₂] \cdot CH₃OH was measured in the temperature range 10–300 K and given in Figure 3.2.3. The $\chi_M T$ value for Cs[Fe(3-OEt-thsa-Me)₂] \cdot CH₃OH is 0.664 cm³ mol⁻¹ K at 300 K, which corresponds to the low-spin value expected for Fe^{III} (0.375 cm³ mol⁻¹ K, $g = 2.00$), revealing no spin transition within the temperature range 10–300 K.

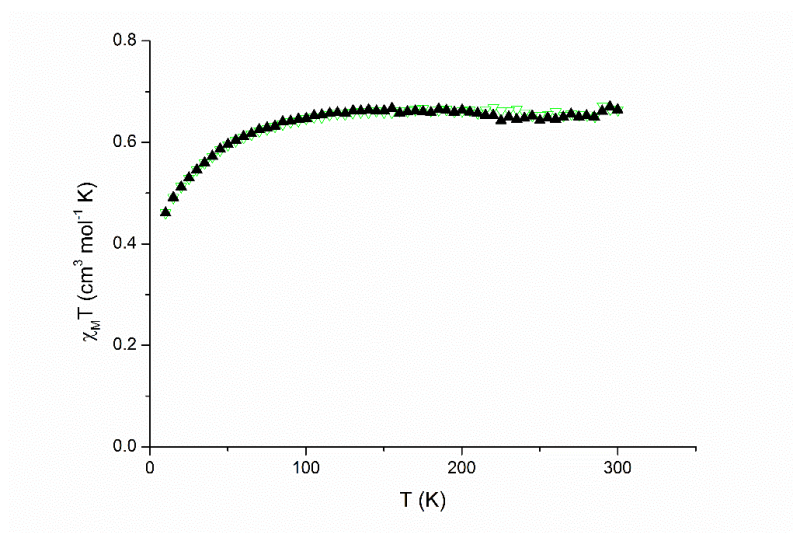
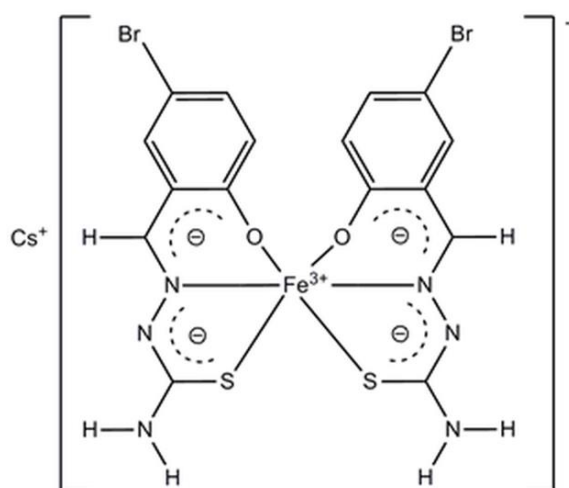


Figure 3.2.3 $\chi_M T$ vs T plot of $\text{Cs}[\text{Fe}(\text{3-OEt-thsa-Me})_2] \cdot \text{CH}_3\text{OH}$. [The sample was heated (\blacktriangle) and subsequently cooled (\blacktriangledown).]

3.3 The crystal structure and magnetic properties of caesium bis(5-bromosalicylaldehyde thiosemicarbazonato(2-)- κ^3 -O, N^1 ,S)ferrate(III)

In this section the magnetic properties of the title Fe^{III} compound, $\text{Cs}[\text{Fe}(\text{5-Br-thsa})_2]$, as illustrated in Scheme 3.3.1, are described, as well as the crystal structure at 293 K. The synthesis of $\text{Cs}[\text{Fe}(\text{5-Br-thsa})_2]$ and the corresponding H_2L ligand, 5-bromosalicylaldehyde thiosemicarbazone, are described in Chapter II – Materials and Methods.



Scheme 3.3.1

3.3.1 Crystal Data and Structure Refinement Details of Cs[Fe(5-Br-thsa)₂]

Crystal data, data collection and structure refinement details are summarised in Table 3.3.1. The structure of Cs[Fe(5-Br-thsa)₂] was routinely solved by direct methods and refined by least squares with hydrogen atoms placed in calculated positions and non-hydrogen atoms given anisotropic displacement parameters. However, the refined parameters did not match the quality of the data set since the unweighted discrepancy index R1 of 0.0916 was much higher than R(int) of 0.0451. Since all 50 of the reflections with the worst discrepancy had F(obs) > F(calc), twinning was suspected; and the closeness of the unit cell β angle to 90° suggested a mechanism for pseudo-merohedral twinning. Application of *ROTAX* [10] indicated 180° rotation about the *a* axis as the likely twin law. Repeating the refinement with this twin law drastically reduced the discrepancy indices.

Now all polar hydrogen atoms were omitted from the model and sought in difference Fourier maps. The H atoms on the secondary amine atoms N13 and N23 were located in difference Fourier maps at peak heights between 0.60 and 0.70 e Å⁻³, while no comparable peaks appeared adjacent to N11, N12, N21, N22 or any O or S atom. In subsequent refinements the amino hydrogen atoms thus established were treated as riding with N–H distances of 0.86 Å and $U_{\text{iso}}(\text{H}) = 1.2U_{\text{eq}}(\text{N})$. The remaining H atoms were included in the refinement in calculated positions and treated as riding on their parent atoms, with C–H = 0.93 Å and $U_{\text{iso}}(\text{H}) = 1.2U_{\text{eq}}(\text{C})$ for aryl (-CH=) H atoms. After final refinement R1 reached 0.0326 and wR2 = 0.0859, and fractional contribution of 0.1306(8) from the minor twin component was indicated.

Table 3.3.1 Crystal data and structure refinement details of Cs[Fe(5-Br-thsa)₂]

Crystal data	
Chemical formula	Cs[Fe(C ₈ H ₆ BrON ₃ S) ₂]
M_r	733.02
Crystal system, space group	Monoclinic, P2 ₁ /c
Temperature (K)	293
a, b, c (Å)	20.2500(14), 12.0868(8), 9.0389(5)
α, β, γ (°)	90, 90.337(1), 90
V (Å ³)	2212.3(2)
Z	4
Radiation type	Mo $K\alpha$
μ (mm ⁻¹)	6.13
Crystal size (mm)	0.08 × 0.08 × 0.01

Table 3.3.1 Crystal data and structure refinement details of Cs[Fe(5-Br-thsa)₂] (continued)

Colour	Green/brown (plate)
Data collection	
Diffractometer	Rigaku AFC12 (Right) diffractometer
Absorption correction	Multi-scan <i>CrystalClear-SM Expert</i> 3.1 b27
No. of measured, independent and observed [$I > 2\sigma(I)$] reflections	29088, 5073, 4211
R_{int}	0.045
$(\sin \theta/\lambda)_{\text{max}}$ (\AA^{-1})	0.649
Refinement	
$R[F^2 > 2\sigma(F^2)]$, $wR(F^2)$, S	0.033, 0.086, 1.03
No. of reflections	5073
No. of parameters	272
No. of restraints	0
H-atom treatment	All H atoms treated by a constrained refinement
$\Delta\rho_{\text{max}}$, $\Delta\rho_{\text{min}}$ (e \AA^{-3})	0.88, -0.85

The program used for data collection, cell refinement and data reduction: *CrystalClear-SM Expert* [12]. The program(s) used for the structure solution and the structure refinement: *ROTAX* [10], *SHELXS* [11] and *SHELXL* [11]. The *ORTEP-3* for Windows [16] program was used to produce the molecular graphics.

3.3.2 Crystallographic study of Cs[Fe(5-Br-thsa)₂]

The crystal structure of caesium bis(5-bromosalicylaldehyde thiosemicarbazonato(2-)- κ^3 -*O,N',S*)ferrate(III) (Figure 3.3.1) was determined at 293 K. Cs[Fe(5-Br-thsa)₂] crystallises in the monoclinic system in the space group $P2_1/c$. The asymmetric unit corresponds to the formula unit, Cs[Fe(L)₂] where L^{2-} = 5-bromosalicylaldehyde thiosemicarbazonato(2-), with no atom on a special position. The central Fe^{III} cation is hexa-coordinated by two dianionic O,N,S-tridentate L^{2-} ligands, displaying a distorted octahedral Fe^{III}O₂N₂S₂ geometry. Deprotonation occurs for the phenol O atoms and thiol S atoms. Selected geometric parameters are listed in Tables 3.3.2 and 3.3.3.

The Fe^{III}O₂N₂S₂ unit is distorted from the ideal octahedral geometry, as indicated by the bond angles (Table 3.3.2) of the donor atoms and the Fe1 atom (*vide infra*). The tridentate L^{2-} ligands are

coordinated to the Fe^{III} cation by the O- and S-donor atoms, which are situated in two perpendicular planes in the *cis* positions, such that the N-donor atoms are situated in mutually *trans* positions.

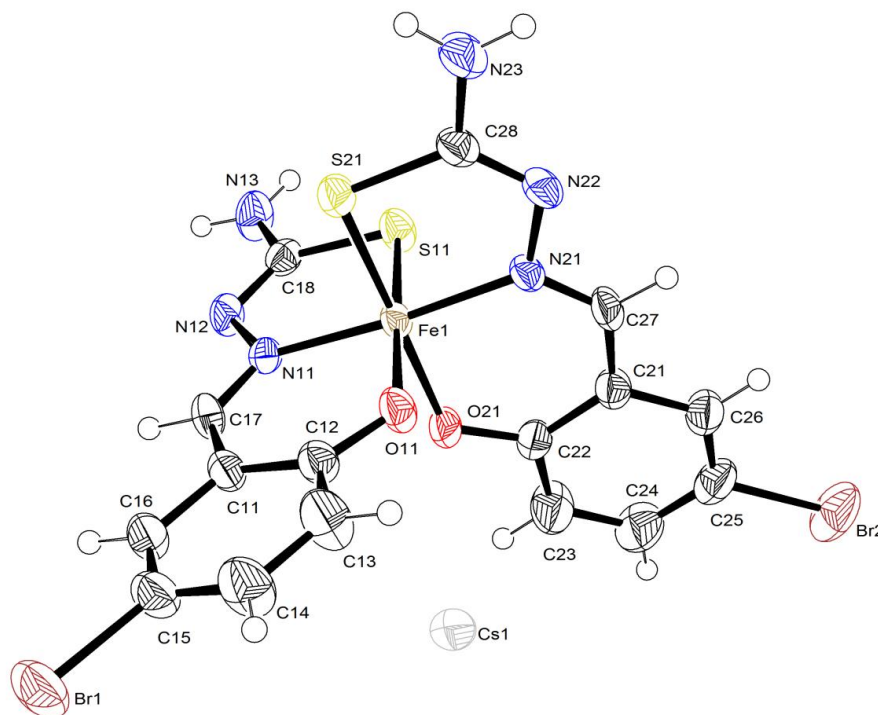


Figure 3.3.1 The molecular structure and atom-numbering scheme for Cs[Fe(5-Br-thsa)₂]. Displacement ellipsoids are drawn at 50% probability level.

Table 3.3.2 Selected geometric parameters of Cs[Fe(5-Br-thsa)₂] (Å, °)

Fe–S11	2.2321(11)	Fe–S21	2.2422(11)
Fe–O11	1.942(3)	Fe–O21	1.956(3)
Fe–N11	1.947(3)	Fe–N21	1.938(3)
Cs1–S11 ⁱ	3.7159(11)	Cs1–N12 ⁱⁱ	3.326(3)
Cs1–S21 ⁱ	3.5564(11)	Cs1–N22 ⁱⁱⁱ	3.470(3)
Cs1–O11	3.220(3)	Cs1–N23 ⁱ	3.699(4)
Cs1–O21	3.129(3)		
S11–Fe–S21	93.66(4)	O11–Fe–N21	89.20(12)
S11–Fe–N11	86.01(9)	O21–Fe–N11	89.40(11)
S11–Fe–O11	177.50(9)	O21–Fe–N21	93.78(12)
S11–Fe–O21	89.78(10)	N11–Fe–N21	175.33(12)
S11–Fe–N21	90.57(9)	C18–S11–Fe	95.12(13)

Table 3.3.2 Selected geometric parameters of Cs[Fe(5-Br-thsa)₂] (Å, °) (continued)

S21–Fe–O11	88.81(9)	C28–S21–Fe	94.61(14)
S21–Fe–O21	176.56(10)	N11–N12–C18	113.5(3)
S21–Fe–N11	90.96(9)	N21–N22–C28	113.6(3)
S21–Fe–N21	86.07(9)	N12–C18–S11	124.3(3)
O11–Fe–O21	87.75(12)	N22–C28–S21	124.8(3)
O11–Fe–N11	94.35(12)		
O11–Cs1–S11 ⁱ	176.98(5)	N12 ⁱⁱ –Cs1–S11 ⁱ	85.01(6)
O11–Cs1–S21 ⁱ	129.54(5)	N12 ⁱⁱ –Cs1–S21 ⁱ	103.23(6)
O11–Cs1–N12 ⁱⁱ	92.97(7)	N12 ⁱⁱ –Cs1–N22 ⁱⁱⁱ	156.35(8)
O11–Cs1–N22 ⁱⁱⁱ	65.82(7)	N12 ⁱⁱ –Cs1–N23 ⁱ	143.33(8)
O11–Cs1–N23 ⁱ	100.65(7)	N22 ⁱⁱⁱ –Cs1–S11 ⁱ	115.72(6)
O11–Cs1–O21	50.34(7)	N22 ⁱⁱⁱ –Cs1–S21 ⁱ	98.64(6)
O21–Cs1–S11 ⁱ	126.82(5)	N22 ⁱⁱⁱ –Cs1–N23 ⁱ	56.10(8)
O21–Cs1–S21 ⁱ	178.78(5)	N23 ⁱ –Cs1–S11 ⁱ	82.29(6)
O21–Cs1–N12 ⁱⁱ	75.63(7)	N23 ⁱ –Cs1–S21 ⁱ	42.99(6)
O21–Cs1–N22 ⁱⁱⁱ	82.42(7)	S21 ⁱ –Cs1–S11 ⁱ	53.27(2)
O21–Cs1–N23 ⁱ	137.96(7)		

Symmetry codes: (i) x, y, z – 1; (ii) x, –y + 1/2, z – 1/2; (iii) x, –y + 3/2, z – 1/2.

X-ray structural data of similar Fe^{III} bis(ligand) compounds containing the dianionic thiosemicarbazonate(2-) ligands show that the Fe–S, Fe–O and Fe–N bond distances are 2.23–2.31 Å, 1.93–1.95 Å and 1.88–1.96 Å, respectively, for low-spin Fe^{III} compounds, and 2.40–2.44 Å, 1.96–1.99 Å and 2.05–2.15 Å, respectively, for corresponding high-spin Fe^{III} compounds [8]. Comparison of the bond distances of Cs[Fe(5-Br-thsa)₂] involving the Fe^{III} atom and the donor atoms (Table 3.3.2) suggests that the present compound contains low-spin Fe^{III} at 293 K.

The distortion of the Fe^{III}O₂N₂S₂ unit results from the constraints imposed by the five- and six-membered chelate rings formed. The six-membered chelate ring involves a significantly wider bite angle than the ideal octahedral 90° [O11–Fe–N11 = 94.35(12)° and O21–Fe–N21 = 93.78(12)°], while the bite angle is narrowed in the five-membered chelate ring [S11–Fe–N11 = 86.01(9)° and S21–Fe–N21 = 86.07(9)°]. There is no major strain relief through puckering: the root mean-square deviations from their least-squares plane of atoms comprising the six-membered [Fe1 N11 C17 C11 C12 O11] and [Fe1 N21 C27 C21 C22 O21] chelate rings are 0.034 and 0.038 Å, respectively; corresponding values for the five-membered [Fe1 N11 N12 C18 S11] and [Fe1 N21 N22 C28 S21] chelate rings are 0.014 and 0.009 Å, respectively. Compared with the 120° angles in a regular hexagon, the O–Fe–N bite angle is deficient by *ca.* 26°; each of the remaining angles in the six-

membered rings is within 2° of 125° . Because the angle at the vertex of a regular pentagon is 108° , the S–Fe–N bite angles are deficient by only 22° . However, the C–S–Fe angles are only about 95° , providing an additional deficiency of 13° and a total which could be neatly offset by increasing the other angles to *ca.* 120° . (In fact, the N–N–C angles are $<120^\circ$ and the N–C–S are $>120^\circ$.) Such 120° angles are consistent with sp^2 hybridisation at C and N atoms. The stability of the Fe^{III} complex is enhanced by the high degree of electron delocalisation throughout the chelated ligands.

The bond distances of the ligands coordinated to the Fe^{III} cation in $\text{Cs}[\text{Fe}(\text{5-Br-thsa})_2]$ can be related to the bond order. The C–S, C–N and N–N bond distances obtained for the present compound show characteristics of a bond order between single and double bonds. As expected, the C18–S11 bond distance of $1.750(4)$ Å and C28–S21 bond distance of $1.753(4)$ Å suggest a partial electron delocalisation of these bonds. Ryabova *et al.*, [21] reported the related low-spin compound $\text{NH}_4[\text{Fe}(\text{5-Br-thsa})_2]$ at 298 K which crystallises in the centrosymmetric space group $Pnca$ with $Z' = 0.5$ (where Z is the number of formula units per unit cell and Z' is the number of formula units per asymmetric unit). Thus the ligands coordinated around the Fe^{III} cation are related by symmetry. The C–S bond distances of $\text{Cs}[\text{Fe}(\text{5-Br-thsa})_2]$ correspond with the C–S bond distance of $1.750(9)$ Å for $\text{NH}_4[\text{Fe}(\text{5-Br-thsa})_2]$ suggesting the occurrence of partial electron delocalisation in both compounds. Furthermore, the electron delocalisation of the ligands is confirmed by a bond order larger than 1 for the C–N bond involving the deprotonated hydrazinic N atom. The bond distances for the C17–N11 and C27–N21 bonds in the present compound are $1.281(5)$ Å and $1.296(5)$ Å, respectively, which are similar to the C–N bond distance ($1.292(10)$ Å) reported for $\text{NH}_4[\text{Fe}(\text{5-Br-thsa})_2]$ [21]. In addition, the N–N bond distances of $\text{Cs}[\text{Fe}(\text{5-Br-thsa})_2]$ are N11–N12 = $1.394(4)$ Å and N21–N22 = $1.401(4)$ Å, respectively, indicating partial electron delocalisation.

The Cs^+ cation of $\text{Cs}[\text{Fe}(\text{5-Br-thsa})_2]$ is at the centre of an irregular seven-donor atom polyhedron, the donor atoms of which originate from three symmetry-related equivalents of both symmetry-independent ligands. Selected geometric parameters are listed in Table 3.3.2.

Several donor atoms coordinated to the Fe atom of $\text{Cs}[\text{Fe}(\text{5-Br-thsa})_2]$ form interactions with the Cs^+ ion in the second coordination sphere, modulating the electron density of the Fe-donor atom bonds and hence influencing the electronic state of the Fe^{III} cation.

The phenolate O11 and O21 Fe^{III} donor atoms bind to the Cs^+ cation within the same Fe^{III} unit. The Cs–O distances are Cs1–O11 = $3.220(3)$ Å and Cs1–O21 = $3.129(3)$ Å, which is somewhat longer than the mean Cs–O bond distance of $3.074(1)$ Å in the hydrated Cs^+ cation [22]. The small O11–Cs1–O21 bond angle of $50.34(7)^\circ$ is a corollary of the closeness of the two ligands bound to Fe^{III} . The Cs1⋯Fe separation involving the \square -diphenolate bridge is $4.2703(6)$ Å and the Cs–O–Fe bond angles are Cs1–O11–Fe = $109.12(11)^\circ$ and Cs1–O21–Fe = $112.16(11)^\circ$.

The thiolate S11ⁱ and S21ⁱ [symmetry code: (i) x, y, z - 1] Fe^{III}-donor atoms coordinate to the Cs⁺ cation with bond distances of 3.7159(11) Å and 3.5564(11) Å, respectively. Moreover, the terminal N23ⁱ atom of the same Fe^{III} unit forms a bond with the Cs⁺ cation, with a Cs1–N23ⁱ bond distance of 3.699(4) Å. The proximity of N23 and S21 is shown by the small N23ⁱ–Cs1–S21ⁱ bond angle of 42.99(6)°, whereas the small S21ⁱ–Cs1–S11ⁱ bond angle of 53.27(2)° is related to the vicinity of the two ligands bound to Fe^{III}. Furthermore, the thiolate S-donor atoms coordinate to the Cs⁺ cation, as well as to the Fe^{III} cation, which gives rise to the Cs1⋯Feⁱ separation of 4.7695(6) Å [symmetry code: (i) x, y, z - 1]. The Cs–S–Fe bond angles involving the □-dithiolate bridge are Cs1–S11ⁱ–Fe = 103.80(4)° and Cs1–S21ⁱ–Fe = 108.55(4)°. In addition, the atoms N12ⁱⁱ and N22ⁱⁱⁱ [symmetry codes: (ii) x, -y + 1/2, z - 1/2; (iii) x, -y + 3/2, z - 1/2] next to the imine N-donor atoms in the first coordination sphere of Fe^{III} are also coordinated to the Cs⁺ cation. The bond distances for the Cs1–N12ⁱⁱ and Cs1–N22ⁱⁱⁱ bonds in Cs[Fe(5-Br-thsa)₂] are 3.326(3) Å and 3.470(3) Å, respectively.

The Cs⁺⋯Cs⁺ separations of 7.4530(5) Å for Cs1⋯Cs1 (x, -y + 3/2, z + 1/2) and 7.6404(5) Å for Cs1⋯Cs1 (x, -y + 1/2, z - 1/2) do correlate with the shortest Fe^{III}⋯Fe^{III} separations in Cs[Fe(5-Br-thsa)₂]. These are 7.5369(9) Å for Fe⋯Fe (x, -y + 3/2, z + 1/2) and 7.5559(6) Å for Fe⋯Fe (x, -y + 1/2, z - 1/2).

The previously reported compound, Cs[Fe(3-OEt-thsa-Me)₂]·CH₃OH, displays Fe^{III}⋯Fe^{III} (x + 1, y, z) separations of 8.486 Å (Section 3.2 *vide supra*). The absence of the solvent molecule in Cs[Fe(5-Br-thsa)₂] allows the Fe^{III} entities to be closer to each other in the crystal lattice compared to those in the latter compound. Furthermore, the R-R'-substituents of the ligands coordinated to the Fe^{III} atom, 5-bromosalicylaldehyde thiosemicarbazone in the present compound and 3-ethoxysalicylaldehyde 4-methylthiosemicarbazone in Cs[Fe(3-OEt-thsa-Me)₂]·CH₃OH, might have some effect as to how the Fe^{III} entities are assembled in the crystal lattice. The size and position of the R, R'-substituted groups are different, as Cs[Fe(5-Br-thsa)₂] contains the Br-substituent on the C15/C25 labelled atom of the salicylaldehyde moiety, whereas Cs[Fe(3-OEt-thsa-Me)₂]·CH₃OH contains a relatively bulky ethoxy group on the C13/C23 atom of the salicylaldehyde moiety as well as a methyl substituent on the terminal nitrogen atom of the thiosemicarbazide moiety. In addition, the Br-substituent of one Fe^{III} unit of Cs[Fe(5-Br-thsa)₂] provides a hydrogen bonding interaction with an amino group of a neighbouring Fe^{III} unit (*vide infra*). The occurrence of the intermolecular hydrogen bonding interactions between the Fe^{III} units in Cs[Fe(5-Br-thsa)₂] contributes to the arrangement of the Fe^{III} entities in the unit cell.

The hydrogen bonding interactions of Cs[Fe(5-Br-thsa)₂] are listed in Table 3.3.3 and displayed in Figure 3.3.2. The main features of the molecular packing of the present compound are the N–H⋯O and N–H⋯Br hydrogen bonds. Although the latter are weak, their grip on the bromine atoms is augmented by C–H⋯Br interactions at similar H⋯Br contact distances. The N13–H13B⋯Br2^v (-x + 1, -y - 1/2, -z + 3/2) and N13–H13A⋯O21^{iv} (x, -y + 1/2, z + 1/2) contacts form hydrogen bonds to

two different ring systems. In turn the O21 atom in the first system and Br2 in the second accept hydrogen bonds from inversion-related N13 ($-x + 1, -y, -z + 2$), giving rise to $R_4^4(18)$ rings [20]. In a similar manner, the N23–H23B \cdots Br1^{vii} ($-x + 2, y + 1/2, -z + 3/2$) and N23–H23A \cdots O11^{vi} ($x, -y + 3/2, z + 1/2$) contacts create $R_4^4(18)$ rings with inversion-related N23 ($-x + 2, -y + 2, -z + 2$). The ring systems created by the hydrogen bonding between the Fe^{III} entities link them in the *a* and *b* directions. Furthermore, the Cs⁺ cations link the Fe^{III} complex anions in a chain along [010].



Figure 3.3.2 A projection showing the unit cell of Cs[Fe(5-Br-thsa)₂]. The Cs⁺ cation has been omitted for clarity. Displacement ellipsoids are drawn at the 50% probability level. Dashed lines indicate hydrogen bonds. [Symmetry codes: (iv) $x, -y + 1/2, z + 1/2$; (v) $-x + 1, y - 1/2, -z + 3/2$; (vi) $x, -y + 3/2, z + 1/2$; (vii) $-x + 2, y + 1/2, -z + 3/2$; (viii) $-x + 2, y + 1/2, -z + 1/2$; (ix) $-x + 1, y - 1/2, -z + 1/2$.]

Table 3.3.3 Hydrogen bond geometry of Cs[Fe(5-Br-thsa)₂] (Å, °)

<i>D</i> –H \cdots <i>A</i>	<i>D</i> –H (Å)	H \cdots <i>A</i> (Å)	<i>D</i> \cdots <i>A</i> (Å)	<i>D</i> –H \cdots <i>A</i> (°)
N13–H13A \cdots O21 ^{iv}	0.86	2.08	2.908(5)	161
N13–H31B \cdots Br2 ^v	0.86	2.73	3.557(4)	163

Table 3.3.3 Hydrogen bond geometry of Cs[Fe(5-Br-thsa)₂] (Å, °) (continued)

<i>D</i> – <i>H</i> ··· <i>A</i>	<i>D</i> – <i>H</i> (Å)	<i>H</i> ··· <i>A</i> (Å)	<i>D</i> ··· <i>A</i> (Å)	<i>D</i> – <i>H</i> ··· <i>A</i> (°)
N23–H23A···O11 ⁱⁱⁱ	0.86	2.10	2.952(5)	171
N23–H23B···Br1 ^{vii}	0.86	2.95	3.590(4)	133
C13–H13···Br1 ^{viii}	0.93	2.83	3.578(5)	139
C23–H23···Br2 ^{ix}	0.93	2.86	3.623(5)	141

Symmetry codes: (iv) $x, -y + 1/2, z + 1/2$; (v) $-x + 1, y - 1/2, -z + 3/2$; (vi) $x, -y + 3/2, z + 1/2$; (vii) $-x + 2, y + 1/2, -z + 3/2$; (viii) $-x + 2, y + 1/2, -z + 1/2$; (ix) $-x + 1, y - 1/2, -z + 1/2$.

3.3.3 Magnetic Studies of Cs[Fe(5-Br-thsa)₂]

The temperature dependence of the $\chi_M T$ product (χ_M being the molar magnetic susceptibility and T, temperature) for the compound Cs[Fe(5-Br-thsa)₂] was measured in the temperature range 10-300 K and is given in Figure 3.3.3. Concomitant with the crystallographic study of Cs[Fe(5-Br-thsa)₂] at 293 K, Cs[Fe(5-Br-thsa)₂] was found to be low-spin at 300 K as $\chi_M T = 0.488 \text{ cm}^3 \text{ mol}^{-1} \text{ K}$, which corresponds to the low-spin value expected for Fe^{III} ($0.375 \text{ cm}^3 \text{ mol}^{-1} \text{ K}$, $g = 2.00$), revealing no spin transition within the temperature range 10-300 K.

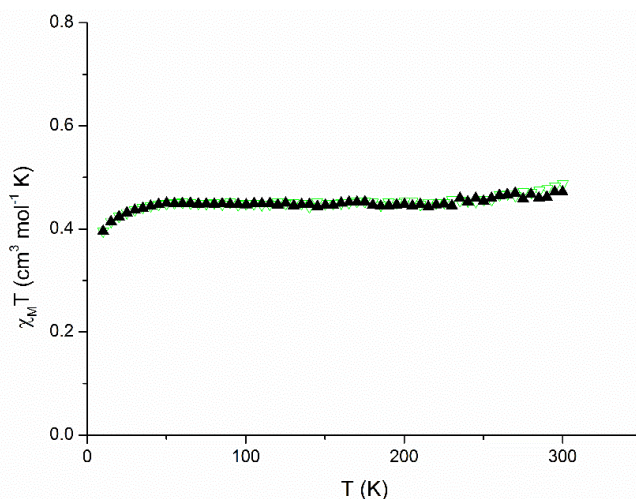


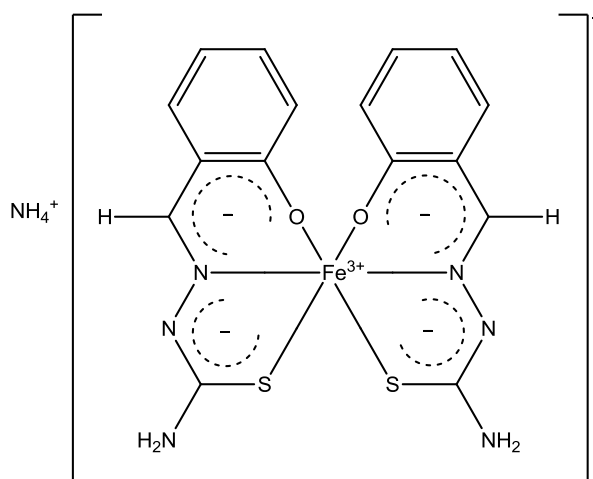
Figure 3.3.3 $\chi_M T$ vs T plot of Cs[Fe(5-Br-thsa)₂]. [The sample was heated (▲) and subsequently cooled (▼).]

3.4 The crystal structure and magnetic properties of ammonium bis(salicylaldehyde thiosemicarbazonato(2-)- κ^3 -O,*N*^I,*S*)ferrate(III)

It has been recognised that ferric complexes, particularly those formed with R-salicylaldehyde 4R'-thiosemicarbazone type ligands are of considerable interest due to their magnetic behaviour. The

spin-crossover properties for $(\text{cation}^+)[\text{Fe}(\text{L}^{2-})_2] \cdot x\text{H}_2\text{O}$ type compounds are quite sensitive to changes in the non-coordinating cation, the number of water molecules, the nature of the R-substituent attached to the salicylaldehyde moiety, and the introduction of the R'-substituent attached to the thiosemicarbazone moiety [2, 3, 6, 8, 18, 19, 21, 25].

In the present section, the variable-temperature magnetic properties and the crystal structure (determined at 100 K) of the complex $\text{NH}_4[\text{Fe}(\text{thsa})_2]$ where thsa is the dianion of salicylaldehyde thiosemicarbazone (as illustrated in Scheme 3.4.1) are described. Ryabova *et al.*, reported the crystallographic data of the related compound $\text{Cs}[\text{Fe}(\text{thsa})_2]$ [18] at 103 and 298 K. The main difference between $\text{NH}_4[\text{Fe}(\text{thsa})_2]$ and $\text{Cs}[\text{Fe}(\text{thsa})_2]$ is the associated outer-sphere cation. The influence of the varying cation on the magnetic properties of these compounds will be investigated by examining the subtle structural and electronic modifications the cation may cause to the crystal packing.



Scheme 3.4.1

3.4.1 Crystal Data and Structure Refinement Details of $\text{NH}_4[\text{Fe}(\text{thsa})_2]$

Crystal data, data collection and structure refinement details are summarized in Table 3.4.1. The position of the hydrogen atoms on the secondary amine nitrogen atoms N3 and N6 were located in difference Fourier maps and were allowed to ride in the refinement, with $U_{\text{iso}}(\text{H}) = 1.2U_{\text{eq}}(\text{N})$. Other hydrogen atoms were included in the refinement in calculated positions, riding on their parent atoms, with $\text{C-H} = 0.96 \text{ \AA}$ and $U_{\text{iso}}(\text{H}) = 1.2U_{\text{eq}}(\text{C})$. The hydrogen atoms on the NH_4^+ cation have not been located but are included in the molecular formula.

Table 3.4.1 Crystal data and structure refinement details of NH₄[Fe(thsa)₂]

Crystal data	
Chemical formula	NH ₄ [Fe(C ₈ H ₇ N ₃ OS) ₂]
M_r	460.30
Crystal system, space group	Monoclinic, $P2_1/n$
Temperature (K)	100
a, b, c (Å)	8.4393(8), 18.2444(17), 11.7635(11)
α, β, γ (°)	90, 90.052(4), 90
V (Å ³)	1811.2(3)
Z	4
Radiation type	Mo $K\alpha$
μ (mm ⁻¹)	1.093
Crystal size (mm)	0.60 × 0.36 × 0.18
Colour	Dark green (rhombic prism)
Data collection	
Diffractometer	Bruker KAPPA APEX II diffractometer
Absorption correction	Multi-scan (SADABS)
T_{\min}, T_{\max}	0.63, 0.82
No. of measured, independent and observed [$I > 2\sigma(I)$] reflections	61584, 5352, 4735
R_{int}	0.0411
Refinement	
$R[F^2 > 2\sigma(F^2)], wR(F^2), S$	0.0418, 0.0543, 3.140 ⁱ
No. of reflections	5352
No. of parameters	280
No. of restraints	40
H-atom treatment	H atoms treated by a mixture of independent and constrained refinement
$\Delta\rho_{\text{max}}, \Delta\rho_{\text{min}}$ (e Å ⁻³)	0.83, -0.76

ⁱ It should be noted that S (goodness of fit) should be close to 1, the goodness of fit value of 3.140 has been reported to the crystallographer at Vienna University of Technology.

The program used for data collection, cell refinement and data reduction: *SAINT-Plus* [23]. The program(s) used for the structure solution and the structure refinement: *SADABS* [23], *SUPERFLIP* [13], *JANA2006* [24]. The *ORTEP-3* for Windows [16] program was used to produce the molecular graphics.

3.4.2 Crystallographic study of $\text{NH}_4[\text{Fe}(\text{thsa})_2]$

The structure of ammonium bis(salicylaldehyde thiosemicarbazonato(2-)- κ^3 -O,N',S)ferrate(III) (Figure 3.4.1) was determined at 100 K. $\text{NH}_4[\text{Fe}(\text{thsa})_2]$ was found to crystallise in the monoclinic system in the space group $P2_1/n$. The asymmetric unit consists of one formula unit, $\text{NH}_4[\text{Fe}(\text{thsa})_2]$, with no atom on a special position. The Fe^{III} cation is coordinated by two dianionic O,N,S-tridentate salicylaldehyde thiosemicarbazonato ligands, displaying a distorted octahedral $\text{Fe}^{\text{III}}\text{O}_2\text{N}_2\text{S}_2$ geometry. Selected geometric parameters are listed in Table 3.4.2. The two-fold deprotonated ligands are coordinated to the Fe^{III} atom with the phenolate-O, thiolate-S and imine-N atoms. These donor atom– Fe^{III} bonds are located in two perpendicular planes, the O and S atoms in the *cis* positions, whereby the S1–Fe–S2 bond angle is $92.06(3)^\circ$ and O1–Fe–O2 bond angle is $88.53(10)^\circ$. Also, the N atoms are situated in *trans* positions which is evidenced by the N1–Fe–N4 bond angle of $176.81(10)^\circ$. The $\text{FeO}_2\text{N}_2\text{S}_2$ coordination core is distorted at 100 K, and the Fe–donor atom distances fall within the range expected for Fe^{III} in the low-spin state [8].

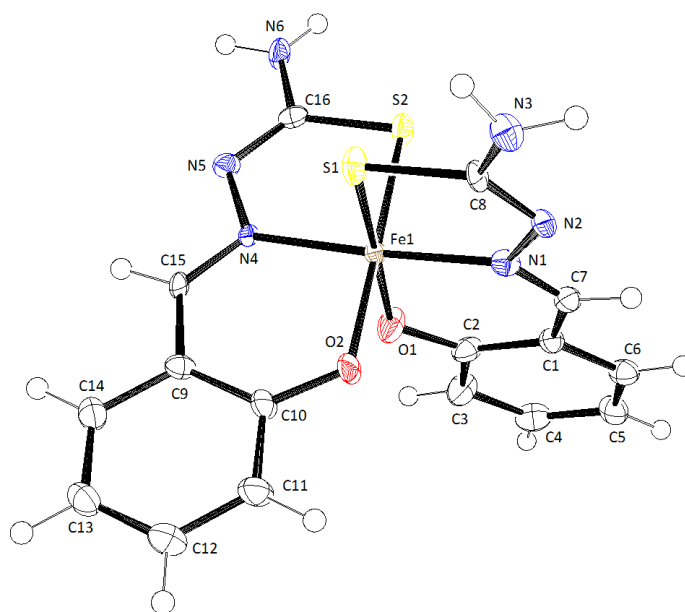


Figure 3.4.1 The molecular structure and atom-numbering scheme for $\text{NH}_4[\text{Fe}(\text{thsa})_2]$. The N atom of the NH_4^+ cation has been omitted from the figure for clarity. Displacements ellipsoids are drawn at the 50% probability level.

The presence of the trivalent iron cation together with the monovalent ammonium cation is supported by the coordination of two two-fold deprotonated ligands to the Fe^{III} ion. In addition, the presence of both dianionic ligands is confirmed by the C–S, C–N and N–N bond distances (listed in Table 3.4.2) obtained for $\text{NH}_4[\text{Fe}(\text{thsa})_2]$, which show characteristics of a bond order between single and double bonds. Ryabova *et al.*, [21] reported the related high-spin compound $\text{Cs}[\text{Fe}(\text{thsa})_2]$ at 103 and

298 K which crystallises in the space group $Pna2_1$ with an asymmetric unit consisting of a Cs^+ cation and a $[\text{Fe}(\text{thsa})_2]^-$ unit. The C–S, C–N and N–N bond distances (C–S = 1.749(9) Å and 1.761(9) Å, C–N = 1.314(10) Å and 1.303(11) Å and N–N = 1.371(11) Å and 1.380(11) Å at 103 K, severally, and C–S = 1.743(14) Å and 1.775(17) Å, C–N = 1.281(19) Å and 1.281(19) Å and N–N = 1.393(18) Å and 1.412(18) Å at 103 K, severally) reported by Ryabova and coworkers [21] for $\text{Cs}[\text{Fe}(\text{thsa})_2]$ at 103 K, correspond to the bond distances for the reported Fe^{III} complex, $\text{NH}_4[\text{Fe}(\text{thsa})_2]$ at 100 K.

Table 3.4.2 Selected geometric parameters of $\text{NH}_4[\text{Fe}(\text{thsa})_2]$ (Å, °)

Fe1–S1	2.2366(9)	Fe1–S2	2.2373(9)
Fe1–O1	1.938(2)	Fe1–O2	1.950(2)
Fe1–N1	1.930(3)	Fe1–N4	1.948(2)
C8–S1	1.742(3)	C16–S2	1.750(3)
C7–N1	1.294(4)	C15–N4	1.291(4)
N1–N2	1.405(3)	N4–N5	1.409(3)
S1–Fe1–S2	92.06(3)	O1–C2–C1	124.4(3)
S1–Fe1–N1	86.53(7)	C2–C1–C7	122.3(3)
S1–Fe1–O1	177.76(7)	C1–C7–N1	126.8(8)
S1–Fe1–O2	89.26(7)	C7–N1–Fe1	126.1(2)
S1–Fe1–N4	91.93(7)	Fe1–O2–C10	126.5(2)
S2–Fe1–O1	90.15(7)	O2–C10–C9	123.7(3)
S2–Fe1–O2	178.58(7)	C10–C9–C15	124.1(3)
S2–Fe1–N1	91.61(7)	C9–C15–N4	126.3(3)
S2–Fe1–N4	85.65(7)	C15–N4–Fe1	124.99(19)
O1–Fe1–O2	88.53(10)	C8–S1–Fe1	94.72(10)
O1–Fe1–N1	93.02(10)	N1–N2–C8	112.9(2)
O1–Fe1–N4	88.63(10)	N2–C8–S1	124.8(2)
O2–Fe1–N1	88.99(10)	C16–S2–Fe1	95.48(10)
O2–Fe1–N4	93.78(10)	N4–N5–C16	113.8(2)
N1–Fe1–N4	176.81(10)	N5–C16–S2	124.2(2)
Fe1–O1–C2	126.5(2)		

The hydrogen bonding interactions of $\text{NH}_4[\text{Fe}(\text{thsa})_2]$ are listed in Table 3.4.3 and are displayed in Figure 3.4.2. The terminal N atoms of the tridentate ligands, N3 and N6, form $\text{N6–Hn62}\cdots\text{O2}$ ($x - 1/2, 1/2 - y, z - 1/2$) and $\text{N3–Hn32}\cdots\text{O1}$ ($x - 1/2, 1/2 - y, 1/2 + z$) contacts with the phenolate O-

donor atoms, O1 and O2, respectively. In this manner, successive Fe^{III} entities are linked in the *c* direction. The ammonium cations are distributed in between the layers of the Fe^{III} entities, with alternate separations of the N atoms of the ammonium cation of 3.915(7) Å (1 + *x*, *y*, *z*) and 4.547(7) Å (1/2 + *x*, 1/2 - *y*, 1/2 + *z*) in the *a* direction. The Fe^{III}...Fe^{III} separations in the present compound are 8.439 Å for Fe^{III}...Fe^{III} (*x* + 1, *y*, *z*) and 9.714 Å for Fe^{III}...Fe^{III} (-*x*, -*y* + 1, -*z* + 1). The Fe^{III} units in NH₄[Fe(*thsa*)₂] are linked by hydrogen bonding interactions between the corresponding Fe^{III} units phenolate O and amino N atoms. The related compound Cs[Fe(5-Br-*thsa*)₂] (Section 3.3, *vide supra*) displays Fe^{III}...Fe^{III} (*x*, 3/2 - *y*, 1/2 + *z*) separations of 7.556 Å and Fe^{III}...Fe^{III} (*x*, 5/2 - *y*, 3/2 + *z*) separations of 7.537 Å. It appears that the addition of the Br-substituent on the salicylaldehyde moiety of the ligand in Cs[Fe(5-Br-*thsa*)₂] may affect how the Fe^{III} units are assembled in the unit cell. The Br-substituent of one Fe^{III} unit of Cs[Fe(5-Br-*thsa*)₂] provides a hydrogen bonding interaction with an amino group of a neighbouring Fe^{III} unit, creating ring systems.

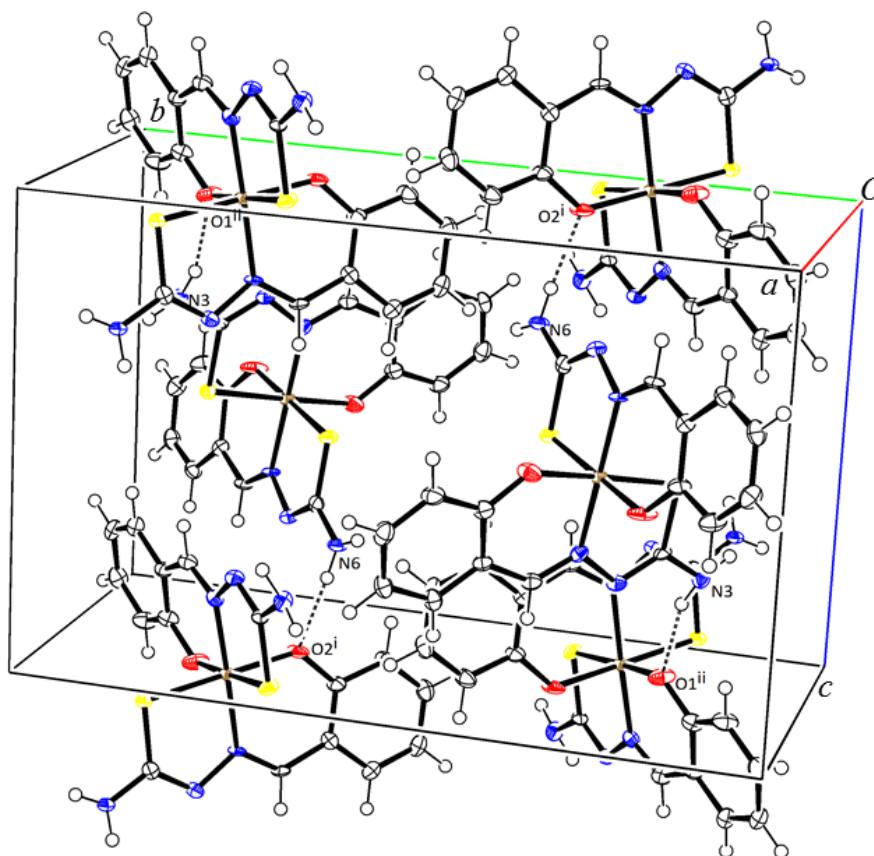


Figure 3.4.2 A projection showing the unit cell of NH₄[Fe(*thsa*)₂]. The N atom of the ammonium cation has been omitted for clarity. Displacement ellipsoids are drawn at the 50% probability level. Dashed lines indicate hydrogen bonds. [Symmetry codes: (i) *x* - 1/2, 1/2 - *y*, *z* - 1/2; (ii) *x* - 1/2, 1/2 - *y*, 1/2 + *z*.]

Table 3.4.3 Hydrogen bond geometry of $\text{NH}_4[\text{Fe}(\text{thsa})_2]$ (\AA , $^\circ$)

$D\text{-H}\cdots A$	$D\text{-H}$	$H\cdots A$	$D\cdots A$	$D\text{-H}\cdots A$
$\text{N6-Hn62}\cdots\text{O2}^{\text{i}}$	0.87 (4)	1.97 (4)	2.387 (3)	173 (3)
$\text{N3-Hn32}\cdots\text{O1}^{\text{ii}}$	0.92 (5)	1.99 (5)	2.880 (4)	160 (4)

Symmetry codes: (i) $x - 1/2, 1/2 - y, z - 1/2$; (ii) $x - 1/2, 1/2 - y, 1/2 + z$.

3.4.3 Magnetic Studies of $\text{NH}_4[\text{Fe}(\text{thsa})_2]$

The temperature dependence of the $\chi_{\text{M}}T$ product (χ_{M} being the molar magnetic susceptibility and T , temperature) for the compound $\text{NH}_4[\text{Fe}(\text{thsa})_2]$ was measured in the temperature range 10-300 K and is given in Figure 3.4.3. At 100 K, the Fe^{III} ion in the crystal structure of $\text{NH}_4[\text{Fe}(\text{thsa})_2]$ was found to be in the low-spin state. The $\chi_{\text{M}}T$ value for $\text{NH}_4[\text{Fe}(\text{thsa})_2]$ corroborates that the Fe^{III} ion is indeed in the low-spin state at this temperature with a $\chi_{\text{M}}T$ value of $0.516 \text{ cm}^3 \text{ mol}^{-1} \text{ K}$ at 100 K. The $\chi_{\text{M}}T$ value for $\text{NH}_4[\text{Fe}(\text{thsa})_2]$ of $0.535 \text{ cm}^3 \text{ mol}^{-1} \text{ K}$ at 300 K reveals no spin transition is observed between the temperature range 10-300 K.

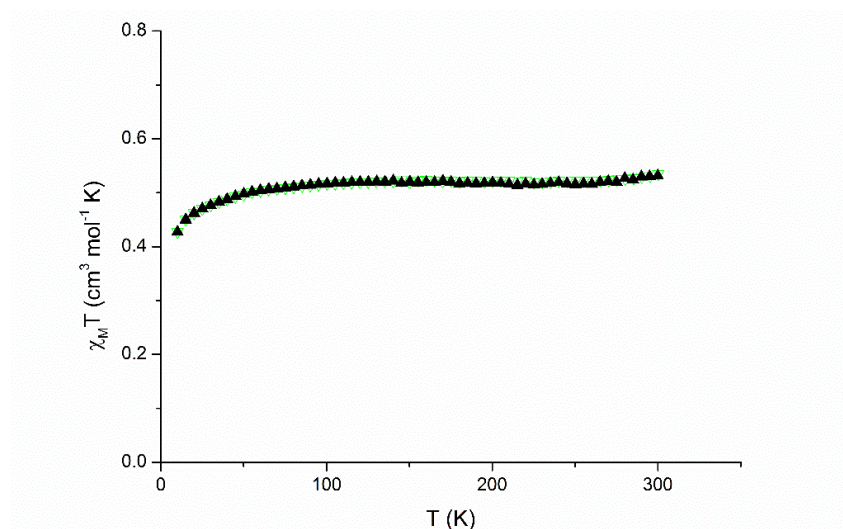


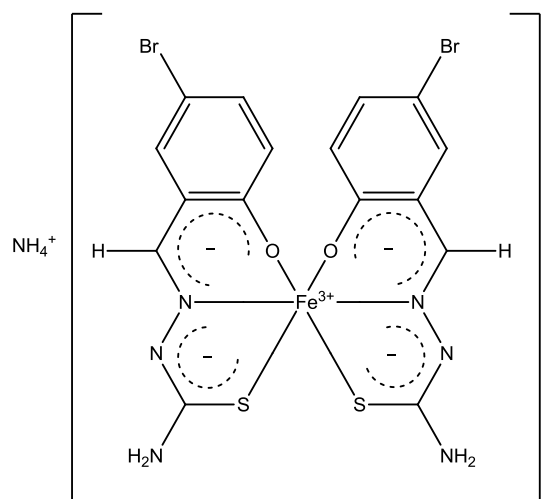
Figure 3.4.3 $\chi_{\text{M}}T$ vs T plot of $\text{NH}_4[\text{Fe}(\text{thsa})_2]$. [The sample was heated (\blacktriangle) and subsequently cooled (\blacktriangledown).]

3.5 The crystal structure and magnetic properties of ammonium bis(5-bromosalicylaldehyde thiosemicarbazonato(2-)- $\kappa^3\text{-O,N}^l\text{,S}$)ferrate(III)

Various $(\text{cation}^+)[\text{Fe}(\text{ligand}^{2-})_2]\cdot n\text{H}_2\text{O}$ type compounds of R-substituted salicylaldehyde thiosemicarbazone have been reported over the past decade [2-4, 8, 18, 19, 21, 25]. This series of compounds has been extensively studied with respect to their crystallographic data in order to attempt to correlate the structural features of these systems with the spin state of Fe^{III} . It is now well

established that significant changes in the electronic state of these Fe^{III} systems may occur due to the associated cation in the complex system, the R-substituents of the salicylaldehyde moiety and/or the R'-substituents of the thioamide group of the thiosemicarbazide moiety and the Fe^{III}O₂N₂S₂ geometry.

In this section, the magnetic behaviour and crystal structure (at 100 K) of NH₄[Fe(5-Br-thsa)₂] (illustrated in Scheme 3.5.1) are described. Ryabova *et al.*, reported the related compound NH₄[Fe(5-Cl-thsa)₂] [19], whereby the structure was determined at 103 and 298 K. The X-ray structure of NH₄[Fe(5-Cl-thsa)₂] at 298 K was found to be isostructural to the tabular form of NH₄[Fe(5-Br-thsa)₂] [21] at 298 K. Both compounds were found to crystallise in the orthorhombic crystal system in the space group *Pnca* at 298 K. It was determined that the ligands coordinated to the Fe^{III} atom by a two-fold rotational symmetry in the Fe^{III} bis(ligand) compounds.



Scheme 3.5.1

In order to attempt to correlate the structures of this family of (cation⁺)[Fe(L²⁻)₂] compounds to their magnetic properties, it has to be considered that the spin transition is governed by subtle structural and electronic modifications tuned by the crystal packing, which determines the ligand field strength and the spin-crossover behaviour. These modifications depend on the nature of the ligands, the non-coordinating cation, the solvent molecules (if any), and the crystal packing. Although, the effects of the aforementioned chemical contributions are not always consistent from one material to another. Indeed, a more systematic approach is required to investigate these modifications on these types of systems. In this regard, comparison of the crystal structure and magnetic properties of NH₄[Fe(5-Br-thsa)₂] (at 100 K) to that of tabular form of NH₄[Fe(5-Br-thsa)₂] (at 298 K) reported by Ryabova *et al.*, [21] are herein described.

3.5.1 Crystal Data and Structure Refinement Details of $\text{NH}_4[\text{Fe}(\text{5-Br-thsa})_2]$

Crystal data, data collection and structure refinement details are summarized in Table 3.5.1. The position of the hydrogen atoms on the secondary amine nitrogen atoms N3 and N6 were located in difference Fourier maps and were allowed to ride in the refinement with $U_{\text{iso}}(\text{H}) = 1.2U_{\text{eq}}(\text{N})$. Other hydrogen atoms were included in the refinement in calculated positions and riding on their parent atoms with $\text{C-H} = 0.96 \text{ \AA}$ and $U_{\text{iso}}(\text{H}) = 1.2U_{\text{eq}}(\text{C})$. The hydrogen atoms on the NH_4^+ cation have not been located but are included in the molecular formula. The ligand molecules in $\text{NH}_4[\text{Fe}(\text{5-Br-thsa})_2]$ are related by a twofold axis of rotation. The ligand shows positional disorder with respect to the following atoms: S1, O1, N4, C2, C3, C4, H3 and H4. Two different sets of positions for these atoms were identified in the difference Fourier synthesis, i.e. S1 and S1', O1 and O1', N4 and N4', C2 and C2', C3 and C3', C4 and C4', H3 and H3', and H4 and H4', severally, which were refined with fixed site occupancy factors (0.5 and 0.5).

3.5.2 Crystallographic study of $\text{NH}_4[\text{Fe}(\text{5-Br-thsa})_2]$

The structure of ammonium bis(5-bromosalicylaldehyde thiosemicarbazonato(2-)- κ^3 -*O,N',S*)ferrate(III) (Figure 3.5.1) was determined at 100 K. $\text{NH}_4[\text{Fe}(\text{5-Br-thsa})_2]$ crystallises in the orthorhombic system in the centrosymmetric space group *Pbcn*, $Z' = 0.5$ (where Z' is the number of formula units per asymmetric unit). The asymmetric unit consists of one NH_4^+ cation and $1/2 [\text{Fe}(\text{5-Br-thsa})_2]$, whereby the ligands coordinated to the Fe^{III} cation are related by two-fold rotational symmetry (symmetry code: (i) $-x, y, -z - 1/2$). The Fe^{III} cation is coordinated by two equivalent dianionic O,N,S-tridentate 5-bromosalicylaldehyde thiosemicarbazonato ligands, displaying a distorted octahedral $\text{Fe}^{\text{III}}\text{O}_2\text{N}_2\text{S}_2$ geometry. Both of the tridentate ligands are found to be in their dianionic form, as no hydrogen atoms were located on the phenolate-O and the thiolate-S atoms. This is also confirmed by the presence of the trivalent iron cation together with the monovalent ammonium cation. Selected geometric parameters are listed in Table 3.5.2.

On the basis of the $\text{FeO}_2\text{N}_2\text{S}_2$ donor bond distances, the spin state of the Fe^{III} ion can be identified. At 100 K, the Fe-S1 and Fe-S1^i ($i = -x, y, -z - 1/2$) distances are $2.263(3) \text{ \AA}$, the Fe-O1 and Fe-O1^i ($i = -x, y, -z - 1/2$) distances are $1.938(6) \text{ \AA}$, and the Fe-N1 and Fe-N1^i ($i = -x, y, -z - 1/2$) distances are $1.9420(18) \text{ \AA}$, typical for low-spin Fe^{III} [8]. Furthermore, the donor atoms of the ligands are situated in two perpendicular planes with O and S atoms in *cis* positions, which is corroborated by the S1-Fe-S1^i bond angle of $82.47(11)^\circ$ and O1-Fe-O1^i bond angle of $73.5(2)^\circ$. In addition, the N atoms are situated in *trans* positions which is confirmed by the N1-Fe-N1^i bond angle of $176.44(7)^\circ$.

Table 3.5.1 Crystal data and structure refinement details of $\text{NH}_4[\text{Fe}(\text{5-Br-thsa})_2]$

Crystal data	
Chemical formula	$\text{NH}_4[\text{Fe}(\text{C}_8\text{H}_6\text{BrN}_3\text{OS})_2]$
M_r	618.10
Crystal system, space group	Orthorhombic, <i>Pbcn</i>
Temperature (K)	100
a, b, c (Å)	11.6901(6), 8.5208(9), 21.0279(15)
α, β, γ (°)	90, 90, 90
V (Å ³)	2094.6(3)
Z	4
Radiation type	Mo $K\alpha$
μ (mm ⁻¹)	4.765
Crystal size (mm)	0.41 × 0.32 × 0.04
Colour	Dark green (rhombic prism)
Data collection	
Diffractometer	Bruker KAPPA APEX II diffractometer
Absorption correction	Multi-scan (<i>SADABS</i>)
T_{\min}, T_{\max}	0.18, 0.83
No. of measured, independent and observed [$I > 2\sigma(I)$] reflections	69081, 3066, 2559
R_{int}	0.0436
Refinement	
$R[F^2 > 2\sigma(F^2)], wR(F^2), S$	0.0287, 0.0416, 2.47 ⁱ
No. of reflections	3066
No. of parameters	184
No. of restraints	24
H-atom treatment	H atoms treated by a mixture of independent and constrained refinement
$\Delta\rho_{\text{max}}, \Delta\rho_{\text{min}}$ (e Å ⁻³)	0.97, -0.64

ⁱ It should be noted that S (goodness of fit) should be close to 1, the goodness of fit value of 2.47 has been reported to the crystallographer at Vienna University of Technology.

The program used for data collection, cell refinement and data reduction: *SAINT-Plus* [23]. The program(s) used for the structure solution and the structure refinement: *SADABS* [23], *SUPERFLIP* [13], *JANA2006* [24]. The *ORTEP-3* for Windows [16] program was used to produce the molecular graphics.

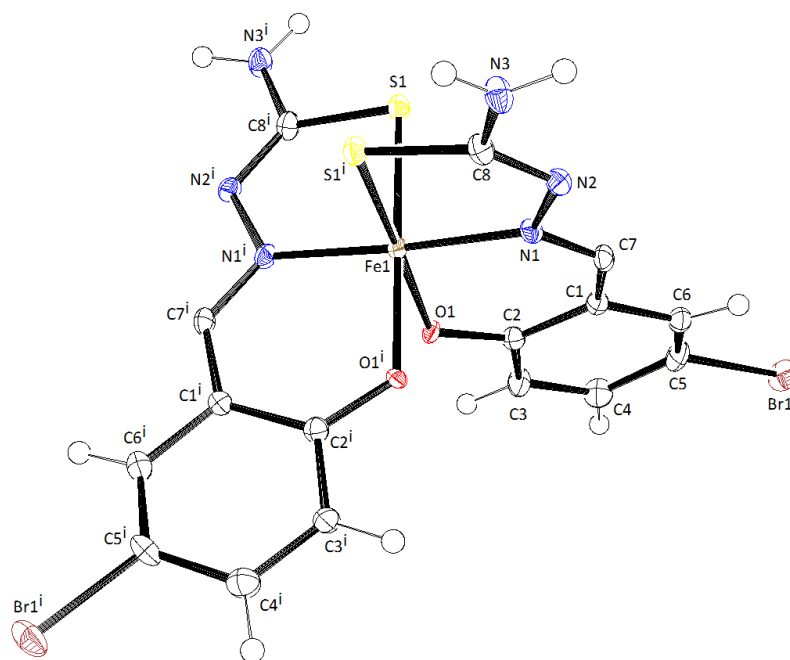


Figure 3.5.1 The molecular structure and atom-numbering scheme for $\text{NH}_4[\text{Fe}(5\text{-Br-thsa})_2]$. The N atom of the NH_4^+ cation, and alternative orientation for O1', S1', C2', C3' and C4' have been omitted from the figure for clarity. Displacements ellipsoids are drawn at the 50% probability level. [Symmetry code: (i) $-x, y, -z - 1/2$.]

Table 3.5.2 Selected geometric parameters of $\text{NH}_4[\text{Fe}(5\text{-Br-thsa})_2]$ (\AA , $^\circ$)

Fe1–S1 ⁱ	2.263(3)	C8 ⁱ –S1 ⁱ	1.769(4)
Fe1–O1 ⁱ	1.938(6)	C7 ⁱ –N1 ⁱ	1.292(4)
Fe1–N1 ⁱ	1.9420(18)	N1 ⁱ –N2 ⁱ	1.401(3)
S1–Fe1–S1 ⁱ	82.47(11)	O1 ⁱ –Fe1–N1	89.9(2)
S1–Fe1–N1	86.10(11)	N1–Fe1–N1 ⁱ	176.44(7)
S1–Fe1–O1	175.46(19)	Fe1–O1–C2	125.1(5)
S1–Fe1–O1 ⁱ	102.00(18)	O1–C2–C1	124.6(5)
S1–Fe1–N1 ⁱ	91.22(11)	C2–C1–C7	122.2(3)
S1 ⁱ –Fe1–O1	102.00(18)	C1–C7–N1	126.2 (19)
S1 ⁱ –Fe1–N1	91.22(11)	C7–N1–Fe1	125.48(15)
O1–Fe1–O1 ⁱ	73.5(2)	C8–S1–Fe1	93.58(16)
O1–Fe1–N1	93.0(2)	N1–N2–C8	113.77(17)
O1–Fe1–N1 ⁱ	89.9(2)	N2–C8–S1	124.5(2)

Symmetry transformation used to generate equivalent atoms: (i) $-x, y, -z - 1/2$.

Both tridentate ligands are found to be in their dianionic form, as no hydrogen atoms were located on the phenolate-O and the thiolate-S atoms. This is also confirmed by the presence of the trivalent iron cation together with the monovalent ammonium cation. Furthermore, this is corroborated by the C–S, C–N and N–N bond distances (listed in Table 3.5.2) obtained for $\text{NH}_4[\text{Fe}(\text{5-Br-thsa})_2]$, which show characteristics of a bond order between single and double bonds. Ryabova *et al.*, [21] reported the structure of the tabular polymorph of the low-spin compound $\text{NH}_4[\text{Fe}(\text{5-Br-thsa})_2]$ at 298 K which crystallises in the centrosymmetric space group *Pnca* with $Z' = 0.5$; the ligands are related by two-fold rotational symmetry. The C–S, C–N and N–N bond distances (C–S = 1.750(9) Å, C–N = 1.294(10) Å and N–N = 1.392(9) Å) reported by Ryabova *et al.*, [21] of this compound are in line with the bond distances for the reported Fe^{III} complex at 100 K.

The crystal packing diagram of $\text{NH}_4[\text{Fe}(\text{5-Br-thsa})_2]$ at 100 K is displayed in Figure 3.5.2 and the hydrogen bonding contacts are listed in Table 3.5.3. The most striking structural feature is the interlinking of mononuclear $[\text{Fe}(\text{L}^{2-})_2]^-$ units by the intermolecular $\text{N3-Hn31}\cdots\text{O1}$ ($1/2 + x, 3/2 - y, -1 - z$) hydrogen bond between the phenolate O-donor atom, O1, and the terminal N3 atom of the symmetry related ligand. A similar intermolecular hydrogen bond is also observed for disordered form of the phenolate O-donor atom, O1', giving rise to the hydrogen bonding contact $\text{N3-Hn31}\cdots\text{O1}'$ ($1/2 + x, 3/2 - y, -1 - z$). These hydrogen bonding interactions between the Fe^{III} entities link them in the *a* direction. The NH_4^+ cations are distributed in between the layers of the Fe^{III} entities, with alternate separations of the N atoms of the ammonium cation of 4.608(4) Å ($1/2 + x, 3/2 + y, -1/2 - z$) and 3.959(4) Å ($1/2 + x, 1/2 + y, -1/2 - z$), respectively, in the *c* direction.

The shortest $\text{Fe}^{\text{III}}\cdots\text{Fe}^{\text{III}}$ separations in $\text{NH}_4[\text{Fe}(\text{5-Br-thsa})_2]$ are 7.233 Å for $\text{Fe}^{\text{III}}\cdots\text{Fe}^{\text{III}}$ ($-x, y + 1, 1/2 - z$) and 7.233 Å for $\text{Fe}^{\text{III}}\cdots\text{Fe}^{\text{III}}$ ($1 - x, y + 1, 1/2 - z$). Additionally, $\text{NH}_4[\text{Fe}(\text{5-Br-thsa})_2]$ displays longer $\text{Fe}^{\text{III}}\cdots\text{Fe}^{\text{III}}$ separations of 8.251 Å for $\text{Fe}^{\text{III}}\cdots\text{Fe}^{\text{III}}$ ($1/2 - x, 1/2 - y, 3/2 + z$) and 8.251 Å for $\text{Fe}^{\text{III}}\cdots\text{Fe}^{\text{III}}$ ($1/2 + x, 3/2 + y, -1/2 - z$). The related compound $\text{Cs}[\text{Fe}(\text{5-Br-thsa})_2]$ (Section 3.3), displays shortest $\text{Fe}^{\text{III}}\cdots\text{Fe}^{\text{III}}$ separations of 7.556 Å for $\text{Fe}^{\text{III}}\cdots\text{Fe}^{\text{III}}$ ($x, 3/2 - y, 1/2 + z$) and 7.537 Å for $\text{Fe}^{\text{III}}\cdots\text{Fe}^{\text{III}}$ ($x, 5/2 - y, 3/2 + z$). Both $\text{NH}_4[\text{Fe}(\text{5-Br-thsa})_2]$ and $\text{Cs}[\text{Fe}(\text{5-Br-thsa})_2]$ contain the dianionic ligand 5-bromosalicylaldehyde thiosemicarbazonato(2-), but differ with respect to the monovalent cation in the crystal lattice. Although both compounds contain the same Br-substituted ligand, the steric effect of the ligand on the manner in which the Fe^{III} units assemble in the unit cell is very different. In $\text{NH}_4[\text{Fe}(\text{5-Br-thsa})_2]$, the Br-substituent of one Fe^{III} unit provides a hydrogen bonding interaction with an amino group of a neighbouring Fe^{III} unit, giving rise to ring systems. However the present compound does not possess hydrogen bonding interactions involving the Br-substituent, and instead corresponding Fe^{III} units are linked in chains by interactions between the phenolate O and imine N atoms (*vide infra*). It appears the hydrogen bonding ring systems in $\text{Cs}[\text{Fe}(\text{5-Br-thsa})_2]$ contribute to the arrangement of the Fe^{III} entities in the unit cell to be closer together compared to that of the present compound's intermolecular hydrogen bonding interactions.

In a similar way to the crystal packing of $\text{NH}_4[\text{Fe}(\text{5-Br-thsa})_2]$ at 100 K, the crystal structure of the tubular polymorph $\text{NH}_4[\text{Fe}(\text{5-Br-thsa})_2]$ reported at 298 K by Ryabova and co-workers [22] indicates that the structural units are linked by $\text{N-H}\cdots\text{O}$ contacts, formed from the terminal N-atom and the phenolate O-donor atom, along the c axis. This indicates that at both 100 K and 298 K, the crystal packing of the Fe^{III} entities are very similar.

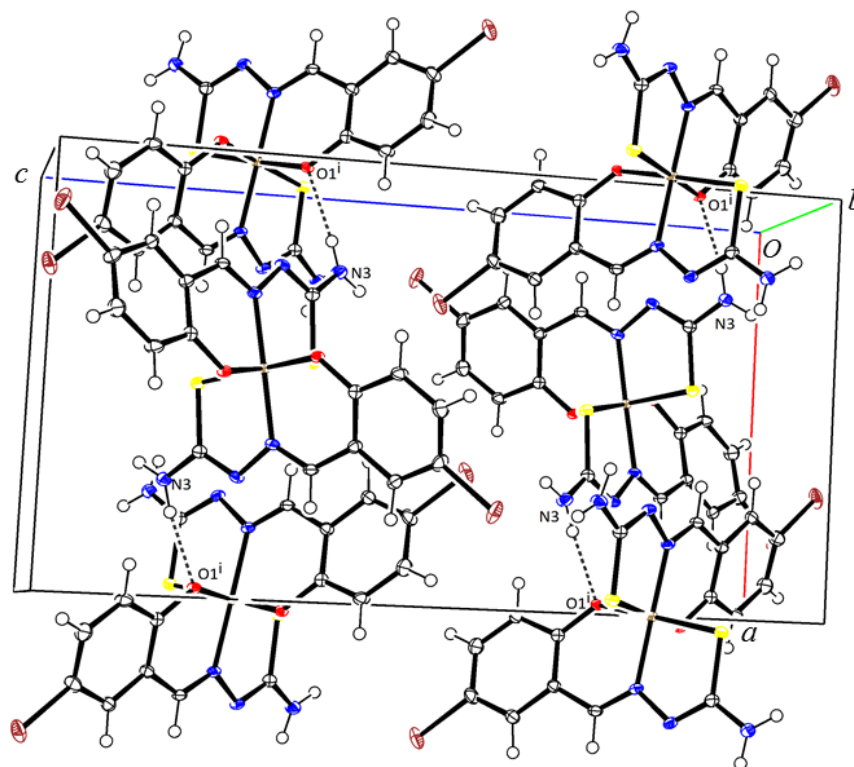


Figure 3.5.2 A projection showing the unit cell of $\text{NH}_4[\text{Fe}(\text{5-Br-thsa})_2]$. The N atom of the NH_4^+ cation and alternative orientation for $\text{O1}'$, $\text{S1}'$, $\text{C2}'$, $\text{C3}'$ and $\text{C4}'$ have been omitted for clarity. Displacements ellipsoids are drawn at the 50% probability level. Dashed lines indicate hydrogen bonds. [Symmetry codes: (i) $1/2 + x, 3/2 - y, -1 - z$; (ii) $1/2 + x, 3/2 - y, -1 - z$.]

Table 3.5.3 Hydrogen bond geometry of $\text{NH}_4[\text{Fe}(\text{5-Br-thsa})_2]$ (\AA , $^\circ$)

$D\text{-H}\cdots A$	$D\text{-H}$	$H\cdots A$	$D\cdots A$	$D\text{-H}\cdots A$
$\text{N3-Hn31}\cdots\text{O1}^{\text{i}}$	0.89 (2)	2.06 (3)	2.935 (7)	168 (3)
$\text{N3-Hn31}\cdots\text{O1}^{\text{ii}}$	0.89 (2)	1.92 (3)	2.807 (7)	177 (2)

Symmetry codes: (i) $1/2 + x, 3/2 - y, -1 - z$; (ii) $1/2 + x, 3/2 - y, -1 - z$.

3.5.3 Magnetic Studies of $\text{NH}_4[\text{Fe}(\text{5-Br-thsa})_2]$

The temperature dependence of the $\chi_M T$ product (χ_M being the molar magnetic susceptibility and T, temperature) for the compound $\text{NH}_4[\text{Fe}(\text{5-Br-thsa})_2]$ was measured in the temperature range 10-300 K and is given in Figure 3.5.3. At 100 K, the Fe^{III} ion in the crystal structure of $\text{NH}_4[\text{Fe}(\text{5-Br-thsa})_2]$ was found to be in the low-spin state which corroborates with the $\chi_M T$ value for $\text{NH}_4[\text{Fe}(\text{5-Br-thsa})_2]$ of being $0.65 \text{ cm}^3 \text{ mol}^{-1} \text{ K}$ at 100 K, which is close to the value expected for a low-spin Fe^{III} ion. Around 200 K, there is an abrupt change in the product $\chi_M T$; the value of $\chi_M T$ for $\text{NH}_4[\text{Fe}(\text{5-Br-thsa})_2]$ increases to $0.85 \text{ cm}^3 \text{ mol}^{-1} \text{ K}$ at 250 K. At this stage, it is important to note that the sample is homogeneous, as the crystals synthesised were found to be in the tabular form. The increase in the product of magnetic susceptibility and temperature could be due to only a minute fraction of the Fe^{III} ions converting into the high-spin state. The observed $\chi_M T$ value at 250 K of $0.85 \text{ cm}^3 \text{ mol}^{-1} \text{ K}$ corresponds to an estimated high-spin fraction of 12 % and an estimated 88 % low-spin fraction of Fe^{III} ions. Thus, observing that the spin transition occurs at $T_{1/2\uparrow} = 200 \text{ K}$ and $T_{1/2\downarrow} = 198 \text{ K}$.

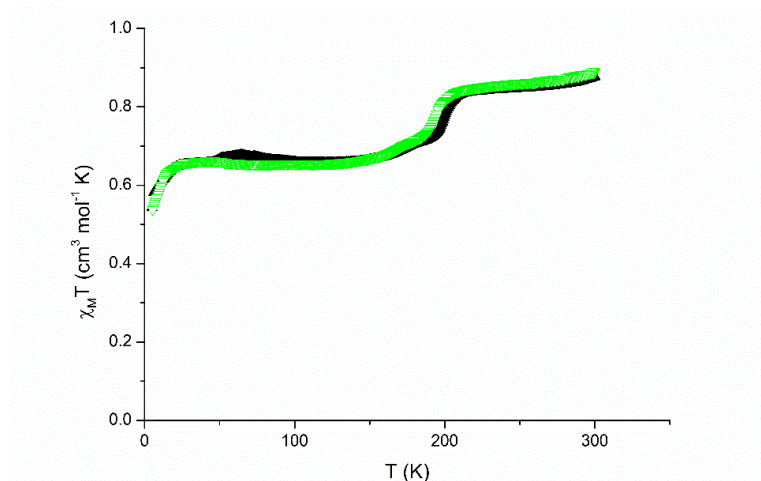


Figure 3.5.3 $\chi_M T$ vs T plot of $\text{NH}_4[\text{Fe}(\text{5-Br-thsa})_2]$. [The sample was heated (\blacktriangle) and subsequently cooled (\blacktriangledown).]

Although, it still remains that for the bulk of the Fe^{III} sample, the Fe^{III} ions are in the low-spin state, as the value of $\chi_M T = 0.85 \text{ cm}^3 \text{ mol}^{-1} \text{ K}$ at 250 K is higher than that expected for a low-spin compound ($\chi_M T = 0.374 \text{ cm}^3 \text{ mol}^{-1} \text{ K}$, when $g = 2.00$) and not as expected for high-spin Fe^{III} ($\chi_M T = 4.37 \text{ cm}^3 \text{ mol}^{-1} \text{ K}$). It should be noted that the value of $\chi_M T = 0.85 \text{ cm}^3 \text{ mol}^{-1} \text{ K}$ at 100 K, which is also higher than the expected value for Fe^{III} ions in the low-spin state, this value slightly higher than expected value may be due to some residual high-spin Fe^{III} ions. Moreover, the decrease of the $\chi_M T$ value between 5-20 K may be due to the zero-field splitting of the high-spin Fe^{III} ions. In order to accurately measure the percentage of Fe^{III} ions which convert to the high-spin state at 200 K, the measurement of the ^{57}Fe Mössbauer spectroscopic data would be advantageous to assess the percentage of the high-spin and low-spin Fe^{III} at particular temperatures.

The DSC curve of $\text{NH}_4[\text{Fe}(\text{5-Br-thsa})_2]$ is displayed in Figure 3.5.4. The DSC curve displays a peak at $T_{\downarrow} = 199 \text{ K}$ in the cooling mode and $T_{\uparrow} = 201 \text{ K}$ in the heating mode. The resultant data corroborates with the temperature dependent magnetic susceptibility data that the Fe^{III} entities exhibit a spin transition at around 200 K.

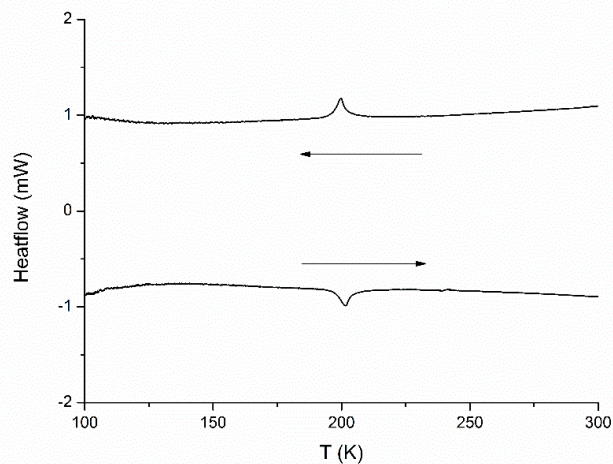
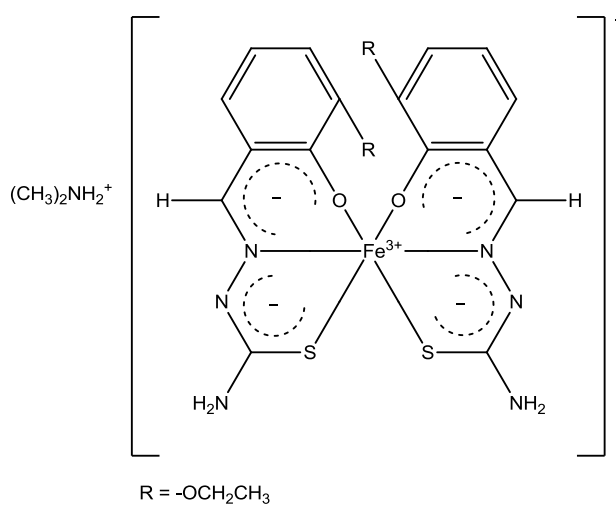


Figure 3.5.4 DSC curves obtained for $\text{NH}_4[\text{Fe}(\text{5-Br-thsa})_2]$ in the temperature range 100-300 K, measured at a scan rate of 5 K min^{-1} .

3.6 The synthesis, structure and magnetic properties of dimethylammonium bis(3-ethoxysalicylaldehyde thiosemicarbazonato(2-)- $\kappa^3\text{-O}^l, \text{N}^l, \text{S}$)ferrate(III)

In the following section the magnetic properties of the compound $(\text{CH}_3)_2\text{NH}_2[\text{Fe}(\text{3-OEt-thsa})_2]$ (illustrated in scheme 3.6.1) are described, as well as the crystal structure at 100 K. The synthesis of $(\text{CH}_3)_2\text{NH}_2[\text{Fe}(\text{3-OEt-thsa})_2]$ and the corresponding H_2L ligand, 3-ethoxysalicylaldehyde thiosemicarbazone is described in Chapter II – Materials and Methods.



Scheme 3.6.1

3.6.1 Crystal Data and Structure Refinement Details of $(\text{CH}_3)_2\text{NH}_2[\text{Fe}(\text{3-OEt-thsa})_2]$

Crystal data, data collection and structure refinement details are summarised in Table 3.6.1. The H-atoms of the terminal amine atoms N103 and N3 were located in difference Fourier maps and refined with restrained N–H distances of 0.86(2) Å and with $U_{\text{iso}}(\text{H}) = 1.2 U_{\text{eq}}(\text{N})$. The remaining H-atoms were included in the refinement in calculated positions and treated as riding on their parent atoms, with N–H distance of 0.91 Å and $U_{\text{iso}}(\text{H}) = 1.2 U_{\text{eq}}(\text{N})$ for the amine N atom of the cation, C–H distance of 0.95 Å and $U_{\text{iso}}(\text{H}) = 1.2 U_{\text{eq}}(\text{C})$ for aryl (–CH=) H-atoms, C–H distance of 0.99 Å and $U_{\text{iso}}(\text{H}) = 1.2 U_{\text{eq}}(\text{C})$ for the secondary (–CH₂–) H-atoms and C–H distance of 0.98 Å and $U_{\text{iso}}(\text{H}) = 1.5 U_{\text{eq}}(\text{C})$ for the methyl (–CH₃) H-atoms.

Table 3.6.1 Crystal data and structure refinement details of $(\text{CH}_3)_2\text{NH}_2[\text{Fe}(\text{3-OEt-thsa})_2]$

Crystal data	
Chemical formula	$(\text{CH}_3)_2\text{NH}_2[\text{Fe}(\text{C}_{10}\text{H}_{11}\text{O}_2\text{N}_3\text{S})_2]$
M_r	576.50
Crystal system, space group	Monoclinic, $P2_1/n$
Temperature (K)	100
a, b, c (Å)	9.4359(3), 16.0265(5), 17.2333(7)
α, β, γ (°)	90, 98.668(4), 90
V (Å ³)	2576.35(17)
Z	4
Radiation type	Mo $K\alpha$
μ (mm ⁻¹)	0.79
Crystal size (mm)	0.08 × 0.05 × 0.01
Colour	Green (plate)
Data collection	
Diffractometer	Rigaku AFC12 four-circle Kappa diffractometer
Absorption correction	Multi-scan (<i>CrystalClear-SM Expert</i> [12])
$T_{\text{min}}, T_{\text{max}}$	0.661, 1.000
No. of measured, independent and observed [$I > 2\sigma(I)$] reflections	16969, 5903, 4415
R_{int}	0.055

Table 3.6.1 Crystal data and structure refinement details of $(\text{CH}_3)_2\text{NH}_2[\text{Fe}(\text{3-OEt-thsa})_2]$ (continued).

Refinement	
$R[F^2 > 2\sigma(F^2)], wR(F^2), S$	0.044, 0.096, 1.02
No. of reflections	5903
No. of parameters	341
No. of restraints	4
H-atom treatment	H atoms treated by a mixture of independent and constrained refinement
$\Delta\rho_{\text{max}}, \Delta\rho_{\text{min}}$ (e \AA^{-3})	0.38, -0.38

The program used for data collection, cell refinement and data reduction: *CrystalClear-SM Expert* [12]. The program(s) used for the structure solution and the structure refinement: *SUPERFLIP* [13], *SHELXL* [11]. The *ORTEP-3* for Windows [16] program was used to produce the molecular graphics.

3.6.2 Crystallographic study of $(\text{CH}_3)_2\text{NH}_2[\text{Fe}(\text{3-OEt-thsa})_2]$

The structure of dimethylammonium bis(3-ethoxysalicylaldehyde thiosemicarbazonato(2-)- κ^3 - O^2, N^1, S)ferrate(III) (Figure 3.6.1) was determined at 100 K. The present compound has been found to crystallise in the monoclinic system in the space group $P2_1/n$ with $Z = 4$. The asymmetric unit consists of one formula unit, $(\text{CH}_3)_2\text{NH}_2[\text{Fe}(\text{3-OEt-thsa})_2]$, with no atom on a special position. The Fe^{III} cation is coordinated by two dianionic O,N,S-tridentate 3-ethoxysalicylaldehyde thiosemicarbazonato(2-) ligands, displaying a distorted octahedral $\text{Fe}^{\text{III}}\text{O}_2\text{N}_2\text{S}_2$ coordination sphere. Selected geometric parameters are listed in Table 3.6.2 and Table 3.6.3.

The $\text{Fe}^{\text{III}}\text{O}_2\text{N}_2\text{S}_2$ coordination sphere displays a distorted octahedral geometry, as indicated by the bond angles (Table 3.6.2) of the donor atoms and the Fe atom (*vide infra*). The donor atoms of the ligands are situated in two perpendicular planes, with the O and S atoms in *cis* positions and N atoms in *trans* positions.

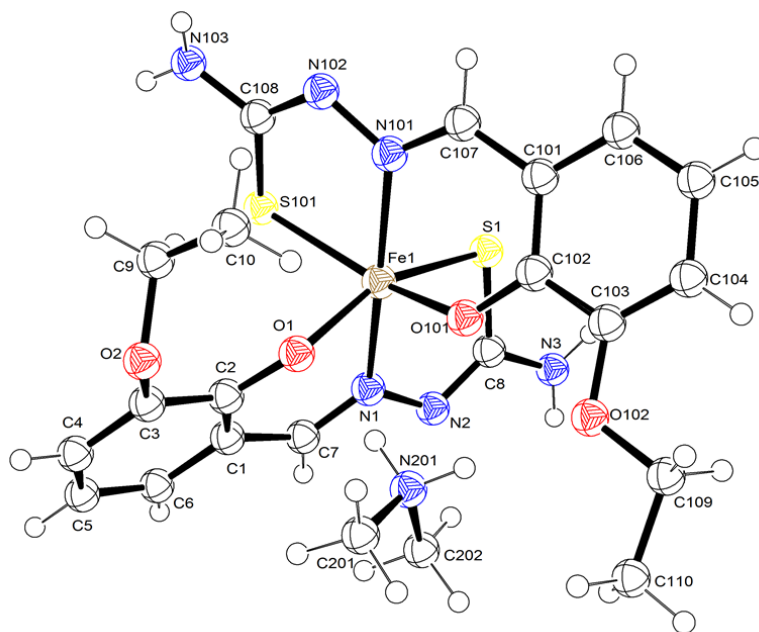


Figure 3.6.1 The molecular structure and atom-numbering scheme for $(\text{CH}_3)_2\text{NH}_2[\text{Fe}(\text{3-OEt-thsa})_2]$. Displacement ellipsoids are drawn at the 50 % probability level.

X-ray structural data of similar Fe^{III} bis(ligand) compounds containing two dianionic thiosemicarbazonato(2-) ligands show that the Fe–S, Fe–O and Fe–N bond distances are 2.23–2.31 Å, 1.93–1.95 Å and 1.88–1.96 Å, severally, for low-spin Fe^{III} compounds and 2.40–2.44 Å, 1.96–1.99 Å and 2.05–2.15 Å, severally, for corresponding high-spin Fe^{III} compounds [8]. The bond distances of $(\text{CH}_3)_2\text{NH}_2[\text{Fe}(\text{3-OEt-thsa})_2]$ involving the Fe atoms and the donor atoms (Table 3.6.2) suggests that the present compound contains high-spin Fe^{III} at 100 K. Furthermore, the spin state of the Fe^{III} cation can also be inferred from the bond angles of the $\text{FeO}_2\text{N}_2\text{S}_2$ coordination core. The bite angle of O–Fe–S is $158.89(5)^\circ$ and $158.48(5)^\circ$, for O1–Fe1–S1 and O101–Fe1–S101, respectively, at 100 K, however for the low-spin compound $\text{Cs}[\text{Fe}(\text{3-OEt-thsa-Me})_2]\cdot\text{CH}_3\text{OH}$, the O–Fe–S angle is $177.88(14)^\circ$ and $178.01(13)^\circ$, O11–Fe1–S11 and O21–Fe1–S21, respectively, at 100 K. This clearly shows that the coordination angles of the Fe^{III} ion in the low-spin state at 100 K are closer to those found in a regular octahedron than those of the high-spin form at 100 K.

The ligands have been found to be in the dianionic form as no hydrogen atoms were located on the phenolate-O (O1 and O101) or the thiolate-S (S1 and S101) atoms. This is associated with the presence of the monovalent dimethylammonium cation together with the trivalent iron cation. The tridentate ligands of the present compound are coordinated to the Fe^{III} cation by the thiolate-S, phenolate-O and imine-N atoms, forming six- and five-membered chelate rings. It has been found that the six membered chelate ring involves a significantly less restricted bite angle [O1–Fe–N1 = $82.17(7)^\circ$ and O101–Fe–N101 = $84.03(7)^\circ$] than the five-membered chelate ring [S1–Fe–N1 =

78.45(5)° and S101–Fe–N101 = 78.93(5)°]. The root mean-square deviations from their least-squares plane of atoms involving the 6-membered chelate ring of both coordinated ligands are 0.197 Å and 0.177 Å, for [Fe1 N11 C17 C11 C12 O11] and [Fe1 N101 C107 C101 C102 O101], respectively, and the analogous values for the 5-membered chelate rings are 0.129 Å and 0.102 Å, for [Fe1 N11 C12 C18 S11] and [Fe1 N101 C102 C108 S101], respectively. It appears that the metal chelate rings deviate slightly from the ideal planar structure. Furthermore, the O–Fe–N and S–Fe–N bite angles of the 6- and 5-membered chelates are deficient by *ca.* 38° and 30°, respectively, compared to the angle at the vertex of a regular hexagon (120°) or pentagon (108°), respectively.

Table 3.6.2 Selected geometric parameters of (CH₃)₂NH₂[Fe(3-OEt-thsa)₂] (Å, °)

Fe1–S1	2.4320(6)	Fe1–S101	2.4389(7)
Fe1–O1	1.9806(16)	Fe1–O101	1.9595(16)
Fe1–N1	2.167(2)	Fe1–N101	2.131(2)
S1–Fe1–S101	98.98(2)	O1–C2–C1	122.4(2)
S1–Fe1–N1	78.45(5)	C2–C1–C7	121.2(2)
S1–Fe1–O1	158.48(5)	C1–C7–N1	125.3(2)
S1–Fe1–O101	94.31(5)	C7–N1–Fe1	124.80(15)
S1–Fe1–N101	93.26(5)	Fe1–O101–C102	130.25(16)
S101–Fe1–O1	91.30(5)	O101–C102–C101	123.1(2)
S101–Fe1–O101	158.89(5)	C102–C101–C107	121.2(2)
S101–Fe1–N1	93.18(5)	C101–C107–N101	125.9(2)
S101–Fe1–N101	78.93(5)	C107–N101–Fe1	123.56(16)
O1–Fe1–O101	81.91(7)	C8–S1–Fe1	95.87(8)
O1–Fe1–N1	82.17(7)	N1–N2–C8	113.96(19)
O1–Fe1–N101	107.31(7)	N2–C8–S1	125.75(17)
O101–Fe1–N1	105.56(7)	C108–S101–Fe1	95.71(8)
O101–Fe1–N101	84.03(7)	N101–N102–C108	114.09(19)
N1–Fe1–N101	167.63(7)	N102–C108–S101	125.65(18)
Fe1–O1–C2	127.41(14)		

In comparison to the other Fe^{III} bis(ligand) compounds reported in this chapter, the deficiency of the bite angle in both the 6- and 5-membered chelate rings is larger than expected. It has been recognised that the other Fe^{III} bis(ligand) compounds reported contain Fe^{III} in the low-spin state, however the present compound contains Fe^{III} in the high-spin state. Subsequently, (CH₃)₂NH₂[Fe(3-OEt-thsa)₂]

displays longer Fe^{III}-donor atom bond distances which could be associated with the bite angles being more restricted. Moreover, the remaining angles of the 6-membered chelate rings (Table 3.7.2) are within *ca.* 5° of 125° as expected. However, the C–S–Fe angles of the 5-membered chelate ring are only about 95°, providing an additional deficiency of 13°. The additional deficiency can be offset by increasing the other angles to *ca.* 120°. It has been found that the N–N–C angles are <120° and the N–C–S angles are >120°, these values (Table 3.7.2) suggest sp² hybridisation at C and N atoms. The stability of the Fe^{III} complex is enhanced by the high degree of electron delocalisation throughout the chelated ligands.

The dianionic ligands coordinated to the Fe^{III} cation of (CH₃)₂NH₂[Fe(3-OEt-thsa)₂] form chelate rings which involve electron delocalisation, which is evident from the geometric parameters. The C–S, C–N and N–N bonds obtained for the present compound, show characteristics of a bond order between single and double bonds. The C8–S1 bond length of 1.746(3) Å and C108–S101 bond length of 1.752(2) Å, suggest partial electron delocalisation of these bonds. A comparison can be made with the related high-spin Fe^{III} compound Cs[Fe(thsa)₂] [18] at 103 K which crystallises in the space group *Pna*2₁. The C–S bond distances of (CH₃)₂NH₂[Fe(3-OEt-thsa)₂] correspond with the C–S bond distances of 1.749(9) and 1.761(9) Å, respectively, for Cs[Fe(thsa)₂], suggesting the occurrence of partial electron delocalisation in both compounds. Additionally, the electron delocalisation of the O,N,S-tridentate ligands is confirmed by a bond order larger than 1 for the C–N bond involving the deprotonated hydrazinic N atom. The bond distances for the C7–N1 and C107–N101, in the present compound are 1.301(3) Å and 1.301(3) Å, respectively. Similarly, the C–N bond distances are 1.314(10) and 1.303(11) Å, respectively, for Cs[Fe(thsa)₂] at 103 K. Moreover, the N–N bond distances of (CH₃)₂NH₂[Fe(3-OEt-thsa)₂] at 100 K, are N1–N2 = 1.395(2) Å and N101–N102 = 1.399(3) Å, respectively, which indicates partial electron delocalisation within the 5-membered chelate.

The hydrogen bonding interactions of (CH₃)₂NH₂[Fe(3-OEt-thsa)₂] are listed in Table 3.6.3 and displayed in Figure 3.6.2. The N atom of the dimethylammonium cation forms two hydrogen bonds; one contact is formed with the phenolate-O of one ligand. The second contact is formed with the O atom of the ethoxy group of the salicylaldehyde moiety of the other ligand. The N201–H20A⋯O102 and N201–H20B⋯O1 contacts form an intramolecular hydrogen bond ring system, giving rise to a R₂²(9) ring [20].

The closely assembled Fe^{III} units in the compound (CH₃)₂NH₂[Fe(3-OEt-thsa)₂] may be due to the size of the R'-substituent groups being different, as (CH₃)₂NH₂[Fe(3-OEt-thsa)₂] contains the amino group whereas Cs[Fe(3-OEt-thsa-Me)₂]-CH₃OH contains a methyl substituent on the terminal N atom of the thiosemicarbazide moiety. Furthermore, both compounds differ in the monovalent cation and the presence/absence of a solvent molecule in the crystal lattice. In addition, (CH₃)₂NH₂[Fe(3-OEt-thsa)₂] forms intramolecular ring systems through hydrogen bonds (*vide infra*), whereas

$\text{Cs}[\text{Fe}(\text{3-OEt-thsa-Me})_2] \cdot \text{CH}_3\text{OH}$ forms intermolecular hydrogen bond ring systems which link the neighbouring Fe^{III} entities. Subsequently, it appears the intermolecular hydrogen bonding interactions of the latter compound contribute to how the Fe^{III} entities are arranged in the unit cell.

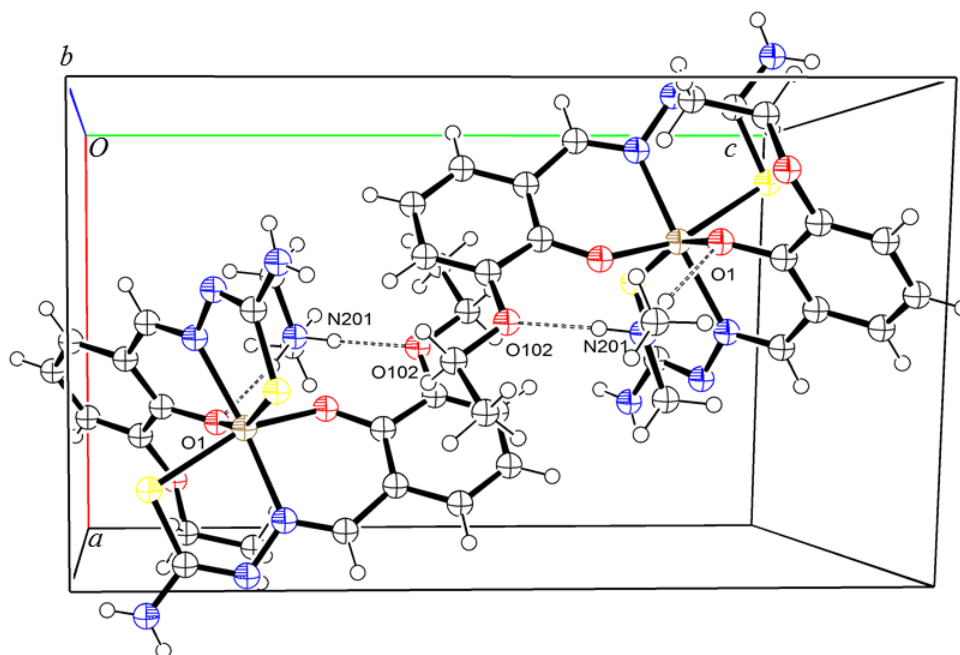


Figure 3.6.2 A projection showing the unit cell of $(\text{CH}_3)_2\text{NH}_2[\text{Fe}(\text{3-OEt-thsa})_2]$. Displacement ellipsoids are drawn at 50% probability level. Dashed lines indicate hydrogen bonds.

Table 3.6.3 Hydrogen bond geometry of $(\text{CH}_3)_2\text{NH}_2[\text{Fe}(\text{3-OEt-thsa})_2]$ (\AA , $^\circ$)

$D\text{-H}\cdots A$	$D\text{-H}$	$H\cdots A$	$D\cdots A$	$D\text{-H}\cdots A$
N201-H20A \cdots O102	0.91	1.97	2.877(3)	173.5
N201-H20B \cdots O1	0.91	1.86	2.766(3)	172.8

3.6.3 Magnetic Studies of $(\text{CH}_3)_2\text{NH}_2[\text{Fe}(\text{3-OEt-thsa})_2]$

The magnetic behaviour of $(\text{CH}_3)_2\text{NH}_2[\text{Fe}(\text{3-OEt-thsa})_2]$ is shown by the temperature dependence of the $\chi_{\text{M}}T$ (χ_{M} being the molar magnetic susceptibility and T being the temperature) measured in the 5-300 K temperature range and is displayed in Figure 3.6.4. The product of magnetic susceptibility and the temperature shows a plateau, revealing the compound to be in the high-spin state over the temperature range 5-300 K, in both the heating and cooling modes. The value of $\chi_{\text{M}}T$ is $4.36 \text{ cm}^3 \text{ K mol}^{-1}$ for $(\text{CH}_3)_2\text{NH}_2[\text{Fe}(\text{3-OEt-thsa})_2]$ at 300 K, which is close to the value expected for high-spin compounds ($S = 5/2$) where $\chi_{\text{M}}T = 4.37 \text{ cm}^3 \text{ K mol}^{-1}$ for $g = 2.00$.

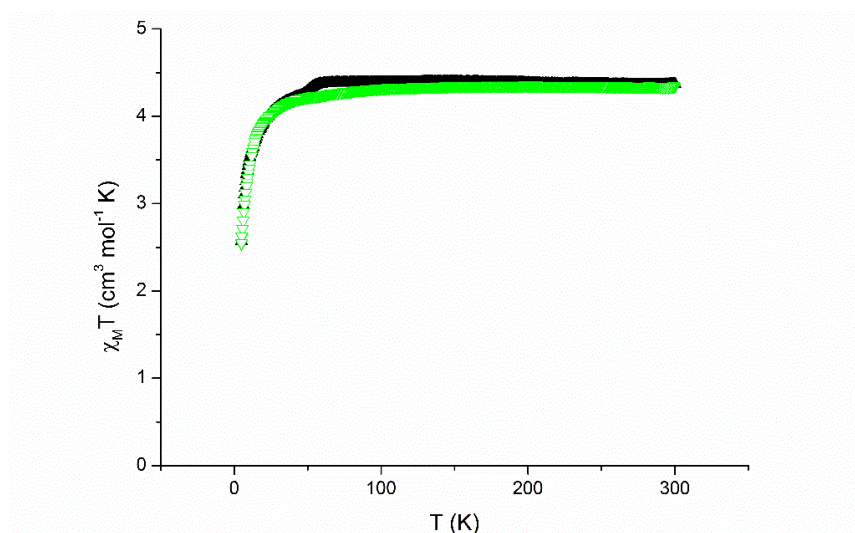


Figure 3.6.3 $\chi_M T$ vs T plot of $(\text{CH}_3)_2\text{NH}_2[\text{Fe}(\text{3-OEt-thsa})_2]$. [The sample was heated (\blacktriangle) and subsequently cooled (\blacktriangledown).]

As illustrated in Figure 3.6.3, the $\chi_M T$ decreases abruptly below the temperature 50 K; this is a consequence of the zero-field splitting of the ground state of the Fe^{III} ion in the high-spin state. This feature has been found to be common in high-spin Fe^{III} compounds [26-27]. The zero-field splitting was calculated using equation (1) [26]:

$$\chi_M = \frac{Ng^2 \beta^2}{4kT} \left[\frac{0.14 + 5.12e^{-3.23X} + 23.85e^{-6.83X}}{1 + e^{-3.23X} + e^{-6.83X}} \right] \quad \text{Eqn (1)}$$

In this equation, $X = D/kT$, D is the zero-field splitting parameter, g is the average g tensor value and the other symbols have their standard meanings (as shown in Chapter I). As reported by Chen *et al.*, [26] equation (1) is the theoretical equation for the magnetic susceptibility resulting from the axial and rhombic zero-field splitting for a Fe^{III} $S = 5/2$ ion. The least-squares fit (Figure 3.6.4) within the temperature range 5-300 K has been obtained with the parameters $D = 0.80 \text{ cm}^{-1}$ and $g = 2.20$ for $(\text{CH}_3)_2\text{NH}_2[\text{Fe}(\text{3-OEt-thsa})_2]$, with a coefficient of determination value of 0.97 and a reduced χ^2 value of 0.000001. The goodness of fit determined for the zero-field splitting parameter can be measured by the reduced χ^2 value; the value of reduced χ^2 is obtained by the following equation:

$$\chi^2 = \left(\sum \frac{\chi_{\text{obs}}^T - \chi_{\text{calc}}^T}{\chi_{\text{obs}}^T} \right)^2 \quad \text{Eqn (2)}$$

In equation (2) $\chi_{\text{obs}} T$ and $\chi_{\text{calc}} T$ represent the observed and calculated product of the magnetic susceptibility and temperature, respectively.

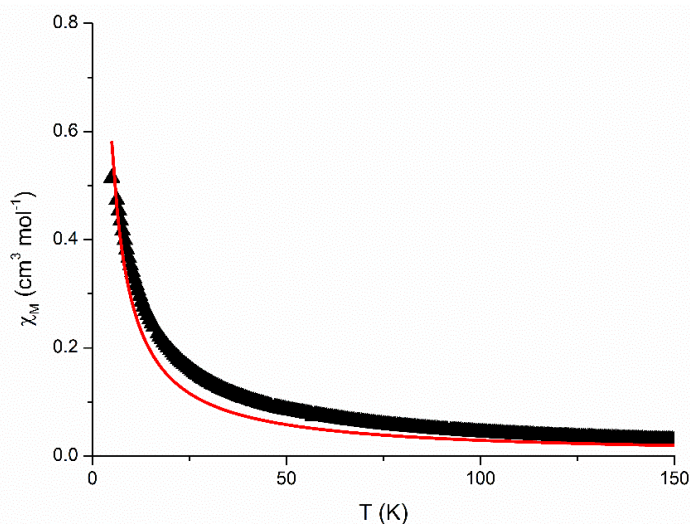


Figure 3.6.4 Temperature dependence of the molar magnetic susceptibility, χ_M , for the compound $(\text{CH}_3)_2\text{NH}_2[\text{Fe}(\text{3-OEt-thsa})_2]$ in the range 5-150 K (\blacktriangle represents the heating mode). Points are the experimental data; solid red line represents the least-squares fit of the data to Equation (1), where $D = 0.80 \text{ cm}^{-1}$ and $g = 2.20$.

3.7 Discussion of Fe^{III} bis(ligand) compounds of R-salicylaldehyde-4R'-thiosemicarbazone

The structures of the $(\text{cation}^+)[\text{Fe}(\text{ligand})_2] \cdot n\text{H}_2\text{O}$ type systems consist of an $\text{Fe}^{\text{III}}\text{O}_2\text{N}_2\text{S}_2$ chromophore which is formed by two chelating tridentate dianionic R-salicylaldehyde 4R'-thiosemicarbazonato(2-) ligands. The $\text{Fe}^{\text{III}}\text{O}_2\text{N}_2\text{S}_2$ chromophore exhibits a distorted octahedral geometry, where the O- and S-donor atoms are in the *cis* positions and the N-donor atoms are in the *trans* positions. The Fe-donor atom distances of the Fe^{III} bis(ligand) compounds described in this chapter are listed in Table 3.7.4.

The Fe^{III} cation in $\text{Cs}[\text{Fe}(\text{3-OEt-thsa-Me})_2] \cdot \text{CH}_3\text{OH}$ is in the low-spin state at 100 K. Moreover, the compounds $\text{Cs}[\text{Fe}(\text{5-Br-thsa})_2]$ at 293 K, $\text{NH}_4[\text{Fe}(\text{thsa})_2]$ at 100 K and $\text{NH}_4[\text{Fe}(\text{5-Br-thsa})_2]$ at 100 K all contain a Fe^{III} cation in the low-spin state, whereas the Fe^{III} cation in $(\text{CH}_3)_2\text{NH}_2[\text{Fe}(\text{3-OEt-thsa})_2]$ is high-spin at 100 K.

In the following, the crystallographic data of the various $(\text{cation}^+)[\text{Fe}(\text{ligand})_2] \cdot n\text{H}_2\text{O}$ compounds (listed in Table 3.7.4) will be compared to similar Fe^{III} bis(ligand) compounds reported in the literature (Table 3.7.5), in an attempt to correlate the structural features of these systems with the spin state of the Fe^{III} cation. It has long been established that the associated cation in the complex system, the R-substituents of the salicylaldehyde moiety and/or the R'-substituents of the thioamide group of the thiosemicarbazide moiety and the $\text{Fe}^{\text{III}}\text{O}_2\text{N}_2\text{S}_2$ chromophore may cause significant changes in the electronic state of the Fe^{III} bis(ligand) compounds. Moreover, the increased hydration

of the Fe^{III} compounds has been associated with the introduction of the R-substituent of the salicylaldehyde moiety or the change in outer-sphere cation [8].

Table 3.7.4 Fe-donor atom bond for various (cation⁺)[Fe(ligand)₂] \cdot n(solvent) compounds of R-salicylaldehyde thiosemicarbazone described in this chapter

Compound ⁱ	T (K)	Space group	Fe–S (Å)	Fe–N (Å)	Fe–O (Å)	Spin State ⁱⁱ
Cs[Fe(3-OEt-thsa-Me) ₂] \cdot CH ₃ OH	100	<i>P</i> -1	2.2686 2.265	1.933 1.939	1.904 1.918	LS
Cs[Fe(5-Br-thsa) ₂]	293	<i>P</i> 2 ₁ / <i>c</i>	2.2321 2.2422	1.947 1.938	1.942 1.956	LS
NH ₄ [Fe(thsa) ₂]	100	<i>P</i> 2 ₁ / <i>n</i>	2.2366 2.2373	1.930 1.948	1.938 1.950	LS
NH ₄ [Fe(5-Br-thsa) ₂] ⁱⁱⁱ	100	<i>Pbcn</i>	2.263	1.942	1.938	LS
(CH ₃) ₂ NH ₂ [Fe(3-OEt-thsa) ₂]	100	<i>P</i> 2 ₁ / <i>n</i>	2.4320 2.4389	2.167 2.131	1.9806 1.9595	HS

ⁱThe geometric parameters for the crystallographically independent ligands are given separately in different lines.

ⁱⁱ The spin states are defined as low-spin (LS) and high-spin (HS).

ⁱⁱⁱ The Fe^{III} ion in the compound NH₄[Fe(5-Br-thsa)₂] becomes partially high-spin around 200 K.

It is noteworthy, that the compounds Cs[Fe(5-Br-thsa)₂], NH₄[Fe(thsa)₂], NH₄[(Fe(5-Br-thsa)₂] and (CH₃)₂NH₂[Fe(3-OEt-thsa)₂] do not contain any solvent molecules in their crystal lattice. This feature has also been observed for the following Fe^{III} compounds: Cs[Fe(thsa)₂] [18], NH₄[Fe(5-Br-thsa)₂] [21] and NH₄[Fe(5-Cl-thsa)₂] [19], for which relevant data are compiled in Table 3.7.5. This table shows the non-solvated Fe^{III} bis(ligand) compounds together with the spin state of the Fe^{III} cation at the temperature at which the crystal structure was determined. Although, this is not the case for the low-spin compound Cs[Fe(3-OEt-thsa-Me)₂] \cdot CH₃OH at 100 K (Table 3.7.4).

The Fe^{III} cation in the compound Cs[Fe(thsa)₂] is in the high-spin state at both 103 K and 298 K [18], whereas the Fe^{III} cation in NH₄[Fe(5-Cl-thsa)₂] is low-spin at 135 K and 298 K [19]. Furthermore, in the compound NH₄[Fe(5-Br-thsa)₂] the Fe^{III} cation is in the low-spin state at 298 K [21]. The Fe^{III} cation in Cs[Fe(5-Br-thsa)₂] is in the low-spin state at 293 K. A transition from low-spin to high-spin Fe^{III} has been detected for similar materials on increasing temperature [25], but crystallographic data are not available for these non-solvated materials. Noting that Cs[Fe(5-Br-thsa)₂] contains low-spin Fe^{III} at 293 K, perhaps, the present compound may exhibit a change in spin state above room

temperature. Furthermore, the possibility of a change in spin state may also occur for the other compounds listed in Table 3.7.4, excluding $(\text{CH}_3)_2\text{NH}_2[\text{Fe}(\text{3-OEt-thsa})_2]$, as the compound is in the high-spin state at 100 K.

Table 3.7.5 Selected average Fe-donor atom bond distances for non-solvated Fe^{III} bis(ligand) compounds of R-salicylaldehyde thiosemicarbazone described in the literature

Compound ⁱ	T (K)	Space group and <i>Z'</i>	Fe–S (Å)	Fe–N (Å)	Fe–O (Å)	Spin State ⁱⁱ	Ref
Cs[Fe(thsa) ₂]	298	<i>Pna2</i> ₁ <i>Z'</i> = 1	2.44	2.12	1.96	HS	[18]
	103	<i>Pna2</i> ₁ <i>Z'</i> = 1	2.44	2.15	1.96	HS	
NH ₄ [Fe(5-Br-thsa) ₂] ⁱⁱⁱ	298	<i>Pnca</i> <i>Z'</i> = 0.5	2.23	1.93	1.95	LS	[21]
NH ₄ [Fe(5-Cl-thsa) ₂]	298	<i>Pnca</i> <i>Z'</i> = 0.5	2.24	1.95	1.93	LS	[19]
	135	<i>Pnca</i> <i>Z'</i> = 0.5	2.23	1.96	1.94	LS	

ⁱ The ligands are defined as follows: H₂L = salicylaldehyde thiosemicarbazone = H₂thsa, so L²⁻ = thsa, H₂L = 5-bromosalicylaldehyde thiosemicarbazone = H₂-5-Br-thsa, so L²⁻ = 5-Br-thsa and H₂L = 5-chlorosalicylaldehyde thiosemicarbazone = H₂-5-Cl-thsa, so L²⁻ = 5-Cl-thsa.

ⁱⁱ The spin states are defined as low-spin (LS) and high-spin (HS).

ⁱⁱⁱ Determined for crystals of tabular form.

The generation of any spin transition is governed by the energy difference between the high-spin and low-spin electronic states. This energy gap can be tuned by variation of the ligand field strength. The features of the second coordination sphere, such as the arrangement of Fe units within a unit cell belonging to a particular crystal system, also influence the ligand field characteristics. The packing of Fe units is evidenced by symmetry requirements which are embedded within the space group in which the material crystallises. X-Ray structural analysis has revealed that the Fe^{III} bis(ligand) type compounds (Table 3.7.5) adopt different crystal systems and space groups in comparison to the (cation⁺)[Fe(ligand)₂] $\cdot n\text{H}_2\text{O}$ compounds listed in Table 3.7.4. The latter compounds display an array of crystal systems and space groups, such as Cs[Fe(3-OEt-thsa-Me)₂] $\cdot \text{CH}_3\text{OH}$ exhibits a triclinic crystal system and the space group *P*-1. Furthermore, the compounds NH₄[Fe(thsa)₂], NH₄[Fe(5-Br-thsa)₂] and (CH₃)₂NH₂[Fe(3-OEt-thsa)₂] display monoclinic crystal systems at 100 K, however with

slightly different orientations of the space group (No. 14) $P2_1/n$, $P2_1/c$ and $P2_1/n$, severally. Moreover, $\text{Cs}[\text{Fe}(\text{5-Br-thsa})_2]$ displays a monoclinic crystal system (at 293 K) and crystallises in the space group $P2_1/c$ with $Z = 4$, or alternatively, $Z' = 1$ (where Z is the number of formula units per unit cell and Z' is the number of formula units per asymmetric unit). In contrast, the non-solvated Fe^{III} bis(ligand) compounds listed in Table 3.7.5, all exhibit an orthorhombic crystal system, however in some cases their space groups differ. For example, $\text{Cs}[\text{Fe}(\text{thsa})_2]$ crystallises in the space group $Pna2_1$ with $Z' = 1$ [18], whereas $\text{NH}_4[\text{Fe}(\text{5-Br-thsa})_2]$ in the tabular form crystallises in the space group $Pnca$ with $Z' = 0.5$ [21]. Moreover, the compound $\text{NH}_4[\text{Fe}(\text{5-Cl-thsa})_2]$ crystallises in the space group $Pnca$, also with $Z' = 0.5$ [19]. The Fe^{III} bis(ligand) entities present variances with respect to their symmetry: In some instances, a value for Z' of 0.5 is encountered which for space group $Pnca$ implies that the ligands coordinated to the Fe^{III} atom are related by two-fold rotational symmetry. Interestingly, Ryabova *et al.*, [21], reported that $\text{NH}_4[\text{Fe}(\text{5-Br-thsa})_2]$ crystallises in two different forms, one form crystallising as tabular plates and the other crystallising as mica-like crystals. It was established that these two different polymorphs exhibit a spin-crossover at different temperature ranges, *i.e.* the mica-like crystals in the region around 200 K, and the tabular plate crystals in the region around 300 K. It appears that the crystallographic data analysed so far for this family of materials do not reveal a relation between Fe^{III} spin state and the crystal system and space group.

It is widely recognised that significant changes in the electronic state of the Fe^{III} bis(ligand) compounds may arise from the associated cation in the complex system, the R-substituents at the benzene ring of the salicylaldehyde moiety and/or the introduction of R'-substituents into the thioamide group of the thiosemicarbazide moiety and the $\text{Fe}^{\text{III}}\text{O}_2\text{N}_2\text{S}_2$ geometry. The main difference observed between the compounds (Table 3.7.5) in comparison to the $(\text{cation}^+)[\text{Fe}(\text{ligand})_2]\cdot n\text{H}_2\text{O}$ compounds reported in this work in Table 3.7.4 is the varying size of the associated cation (either NH_4^+ , $(\text{CH}_3)_2\text{NH}_2^+$ or Cs^+) in the crystal lattice and the variation in slight distortions of the octahedral $\text{Fe}^{\text{III}}\text{O}_2\text{N}_2\text{S}_2$ coordination sphere. It appears that the variation of the associated cation in the Fe^{III} bis(ligand) compounds may have an indirect impact on the spin state of Fe^{III} by influencing the crystal packing. In addition to the difference in size between NH_4^+ , $(\text{CH}_3)_2\text{NH}_2^+$ and Cs^+ ions, the two former may engage in directed interactions through hydrogen bonding while the latter presents a more uniform electrostatic field without a preferred direction for hydrogen bonds. The R,R'-substituents of the ligand may exhibit steric and electronic effects (including being involved in hydrogen bonding, via the R,R'-substituents in the $(\text{cation}^+)[\text{Fe}(\text{ligand})_2]\cdot n\text{H}_2\text{O}$ compounds (Table 3.7.4)), but at this stage it is unclear how these features may be harnessed to induce a particular spin state for Fe^{III} .

The $\text{Fe}^{\text{III}}\text{O}_2\text{N}_2\text{S}_2$ coordination spheres of the compounds are slightly distorted from the ideal octahedral geometry. It has been acknowledged that there are subtle differences in the Fe^{III}

coordination geometry among the members of this particular type of compound. Clearly, the stabilisation of Fe^{III} in a particular spin state is governed by a subtle balance of geometric parameters, as is implied by the fact that a single compound (NH₄[Fe(5-Br-thsa)₂] [21]) exists in slightly different polymorphs each with its distinct magnetic behaviour. The latter example shows that it is too early for deriving a possible relation between Fe^{III} spin state and Fe^{III}O₂N₂S₂ geometry and crystal packing (the latter evidenced by crystal system and space group).

The development of a strategy towards the synthesis of Fe^{III} bis(ligand) compounds with a pre-determined spin state will require the measurement and analysis of crystallographic data of a larger number of Fe^{III} compounds of this family, including these having different R and/or R'-substituents and a variety of associated cations. Furthermore, other parameters that we are currently considering in our studies are the alteration of the degree of solvation and the tuning of the deprotonation characteristics of the R-salicylaldehyde R'-thiosemicarbazone ligand.

3.8 References

1. Gütlich, P. and Goodwin, H. A. (2004). Editors. *Spin Crossover in Transition Metal Compounds I*, edited by Gütlich, P. and Goodwin, H. A., *Top. Curr. Chem.* Berlin: Springer, **233**, pp. 1-47.
2. Floquet, S., Boillot M.-L., Rivière, E., Varret, F., Boukheddaden, K., Morineau, D. and Négrier, P. (2003). *New. J. Chem.* **27**, pp. 341-348.
3. Floquet, S., Guillou, N., Négrier, P., Rivière, E. and Boillot M.-L. (2006). *New. J. Chem.* **30**, pp. 1621-1627.
4. Floquet, S., Muñoz, M. C., Guillot, R., Rivière, E., Blain, G., Réal, J. A. and Boillot, M.-L. (2009). *Inorg. Chim. Acta.* **362**(1), pp. 56-64.
5. Li, Z.-Y., Dai, J.-W., Shiota, Y., Yoshizawa, K., Kanegawa, S. and Sato, O. (2013). *Chem. Eur. J.* **19**, pp. 12948-12952.
6. Yemeli Tido, E. W. (2010). PhD Thesis, University of Groningen, The Netherlands.
7. Yemeli Tido, E. W., Alberda van Ekenstein, G. O. R., Meetsma, A. and Koningsbruggen, P. J. van. (2008). *Inorg. Chem.* **47**, pp. 143-153.
8. Koningsbruggen, P. J. van, Maeda, Y. and Oshio, H. (2004). *Spin Crossover in Transition Metal Compounds I*, edited by Gütlich, P. and Goodwin, H. A., *Top. Curr. Chem.* **233**, pp. 259-324.
9. Yemeli Tido, E. W., Faulmann, R., Roswanda, A., Meetsma, A. and Koningsbruggen, P. J. van. (2010). *Dalton Trans.* **39**(6), pp. 1643-1651.
10. Cooper, R. I., Gould, R.O., Parsons, S. and Watkin, D. J. (2002). *J. Appl. Cryst.* **35**, pp. 168-174.
11. Sheldrick, G. M. (2008). *Acta. Cryst.* **A64**, pp. 112-122.

12. Rigaku (2013). *CrystalClear-SM Expert 2.1 b29*. Rigaku Corporation, The Woodlands, Texas, USA.
13. Palatinus, L. and Chapuis, G. (2007). *J. Appl. Cryst.* **40**, pp. 786-790.
14. Palatinus, L., Prathapa, S. J. and Smaalen, S. van. (2012). *J. Appl. Cryst.* **45**, pp. 575-580.
15. Palatinus, L. and Lee, D. van der. (2008). *J. Appl. Cryst.* **41**, pp. 975-984.
16. Farrugia, L. J. (2012). *J. Appl. Cryst.* **45**, pp. 849-854.
17. Dolomanov, O. V., Bourhis, L. J., Gildea, R. J., Howard, J. A. K. and Puschmann, H. (2009) *J. Appl. Cryst.* **42**, pp. 339-341.
18. Ryabova, N. A., Ponomarev, V. I., Zelentsov, V. V. and Atovmyan, L. O. (1981). *Kristallografiya.* **26**(1), pp. 101-108.
19. Ryabova, N. A., Ponomarev, V. I., Atovmyan, L. O., Zelentsov, V. V. and Shipilov, V. I. (1978). *Koord. Khim.* **4**, pp. 119-126.
20. Bernstein, J., Davis, R. E., Shimoni, L. and Chang, N. L. (1995). *Angew. Chem. Int. Ed.* **34**(15), pp. 1555-1573.
21. Ryabova, N. A., Ponomarev, V. I., Zelentsov, V. V., Shipilov, V. I. and Atovmyan, L. O. (1981). *J. Struct. Chem.* **22**, pp. 111-115.
22. Mähler, J. and Persson, I. (2011). *Inorg. Chem.* **51**(1), pp. 425-438.
23. Bruker (2012). *SAINT-Plus*. Bruker AXS Inc., Madison, Wisconsin, USA.
24. Petricek, V. and Dusek, M. (2006). *JANA2006*. Institute of Physics, Czech Academy of Sciences, Prague, Czech Republic.
25. Ryabova, N. A., Ponomarev, V. I., Zelentsov, V. V. and Atovmyan, L. O. (1982). *Kristallografiya.* **27**(1), pp. 81-91.
26. Chen, C.-H., Lee, Y.-Y., Liao, B.-C., Shanmugham, E., Chen, J.-H., Hsieh, H.-Y, Liao, F.-L. Wang, S.-L. and Hwang, L.-P. (2002). *J. Chem. Soc., Dalton. Trans.*, pp. 3001-3006.
27. Boča, R. (2004). *Coord. Chem. Rev.* **248**, pp. 757-815.

Chapter IV
Neutral Fe(III) Complexes of
R-salicylaldehyde 4-R'-thiosemicarbazones

4.0 Neutral Fe(III) Complexes of R-salicylaldehyde 4R'-thiosemicarbazones

4.1 Introduction

Transition metal fragments displaying switching behaviour are appealing materials, which may be used in a functional way in research and technology [1-5]. It is now established that some molecular species containing transition metal ions may exhibit a crossover between states having a different magnetic moment. Among these, Fe^{III} occupies a unique position in the development of the spin-crossover area since it was for Fe^{III} tris(dithiocarbamates) that the temperature induced phenomenon was first discovered [6-7]. The magnetic interconversion between the low-spin ($S = 1/2$) and high-spin ($S = 5/2$) state in Fe^{III} systems has now been found to be triggered by a change in temperature, pressure or by light irradiation [4, 8-9].

Generation of Fe^{III} spin-crossover behaviour has been demonstrated for a variety of ligand systems [4]. Among these, particular interest is focused on Fe^{III} entities containing two tridentate O,N,S-thiosemicarbazonato ligands which exhibit a thermal spin transition [10-18]. Previous research by Yemeli Tido and co-workers first focused on using derivatives of pyridoxal-4-R-thiosemicarbazone for generating Fe^{III} spin-crossover, resulting in the octahedral Fe^{III}O₂N₂S₂ entity [Fe^{III}(HL)(L)]·2H₂O, where HL⁻ and L²⁻ are the mono- and dianionic form of pyridoxal-4-methylthiosemicarbazone, respectively [19]. The crystal structure of this compound has been determined at 100 K and from the values of the geometric parameters, it could be inferred that the Fe^{III} cation is in the low-spin state. Temperature dependent magnetic susceptibility measurements (5–300 K) showed that this spin state is retained over this temperature range. Complete dehydration of the compound results in an Fe^{III} high-spin material [19]. Furthermore, it appeared that varying the pH during the synthesis of the Fe^{III} entities leads to the formation of Fe^{III} compounds differing in the degree of deprotonation of the ligand [20]. In addition, Yemeli Tido [20] identified the photo-induced spin transition through the light-induced excited spin state trapping (LIESST) of Fe^{III} in [Fe^{III}(HL)(L)]·xH₂O, where HL⁻ = 5-chlorosalicylaldehyde thiosemicarbazonate(1-) and L²⁻ = 5-chlorosalicylaldehyde thiosemicarbazonate(2-) ($x = 1$), or HL⁻ = 5-bromosalicylaldehyde thiosemicarbazonate(1-) and L²⁻ = 5-bromosalicylaldehyde thiosemicarbazonate(2-) ($x = 1/2$) [20]. The magnetic properties and crystallographic studies (obtained from powder X-ray diffraction) reveal the compounds exhibit a one-step spin-transition [20]. In addition, Li *et al.*, reported the single crystal X-ray structures of the photo-responsive neutral spin-crossover compounds [Fe^{III}(H-5-Br-thsa)(5-Br-thsa)]·H₂O [18] (where H-5-Br-thsa, HL⁻ = 5-bromosalicylaldehyde thiosemicarbazonate(1-) and 5-Br-thsa, L²⁻ = 5-bromosalicylaldehyde thiosemicarbazonate(2-)) and [Fe^{III}(H-5-Cl-thsa-Me)(5-Cl-thsa-Me)]·H₂O [21] (where H-5-Cl-thsa-Me, HL⁻ = 5-chlorosalicylaldehyde 4-methylthiosemicarbazonate(1-) and 5-Cl-thsa-Me, L²⁻ = 5-chlorosalicylaldehyde 4-methylthiosemicarbazonate(2-)). In contrast to the one-step spin transition

of the neutral compound $[\text{Fe}^{\text{III}}(\text{H-5-Br-thsa})(5\text{-Br-thsa})]\cdot(\text{H}_2\text{O})_{1/2}$ (reported by Yemeli Tido [20]), the compound $[\text{Fe}^{\text{III}}(\text{H-5-Br-thsa})(5\text{-Br-thsa})]\cdot\text{H}_2\text{O}$ [18] studied by Li and co-workers revealed a rare multi-step spin-transition, which reportedly is accompanied by a two-step reversible crystallographic symmetry breaking process. In recent years, it has been suggested in the literature that multifunctional spin-crossover compounds which respond to magnetic and electric stimuli are highly desirable [21-29]. Li *et al.*, reported the mononuclear ferric compound $[\text{Fe}^{\text{III}}(\text{H-5-Cl-thsa-Me})(5\text{-Cl-thsa-Me})]\cdot\text{H}_2\text{O}$ exhibits a two-step spin transition and dielectric anomalies, also, the material is photo-responsive [21].

The aim of the work described in this research chapter is to design, synthesise and study the magnetic behavior of hydrated ferric spin-crossover materials containing both the mono- and dianionic form of the R-salicylaldehyde 4R'-thiosemicarbazone type ligand, with emphasis on the variation of the R substituent and its position on the salicylaldehyde moiety and the nature of the R' substituent of the thiosemicarbazone moiety. The study of these compounds will be considered in conjunction with the structural features of the spin-crossover materials reported by Li *et al.*, [18, 21], Yemeli Tido [20] and Floquet *et al.*, [30]. Detailed discussion of how the structural features might influence the possibility of the material to exhibit a temperature dependent spin transition will be closely examined and compared with the related results published in the literature [18, 20-21, 30].

Herein, we report the crystallographic studies (at 100 K) and magnetic properties of three novel neutral ferric complexes: $[\text{Fe}^{\text{III}}(\text{H-thsa-Me})(\text{thsa-Me})]\cdot\text{H}_2\text{O}$, $[\text{Fe}^{\text{III}}(\text{H-3-OEt-thsa-Me})(3\text{-OEt-thsa-Me})]\cdot\text{H}_2\text{O}$ and $[\text{Fe}^{\text{III}}(\text{H-5-Cl-thsa-Me})(5\text{-Cl-thsa-Me})]\cdot\text{H}_2\text{O}$. The featured compounds contain both the doubly and singly deprotonated forms of the R-salicylaldehyde 4R'-thiosemicarbazone derivatives (ligand structures illustrated in Figure 4.1.1.)

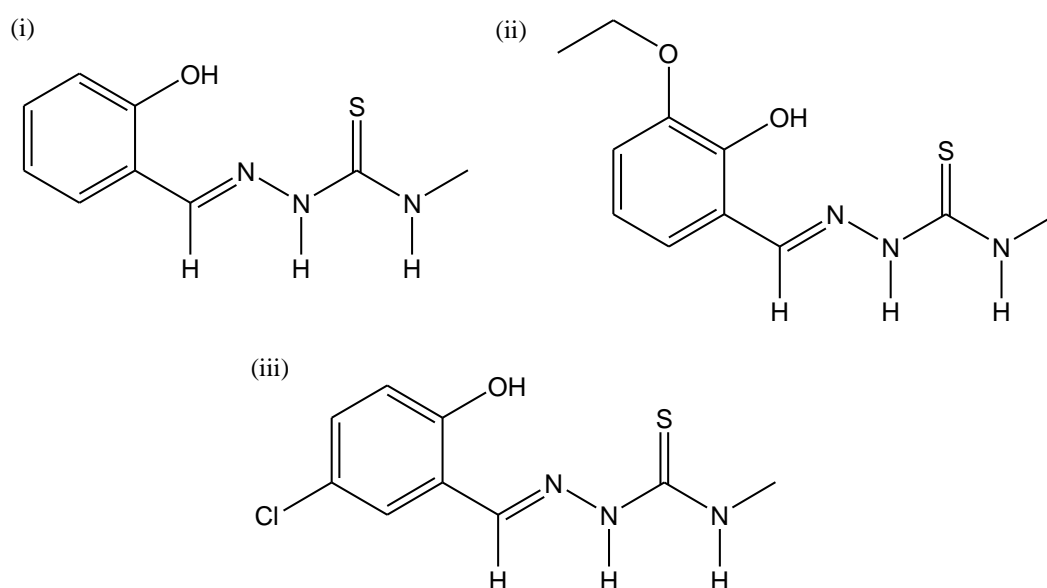


Figure 4.1.1 Molecular structure of the R-salicylaldehyde 4R'-thiosemicarbazone ligands (i) H_2 -thsa-Me, (ii) H_2 -3-OEt-thsa-Me and (iii) H_2 -5-Cl-thsa-Me.

4.2 The crystal structure and magnetic properties of [Fe(H-thsa-Me)(thsa-Me)]·H₂O

In this section the magnetic properties of the compound [Fe(H-thsa-Me)(thsa-Me)]·H₂O are described, as well as the crystal structure at 100 K. Furthermore, the infrared spectroscopic studies of the free ligand and ferric complex are also discussed. The synthesis of [Fe(H-thsa-Me)(thsa-Me)]·H₂O and the corresponding H₂L ligand, salicylaldehyde 4-methylthiosemicarbazone, is described in Chapter II – Materials and Methods.

4.2.1 Crystal Data and Structure Refinement Details of [Fe(H-thsa-Me)(thsa-Me)]·H₂O

Crystal data, data collection and structure refinement details are summarised in Table 4.2.1. The Fe1 atom has a site occupancy position of 0.5, whereby the symmetry transformation (i) $-x + 1, -y + 1, z$ generates the equivalent atoms of the coordinated anionic ligand salicylaldehyde methylthiosemicarbazone. The H-atoms of the secondary amine atoms N2, N2ⁱ, N3 and N3ⁱ were located in difference Fourier maps and refined with restrained N–H distances of 0.88(2) Å and with $U_{\text{iso}}(\text{H}) = 1.2 U_{\text{eq}}(\text{N})$. Moreover, the H -atom bound to the N2-atom has a site occupancy factor of 0.5. The water solvent molecule has a site occupancy of 0.5. The H-atoms bound to the O-atom of the water molecule were located in difference Fourier maps and refined with an O–H distance restraint of 0.87(2) Å and with $U_{\text{iso}}(\text{H}) = 1.5 U_{\text{eq}}(\text{O})$. The remaining H-atoms were included in the refinement in calculated positions and treated as riding on their parent atoms, with a C–H distance of 0.95 Å and $U_{\text{iso}}(\text{H}) = 1.2 U_{\text{eq}}(\text{C})$ for aryl (-CH=) H-atoms and a C–H distance of 0.98 Å and $U_{\text{iso}}(\text{H}) = 1.5 U_{\text{eq}}(\text{C})$ for the methyl (-CH₃) H-atoms.

Table 4.2.1 Crystal data and structure refinement details of [Fe(H-thsa-Me)(thsa-Me)]·H₂O

Crystal data	
Chemical formula	[Fe(C ₉ H ₉ N ₃ OS)(C ₉ H ₁₀ N ₃ OS)]·H ₂ O
M_r	489.38
Crystal system, space group	Orthorhombic, <i>Aea</i> 2
Temperature (K)	100
a, b, c (Å)	11.354 (3), 19.433 (5), 9.097 (2)
α, β, γ (°)	90, 90, 90
V (Å ³)	2007.2 (9)
Z	4
Radiation type	Mo $K\alpha$
μ (mm ⁻¹)	0.994

Table 4.2.1 Crystal data and structure refinement details of [Fe(H-thsa-Me)(thsa-Me)]·H₂O (continued)

Crystal size (mm)	0.06 x 0.06 x 0.01
Data collection	
Diffractometer	Rigaku AFC12 four-circle Kappa diffractometer
Absorption correction	Multi-scan (<i>CrystalClear-SM Expert 3.1 b27</i> [31])
T_{\min} , T_{\max}	0.618, 1.000
No. of measured, independent and observed [$I > 2\sigma(I)$] reflections	6620, 2270, 1741
R_{int}	0.096
Refinement	
$R[F^2 > 2\sigma(F^2)]$, $wR(F^2)$, S	0.060, 0.188, 1.04
No. of reflections	2270
No. of parameters	150
No. of restraints	6
H-atom treatment	H atoms treated by a mixture of independent or constrained refinement
$\Delta\rho_{\text{max}}$, $\Delta\rho_{\text{min}}$ (e Å ⁻³)	0.74, -0.49

The program used for the structure solution: *SUPERFLIP* [32]; the structure refinement used the program *SHELXL-2014* [33]. The *OLEX2* [34] and *ORTEP-3* for Windows [35] programs were used to produce the molecular graphics [35].

4.2.2 Crystallographic study of [Fe(H-thsa-Me)(thsa-Me)]·H₂O

The crystal structure of [Fe(H-thsa-Me)(thsa-Me)]·H₂O (Figure 4.2.1) was determined at 100 K. The present compound crystallises in the orthorhombic polar space group *Aea2* with $Z = 4$ and $Z' = 0.5$ (where Z is the number of formula units per unit cell and Z' is the number of formula units per asymmetric unit). The asymmetric unit consists of 1/2 [Fe(H-thsa-Me)(thsa-Me)] unit and half of a solvent water molecule. The ligands coordinated around the Fe^{III} cation are related by symmetry (symmetry code: (i) $-x + 1, -y + 1, z$).

The Fe^{III} cation is coordinated by an anionic O,N,S-tridentate salicylaldehyde 4-methylthiosemicarbazone(1-) and a dianionic ligand salicylaldehyde 4-methylthiosemicarbazone(2-) which are related by symmetry [(i) $-x + 1, -y + 1, z$]. The crystallographic model for both ligands involves a hydrogen atom bound to the hydrazinic N atom of each ligand (N2 and N2ⁱ) having a site occupancy factor of 0.5, therefore this hydrogen atom is

disordered over both the N2 and N2ⁱ sites (50:50). The disorder of the hydrogen atoms of the hydrazinic N atoms gives rise to the ferric complex containing a dianionic ligand and an anionic ligand (*vide infra*).

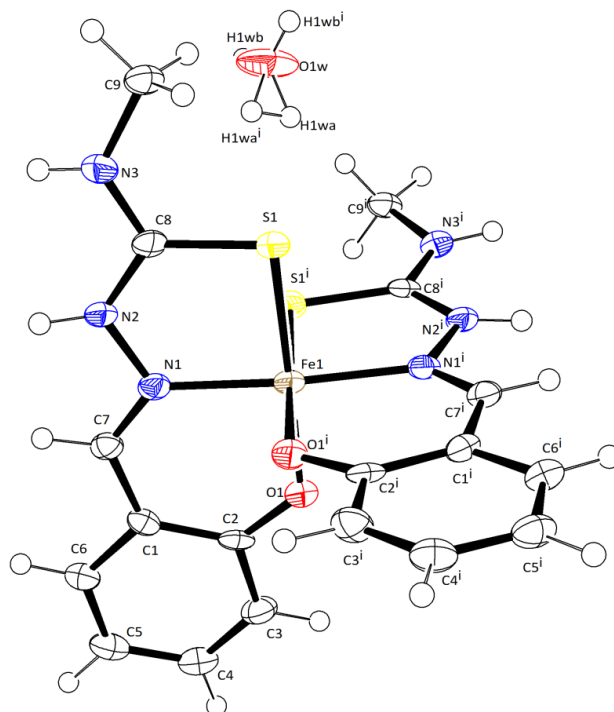


Figure 4.2.1 The molecular structure and atom-numbering scheme of [Fe(H-thsa-Me)(thsa-Me)]·H₂O, whereby the second ligand bound to Fe1 atom is generated by the symmetry operation: (i) $-x + 1, -y + 1, z$. The hydrogen atom bound to N2 and N2ⁱ atoms has a site occupancy factor of 0.5, *i.e.* the atom is disordered over the N2 and N2ⁱ sites (50:50). Displacement ellipsoids are drawn at the 50% probability level.

The Fe^{III} cation forms an Fe^{III}O₂N₂S₂ octahedral environment with the coordinated O,N,S-donor atoms of both ligands. The Fe^{III}-donor atom bond distances are Fe1–S1 and Fe1–S1ⁱ = 2.249(2) Å, Fe1–O1 and Fe1–O1ⁱ = 1.932(5) Å and Fe–N1 and Fe1–N1ⁱ = 1.9246(5) Å. Selected geometric parameters are displayed in Table 4.2.2.

X-ray structural data of Fe^{III} bis(ligand) type compounds reveal that the Fe–S, Fe–O and Fe–N distances are 2.23 – 2.31 Å, 1.93 – 1.95 Å and 1.88 – 1.96 Å, severally, for low-spin Fe^{III} compounds, and 2.40 – 2.44 Å, 1.96 – 1.99 Å and 2.05 – 2.15 Å, severally, for the corresponding high-spin Fe^{III} compounds [4]. These details in comparison with the present compound's Fe-donor atom bond distances suggest that the Fe^{III} cation is in the low-spin state at 100 K. In addition, the X-ray structural data of the low-spin compound [Fe(H-5-Br-thsa)(5-Br-thsa)]·H₂O at 123 K, reveal that the Fe–S and Fe–N bonds distances of are 2.2718(17)/2.2463(17) Å and 1.952(5)/1.955(4) Å, respectively, which

too suggests that the Fe^{III} cation is in the low-spin state at 100 K for the compound [Fe(H-thsa-Me)(thsa-Me)]·H₂O.

Table 4.2.2 Selected geometric parameters of [Fe(H-thsa-Me)(thsa-Me)]·H₂O (Å, °)

Fe1–S1	2.249 (2)	Fe1–N1	1.946 (5)
Fe1–O1	1.932 (5)		
S1–Fe1–S1 ⁱ	90.08 (12)	Fe1–O1–C2	127.6 (5)
S1–Fe1–N1	86.5 (2)	O1–C2–C1	123.3 (7)
S1–Fe1–O1	179.4 (2)	C2–C1–C7	123.8 (8)
S1–Fe1–O1 ⁱ	89.67 (16)	C1–C7–N1	125.4 (7)
S1–Fe1–N1 ⁱ	90.2 (2)	C7–N1–Fe1	126.7 (7)
O1–Fe1–O1 ⁱ	90.6 (3)	C8–S1–Fe1	95.9 (3)
O1–Fe1–N1	92.9 (3)	N1–N2–C8	116.1 (6)
O1–Fe1–N1 ⁱ	90.4 (3)	N2–C8–S1	122.3 (6)
N1–Fe1–N1 ⁱ	175.4 (5)		

Symmetry transformation used to generate equivalent atoms: (i) $-x + 1, -y + 1, z$.

The donor atoms of the salicylaldehyde 4-methylthiosemicarbazonato ligands are located in two mutually perpendicular planes with the phenolate-O and thiolate-S in *cis* positions and the imine-N atom in the *trans* position. The distortion of the Fe^{III}O₂N₂S₂ octahedral geometry results from the constraints imposed by the five- and six-membered chelate rings formed. As expected the six-membered chelate ring involves a significantly wider bite angle than the ideal octahedral 90° [O1–Fe1–N1 bite angle of 92.9(3)°] while the bite angle is narrowed in the five-membered chelate ring [S1–Fe1–N1 bite angle of 86.5(2)°]; selected geometric parameters are displayed in Table 4.2.2. There is no major strain relief through puckering: the root mean-square deviations from their least-squares plane of atoms comprising the six membered [Fe1 N1 C7 C1 C2 O1] chelate ring are 0.020 Å and the corresponding values for the five-membered [Fe1 N1 N2 C8 S1] chelate ring are 0.007 Å. The Fe^{III} chelating O,N,S-tridentate ligands' bond distances suggest that there is electron delocalisation over the five- and six-membered chelates. It should be noted that the bond distances and angles for the [Fe(H-thsa-Me)(thsa-Me)]·H₂O compound are an average for the one-fold and two-fold deprotonated ligand forms, due to the ligands being related by symmetry. Furthermore, it is significant to note that the ligands are chemically inequivalent *i.e.* one ligand is anionic and the other dianionic, but the ligands are crystallographically equivalent, due to the ligands being related by the symmetry operation (i) $-x + 1, -y + 1, z$. This geometric feature is shown by the bond distances

of the C–S, C–N and N–N bonds of the symmetry related ligands. The N1–N2, N2–C8 and C8–S1 bonds are involved in the structure of the five-membered chelate, in which the bond distances at 100 K are 1.396(9) Å, 1.340(9) Å and 1.726(7) Å, respectively. This corresponds to the N–N, N–C and C–S bond distances reported for the crystallographically independent ligands in the related compound [Fe(5-Cl-thsa-Me)(H-5-Cl-thsa-Me)]·H₂O at 110 K, reported by Li *et al.* [21].

The salicylaldehyde 4-methylthiosemicarbazone ligand can coordinate to the Fe^{III} cation in two different tautomeric forms, the thione and the thiol form. In this instance, the thione form is a singly deprotonated ligand which possesses a hydrogen atom at the hydrazinic nitrogen atoms, whereas the thiol form of the tautomer is doubly deprotonated and therefore has no hydrogen atom bound to the hydrazinic nitrogen. Each Fe^{III} ion is coordinated by one singly deprotonated ligand, *i.e.* thione tautomer. The other ligand is generated by the symmetry operation (i) $-x + 1, -y + 1, z$. Considering that one ligand is generated from the other by symmetry, the disorder of the hydrazinic proton, with a N2 site occupancy of 50% and N2ⁱ site occupancy of 50%, suggests that the hydrogen atom can take up either N2 or the N2ⁱ site, which suggests that both an anionic ligand and dianionic ligand are bound to the Fe^{III} cation.

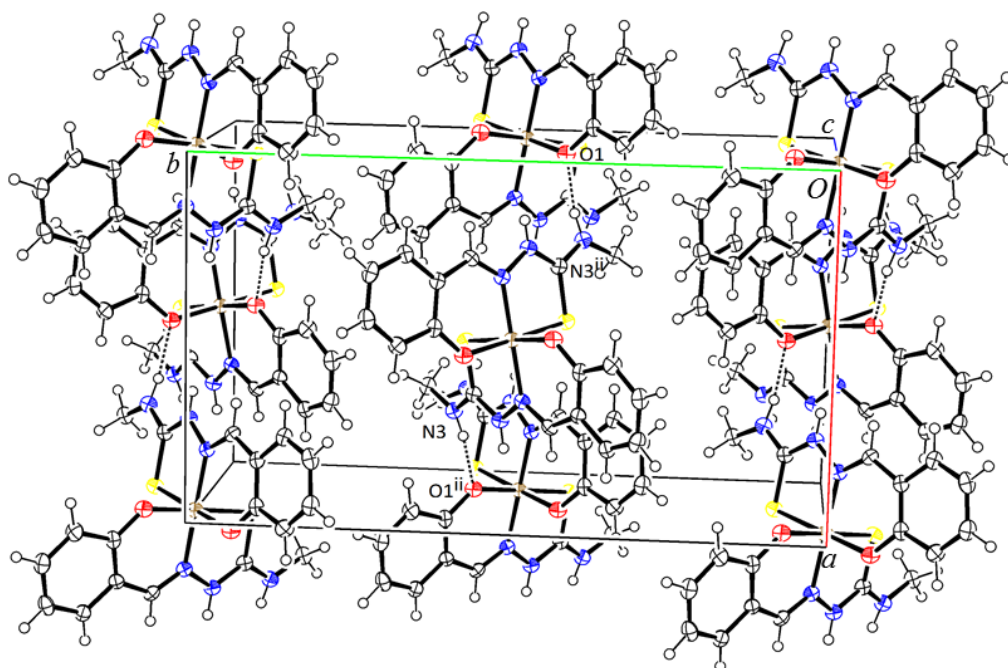


Figure 4.2.2 A projection showing the unit cell of [Fe(H-thsa-Me)(thsa-Me)]·H₂O. The disordered H₂O molecule has been omitted for clarity. Displacement ellipsoids are drawn at the 50% probability level. Dashed lines indicate hydrogen bonds. [Symmetry code: (ii) $x - 1/2, -y + 1, z + 1/2$]

The shortest Fe^{III}...Fe^{III} separations for the present compound are 7.2744(13) Å for Fe1...Fe1 ($x - 1/2, -y + 1, z + 1/2$) and 9.097(2) Å for Fe1...Fe1 ($-x + 1, -y + 1, z - 1$). The Fe^{III} units of [Fe(H-thsa-Me)(thsa-Me)]·H₂O are linked in the *a* direction by the N-H...O contacts (as displayed in Figure 4.2.2). The N3-H3...O1 ($x - 1/2, -y + 1, z + 1/2$) contact is formed by the terminal nitrogen atom, N3, which hydrogen bonds to the phenolate-O Fe^{III} donor atom, O1. The hydrogen bonding geometry of [Fe(H-thsa-Me)(thsa-Me)]·H₂O is listed in Table 4.3.3.

Table 4.3.3 Hydrogen bond geometry of [Fe(H-thsa-Me)(thsa-Me)]·H₂O (Å, °)

<i>D-H...A</i>	<i>D-H</i>	<i>H...A</i>	<i>D...A</i>	<i>D-H...A</i>
N3-H3...O1 ⁱⁱ	0.880 (3)	1.894 (19)	2.759 (9)	167 (7)

Symmetry code: (ii) $x - 1/2, -y + 1, z + 1/2$.

4.2.3 Infrared spectroscopic studies of [Fe(H-thsa-Me)(thsa-Me)]·H₂O and the ligand salicylaldehyde 4-methylthiosemicarbazone, H₂-thsa-Me

Several key structural features regarding the ferric complexes and ligands can be drawn from the infrared spectra (given in the appendix). In contrast to the infrared spectrum of the ferric complex, the infrared spectrum of the ligand salicylaldehyde 4-methylthiosemicarbazone shows a νOH peak at 3362 cm⁻¹ which indicates the presence of the OH group of the phenol. As the ligand binds to the Fe^{III} ion, it is possible for the tridentate ligand to be present in the anionic or dianionic form. The anionic ligand is singly deprotonated at the phenolate-O atom and the dianionic ligand is doubly deprotonated thus no hydrogen atom would be located at the phenolate-O and thiolate-S atoms. The present ferric complex contains both the anionic and dianionic form of the ligand; subsequently the OH group of the phenol is not present in the infrared spectrum of the ferric complex as expected. The deprotonation of the phenolate-O atom after complexation to the metal ion is also supported by the shift of the frequency of the νC-O band from 1100 cm⁻¹ to 1323 cm⁻¹, in the ligand to the ferric complex, respectively [18, 21]. The positive shift of the νC-O band frequency indicates the coordination of the Fe^{III} ion to the phenolate-O atom. The azomethine nitrogen atom is confirmed to have coordinated to the metal ion due to the shift of the C=N band from 1604 cm⁻¹ in the free ligand to 1600 cm⁻¹ in the complex [18, 21, 37]. The absence of the S-H bond in the range 2600-2800 cm⁻¹ in the infrared spectrum of the ligand, indicates the ligand is present in the thione form, which is confirmed by the vibration at 1201 cm⁻¹ which corresponds to the C=S band [18, 21, 37]. Furthermore, the coordination of the S atom to the Fe^{III} ion is corroborated by the shift of the C-S band to 815 cm⁻¹ in the ferric complex from 1020 cm⁻¹ (νC=S) with regard to the free ligand [37].

4.2.4 Magnetic properties of [Fe(H-thsa-Me)(thsa-Me)]·H₂O

The temperature dependence of the $\chi_M T$ value (χ_M being the molar magnetic susceptibility and T being the temperature) of [Fe(H-thsa-Me)(thsa-Me)]·H₂O was measured in the 5-300 K temperature range and is displayed in Figure 4.2.3. The magnetic behaviour of the present compound reveals that the Fe^{III} ion is in the low-spin state over the temperature range 5-300 K, in both the heating and cooling modes. The product of magnetic susceptibility and the temperature clearly indicates a plateau with the low-spin value (0.55 cm³ K mol⁻¹) for [Fe(H-thsa-Me)(thsa-Me)]·H₂O being slightly higher than the value expected for low-spin compounds ($S = 1/2$) where $\chi_M T = 0.375$ cm³ K mol⁻¹ for $g = 2.00$. The $\chi_M T$ value slowly increases at temperatures above ca. 280 K, this will be further investigated (*vide infra*).

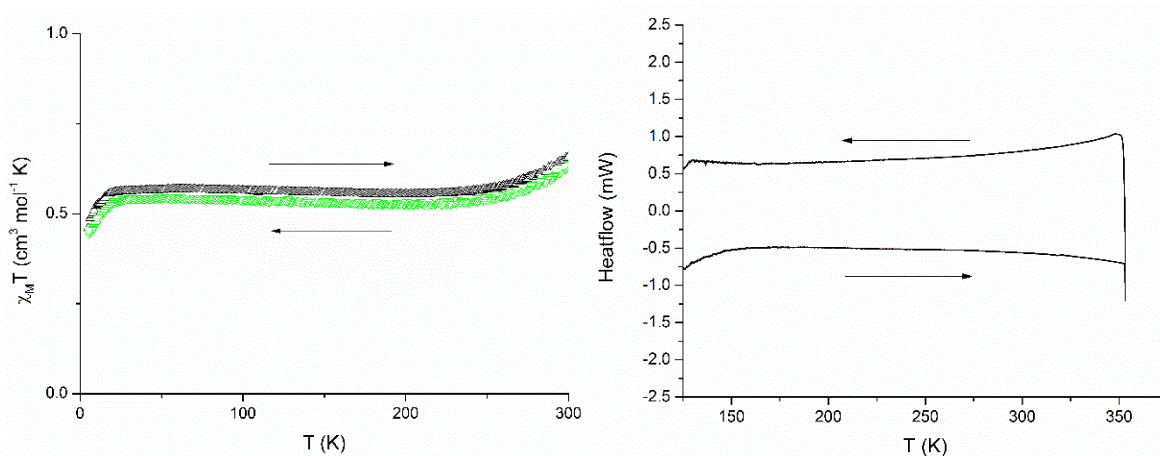


Figure 4.2.3 $\chi_M T$ vs T plot of [Fe(H-thsa-Me)(thsa-Me)]·H₂O (left). The sample was warmed (▲) and then subsequently cooled (▼) in the temperature region of 5-300 K, at a rate of 2 K min⁻¹. DSC curves (right) obtained for [Fe(H-thsa-Me)(thsa-Me)]·H₂O at a scan rate of 5 K min⁻¹.

As observed from Figure 4.2.3 the $\chi_M T$ vs T plot of [Fe(H-thsa-Me)(thsa-Me)]·H₂O (5-300 K) shows that the value of the $\chi_M T$ slightly increases in the temperature range 250-300 K. In order to investigate this increase of $\chi_M T$, higher temperature magnetic measurements were conducted and are displayed in Figure 4.2.4. At 400 K, $\chi_M T = 2.52$ cm³ K mol⁻¹ for the Fe^{III} complex, however, this is much lower than the expected $\chi_M T$ value (4.37 cm³ K mol⁻¹, $S = 5/2$, $g = 2.0023$) for the corresponding Fe^{III} ion in the high-spin state. The increase in the product of magnetic susceptibility and temperature may be due to the Fe^{III} ion exhibiting in an incomplete spin transition, whereby only a fraction of the Fe^{III} ions convert into the high-spin state. The observed $\chi_M T$ values at 300 K and 400 K are 0.66 cm³ K mol⁻¹ and 2.52 cm³ K mol⁻¹, which correspond to the estimated high-spin fractions of 7 % and 54 %, respectively.

The DSC curve (125-350 K) of $[\text{Fe}(\text{H-thsa-Me})(\text{thsa-Me})]\cdot\text{H}_2\text{O}$, as displayed in Figure 4.2.3, shows a slight increase in the curve above *ca.* 280 K in both the heating and cooling mode, which confirms the onset of the spin-crossover in this temperature range. This result correlates with the temperature dependent magnetic data recorded from 5 to 300 K.

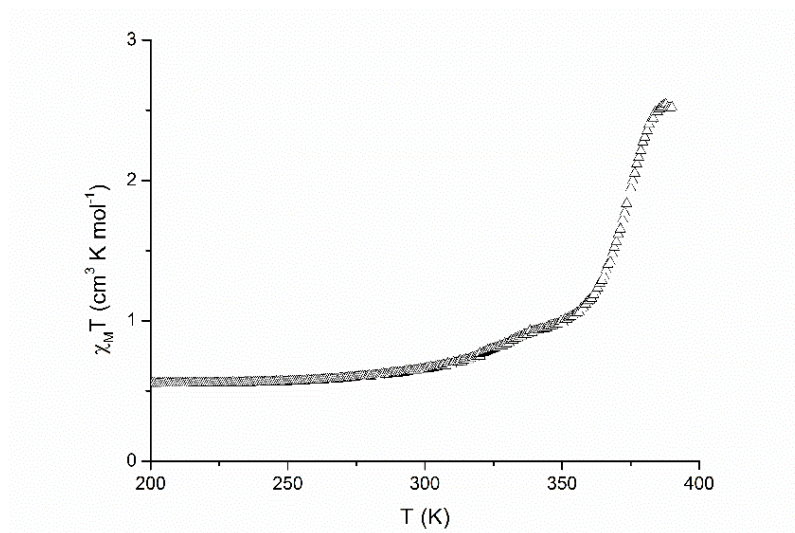


Figure 4.2.4 $\chi_{\text{M}}T$ vs T plot of $[\text{Fe}(\text{H-thsa-Me})(\text{thsa-Me})]\cdot\text{H}_2\text{O}$. The sample was warmed (\blacktriangle) in the temperature region of 200-400 K, at a rate of 2 K min^{-1} .

4.3 The structure and magnetic properties of $[\text{Fe}(\text{H-3-OEt-thsa-Me})(3\text{-OEt-thsa-Me})]\cdot\text{H}_2\text{O}$

In this section the crystallographic data and magnetic properties of the ferric complex $[\text{Fe}(\text{H-3-OEt-thsa-Me})(3\text{-OEt-thsa-Me})]\cdot\text{H}_2\text{O}$ are reported. Furthermore, the infrared spectroscopic studies of the free ligand and ferric complex are also discussed.

The synthesis of $[\text{Fe}(\text{H-3-OEt-thsa-Me})(3\text{-OEt-thsa-Me})]\cdot\text{H}_2\text{O}$ and corresponding H_2L ligand, 3-ethoxysalicylaldehyde 4-methylthiosemicarbazone ($\text{H}_2\text{-3-OEt-thsa-Me}$), are detailed in Chapter II – Materials and Methods.

4.3.1 Crystal Data and Structure Refinement Details of $[\text{Fe}(\text{H-3-OEt-thsa-Me})(3\text{-OEt-thsa-Me})]\cdot\text{H}_2\text{O}$

Data was collected on the Beamline I19 situated on an undulator insertion device with a combination of double crystal monochromator, vertical and horizontal focussing mirrors and a series of beam slits (primary white beam and either side of the focussing mirrors). The experimental hutch (EH1) is equipped with a Crystal Logic 4-circle kappa geometry goniometer with a Rigaku Saturn 724 CCD detector and an Oxford Cryosystems Cryostream plus cryostat (80-500 K). For conventional service

crystallography the beamline operates at a typical energy of 18 keV (Zr K absorption edge). The cell determination and data collection were carried out on the software *CrystalClear-SM Expert 2.0 r5* [38]. The data reduction, cell refinement and absorption correction were made using *CrystalClear-SM Expert 2.0 r5* [38] and the structure solution was made using the program *SUPERFLIP* [32]. *OLEX2* [34] and *ORTEP-3* for Windows [35] programs were used to produce the molecular graphics [35].

The crystal data, data collection and structure refinement details are summarised in Table 4.3.1. All H-atoms were included in the refinement in calculated positions and treated as riding on their parent atoms, with N–H distance of 0.86 Å and $U_{\text{iso}}(\text{H}) = 1.2 U_{\text{eq}}(\text{C})$ for amide H-atoms, C–H distance of 0.93 Å and $U_{\text{iso}}(\text{H}) = 1.2 U_{\text{eq}}(\text{C})$ for aryl (-CH=) H-atoms, C–H distances of 0.97 Å and $U_{\text{iso}}(\text{H}) = 1.2 U_{\text{eq}}(\text{C})$ for secondary (-CH₂-) H-atoms and C–H distance of 0.92 Å and $U_{\text{iso}}(\text{H}) = 1.5 U_{\text{eq}}(\text{C})$ for the methyl (-CH₃) H-atoms. The remaining non-hydrogen atoms have been refined as a rigid body, using the rigid body restraint RIGU, with the sigma for 1-2 distances of 0.004 and sigma for 1-3 distances of 0.0004. The O401 and O501 atoms of the H₂O solvent molecules, both have a site occupancy factor of 0.5; due to the disorder associated with the H₂O solvent molecules, the H-atoms have not been located explicitly, although they are included in the sum formula of the ferric complex. The large residual density ($\Delta\rho_{\text{max}} = 0.892 \text{ e } \text{Å}^{-3}$) on the difference Fourier map included peaks near the Fe atom and the largest peak being near the O atom; a fraction of the large residual density may be due to the positional disorder of the ethoxy group of one of the ligands. Thus, the peaks which represent a fraction of the electrons in ethoxy group, were assumed to arise from limitations of the data.

4.3.2 Crystallographic study of [Fe(H-3-OEt-thsa-Me)(3-OEt-thsa-Me)]·H₂O

The structure of [Fe(H-3-OEt-thsa-Me)(3-OEt-thsa-Me)]·H₂O (Fig. 4.3.1) was determined at 100 K. The present compound crystallises in the triclinic system in the space group *P*-1, with *Z* = 2. The asymmetric unit of [Fe(H-3-OEt-thsa-Me)(3-OEt-thsa-Me)]·H₂O contains two crystallographically independent Fe^{III} entities, defined as sites Fe1 and Fe11, respectively. Both Fe^{III} cations are coordinated by a dianionic O,N,S-tridentate ligand, 3-ethoxysalicylaldehyde 4-methylthiosemicarbazonato(2-) (L²⁻) and an anionic O,N,S-tridentate ligand, 3-ethoxysalicylaldehyde 4-methylthiosemicarbazonato(1-) (HL⁻).

Examination of the structure of [Fe(H-3-OEt-thsa-Me)(3-OEt-thsa-Me)]·H₂O revealed that both the Fe^{III} ions (Fe1 and Fe11) have octahedral coordination with an Fe^{III}O₂N₂S₂ geometry. The bond distances of the Fe^{III}-donor atoms are given in Table 4.3.2 and are consistent with those typical for high-spin Fe^{III} bis(ligand) compounds containing both the anionic and dianionic form of the R-salicylaldehyde 4R'-thiosemicarbazonate ligand [18, 20-21]. The Fe^{III}O₂N₂S₂ coordination spheres

of Fe1 and Fe11 display slightly distorted octahedral geometries, as indicated by the bond angles (Table 4.3.2) of the donor atoms and the Fe1 and Fe11 atoms (*vide infra*). The distorted Fe^{III}O₂N₂S₂ geometry is evidenced by the two mutually perpendicular ligand planes whereby the donor atoms O and S are in the *cis* positions and N atoms in *trans* positions.

Table 4.3.1 Crystal data and structure refinement details of [Fe(H-3-OEt-thsa-Me)(3-OEt-thsa-Me)]·H₂O

Crystal data	
Chemical formula	[[Fe(C ₁₁ H ₁₃ N ₃ O ₂ S)(C ₁₁ H ₁₄ N ₃ O ₂ S)]·H ₂ O] ₂
M_r	1136.44
Crystal system, space group	Triclinic, <i>P</i> -1
Temperature (K)	100
a, b, c (Å)	12.264 (2), 12.829 (2), 17.214 (2)
α, β, γ (°)	91.768 (8), 90.822 (6), 104.854 (9)
V (Å ³)	2615.9 (7)
Z	2
Radiation type	Mo $K\alpha$
μ (mm ⁻¹)	0.721
Crystal size (mm)	0.04 x 0.04 x 0.04
Data collection	
Diffractometer	Beamline I19 (Synchrotron)
Absorption correction	Multi-scan (<i>CrystalClear-SM Expert 2.0 r5</i> [38])
T_{\min}, T_{\max}	0.445, 1.000
No. of measured, independent and observed [$I > 2\sigma(I)$] reflections	21479, 9060, 4095
R_{int}	0.1949
Refinement	
$R[F^2 > 2\sigma(F^2)], wR(F^2), S$	0.1253, 0.2922, 1.053
No. of reflections	9060
No. of parameters	649
No. of restraints	19
H-atom treatment	H atoms treated by constrained refinement
$\Delta\rho_{\max}, \Delta\rho_{\min}$ (e Å ⁻³)	0.892, -0.710

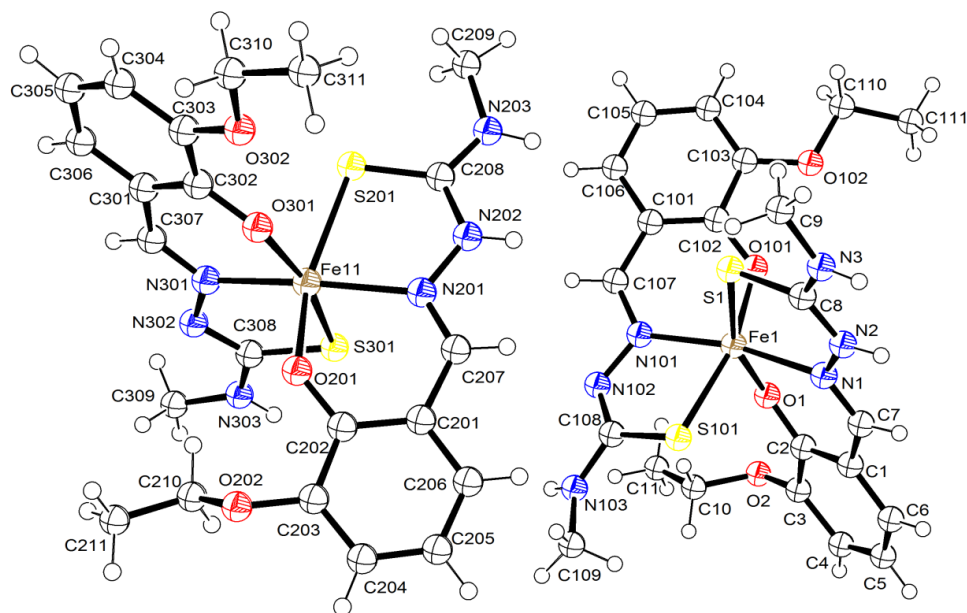


Figure 4.3.1 The molecular structure and atom-numbering scheme for the asymmetric unit of $[\text{Fe}(\text{H-3-OEt-thsa-Me})(3\text{-OEt-thsa-Me})]\cdot\text{H}_2\text{O}$. The two H_2O molecules have been omitted for clarity. Displacement ellipsoids are drawn at the 50% probability level.

The single crystal structure of $[\text{Fe}(\text{H-3-OEt-thsa-Me})(3\text{-OEt-thsa-Me})]\cdot\text{H}_2\text{O}$ has revealed that the Fe^{III} ion is in the high-spin state at 100 K, whereas the Fe^{III} ion of the complex $[\text{Fe}(\text{H-thsa-Me})(\text{thsa-Me})]\cdot\text{H}_2\text{O}$ (*vide supra*) is in the low-spin state at 100 K. It is recognised that there is a difference in the bond distances of the Fe^{III} -donor atoms between the high-spin and low-spin forms [20, 21]. Bond distances between the Fe^{III} atom and the O,N,S-donor atoms for selected $[\text{Fe}^{\text{III}}(\text{HL})(\text{L})]\cdot\text{H}_2\text{O}$ type spin-crossover compounds are summarised in Table 4.3.3.

Table 4.3.2 Selected geometric parameters of $[\text{Fe}(\text{H-3-OEt-thsa-Me})(3\text{-OEt-thsa-Me})]\cdot\text{H}_2\text{O}$ (Å, °)

Fe1–S1	2.473 (4)	Fe1–S101	2.442 (4)
Fe1–O1	1.939 (9)	Fe1–O101	1.996 (9)
Fe1–N1	2.168 (10)	Fe1–N101	2.085 (10)
Fe11–S201	2.482 (4)	Fe11–S301	2.417 (4)
Fe11–O201	1.958 (9)	Fe11–O301	1.994 (8)
Fe11–N201	2.146 (5)	Fe11–N301	2.096 (11)
S1–Fe1–S101	95.02 (13)	S201–Fe11–S301	95.75 (13)
S1–Fe1–N1	79.5 (3)	S201–Fe11–N201	79.1 (3)

Table 4.3.2 Selected geometric parameters of [Fe(H-3-OEt-thsa-Me)(3-OEt-thsa-Me)]·H₂O (Å, °) (continued)

S1–Fe1–O1	160.2 (3)	S201–Fe11–O201	159.7 (3)
S1–Fe1–O101	86.4 (3)	S201–Fe11–O301	88.0 (3)
S1–Fe1–N101	100.1 (3)	S201–Fe11–N301	97.7 (4)
S101–Fe1–O1	95.8 (3)	S301–Fe11–O201	94.8 (3)
S101–Fe1–O101	165.3 (3)	S301–Fe11–O301	166.2 (3)
S101–Fe1–N1	87.3 (3)	S301–Fe11–N201	84.9 (3)
S101–Fe1–N101	78.9 (3)	S301–Fe11–N301	80.5 (3)
O1–Fe1–O101	87.3 (4)	O201–Fe11–O301	85.8 (4)
O1–Fe1–N1	84.4 (4)	O201–Fe11–N201	84.7 (4)
O1–Fe1–N101	98.3 (4)	O201–Fe11–N301	101.1 (4)
O101–Fe1–N1	107.3 (3)	O301–Fe11–N201	108.9 (3)
O101–Fe1–N101	86.4 (4)	O301–Fe11–N301	85.8 (4)
N1–Fe1–N101	166.2 (4)	N201–Fe11–N301	164.6 (4)

In the high-spin compound [Fe(H-3-OEt-thsa-Me)(3-OEt-thsa-Me)]·H₂O, the Fe–O, Fe–S and Fe–N bond distances of the anionic ligand (H-3-OEt-thsa-Me) are Fe1–O1 = 1.939(4) Å and Fe11–O201 = 1.958(5) Å; Fe1–S1 = 2.473(4) Å and Fe11–S201 = 2.482(2) Å; and Fe1–N1 = 2.168(10) Å and Fe11–N201 = 2.146(5) Å, severally. Furthermore, the Fe–O, Fe–S and Fe–N bond distances of the dianionic ligand (3-OEt-thsa-Me) are Fe1–O101 = 1.996(9) Å and Fe11–O301 = 1.994(8) Å; Fe1–S101 = 2.442(4) Å and Fe11–S301 = 2.417(4) Å; and Fe1–N101 = 2.085(10) Å and Fe11–N301 = 2.096(11) Å, severally. In the low-spin compound [Fe(H-thsa-Me)(thsa-Me)]·H₂O, the Fe–O, Fe–S and Fe–N bond distances are Fe1–O1ⁱ = 1.932(5) Å, Fe1–S1ⁱ = 2.249(2) Å and Fe1–N1ⁱ = 1.946(5) Å ((i) –x + 1, –y + 1, z), severally. It should be noted that the bond distances for the [Fe(H-thsa-Me)(thsa-Me)]·H₂O compound are an average for the one-fold and two-fold deprotonated ligand forms, as the ligands are crystallographically equivalent, due to the ligands being related by the symmetry operation (i) –x + 1, –y + 1, z. These differences between the high-spin and low-spin form result in the bond distances of the anionic ligands (HL[–]) of ΔFe–O = 0.01 Å, ΔFe–S = 0.22 Å and ΔFe–N = 0.21 Å, severally, and for the dianionic ligand (L^{2–}) of ΔFe–O = 0.06 Å, ΔFe–S = 0.17 Å and ΔFe–N = 0.15 Å, severally, for the reported compounds [Fe(H-3-OEt-thsa-Me)(3-OEt-thsa-Me)]·H₂O and [Fe(H-thsa-Me)(thsa-Me)]·H₂O. The Fe^{III}-donor atom bond distances of the compounds [Fe(H-5-Br-thsa)(5-Br-thsa)]·H₂O and [Fe(H-5-Cl-thsa-Me)(5-Cl-thsa-Me)]·H₂O (displayed in Table 4.3.3) differences for the anionic ligand are ΔFe–O = 0.004–0.028 Å, ΔFe–S = 0.196–0.213 Å and ΔFe–N = 0.176–0.201 Å, severally, the corresponding differences between the

Fe^{III}-donor atom bond distances for the dianionic ligand are $\Delta\text{Fe-O} = 0.003\text{-}0.024 \text{ \AA}$, $\Delta\text{Fe-S} = 0.152\text{-}0.171 \text{ \AA}$ and $\Delta\text{Fe-N} = 0.118\text{-}0.176 \text{ \AA}$, severally.

Table 4.3.3 The Fe–O, Fe–N and Fe–S bond distances (Å), and the bond distances differences between the low-spin and high-spin state for selected [Fe^{III}(HL)(L)]·H₂O spin-crossover compounds

Fe ^{III} compounds ⁱ	Fe–O	Fe–N	Fe–S	$\Delta\text{Fe-O}$	$\Delta\text{Fe-N}$	$\Delta\text{Fe-S}$
	LS/HS ⁱⁱ	LS/HS ⁱⁱ	LS/HS ⁱⁱ			
[Fe(H-5-Br-thsa)(5-Br-thsa)]·H ₂ O ⁱⁱⁱ [18]	1.941(4)	1.952(5)	2.2718(17)	0.028	0.201	0.213
	1.949(4)	1.955(4)	2.2463(17)	0.003	0.176	0.171
	/	/	/			
	1.969(4)	2.153(4)	2.4845(18)			
	1.952(4)	2.131(4)	2.4177(19)			
[Fe(H-5-Cl-thsa-Me)(5-Cl-thsa-Me)]·H ₂ O ⁱⁱⁱ [21]	1.933(4)	1.948(5)	2.2566(16)	0.004	0.176	0.196
	1.940(4)	1.993(5)	2.2389(15)	0.024	0.118	0.152
	/	/	/			
	1.937(9)	2.124(9)	2.453(4)			
	1.916(9)	2.111(10)	2.391(4)			

ⁱ The H₂L ligands are defined as follows: 5-bromosalicylaldehyde thiosemicarbazone = H₂-5-Br-thsa and 5-chlorosalicylaldehyde 4-methylthiosemicarbazone = H₂-5-Cl-thsa-Me.

ⁱⁱ HS and LS represent high-spin and low-spin states, respectively.

ⁱⁱⁱ The geometric parameters of the HL and L ligands are given on subsequent lines.

It is significant to note that the Fe–O distances seem to be less sensitive to change in Fe^{III} spin state than the Fe–N and Fe–S distances, which may be related to the π -acceptor capability of the N- and S-donor atoms opposed to the π -donor capability of the O-donor atoms. This is of particular significance when Fe^{III} is in the low-spin state, as increased back-bonding will lead to comparatively more pronounced shortening of the Fe–N and Fe–S bonds than of the Fe–O bonds. Furthermore, the changes in the Fe^{III}-donor atoms' bond distances are due to the Fe^{III} ion switching from the low-spin to the high-spin state, as it is recognised that with a spin transition the size of the ionic radius of the metal ion changes.

The packing diagram of the high-spin compound [Fe(H-3-OEt-thsa-Me)(3-OEt-thsa-Me)]·H₂O is given in Figure 4.3.2. The Fe^{III}...Fe^{III} separations of the Fe1 units of the compound [Fe(H-3-OEt-thsa-Me)(3-OEt-thsa-Me)]·H₂O are 9.942(4) Å for Fe1...Fe1 (–x + 1, –y + 1, –z + 1) and 12.829(2) Å for Fe1...Fe1 (x, y + 1, z). The Fe11...Fe11 separations of 17.555(4) Å for Fe11...Fe11 (–x + 1, –y + 1, –z + 1) and 12.829(2) Å for Fe11...Fe11 (x, y + 1, z) correlate with the Fe1...Fe1 separations in [Fe(H-3-OEt-thsa-Me)(3-OEt-thsa-Me)]·H₂O. The Fe1 and Fe11 units are assembled with Fe1...Fe11 (–x + 1, –y + 1, –z + 1) separations of 9.644(3) Å and Fe1...Fe11 (–x + 2, –y + 1, –z + 1)

10.371(3) Å. The hydrogen bonding interactions of $[\text{Fe}(\text{H-3-OEt-thsa-Me})(3\text{-OEt-thsa-Me})]\cdot\text{H}_2\text{O}$ are listed in Table 4.3.4. The terminal N atom N3 of the anionic ligand coordinated to Fe1 forms an $\text{N3-H3}\cdots\text{O401}$ contact involving the water solvent oxygen atom O401.

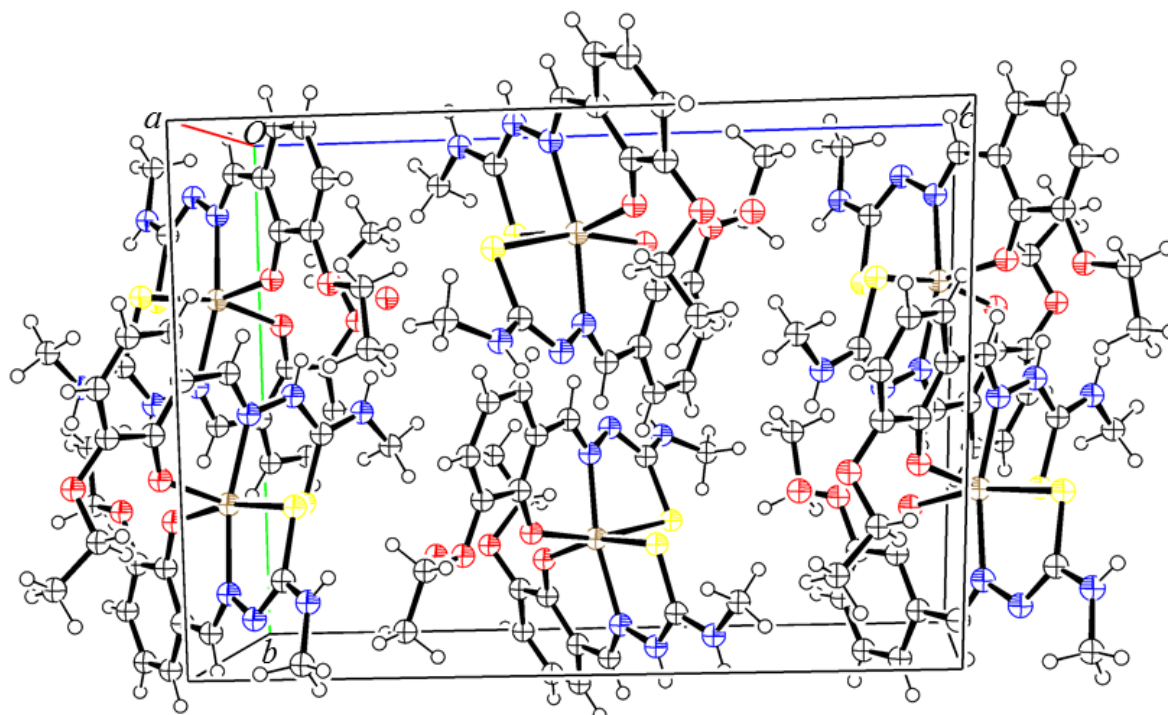


Figure 4.3.2 A projection of the unit cell of $[\text{Fe}(\text{H-3-OEt-thsa-Me})(3\text{-OEt-thsa-Me})]\cdot\text{H}_2\text{O}$. Displacement ellipsoids are drawn at the 50% probability level.

Table 4.3.4 Hydrogen bond geometry of $[\text{Fe}(\text{H-3-OEt-thsa-Me})(3\text{-OEt-thsa-Me})]\cdot\text{H}_2\text{O}$ (Å, °)

$D\text{-H}\cdots A$	$D\text{-H}$	$\text{H}\cdots A$	$D\cdots A$	$D\text{-H}\cdots A$
$\text{N3-H3}\cdots\text{O401}$	0.86	2.01	2.82 (3)	155.0

4.3.3 Infrared spectroscopic studies of $[\text{Fe}(\text{H-3-OEt-thsa-Me})(3\text{-OEt-thsa-Me})]\cdot\text{H}_2\text{O}$ and the ligand 3-ethoxysalicylaldehyde 4-methylthiosemicarbazone, $\text{H}_2\text{-3-OEt-thsa-Me}$

Similarly to compound $[\text{Fe}(\text{H-thsa-Me})(\text{thsa-Me})]\cdot\text{H}_2\text{O}$, the infrared spectrum of $[\text{Fe}(\text{H-3-OEt-thsa-Me})(3\text{-OEt-thsa-Me})]\cdot\text{H}_2\text{O}$ displays the relevant bands corresponding to the typical peaks expected for a ferric complex containing both a thione and thiol tautomeric form of the ligand. The assignments of the main infrared spectroscopic bands of the Fe^{III} complex and corresponding ligand, 3-ethoxysalicylaldehyde 4-methylthiosemicarbazone, are listed in Table 4.3.5. The infrared spectrum of the free ligand exhibits bands in the regions 1606 cm^{-1} and 1107 cm^{-1} , which are assigned

to $\nu\text{C}=\text{N}$ and νCS bands, respectively, indicating the free ligand is in the thione form. The coordination of the ligand to the Fe^{III} is accompanied by negative shifts of the $\nu\text{C}=\text{N}$ and νCS bands and a positive shift of the νCO band with regards to the free ligand, therefore indicating the coordination of the Fe^{III} ion to the O,N,S-donor atoms.

Table 4.3.5 Selected infrared spectroscopic bands (cm^{-1}) with assignments of $[\text{Fe}(\text{H-3-OEt-thsa-Me})(3\text{-OEt-thsa-Me})]\cdot\text{H}_2\text{O}$ and H_2L ligand, 3-ethoxysalicylaldehyde 4-methylthiosemicarbazone.

Compound	$\nu\text{C}=\text{N}$	$\nu\text{N}=\text{C}$	νNN	νCS	νCO
H_2L	1606	-	1167	1107	1061
$[\text{Fe}(\text{H-3-OEt-thsa-Me})(3\text{-OEt-thsa-Me})]\cdot\text{H}_2\text{O}$	1597	1582	1239	727	1213

4.3.4 Magnetic properties of $[\text{Fe}(\text{H-3-OEt-thsa-Me})(3\text{-OEt-thsa-Me})]\cdot\text{H}_2\text{O}$

The magnetic behaviour of $[\text{Fe}(\text{H-3-OEt-thsa-Me})(3\text{-OEt-thsa-Me})]\cdot\text{H}_2\text{O}$ is shown by the temperature dependence of the $\chi_{\text{M}}T$ value (χ_{M} being the molar magnetic susceptibility and T being the temperature) measured in the 5-300 K temperature range and is displayed in Figure 4.3.3. The product of magnetic susceptibility and the temperature shows a plateau, revealing the compound to be in the high-spin state over the temperature range 5-300 K, in both the heating and cooling modes. The value of $\chi_{\text{M}}T$ is $4.09 \text{ cm}^3 \text{ K mol}^{-1}$ for $[\text{Fe}(\text{H-3-OEt-thsa-Me})(3\text{-OEt-thsa-Me})]\cdot\text{H}_2\text{O}$ at 300 K, which is close to the value expected for high-spin compounds ($S = 5/2$) where $\chi_{\text{M}}T = 4.37 \text{ cm}^3 \text{ K mol}^{-1}$ for $g = 2.00$. The lower than expected value of $\chi_{\text{M}}T$ of $4.09 \text{ cm}^3 \text{ K mol}^{-1}$ for $[\text{Fe}(\text{H-3-OEt-thsa-Me})(3\text{-OEt-thsa-Me})]\cdot\text{H}_2\text{O}$ at 300 K, may be due to residual low-spin Fe^{III} , with a corresponding low-spin fraction estimated at 6%.

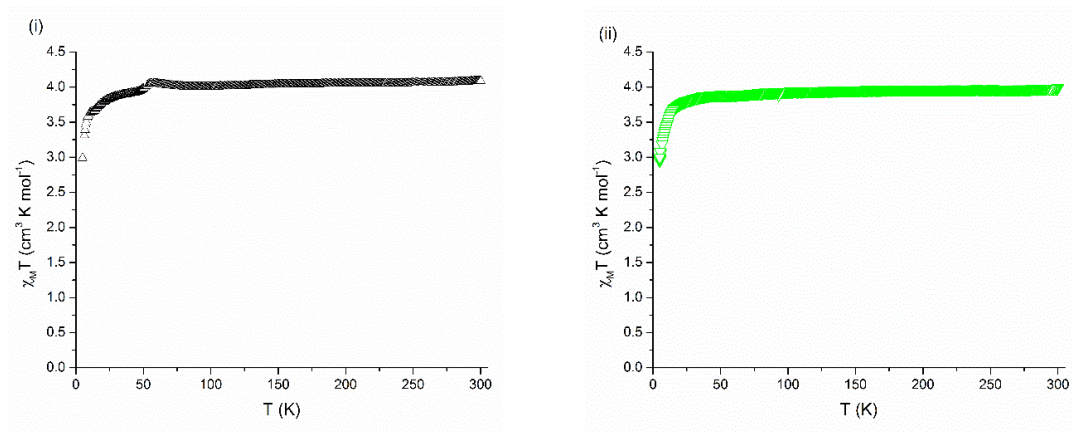


Figure 4.3.3 $\chi_{\text{M}}T$ vs T plot of $[\text{Fe}(\text{H-3-OEt-thsa-Me})(3\text{-OEt-thsa-Me})]\cdot\text{H}_2\text{O}$ in the temperature range of 5 – 300 K, measured at a rate of 2 K min^{-1} . (i) The heating mode is shown on the left and represented by the symbol (Δ) and (ii) the cooling mode on the right is represented by the symbol (∇).

The DSC curves of [Fe(H-3-OEt-thsa-Me)(3-OEt-thsa-Me)]·H₂O, as displayed in Figure 4.3.4, correlates with the temperature dependent magnetic susceptibility data that a phase transition in the temperature range 5-300 K is absent.

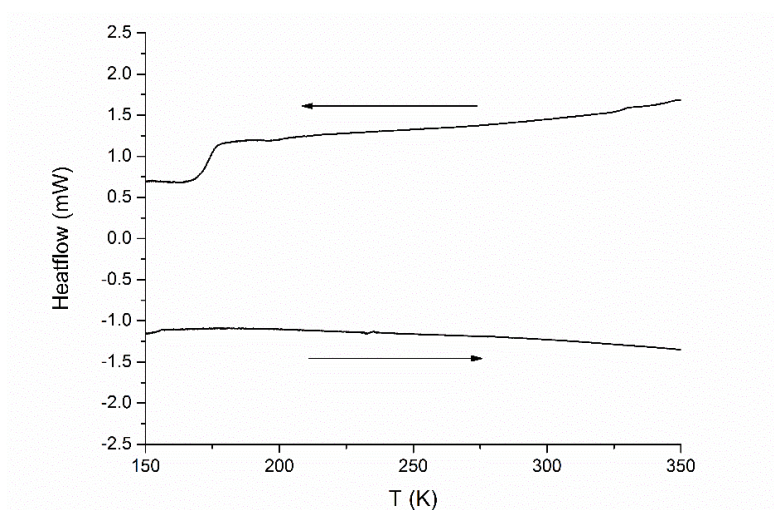


Figure 4.3.4 DSC curves obtained for [Fe(H-3-OEt-thsa-Me)(3-OEt-thsa-Me)]·H₂O in the temperature range 150-350 K, measured at a scan rate of 5 K min⁻¹.

As illustrated in Figure 4.3.3, the $\chi_M T$ value decreases abruptly below the temperature 50 K; this is a consequence of the significant zero-field splitting of the ground state Fe^{III} ion in the high-spin state. This feature has been found to be common in high-spin Fe^{III} compounds [39-40]. The zero-field splitting was calculated using equation (1) [39]:

$$\chi_M = \frac{Ng^2 \beta^2}{4kT} \left[\frac{0.14 + 5.12e^{-3.23X} + 23.85e^{-6.83X}}{1 + e^{-3.23X} + e^{-6.83X}} \right] \quad \text{Eqn (1)}$$

In this equation, $X = D/kT$, D is the zero-field splitting parameter, g is the average g tensor value and the other symbols have their standard meanings (as shown in Chapter I). As reported by Chen *et al.*, [39] equation (1) is the theoretical equation for the magnetic susceptibility resulting from the axial and rhombic zero-field splitting for a Fe^{III} $S = 5/2$ ion. The least squares fit (Figure 4.3.5) between the temperature range 5-150 K has been obtained with the parameters $D = 2.85 \text{ cm}^{-1}$ and $g = 2.18$, for [Fe(H-3-OEt-thsa-Me)(3-OEt-thsa-Me)]·H₂O, with a coefficient of determination value of 0.99 and a reduced χ^2 value of 0.0001.

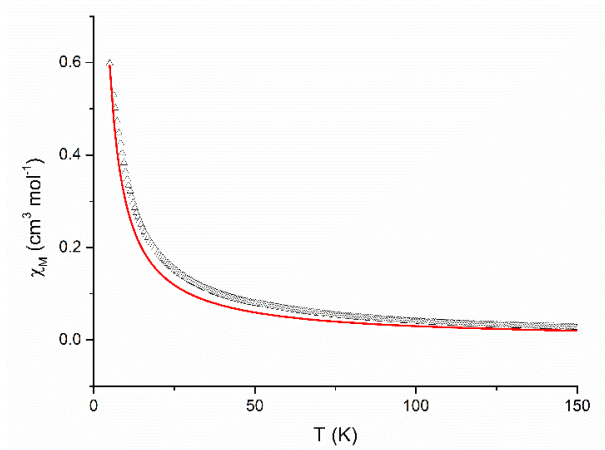


Figure 4.3.5 Temperature dependence of the molar magnetic susceptibility, χ_M , for the compound $[\text{Fe}(\text{H}-3\text{-OEt-thsa-Me})(3\text{-OEt-thsa-Me})]\cdot\text{H}_2\text{O}$ in the range 5-150 K. Points represent the cooling mode experimental data; solid red line represents the least-squares fit of the data to Equation (1), where $D = 2.85 \text{ cm}^{-1}$ and $g = 2.18$.

4.4 The crystal structure and magnetic properties of $[\text{Fe}(\text{H}-5\text{-Cl-thsa-Me})(5\text{-Cl-thsa-Me})]\cdot\text{H}_2\text{O}$ ¹

In this section the crystallographic data and magnetic properties of the ferric complex $[\text{Fe}(\text{H}-5\text{-Cl-thsa-Me})(5\text{-Cl-thsa-Me})]\cdot\text{H}_2\text{O}$ are reported. Furthermore, the infrared spectroscopic studies of the free ligand and ferric complex are also discussed. The synthesis of $[\text{Fe}(\text{H}-5\text{-Cl-thsa-Me})(5\text{-Cl-thsa-Me})]\cdot\text{H}_2\text{O}$ and corresponding H_2L ligand, 5-chlorosalicylaldehyde 4-methylthiosemicarbazone ($\text{H}_2-5\text{-Cl-thsa-Me}$), is detailed in Chapter II – Materials and Methods.

4.4.1 Crystal Data and Structural Refinement Details of $[\text{Fe}(\text{H}-5\text{-Cl-thsa-Me})(5\text{-Cl-thsa-Me})]\cdot\text{H}_2\text{O}$

Crystal data, data collection and structure refinement details are summarised in Table 4.4.1. The Fe1 atom has a site occupancy of 0.5, whereby the symmetry transformation (i) $-x + 1, -y + 1, z$ generates the equivalent atoms of the coordinated ligand 5-chlorosalicylaldehyde methylthiosemicarbazone. The position of the hydrogen atoms on the secondary amine nitrogen atoms N2, N2ⁱ, N3 and N3ⁱ were located in difference Fourier maps and refined with restrained N–H distances of 0.88(2) Å and with $U_{\text{iso}}(\text{H}) = 1.2 U_{\text{eq}}(\text{N})$. The hydrogen atoms attached to the O1W of the water molecule were

¹ An article was published during the preparation of this thesis regarding the compound $[\text{Fe}(\text{H}-5\text{-Cl-thsa-Me})(5\text{-Cl-thsa-Me})]\cdot\text{H}_2\text{O}$. Reference: Li, Z.-Y., Dai, J.-W., Gagnon, K. J., Cai, H.-L., Yamamoto, T., Einaga, Y., Zhao, H.-H., Kanegawa, S., Sato, O., Dunbar, K. R. and Xiong, R.-R. (2013). *Dalton. Trans.* **42**, pp. 14685-14688.

located in a difference Fourier map and refined with restrained O–H distances of 0.87(2) Å and with $U_{\text{iso}}(\text{H}) = 1.5 U_{\text{eq}}(\text{O})$. Moreover, the H2 atom bound to the N2 atom has a site occupancy factor of 0.5. The water solvent molecule has a site occupancy of 0.5. The remaining hydrogen atoms were included in the refinement in calculated positions, riding on their parent atoms, with C–H = 0.95 Å and $U_{\text{iso}}(\text{H}) = 1.2 U_{\text{eq}}(\text{C})$ for aryl H atoms.

Table 4.4.1 Crystal data and structure refinement details of [Fe(H-5-Cl-thsa-Me)(5-Cl-thsa-Me)]·H₂O

Crystal data	
Chemical formula	[Fe(C ₉ H ₈ ClN ₃ OS)(C ₉ H ₉ ClN ₃ OS)]·H ₂ O
M _r	558.26
Crystal system, space group	Orthorhombic, Aea2
Temperature (K)	100
a, b, c (Å)	11.4264 (8), 22.6178 (16), 8.7809 (6)
α, β, γ (°)	90, 90, 90
V (Å ³)	2269.3 (3)
Z	4
Radiation type	Mo Kα
μ (mm ⁻¹)	1.12
Crystal size (mm)	0.09 x 0.09 x 0.01
Data collection	
Diffractometer	Rigaku AFC12 four-circle Kappa diffractometer
Absorption correction	Multi-scan (<i>CrystalClear-SM Expert</i> [31])
T _{min} , T _{max}	0.663, 1.000
No. of measured, independent and observed [I > 2σ(I)] reflections	14234, 2541, 1877
R _{int}	0.114
Refinement	
R[F ² > 2σ(F ²)], wR(F ²), S	0.077, 0.173, 0.95
No. of reflections	2541
No. of parameters	159
No. of restraints	6
H-atom treatment	H atoms treated by a mixture of independent and constrained refinement
Δρ _{max} , Δρ _{min} (e Å ⁻³)	1.20, -0.39

The program used for the structure solution: *CrystalClear-SM Expert* 2.1 b29 [31]; the structure refinement used the programs *SUPERFLIP* [32] and *SHELXL-2014* [33]. The *OLEX2* [34] and *ORTEP-3* for Windows [35] programs were used to produce the molecular graphics [35].

4.4.2 Crystallographic study of $[\text{Fe}(\text{H-5-Cl-thsa-Me})(5\text{-Cl-thsa-Me})]\cdot\text{H}_2\text{O}$

The crystal structure of the compound $[\text{Fe}(\text{H-5-Cl-thsa-Me})(5\text{-Cl-thsa-Me})]\cdot\text{H}_2\text{O}$ was determined at 100 K, and is illustrated in Figure 4.4.1. It crystallises in the orthorhombic crystal system in the space group *Aea*2, where $Z = 4$ and $Z' = 0.5$ (where Z is the number of formula units per unit cell and Z' is the number of formula units per asymmetric unit). The asymmetric unit consists of $1/2$ $[\text{Fe}(\text{HL})(\text{L})]$ fragment and half of a solvent water molecule. The ligands coordinated around the Fe^{III} cation are related by symmetry, and are generated by the symmetry transformation $(-x + 1, -y + 1, z)$. The Fe^{III} atom of the present compound is coordinated to two O,N,S-tridentate ligands, a two-fold deprotonated ligand [$\text{L} = 5\text{-chlorosalicylaldehyde 4-methylthiosemicarbazonato}(2-)$] and a one-fold deprotonated ligand [$\text{HL} = 5\text{-chlorosalicylaldehyde 4-methylthiosemicarbazonato}(1-)$]. However, due to the disorder of the H-atom on the imine N-atoms, N2 and N2ⁱ, within each Fe^{III} unit it is not clear which ligand is (-2) or (-1) charged. The compound $[\text{Fe}(\text{H-5-Cl-thsa-Me})(5\text{-Cl-thsa-Me})]\cdot\text{H}_2\text{O}$ has been found to be isostructural to $[\text{Fe}(\text{H-thsa-Me})(\text{thsa-Me})]\cdot\text{H}_2\text{O}$.

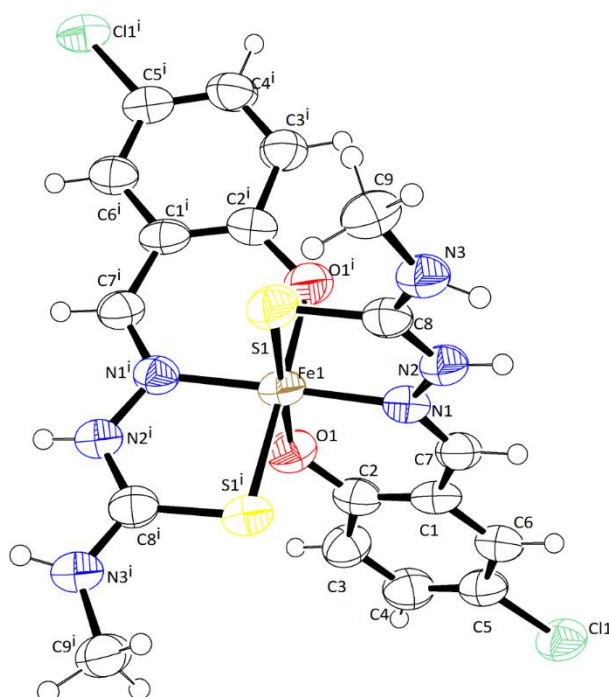


Figure 4.4.1 The molecular structure and atom-numbering scheme for $[\text{Fe}(\text{H-5-Cl-thsa-Me})(5\text{-Cl-thsa-Me})]\cdot\text{H}_2\text{O}$, whereby the second ligand bound to Fe1 atom is generated by the symmetry operation (i) $-x + 1, -y + 1, z$. The hydrogen atom bound to N2 and N2ⁱ atoms has a site occupancy

factor of 0.5, *i.e.* the atom is disordered over the N2 and N2ⁱ sites (50:50). The H₂O molecule has been omitted for clarity. Displacement ellipsoids are drawn at the 50% probability level.

The dianionic and anionic O,N,S-tridentate ligands coordinate to the Fe^{III} cation to form an distorted octahedral FeO₂N₂S₂ geometry. The dianionic ligand is deprotonated at the phenolate-O and the thiolate-S, whereas the anionic ligand is deprotonated at the phenolate-O atom, only. The donor atoms of the ligands are orientated in two perpendicular planes, with the O and S atoms in the *cis* positions [O1–Fe1–O1ⁱ = 89.6 (4)° and S1–Fe1–S1ⁱ = 92.02 (15)°] and the N atoms in the *trans* positions [N1–Fe1–N1ⁱ = 175.2 (5)°]. Selected geometric parameters are listed in Table 4.4.2.

Table 4.4.2 Selected geometric parameters of [Fe(H-5-Cl-thsa-Me)(5-Cl-thsa-Me)]·H₂O (Å, °)

Fe1–S1 ⁱ	2.255 (3)	Fe1–N1 ⁱ	1.969 (6)
Fe1–O1 ⁱ	1.951 (7)		
S1–Fe1–S1 ⁱ	92.02 (15)	O1 ⁱ –Fe1–N1	90.5 (3)
S1–Fe1–N1	86.2 (2)	N1–Fe1–N1 ⁱ	175.2 (5)
S1–Fe1–O1	178.5 (2)	Fe1–O1–C2	125.4 (6)
S1–Fe1–O1 ⁱ	89.2 (2)	O1–C2–C1	125.2 (8)
S1–Fe1–N1 ⁱ	90.5 (2)	C2–C1–C7	123.2 (8)
S1 ⁱ –Fe1–O1	89.2 (2)	C1–C7–N1	126.1 (8)
S1 ⁱ –Fe1–N1	90.5 (2)	C7–N1–Fe1	126.1 (6)
O1–Fe1–O1 ⁱ	89.6 (4)	C8–S1–Fe1	95.8 (3)
O1–Fe1–N1	92.9 (3)	N1–N2–C8	116.2 (7)
O1–Fe1–N1 ⁱ	90.5 (3)	N2–C8–S1	122.5 (7)

Symmetry transformation used to generate equivalent atoms: (i) $-x + 1, -y + 1, z$.

The Fe-donor atom bond distances suggest that the Fe^{III} cation in the present compound is in the low-spin state at 100 K. Typical distances for Fe–S, Fe–O and Fe–N bonds are 2.23–2.31, 1.93–1.95 and 1.88–1.96 Å, respectively, for low-spin Fe^{III} compounds of this family, and 2.40–2.44, 1.96–1.99 and 2.05–2.15 Å, respectively, for the corresponding high-spin Fe^{III} compounds [4]. Comparison of the bond distances of the present compound involving the Fe^{III} atom and the donor atoms (Table 4.4.2) suggests that the present compound contains low-spin Fe^{III} at 100 K.

The Fe^{III}O₂N₂S₂ chromophore is formed by two six-membered chelates and two five-membered chelates via the two-fold and one-fold deprotonated tridentate 5-chlorosalicylaldehyde 4-

methylthiosemicarbazone ligands. The five-membered chelate rings bite angle is significantly restricted [$S1-Fe1-N1 = S1^i-Fe1-N1^i = 86.2(2)^\circ$] in comparison to the wider bite angles of the six-membered chelate rings [$O1-Fe1-N1 = O1^i-Fe1-N1^i = 92.9(3)^\circ$]. The ligands coordinated to the Fe^{III} cation show no major strain relief through puckering of the five- and six-membered chelate rings. The five-membered chelate ring shows root-mean-square deviations of 0.08 Å; the corresponding values are 0.045 Å for the six-membered chelate ring. In comparison to the bite angle of the regular hexagon of 120° , the O–Fe1–N bite angles of the six-membered chelate rings are deficient by ca. 27° . The remaining bite angles (listed in Table 4.4.2) of the six-membered chelate are within 2° of 125° . Moreover, the five-membered chelate S–Fe1–N bite angles are deficient by ca. 23° of the vertex angle (108°) expected for the regular pentagon. The C–S–Fe1 angles form an additional deficiency of 13° , which suggests the remaining bite angles (listed in table 4.2.2) of the 5-membered chelate ring would be expected to be ca. 120° . However, the N–N–C angle is $115.9(7)^\circ$ and the N–C–S angles are $123.0(7)^\circ$. The chelating O,N,S-tridentate ligands allows for further stabilisation of the present compound through the near alternation of the single and double bonds, giving rise to a high degree of π -electron delocalisation throughout the chelate rings.

Li *et al.*, reported the structure of the compound $[Fe(H-5-Cl-thsa-Me)(5-Cl-thsa-Me)] \cdot H_2O$ at 110, 260 and 293 K [26]. Single crystal X-ray structure determination revealed the compound to crystallise in the monoclinic system and the polar *Cc* space group at 110, 260 and 293 K. The noticeable difference between the compound $[Fe(H-5-Cl-thsa-Me)(5-Cl-thsa-Me)] \cdot H_2O$ reported by Li *et al.*, and in this thesis, is the space group the compound crystallises. Li *et al.*, reported the monoclinic space group *Cc*, whereas the present work reports orthorhombic space group, *Aea2*. The major difference between the unit cells is the β angle, for the space group *Cc* the β angle is $91.301(3)^\circ$ (at 110 K) whereas for *Aea2* the β angle = 90.00° .

The Fe^{III} cation was found to be in the low-spin state at 110 K and in the high-spin state at 293 K. The compound $[Fe(H-5-Cl-thsa-Me)(5-Cl-thsa-Me)] \cdot H_2O$ [26] displays an $Fe^{III}O_2N_2S_2$ octahedral environment which is comprised of both the anionic and dianionic ligand, therefore the 5-chlorosalicylaldehyde 4-methylthiosemicarbazone ligands are in the thione and thiol tautomeric form, respectively. In the present compound $[Fe(5-Cl-thsa-Me)(H-5-Cl-thsa-Me)] \cdot H_2O$, it should be noted that the bond distances are an average for the anionic and dianionic deprotonated ligand forms, due to the ligands being related by symmetry. This geometric feature is shown by the bond distances of the C–S, C–N and N–N bonds of the symmetry related ligands. The N1–N2, N2–C8 and C8–S1 bonds distances at 100 K are 1.395(10) Å, 1.328(11) Å and 1.748(8) Å, respectively. This corresponds to the N–N, N–C and C–S bond distances the compound $[Fe(H-5-Cl-thsa-Me)(5-Cl-thsa-Me)] \cdot H_2O$ at 110 K, reported by Li *et al.*, [26].

The packing of $[\text{Fe}(\text{H-5-Cl-thsa-Me})(5\text{-Cl-thsa-Me})]\cdot\text{H}_2\text{O}$ is displayed in Figure 4.4.2 and the hydrogen bonding interactions are listed in Table 4.4.3 and displayed in Figure 4.4.3. $[\text{Fe}(\text{H-5-Cl-thsa-Me})(5\text{-Cl-thsa-Me})]\cdot\text{H}_2\text{O}$ displays $\text{Fe}^{\text{III}}\cdots\text{Fe}^{\text{III}}$ ($x - 1/2, -y + 1, z - 1/2$) separations of 7.1829(18) Å; 8.747(3) Å for $\text{Fe}\cdots\text{Fe}$ ($-x + 1, -y + 1, z - 1$) and 12.093(4) Å for $\text{Fe}\cdots\text{Fe}$ ($-x + 1, -y + 1/2, z - 1/2$). The Fe^{III} units are linked together by $\text{N-H}\cdots\text{O}$ hydrogen bonds in the a direction. The $\text{N3-H3}\cdots\text{O1}^{\text{iii}}$ ($x + 1/2, -y + 1, z + 1/2$) contact is formed between the terminal amide nitrogen atom, N3 and the phenolate-O atom O1. The water solvent molecule is involved in hydrogen bonding with the metal complex units within the unit cell. Firstly, the hydrazinic nitrogen atom, N2 forms the contact $\text{N2-H2}\cdots\text{O1W}^{\text{ii}}$ ($-x + 3/2, y, z + 1/2$) with the oxygen atom of the water molecule, O1W.

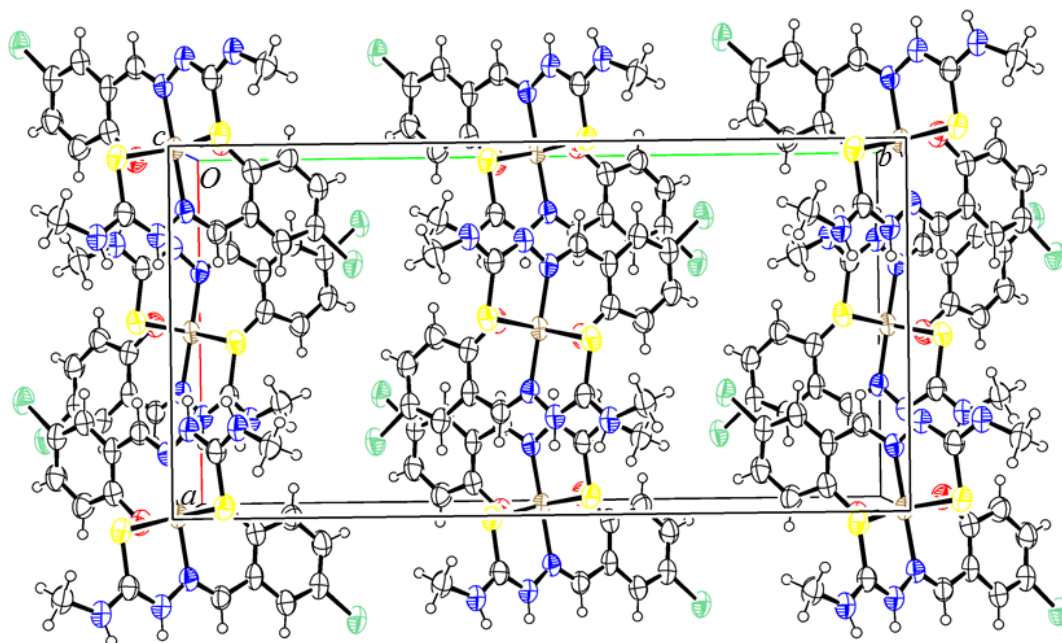


Figure 4.4.2 A projection showing the unit cell of $[\text{Fe}(\text{H-5-Cl-thsa-Me})(5\text{-Cl-thsa-Me})]\cdot\text{H}_2\text{O}$. The disordered H_2O molecule has been omitted for clarity. The displacement ellipsoids are drawn at the 50% probability level.

The O1W atom of the water solvent molecule also forms a hydrogen bond with the phenolate-O1 and O1^{i} atoms, $\text{O1W-H1WB}\cdots\text{O1}$ and $\text{O1W-H1WB}\cdots\text{O1}^{\text{i}}$ ($-x + 1, -y + 1, z$). A ring system is created by the following hydrogen bonds: $\text{N3-H3}\cdots\text{O1}^{\text{iii}}$ ($x + 1/2, -y + 1, z + 1/2$), $\text{N2-H2}\cdots\text{O1W}^{\text{ii}}$ and $\text{O1W-H1WB}\cdots\text{O1}$. This particular ring system is formed by two acceptor atoms [the phenolate O1 and solvent oxygen O1W atoms] and 3 donor atoms, thus forming a $\text{R}^2_3(8)$ system [27]. Furthermore, the $\text{O1W-H1WB}\cdots\text{O1}$ and $\text{O1W-H1WB}\cdots\text{O1}^{\text{i}}$ ($-x + 1, -y + 1, z$) contacts form a hydrogen bonding ring system. In turn, the phenolate O1 and symmetry related phenolate O1^{i} atoms acts as a hydrogen acceptor of the H-atom, H1WB, from the solvent water oxygen atom O1W, giving rise to a $\text{R}^2_1(4)$ ring [27]. It should be noted that the hydrogen bond ring system involving the

phenolate-O atoms (O1 and O1ⁱ) which are coordinated to the Fe^{III} atom, could affect the Fe-O donor atom bond distances, and therefore the spin state of Fe^{III}.

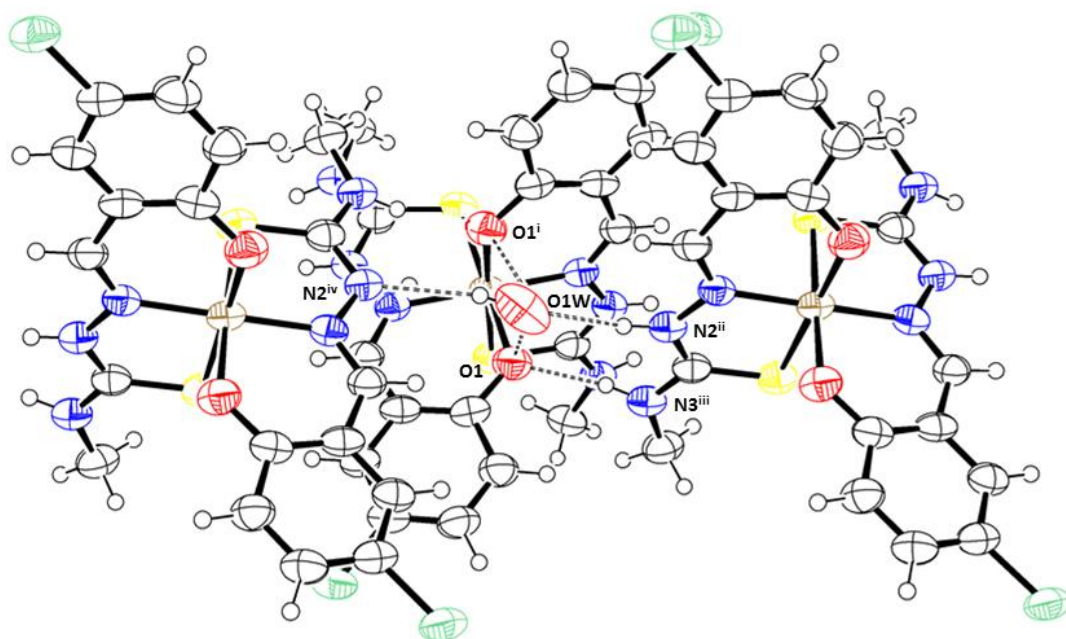


Figure 4.4.3 Hydrogen bonding system of [Fe(H-5-Cl-thsa-Me)(5-Cl-thsa-Me)]·H₂O in the *a* direction. An alternative orientation for H1WA and H1WB has been omitted for clarity. The displacement ellipsoids are drawn at the 50% probability level. [Symmetry codes: (i) $-x + 1, -y + 1, z$; (ii) $-x + 3/2, y, z + 1/2$; (iii) $x + 1/2, -y + 1, z + 1/2$; (iv) $-x + 3/2, y, z - 1/2$.]

Table 4.4.3 Hydrogen bond geometry of [Fe(H-5-Cl-thsa-Me)(5-Cl-thsa-Me)]·H₂O (Å, °)

D-H...A	D-H	H...A	D...A	D-H...A
N2-H2...O1W ⁱⁱ	0.88 (3)	2.22 (6)	3.085 (7)	166 (18)
N3-H3...O1 ⁱⁱⁱ	0.87 (3)	1.94 (3)	2.807 (11)	176 (10)
O1W-H1WA...N2 ^{iv}	0.86 (3)	2.28 (14)	3.085 (7)	157 (32)
O1W-H1WB...O1 ⁱ	0.85 (3)	2.3 (3)	3.008 (14)	135 (33)
O1W-H1WB...O1	0.85 (3)	2.3 (4)	3.008 (14)	140 (49)

Symmetry codes: (i) $-x + 1, -y + 1, z$; (ii) $-x + 3/2, y, z + 1/2$; (iii) $x + 1/2, -y + 1, z + 1/2$; (iv) $-x + 3/2, y, z - 1/2$.

4.4.3 Infrared spectroscopic study of $[\text{Fe}(\text{H-5-Cl-thsa-Me})(\text{5-Cl-thsa-Me})]\cdot\text{H}_2\text{O}$ and the corresponding ligand 5-chlorosalicylaldehyde 4-methylthiosemicarbazone, $\text{H}_2\text{-5-Cl-thsa-Me}$

Similarly, to compound $[\text{Fe}(\text{H-thsa-Me})(\text{thsa-Me})]\cdot\text{H}_2\text{O}$, the infrared spectrum of $[\text{Fe}(\text{H-5-Cl-thsa-Me})(\text{5-Cl-thsa-Me})]\cdot\text{H}_2\text{O}$ displays the relevant bands to give rise the typical peaks expected for a ferric complex containing both a thione and thiol tautomeric form of the ligand. The infrared spectra of $[\text{Fe}(\text{H-5-Cl-thsa-Me})(\text{5-Cl-thsa-Me})]\cdot\text{H}_2\text{O}$ and the corresponding free ligand, 5-chlorosalicylaldehyde 4-methylthiosemicarbazone, are given in the appendix. In contrast to the ferric complex spectrum, the infrared spectrum of the ligand 5-chlorosalicylaldehyde 4-methylthiosemicarbazone shows a νOH peak at 3397 cm^{-1} which indicates the presence of the OH group of the phenol. As the ligand binds to the central metal Fe^{III} ion, it is possible for the tridentate ligand to be present in the anionic and dianionic form. The anionic ligand is singly deprotonated at the phenolate-O atom and the dianionic ligand is doubly deprotonated thus no hydrogen atom would be located at the phenolate-O or thiolate-S atoms. The present ferric complex contains both the anionic and dianionic form of the ligand, subsequently the vibration of the OH group of the phenol is not present in the ferric complex spectrum as expected. The deprotonation of the phenolate-O atom after complexation to the metal ion is also supported by the shift of the frequency of the $\nu\text{C-O}$ band from 1100 cm^{-1} to 1315 cm^{-1} , in the ligand to the ferric complex, respectively [18, 21]. The positive shift of the $\nu\text{C-O}$ band frequency indicates the coordination of the Fe^{III} ion to the phenolate-O atom. The azomethine nitrogen atom is confirmed to have coordinated to the metal ion due to the shift of the C=N band from 1604 cm^{-1} in the free ligand to 1600 cm^{-1} in the complex [18, 21, 37]. The absence of the S-H bond in the range $2600\text{-}2800\text{ cm}^{-1}$ in the infrared spectrum of the ligand, indicates the ligand is present in the thione form, which is confirmed by the vibration at 1182 cm^{-1} which corresponds to the CS band [18, 21, 37]. Furthermore, the coordination of the S atom to the Fe^{III} ion is corroborated by the shift of the C-S band to 815 cm^{-1} in the ferric complex from 1028 cm^{-1} νCS with regards to the free ligand [37].

4.4.4 Magnetic properties of $[\text{Fe}(\text{H-5-Cl-thsa-Me})(\text{5-Cl-thsa-Me})]\cdot\text{H}_2\text{O}$

The temperature dependence of the $\chi_{\text{M}}T$ product (χ_{M} being the molar magnetic susceptibility and T, the temperature) for $[\text{Fe}(\text{H-5-Cl-thsa-Me})(\text{5-Cl-thsa-Me})]\cdot\text{H}_2\text{O}$ was measured in the temperature range 5-320 K and is presented in Figure 4.4.4. The magnetic properties of the present compound reveal a rare two-step spin transition between low-spin ($S = 1/2$) and high-spin ($S = 5/2$) states of the Fe^{III} ion, with an observed hysteresis effect. The value of $\chi_{\text{M}}T$ is $3.80\text{ cm}^3\text{ mol}^{-1}\text{ K}$ at 320 K, which corresponds to the expected value of high-spin Fe^{III} , $\chi_{\text{M}}T = 4.37\text{ cm}^3\text{ mol}^{-1}\text{ K}$ ($g = 2.00$). Furthermore, at 100 K, the magnetic properties of $[\text{Fe}(\text{H-5-Cl-thsa-Me})(\text{5-Cl-thsa-Me})]\cdot\text{H}_2\text{O}$ indicate that the value of $\chi_{\text{M}}T$ ($0.65\text{ cm}^3\text{ mol}^{-1}\text{ K}$) is slightly higher than the value expected for a low-spin Fe^{III} ion,

$\chi_M T = 0.375 \text{ cm}^3 \text{ mol}^{-1} \text{ K}$ for $g = 2.00$. The transition temperatures of the two steps are centered at temperatures of $T_{1/2(S1)\uparrow} = 249 \text{ K}$ and $T_{1/2(S2)\uparrow} = 277 \text{ K}$ (where S1 and S2 represent the spin transition temperature of step 1 and step 2, respectively), respectively, and $T_{1/2(S1)\downarrow} = 240 \text{ K}$ and $T_{1/2(S2)\downarrow} = 271 \text{ K}$, respectively. These values give rise to a thermal hysteresis for $T_{1/2(S1)}$ and $T_{1/2(S2)}$ of about 9 K and 6 K, respectively.

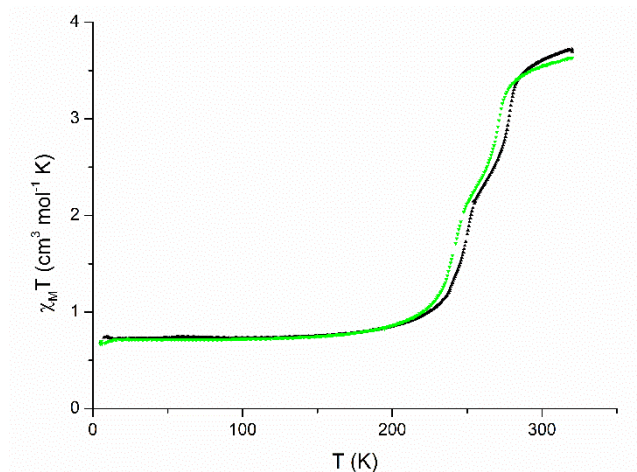


Figure 4.4.4 $\chi_M T$ vs T plot of $[\text{Fe}(\text{H-5-Cl-thsa-Me})(\text{5-Cl-thsa-Me})] \cdot \text{H}_2\text{O}$. The sample was warmed (▲) and then subsequently cooled (▼) in the temperature region of 5–320 K, at a rate of 2 K min^{-1} .

The DSC curves of $[\text{Fe}(\text{H-5-Cl-thsa-Me})(\text{5-Cl-thsa-Me})] \cdot \text{H}_2\text{O}$ is displayed in Figure 4.4.5. The DSC curves displays a peak at $T_{\downarrow} = 242$ and 269 K in the cooling mode and $T_{\uparrow} = 247$ and 274 K in the heating mode. The data corroborates with the temperature dependent magnetic susceptibility data in that the ferric complex exhibits a two-step spin transition.

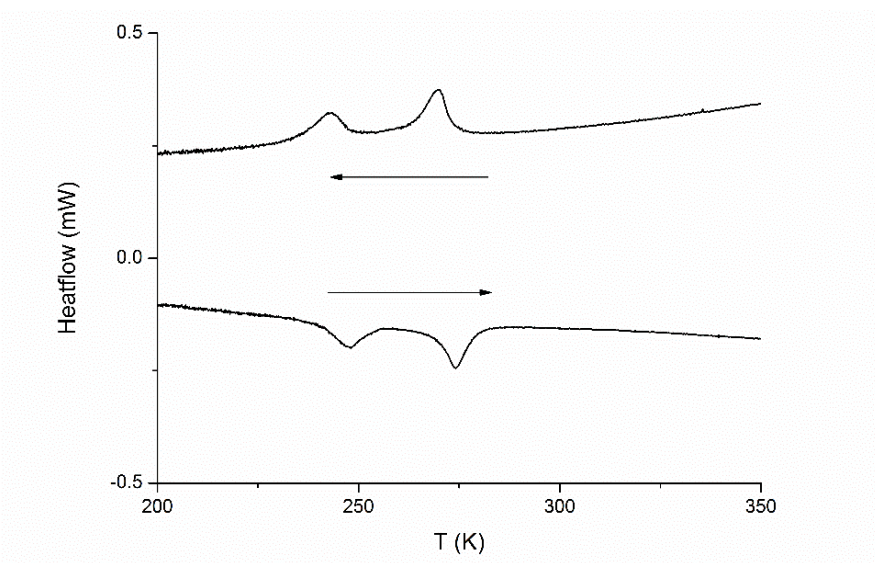


Figure 4.4.5 DSC curves obtained for $[\text{Fe}(\text{H-5-Cl-thsa-Me})(\text{5-Cl-thsa-Me})] \cdot \text{H}_2\text{O}$ in the temperature range 200–350 K, measured at a scan rate of 5 K min^{-1} .

4.5 Discussion

This chapter reported the structural characterisation and magnetic behaviour of three novel mononuclear Fe^{III} compounds, containing a one-fold and a two-fold deprotonated R-salicylaldehyde 4R'-thiosemicarbazone ligand. The aim of this study is to attempt to construct correlations between the steric and electronic effects imposed by the R- and R'-substituents of the ligands to the Fe^{III} ions and the magnetic properties observed. The structures of [Fe(H-thsa-Me)(thsa-Me)]·H₂O, [Fe(H-3-OEt-thsa-Me)(3-OEt-thsa-Me)]·H₂O and [Fe(H-5-Cl-thsa-Me)(5-Cl-thsa-Me)]·H₂O consist of an Fe^{III}O₂N₂S₂ chromophore which is formed by a chelating tridentate anionic R-salicylaldehyde 4R'-thiosemicarbazonato(1-) ligand and a dianionic R-salicylaldehyde 4R'-thiosemicarbazonato(2-) ligand. The Fe^{III}O₂N₂S₂ chromophore exhibits a distorted octahedral geometry, where the O- and S-donor atoms are in the *cis* positions and the N-donor atoms are in the *trans* positions. It should be noted that for the isostructural compounds, [Fe(H-thsa-Me)(thsa-Me)]·H₂O and [Fe(H-5-Cl-thsa-Me)(5-Cl-thsa-Me)]·H₂O the ligands coordinated to the Fe^{III} atom are related by symmetry. Interestingly, the two compounds [Fe(H-thsa-Me)(thsa-Me)]·H₂O and [Fe(H-5-Cl-thsa-Me)(5-Cl-thsa-Me)]·H₂O are chiral, although this is a rare occurrence due to the fact that no chiral compounds were used in the synthesis of the ferric complexes to induce chirality. The Fe-donor atom bond distances of the [Fe(HL)(L)]·H₂O compounds described in this chapter are listed in Table 4.5.1.

The compounds [Fe(H-thsa-Me)(thsa-Me)]·H₂O and [Fe(H-5-Cl-thsa-Me)(5-Cl-thsa-Me)]·H₂O at 100 K both contain a Fe^{III} cation in the low-spin state, whereas the Fe^{III} cation in [Fe(H-3-OEt-thsa-Me)(3-OEt-thsa-Me)]·H₂O is high-spin at 100 K.

In the following, the crystallographic data of [Fe(H-thsa-Me)(thsa-Me)]·H₂O, [Fe(H-3-OEt-thsa-Me)(3-OEt-thsa-Me)]·H₂O and [Fe(H-5-Cl-thsa-Me)(5-Cl-thsa-Me)]·H₂O will be compared to similar Fe^{III} bis(ligand) compounds reported in the literature (listed in Table 4.5.2) in an attempt to correlate the structural features of these materials with the spin state of the Fe^{III} cation. Table 4.5.2 shows the Fe-donor atom bond distances of the [Fe(HL)(L)]·H₂O type compounds together with the spin state of the Fe^{III} cation at the temperature at which the crystal structure was determined.

The compounds [Fe(H-thsa)(thsa)]·H₂O and [Fe(H-5-Cl-thsa)(5-Cl-thsa)]·H₂O at 293 K both contain a Fe^{III} cation in the high-spin state [20]. The Fe^{III} cation in [Fe(H-5-Br-thsa)(5-Br-thsa)]·H₂O is high-spin at 303 K and low-spin at 123 K [18]. Furthermore, in the compound [Fe(H-5-Cl-thsa-Me)(5-Cl-thsa-Me)]·H₂O the Fe^{III} cation is in the low-spin state at 110 K and in the high-spin state at 293 K [21].

Table 4.5.1 Selected crystallographic data and spin state for [Fe(HL)(L)]·H₂O type complexes of R-salicylaldehyde 4R'-thiosemicarbazone ligands described in this chapter.

Compound ⁱ	T ⁱⁱ (K)	Space group	Fe–S (Å)	Fe–N (Å)	Fe–O (Å)	Spin State ⁱⁱⁱ
[Fe(H-thsa-Me)(thsa-Me)]·H ₂ O ^{iv}	100	<i>Aea2</i>	2.249(2) 2.249(2)	1.946(5) 1.946(5)	1.932(5) 1.932(5)	LS
[Fe(H-3-OEt-thsa-Me)(3-OEt-thsa-Me)]·H ₂ O ^v	100	<i>P-1</i>	2.473(4) 2.442(4) 2.482(2) 2.417(4)	2.168(10) 2.085(10) 2.416(5) 2.096(11)	1.939(4) 1.996(9) 1.958(5) 1.994(8)	Fe1 HS Fe11 HS
[Fe(H-5-Cl-thsa-Me)(5-Cl-thsa-Me)]·H ₂ O ^{iv}	100	<i>Aea2</i>	2.255(3) 2.255(3)	1.969(6) 1.969(6)	1.951(7) 1.951(7)	LS

ⁱ The ligands are defined as follows: salicylaldehyde 4-methylthiosemicarbazone = H₂-thsa-Me (H₂L form), 3-ethoxysalicylaldehyde 4-methylthiosemicarbazone = H₂-3-OEt-thsa-Me (H₂L form) and 5-chlorosalicylaldehyde 4-methylthiosemicarbazone = H₂-5-Cl-thsa-Me (H₂L form); in the case that there are different ligands coordinated to the Fe atom, the geometric parameters involving each ligand (HL and L) are given in separate lines.

ⁱⁱ T represents the measurement temperature.

ⁱⁱⁱ The spin states are defined as low-spin (LS) and high-spin (HS).

^{iv} Fe^{III} donor atom bond distances are an average for the one-fold and two-fold deprotonated ligand forms, due to the ligands being related by the symmetry operation: $-x + 1, -y + 1, z$.

^v Compound contains two crystallographically independent Fe sites (Fe1 and Fe11).

As significant changes in the electronic state of Fe^{III} bis(ligand) compounds may arise from the associated R- and R'-substituents of the ligand; in addition to the steric effects we may consider the electronic effects imposed by the position on a particular R-group on the salicylaldehyde moiety. Dependent upon the R-group and the position of the R-group on the benzene ring, the R-group may be electron withdrawing or an electron donating group, which may affect the phenolate C–O bond length, whereby the phenolate O-atom is bound to the central metal ion, Fe^{III}. As the bond distances of the Fe-donor atoms may reveal what spin state the Fe^{III} cation may exhibit (in a specific temperature range), it may be stated that the position of the R-group and the type of R-group of the benzene ring may affect whether the ferric complexes exhibit an spin transition. Although, it must be duly noted that the Fe–O bond distances seem to be less sensitive to change in Fe^{III} spin state than Fe–N and Fe–S bond distances, which may be related to the π -acceptor capability of the N- and S-donor atoms opposed to the π -donor capability of the O-donor atoms. This is of particular significance when the Fe^{III} is in the low-spin state, as increased π back-bonding will lead to comparatively more pronounced shortening of the Fe–N and Fe–S bonds than of the Fe–O bonds.

Table 4.5.2 Selected Fe-donor atom bond distances and spin state for [Fe(HL)(L)]·H₂O type complexes of R-salicylaldehyde 4R'-thiosemicarbazone ligands described in the literature.

Compound ⁱ	T ⁱⁱ (K)	Space group	Fe–S (Å)	Fe–N (Å)	Fe–O (Å)	Spin State ⁱⁱⁱ
[Fe(H-thsa)(thsa)]·H ₂ O [20]	293	<i>P2₁/n</i>	2.444(7) 2.370(7)	2.111(6) 2.166(6)	1.927(5) 1.894(5)	HS
[Fe(H-5-Cl-thsa)(5-Cl-thsa)]·H ₂ O [20]	293	<i>P2₁/n</i>	2.386(13) 2.346(13)	2.210(11) 2.118(12)	1.920(17) 1.902(16)	HS
[Fe(H-5-Br-thsa)(5-Br-thsa)]·H ₂ O [18]	303	<i>P2₁/n</i>	2.4845(18) 2.4177(19)	2.153(4) 2.131(4)	1.969(4) 1.952(4)	HS
	123	<i>P2₁/n</i>	2.2718(17) 2.2463(17)	1.952(5) 1.955(4)	1.941(4) 1.949(4)	LS
[Fe(H-5-Cl-thsa-Me)(5-Cl-thsa-Me)]·H ₂ O [21]	293	<i>Cc</i>	2.453(4) 2.391(4)	2.124(9) 2.11(10)	1.937(9) 1.916(9)	HS
	110	<i>Cc</i>	2.2566(16) 2.2389(150)	1.948(5) 1.993(5)	1.933(4) 1.940(4)	LS

ⁱ The ligands are defined as follows: salicylaldehyde thiosemicarbazone = H₂thsa (H₂L form), 5-chlorosalicylaldehyde thiosemicarbazone = H₂-5-Cl-thsa (H₂L form), 5-bromosalicylaldehyde thiosemicarbazone = H₂-5-Br-thsa (H₂L form) and 5-chlorosalicylaldehyde 4-methylthiosemicarbazone = H₂-5-Cl-thsa-Me (H₂L form); in the case that there are different ligands coordinated to the Fe atom, the geometric parameters involving each ligand (HL and L) are given in separate lines.

ⁱⁱ T represents the measurement temperature.

ⁱⁱⁱ The spin states are defined as low-spin (LS) and high-spin (HS).

In the following, the electronic and steric effects of the R and R'-substituents of the R-salicylaldehyde 4R'-thiosemicarbazone ligand on the magnetic properties of the ferric complexes will be discussed, as well as the affects imposed by the R, R'-substituents intermolecular interactions formed between the Fe^{III} units.

4.5.1 Electronic effects of R and R'-substituents of the R-salicylaldehyde 4R'-thiosemicarbazone ligand

Studies conducted by Zelentsov *et al.*, [10] revealed that replacing the H atom (R-substituent) of carbon atom 5 (illustrated in Figure 4.5.1) of the benzene ring of salicylaldehyde may lead to significant changes in the magnetic properties of the ferric bis(ligand) compounds. The transition from the low-spin ($S = 1/2$) to the high-spin ($S = 5/2$) state is governed by the energy difference

between these two electronic states; this energy gap can be tuned by the variation of the ligand field strength, which can be influenced by the R-group of the benzene ring, as the transfer of electronic properties of the substituent through the benzene ring is enabled by the π -delocalisation in this ring [10].

If one considers the influence of the inductive effect caused by various R-substituents, the R-substituents can be organised according to the magnitude of electron density that is withdrawn or donated to the benzene ring via electron withdrawing groups and electron donating groups, respectively. The following list of groups show the magnitude of inductive effects in different substituents:

- (i) Decreasing order of electron withdrawing effect of these substituents:



- (ii) Decreasing order of electron donating effect of these substituents:

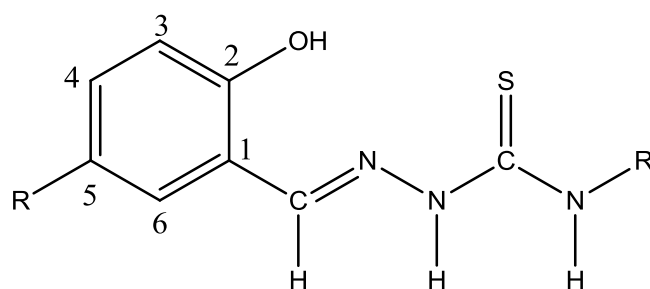
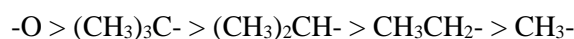


Figure 4.5.1 Atom labelling of the benzene ring of the R-salicylaldehyde 4R'-thiosemicarbazone ligand.

Zelentsov and co-workers found that the substituents studied for Fe^{III} bis(ligand) compounds containing two dianionic R-salicylaldehyde 4R'-thiosemicarbazone(2-) ligands, whereby the R-substituent replaces the H atom of the carbon atom 5 (illustrated in Figure 4.5.1), have been categorised in the following sequence according to the capability of favouring low-spin state of Fe^{III}: NO₂ > H > CH₃ > Cl > Br [10].

The compounds reported in this chapter, [Fe(H-thsa-Me)(thsa-Me)]·H₂O, [Fe(H-3-OEt-thsa-Me)(3-OEt-thsa-Me)]·H₂O and [Fe(H-5-Cl-thsa-Me)(5-Cl-thsa-Me)]·H₂O (listed in Table 4.5.1), contain the R-substituents, R = H, R = 3-OEt and R = 5-Cl, respectively, and all of the compounds contain the R'-substituent, R' = Me. In accordance with the sequence of the capability of favouring low-spin state of Fe^{III} in ferric bis(R-salicylaldehyde 4R'-thiosemicarbazone) compounds, the three novel compounds reported have been categorised in the following sequence: H > Cl > -OEt. An attempt to reveal the electronic effect of the R-substituents are accounted for by the Hammett constants (normal

σ^n values) of the R group of the R-salicylaldehyde 4R'-thiosemicarbazone ligand system, R = H where $\sigma^n = 0.00$, R = 3-OEt where $\sigma^n = 0.10$, and R = 5-Cl where $\sigma^n = 0.37$ [1]. Typically it has been found that for coordination complexes the higher the spin transition temperature, the larger the electron withdrawing effect, which is corroborated by the linear relationship between the Hammett parameter (σ^n) and the spin-transition temperature ($T_{1/2}$). For the series of compounds containing both the anionic and dianionic R-salicylaldehyde 4R'-thiosemicarbazone ligand, the complex with R = 3-OEt remains in the high-spin state, where R = H no spin transition is observed and for the compound containing R = 5-Cl, the complex exhibits a rare two-step spin transition. It could be suggested that electron donating groups could stabilise the high spin state with the addition of the steric hindrance the ortho-OEt R-substituents presents, *i.e.* the π -back bonding decreases, whilst the electron withdrawing groups (R = H, or Cl) results in increasing π -back bonding and decreasing in the σ -bonding in the Fe-O(R-thsa-R') bond. As a result of increased π -back bonding, the larger the π -acceptor properties of the Fe-donor atom bonds are, subsequently giving rise to softer acidity of the Fe^{III} ion. Consequently, the Fe^{III} ion is more likely to adopt the low-spin Fe^{III} electronic configuration, as well as a higher spin-crossover temperature ($T_{1/2}$) dependent upon the R-substituent. Similar compounds reported in the literature such as [Fe(H-thsa)(thsa)]·H₂O [20], [Fe(H-5-Cl-thsa)(5-Cl-thsa)]·H₂O [20] and [Fe(H-5-Br-thsa)(5-Br-thsa)]·H₂O [18] (spin state and $T_{1/2}$ displayed in Table 4.5.2 and 4.5.3, respectively), also show the similar trend between the Hammett parameter and the electron withdrawing effect, with respect to favouring the low-spin state. In this series of compounds and similar Fe^{III} compounds reported in the literature [18,20], the electronic effect on the spin-crossover behaviour of the R-groups suggests that the larger the electron withdrawing effect the lower the $T_{1/2}$ which is corroborated by the linear relationship between $T_{1/2}$ and the Hammett parameters H (0.00) > 5-Cl (0.37) > 5-Br (0.39).

4.5.2 Steric effects of R- and R'-substituents of the R-salicylaldehyde 4R'-thiosemicarbazone ligand

In an attempt to correlate the structural features of the R-salicylaldehyde 4R'-thiosemicarbazone ligands to the Fe^{III} spin-state, one needs to consider the introduction of the substituents into the benzene ring of the salicylaldehyde moiety or the integration of a substituent into the thioamide of the thiosemicarbazone moiety. The compounds reported in this chapter, [Fe(H-thsa-Me)(thsa-Me)]·H₂O, [Fe(H-3-OEt-thsa-Me)(3-OEt-thsa-Me)]·H₂O and [Fe(H-5-Cl-thsa-Me)(5-Cl-thsa-Me)]·H₂O (listed in Table 4.5.1), contain the R-substituents, R = H, R = 3-OEt and R = 5-Cl, respectively, and all of the compounds contain the R'-substituent, R' = Me. The related Fe^{III} bis(ligand) compounds displayed in Table 4.5.2 contain the following R- and R'-substituents, [Fe(H-thsa)(thsa)]·H₂O, R and R' = H, [Fe(H-5-Cl-thsa)(5-Cl-thsa)]·H₂O, R = 5-Cl and R' = H, [Fe(H-5-

Br-thsa)(5-Br-thsa)]·H₂O, R = 5-Br and R' = H, [Fe(H-5-Cl-thsa-Me)(5-Cl-thsa-Me)]·H₂O, R = 5-Cl and R' = Me. Firstly, we consider the influence of the substituent R-group on the benzene ring on the magnetic behaviour of the ferric complexes, as this is the main difference between the compounds discussed in this chapter and the compounds listed in Table 4.5.2. The R-substituents present in the ferric complexes listed in Tables 4.5.1 and 4.5.2, R = H, -5-Cl, -5-Br or -3-OEt all have an electron withdrawing effect on the benzene ring of the salicylaldehyde moiety. It would appear that the R-substituents R = -H, -5-Cl or -5-Br, facilitate an increase in Δ_o (octahedral crystal field splitting parameter) and assist the Fe^{III} cation to exhibit a spin transition, as shown by compounds [Fe(H-5-Cl-thsa-Me)(5-Cl-thsa-Me)]·H₂O (Chapter IV), [Fe(H-thsa)(thsa)]·H₂O [20], [Fe(H-5-Cl-thsa)(5-Cl-thsa)]·H₂O [20] and [Fe(H-5-Br-thsa)(5-Br-thsa)]·H₂O [18]. The presence of the R-substituent at the 5-position of the salicylaldehyde moiety impacts the operating temperature of the spin transition, in this case the ability of the R-substituents R = -H, -5-Cl or -5-Br to increase Δ_o can be arranged in the following sequence: -H > -5-Cl > -5-Br [18, 20]. However, the presence of the R-substituent (R = H or -3-OEt) does not facilitate an increase in the Δ_o in order to generate a spin transition for the reported spin-crossover inactive compounds [Fe(H-thsa-Me)(thsa-Me)]·H₂O and [Fe(H-3-OEt-thsa-Me)(3-OEt-thsa-Me)]·H₂O. It could be suggested that the replacement of the H atom with the methyl group on the terminal nitrogen atom of the thiosemicarbazone moiety has both electronic and steric effects on the spin-crossover behaviour of these two compounds. The integration of the R' = Me within the thiosemicarbazone moiety for the spin-crossover compound [Fe(H-5-Cl-thsa-Me)(5-Cl-thsa-Me)]·H₂O [Chapter IV, 21] reveals that the temperature at which the transition occurs is much higher than that observed for spin-crossover compounds with R' = H; the spin-transition temperatures are listed in Table 4.5.3. Furthermore, the obvious steric interactions induced by the presence of the halogen at 5-position of the R-salicylaldehyde fragment causes the spin-state transition to operate at lower temperature, thereby affecting the temperature at which the spin transition occurs.

By comparison, for the low-spin [Fe(H-thsa-Me)(thsa-Me)]·H₂O, the Fe^{III}-donor atom bond distances are 2.249(2) Å (Fe-S), 1.946(5) Å (Fe-N) and 1.932(5) Å (Fe-O) at 100 K, while at the same temperature, for [Fe(H-3-OEt-thsa-Me)(3-OEt-thsa-Me)]·H₂O the coordination bond distances for the anionic ligand (H-3-OEt-thsa-Me) are Fe1-O1 = 1.939(4) Å and Fe11-O201 = 1.958(5) Å; Fe1-S1 = 2.473(4) Å and Fe11-S201 = 2.482(2) Å; and Fe1-N1 = 2.168(10) Å and Fe11-N201 = 2.146(5) Å, severally. Furthermore, the Fe-O, Fe-S and Fe-N bond distances for the dianionic ligand (3-OEt-thsa-Me) are Fe1-O101 = 1.996(9) Å and Fe11-O301 = 1.994(8) Å; Fe1-S101 = 2.442(4) Å and Fe11-S301 = 2.417(4) Å; and Fe1-N101 = 2.085(10) Å and Fe11-N301 = 2.096(11) Å, severally. 2.455 Å (Fe-S), 2.125 Å (Fe-N) and 1.975 Å (Fe-O), which are characteristic of a high-spin species. It appears that the R-group could sterically prohibit the corresponding system [Fe(H-3-OEt-thsa-Me)(3-OEt-thsa-Me)]·H₂O to exhibit spin-crossover properties: it may be that the 3-

ethoxy substituent group does not allow the contraction of the octahedron typically observed during the high-spin to low-spin transition. The hindered contraction of the octahedron could be caused by the positioning of the ethoxy group on the benzene ring, as the ethoxy group is bound at the carbon 3 atom, which is next to the carbon atom bound to the phenolate-O donor atom. Moreover, the strong steric interactions of the “bulky” ethoxy group in the complex apparently prevents such shortening in the Fe-donor atom distances, so the Fe^{III} ion remains in the high-spin state.

Table 4.5.3 Transition temperatures (K) for selected spin-crossover [Fe(HL)(L)]·H₂O compounds.

Compound ⁱ	T _{1/2} [↑] ⁱⁱ	T _{1/2} [↓] ⁱⁱⁱ	Ref
[Fe(H-thsa)(thsa)]·H ₂ O	275	(1) 262 (2) 232	[20]
[Fe(H-5-Cl-thsa)(5-Cl-thsa)]·H ₂ O	231	230	[20]
[Fe(H-5-Br-thsa)(5-Br-thsa)]·H ₂ O	(1) 148 (2) 173 (3) 194 (4) 212 (5) 245	(1) 242 (2) 238 (3) 211 (4) 194 (5) 170 (6) 144	[18]
[Fe(H-5-Cl-thsa-Me)(5-Cl-thsa-Me)]·H ₂ O	(1) 249 (2) 278	(1) 270 (2) 245	[21]

ⁱ The ligands are defined as follows: salicylaldehyde thiosemicarbazone = H₂thsa (H₂L form), 5-chlorosalicylaldehyde thiosemicarbazone = H₂-5-Cl-thsa (H₂L form), 5-bromosalicylaldehyde thiosemicarbazone = H₂-5-Br-thsa (H₂L form) and 5-chlorosalicylaldehyde 4-methylthiosemicarbazone = H₂-5-Cl-thsa-Me (H₂L form).

ⁱⁱ Transition temperature in heating mode (K). NB: Multiple step transitions are numbered.

ⁱⁱⁱ Transition temperature in cooling mode (K). NB: Multiple step transitions are numbered.

4.5.3 R- and R'-substituents as hydrogen bonding donor or acceptor atoms and π - π stacking interactions

It would appear the steric and electronic features of either the R or R'-substituent may have an impact on the spin state of Fe^{III} cations, and affect at which temperature the spin transition occurs. Moreover, the steric and electronic features may affect the degree of cooperativity between Fe^{III} entities due to the packing arrangement of the Fe^{III} units within the unit cell imposed by intermolecular interactions of the coordinated R-salicylaldehyde 4R'-thiosemicarbazone ligands. The R and/or R'-substituent may assist the intricate formation of hydrogen bonding networks as well as the possibility of the benzene rings forming π - π stacking interactions between the Fe^{III} entities. It is evidenced throughout

that spin-crossover materials reported in the literature reveal that the symmetry and packing arrangements within the unit cell of these types of materials influence whether the materials exhibit a spin transition. It is recognised that in these type of spin-crossover systems strong cooperativity can be influenced by the packing arrangements of the Fe^{III} entities within the unit cell. There are two possible features that may cause the behaviour of strong cooperativity: (i) the intermolecular π - π stacking interactions between the benzene rings of the salicylaldehyde fragment and (ii) the hydrogen bonding networks. In comparison to the low-spin compounds [Fe(H-thsa-Me)(thsa-Me)]·H₂O and [Fe(H-5-Cl-thsa-Me)(5-Cl-thsa-Me)]·H₂O and the high-spin compound [Fe(H-3-OEt-thsa-Me)(3-OEt-thsa-Me)]·H₂O, it appears that the compounds listed in Table 4.5.2 exhibit π - π stacking and have extensive hydrogen bonding networks [18, 20-21]. In addition, if the hydrogen bonding network connecting the Fe^{III} entities, involves a coordinating donor atom and/or an atom next to the Fe^{III} donor atom, may cause an electronic effect, which could then prohibit the ferric complex to generate the spin conversion from the low- to high-spin state for Fe^{III}. However, it is unclear at this stage how these particular features can be harnessed to induce a particular spin-state for Fe^{III}.

4.6 Conclusion

In this chapter, three neutral ferric complexes, [Fe(H-thsa-Me)(thsa-Me)]·H₂O, [Fe(H-3-OEt-thsa-Me)(3-OEt-thsa-Me)]·H₂O and [Fe(H-5-Cl-thsa-Me)(5-Cl-thsa-Me)]·H₂O, were synthesised with the aim of ligand modification in an approach to tune spin-crossover properties of [Fe^{III}(HL)(L)]·xH₂O type compounds. Single crystal X-ray crystallographic measurements at 100 K determined that the Fe^{III} cations of the compounds [Fe(H-thsa-Me)(thsa-Me)]·H₂O and [Fe(H-5-Cl-thsa-Me)(5-Cl-thsa-Me)]·H₂O were in the low-spin state and [Fe(H-3-OEt-thsa-Me)(3-OEt-thsa-Me)]·H₂O was in the high-spin state. Magnetic measurements performed on these compounds evidenced that the two neutral compounds [Fe(H-thsa-Me)(thsa-Me)]·H₂O and [Fe(H-3-OEt-thsa-Me)(3-OEt-thsa-Me)]·H₂O do not exhibit a temperature dependent spin transition in the temperature range 5-300 K, which was corroborated by the DSC measurements. A rare two-step spin-crossover was observed for the compound [Fe(H-5-Cl-thsa-Me)(5-Cl-thsa-Me)]·H₂O in the temperature range 5-320 K. Similar compounds have been reported in the literature by Yemeli Tido [20], Li *et al.*, [18, 21] and Floquet *et al.* [30] and have been compared to the three neutral compounds reported in this chapter. In an attempt to correlate the structural properties of these Fe^{III} compounds and their corresponding R-salicylaldehyde 4R'-thiosemicarbazone ligands and the magnetic behaviours, the discussion's main focus considered the ligand modification in terms of the electronic and steric effects caused by the variation of the R- and R'-substituents and how these features influenced the crystal packing and the magnetic behaviour exhibited by the ferric complexes. It has been recognised that the increased steric interactions induced by the presence of the R-substituents, R = -5-Cl or -5-

Br of the R-salicylaldehyde moiety cause the spin-state transition to operate at lower temperature. Moreover, the introduction of R' = Me to the thiosemicarbazone moiety for the spin-crossover compound [Fe(H-5-Cl-thsa-Me)(5-Cl-thsa-Me)]·H₂O reveals the spin-state transition operates at a higher temperature than the transition temperature observed for spin-crossover compounds with R' = H. The low-spin compound [Fe(H-thsa-Me)(thsa-Me)]·H₂O exhibits an incomplete spin-transition in the temperature range 5-400 K; it could be suggested that the presence of the R' = Me causes electronic and steric effects which prevent the full spin-state conversion from the low-spin to the high-spin state. Furthermore, for the spin-crossover inactive compound [Fe(H-3-OEt-thsa-Me)(3-OEt-thsa-Me)]·H₂O, the electronic effects and the steric interactions of both the R and R'-substituents (R = -3-OEt and R' = Me) do not allow the contraction of the FeO₂N₂S₂ octahedron typically observed during the high-spin to low-spin transition, so as observed in the magnetic behaviour, the ferric complex remains in the high-spin state in temperature range 5-300 K. In order to develop a strategy to tune this type of ferric complex to exhibit a temperature dependent spin transition, it is evident a larger number of magnetic measurements and analysis of crystallographic data will be required.

4.7 References

1. Létard, J.-F., Guionneau, P. and Goux-Capes, L. (2004). *Spin Crossover in Transition Metal Compounds III*, edited by Gütllich, P. and Goodwin, H. A., *Top. Curr. Chem.* Berlin: Springer, **235**, pp. 221-249.
2. Gütllich, P., Koningsbruggen, P. J. van., Renz, F. (2004). *Struct. Bonding.*, **107**, pp. 27-75.
3. Gütllich, P. and Goodwin, H. A. (2004). Editors. *Spin Crossover in Transition Metal Compounds I*, edited by Gütllich, P. and Goodwin, H. A., *Top. Curr. Chem.* Berlin: Springer, **233**, pp. 1-47.
4. Koningsbruggen, P. J. van., Maeda, Y. and Oshio, H. (2004). *Spin Crossover in Transition Metal Compounds I*, edited by Gütllich, P. and Goodwin, H. A., *Top. Curr. Chem.* Berlin: Springer, **233**, pp. 259-324.
5. Koningsbruggen, P. J. van. (2004). *Spin Crossover in Transition Metal Compounds I*, edited by Gütllich, P. and Goodwin, H. A., *Top. Curr. Chem.* Berlin: Springer, **233**, pp. 123-149.
6. Cambi, L. and Szegö, L. (1931). *Ber. dtsh. Chem. Ges A/B*, **64**, pp. 2591-2598.
7. Cambi, L. and Szegö, L. (1933). *Ber. dtsh. Chem. Ges A/B*, **66**, pp. 656-661.
8. Hayami, S., Gu, Z. Z., Shiro, M., Einaga, Y., Fujishima, A. and Sato, O. (2000). *J. Am. Chem. Soc.*, **122**(29), pp. 7126-7127.
9. Hayami, S., Hiki, K., Kawahara, T., Maeda, Y., Urakami, D., Inoue, K., Ohama, M., Kawata, S. and Sato, O. (2009). *Chem. Eur. J.*, **15**(14), pp. 3497-3508.

10. Zelentsov, V. V., Bogdanova, L. G., Ablov, A. V., Gerbelev, N. V. and Dyatlova, Ch. V. (1973). *Russ. J. Inorg. Chem.* **18**(10), pp. 1410-1412.
11. Ryabova, N. A., Ponomarev, V. I., Atovmyan, L. O., Zelentsov, V. V. and Shipilov, V. I. (1978). *Koord. Khim.* **4**, pp. 119-126.
12. Ryabova, N. A., Ponomarev, V. I., Zelentsov, V. V. and Atovmyan, L. O. (1981). *Kristallografiya.* **26**(1), pp. 101-108.
13. Ryabova, N. A., Ponomarev, V. I., Zelentsov, V. V., Shipilov, V. I. and Atovmyan, L. O. (1981). *J. Struct. Chem.* **22**(2), pp. 234-238.
14. Ryabova, N. A., Ponomarev, V. I., Zelentsov, V. V. and Atovmyan, L. O. (1982). *Sov. Phys. Crystallogr.* **27**(1), pp. 81-91.
15. Floquet, S., Boillot, M. L., Rivière, E., Varret, F., Boukheddaden, K., Morineau, D. and Négrier, P. (2003). *New. J. Chem.* **27**, pp. 341-348.
16. Floquet, S., Guillou, N., Négrier, P., Rivière, E. and Boillot, M. L. (2006). *New. J. Chem.* **30**, pp. 1621-1627.
17. Floquet, S., Muñoz, M. C., Guillot, R., Rivière, E., Blain, G., Réal, J. A. and Boillot, M. L. (2009). *Inorg. Chim. Acta.* **362**, pp. 56-64.
18. Li, Z.-Y., Dai, J. W., Shiota, Y., Yoshizawa, K., Kanegawa, S. and Sato, O. (2013). *Chem. Eur. J.* **19**(39), pp. 12948-12952.
19. Yemeli Tido, E. W., Alberda van Ekenstein, G. O. R., Meetsma, A. and Koningsbruggen, P. J. van. (2008). *Inorg. Chem.* **47**, pp. 143-153.
20. Yemeli Tido, E.W. (2010). PhD Thesis, University of Groningen: The Netherlands.
21. Li, Z.-Y., Dai, J.-W., Gagnon, K. J., Cai, H.-L., Yamamoto, T., Einaga, Y., Zhao, H.-H., Kanegawa, S., Sato, O., Dunbar, K. R. and Xiong, R.-R. (2013). *Dalton. Trans.* **42**, pp. 14685-14688.
22. Tao, J., Wei, R. J., Huang, R. B. and Zheng, L. S. (2012). *Chem. Soc. Rev.* **41**, pp. 703-737.
23. Dechambenoit, P. and Long, J. R. (2011). *Chem. Soc. Rev.* **40**, pp. 3249-3265.
24. Clemente-Leon, M., Coronado, E., Lopez-Jorda, M., Espallargas, G. M., Soriano-Portillo, A. and Waerenborgh, J. C. (2010). *Chem. Eur. J.* **16**(7), pp. 2207-2219.
25. Zhu, D. R., Qi, L., Cheng, H.M., Shen, X. A. and Lu, W. (2009). *Prog. Chem.* **21**, pp. 1187.
26. Gaspar, A. B., Seredyuk, M. and Gütllich, P. (2009). *J. Mol. Struct.* **924-926**, pp. 9- 19.
27. Seredyuk, M., Gaspar, A. B., Ksenofontov, V., Reiman, S., Galyametdinov, Y., Haase, W., Rentschler, E. and Gütllich, P. (2005). *Hyperfine Interact.* **166**, pp. 385-390.
28. Itkis, M. E., Chi, X., Cordes, A. W. and Haddon, R. C. (2002). *Science.* **296**, pp. 1443-1445.
29. Bonhommeau, S., Guillon, T., Daku, L. M. L., Demont, P., Costa, J. S., Létard, J. F., Molnár, G. and Bousseksou, A. (2006). *Angew. Chem.*, **118**, pp. 1655-1659.
30. Floquet, S., Rivière, E., Boukheddaden, K., Morineau, D. and Boillot, M.-L. (2014). *Polyhedron.*, **80**, pp. 60-68.

31. Rigaku (2014). *CrystalClear-SM Expert 3.1 b27*. Rigaku Corporation, The Woodlands, Texas, USA.
32. Palatinus, L. and Chapuis, G. (2007). *J. Appl. Cryst.* **40**, pp. 786-790.
33. Sheldrick, G.M. (2008). *Acta Cryst.* **A64**, pp. 112-122.
34. Dolomanov, O. V., Bourhis, L. J., Gildea, R. J., Howard, J. A. K. and Puschmann, H. (2009) *J. Appl. Cryst.* **42**, pp. 339-341.
35. Farrugia, L. J. (2012). *J. Appl. Cryst.* **45**, pp. 849-854.
36. *International Tables for Crystallography* (2006). Volume A, *Space-group symmetry*.
37. Kazou, N. (1986). *Infrared and Raman Spectra of Inorganic and Coordination Compounds.*, 4th Ed. New York: Wiley.
38. Rigaku (2010). *CrystalClear-SM Expert 2.0 r5*. Rigaku Corporation, The Woodlands, Texas, USA.
39. Chen, C.-H., Lee, Y.-Y., Liao, B.-C., Shanmugham, E., Chen, J.-H., Hsieh, H.-Y, Liao, F.-L. Wang, S.-L. and Hwang, L.-P. (2002). *J. Chem. Soc., Dalton. Trans.*, pp. 3001-3006.
40. Boča, R. (2004). *Coord. Chem. Rev.* **248**, pp. 757-815.
41. Hansch, C., Leo, A. and Taft, R. W. (1991). *Chem. Rev.* **99**, pp.165-195.

Chapter V
Cationic Fe(III) Complexes of
R-salicylaldehyde 4-R'-thiosemicarbazones

5.0 Cationic Fe(III) Complexes of R-salicylaldehyde 4R'-thiosemicarbazones

5.1 Introduction

In the preceding chapters, the magnetic behaviour of $(\text{cation}^+)[\text{Fe}(\text{L}^{2-})_2] \cdot x(\text{solvent})$ (Chapter III) and $[\text{Fe}(\text{HL}^-)(\text{L}^{2-})] \cdot \text{H}_2\text{O}$ (Chapter IV) type compounds were investigated on the basis of the structural data collected for each reported system. The structural and magnetic studies of the $(\text{cation}^+)[\text{Fe}(\text{L}^{2-})_2] \cdot x(\text{solvent})$ and $[\text{Fe}(\text{HL}^-)(\text{L}^{2-})] \cdot \text{H}_2\text{O}$ compounds demonstrated that the nature of the spin state of Fe^{III} ion is strongly influenced by different structural parameters. Thus far, studies focused on the Fe^{III} bis(R-salicylaldehyde 4R'-thiosemicarbazone) compounds have shown that the spin-crossover behaviour, the conversion from the low-spin ($S = 1/2$) state to the high-spin ($S = 5/2$) state, may be harnessed by the following structural parameters: the variation of the counter cation, the degree of deprotonation of the ligand, the integration of different R- and R'-substituents to the salicylaldehyde and thiosemicarbazone moieties, respectively, and the solvation of the Fe^{III} bis(ligand) complexes [1-12]. Furthermore, comparing the crystal structures of the $(\text{cation}^+)[\text{Fe}(\text{L}^{2-})_2] \cdot x(\text{solvent})$ and $[\text{Fe}(\text{HL}^-)(\text{L}^{2-})] \cdot \text{H}_2\text{O}$ type compounds reported in Chapter III and Chapter IV, respectively, to similar compounds reported in this research area [1-12], revealed that the different behaviours in magnetic properties of the Fe^{III} bis(R-salicylaldehyde 4R'-thiosemicarbazone) compounds may be due to the variation of significant intermolecular interactions such as hydrogen bonding in the system and whether the complexes are linked by π - π stacking interactions, thus giving rise to the modulation of the cooperativity in the R-salicylaldehyde 4R'-thiosemicarbazone containing compounds.

In this context, changing the degree of deprotonation of the ligand, the type of R- and R'-substituents of the ligand, and the type of anion present in the crystal lattice, may alter the supramolecular assembly of the Fe^{III} entities in the lattice and therefore the cooperativity of the spin-crossover behaviour of the Fe^{III} entities, and with it the magnetic behaviour of the Fe^{III} bis(ligand) complexes.

In this chapter, the crystallographic structures (at 100 K) and magnetic properties of $[\text{Fe}(\text{H-5-Br-thsa-Et})_2](\text{NO}_3) \cdot \text{H}_2\text{O}$ and $[\text{Fe}(\text{H-4-OH-thsa})_2]_4 \cdot (\text{SO}_4)_2 \cdot 9\text{H}_2\text{O}$ are reported. The ligands used to generate these ferric compounds are displayed in Figure 5.1.1. The effect of the anion, the R- and R'-substituents and the degree of solvation on the magnetic properties of the two $[\text{Fe}(\text{HL}^-)_2](\text{anion}^-) \cdot x\text{H}_2\text{O}$ type compounds will be discussed, and will propose the structural impact of the ligand modification, anion variation and degree of solvation on the magnetic behaviour of these two $[\text{Fe}(\text{HL}^-)_2](\text{anion}^-) \cdot x\text{H}_2\text{O}$ type compounds.

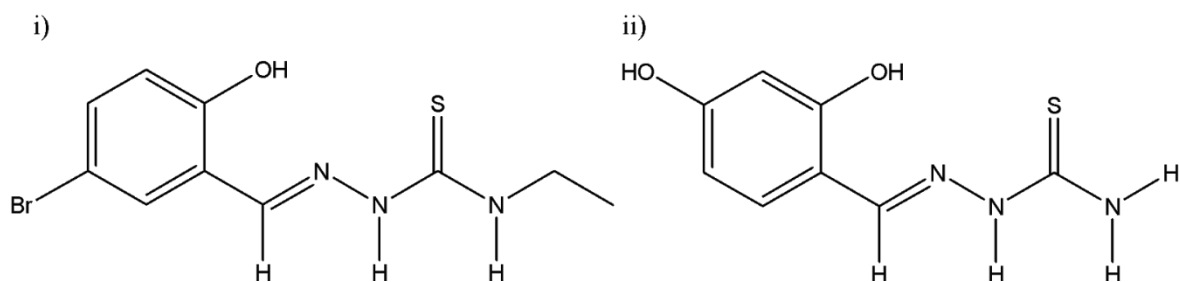


Figure 5.1.1 Molecular structure of the R-salicylaldehyde 4R'-thiosemicarbazone ligands (i) H₂-5-Br-thsa-Et and (ii) H₂-4-OH-thsa

5.2 The crystal structure and magnetic properties of [Fe(H-5-Br-thsa-Et)₂](NO₃)·H₂O

The magnetic properties are herein reported of the novel Fe^{III} compound [Fe(H-5-Br-thsa-Et)₂](NO₃)·H₂O containing two anionic tridentate 5-bromosalicylaldehyde 4-ethylthiosemicarbazone(1-) (HL⁻) ligands and the determination and description of its structure at 100 K. Furthermore, the infrared spectroscopic studies of the free ligand and ferric complex are discussed.

The experimental data is reported in Chapter II for the synthesis of [Fe(H-5-Br-thsa-Et)₂](NO₃)·H₂O and corresponding ligand, 5-bromosalicylaldehyde 4-ethylthiosemicarbazone.

5.2.1 Crystal Data and Structure Refinement Details of [Fe(H-5-Br-thsa-Et)₂](NO₃)·H₂O

Crystal data, data collection and structure refinement details are summarised in Table 5.2.1. The hydrogen atoms H10B and H10A of the water solvent molecule form hydrogen bonds with the O202 atom of the nitrate anion and the O11 phenolate donor atom, respectively; these bond distances were restrained by using the DFIX command to fix the geometry of the unbound nitrate anion and the solvent water molecule. The other hydrogen atoms were included in the refinement in calculated positions, and riding on their parent atoms, with N-H = 0.88 Å and $U_{\text{iso}}(\text{H}) = 1.2U_{\text{eq}}(\text{N})$, C-H = 0.95 Å and $U_{\text{iso}}(\text{H}) = 1.2U_{\text{eq}}(\text{C})$, C-H = 0.99 Å and $U_{\text{iso}}(\text{H}) = 1.2U_{\text{eq}}(\text{C})$, C-H = 0.98 Å and $U_{\text{iso}}(\text{H}) = 1.5U_{\text{eq}}(\text{C})$ for the amide (N-H), methine (-CH=), methylene (-CH₂-) and methyl (-CH₃) hydrogen atoms, severally. Additional details towards the structure refinement of [Fe(H-5-Br-thsa-Et)₂](NO₃)·H₂O are as follows: *SMTBX* solvent masking routine as implemented within Olex2 was used to mask residual electron density from unidentified solvent [13].

The program used for the structure solution: *SUPERFLIP* [15]; the structure refinement used the program *SHELXL-2014* [16]. The *OLEX2* [13] and *ORTEP-3* for Windows [17] programs were used to produce the molecular graphics.

Table 5.2.1 Crystal data and structure refinement details of [Fe(H-5-Br-thsa-Et)₂](NO₃)·H₂O

Crystal data	
Chemical formula	[Fe(H-5-Br-thsa-Et) ₂](NO ₃)·H ₂ O
M_r	738.35
Crystal system, space group	Orthorhombic, <i>Pnna</i>
Temperature (K)	100
a, b, c (Å)	12.3654(4), 23.2809(6), 19.6468(7)
α, β, γ (°)	90, 90, 90
V (Å ³)	5655.9(3)
Z	8
Radiation type	Mo $K\alpha$
μ (mm ⁻¹)	3.555
Crystal size (mm)	0.19 x 0.01 x 0.01
Data collection	
Diffractometer	Rigaku AFC12 four-circle Kappa diffractometer
Absorption correction	Multi-scan (<i>CrysAlisPro</i> [14])
T_{\min}, T_{\max}	0.67549, 1.000
No. of measured, independent and observed [$I > 2\sigma(I)$] reflections	13173, 6540, 4299
R_{int}	0.0888
Refinement	
$R[F^2 > 2\sigma(F^2)], wR(F^2), S$	0.0599, 0.1397, 1.045
No. of reflections	6540
No. of parameters	348
No. of restraints	2
H-atom treatment	H atoms treated by a mixture of independent and constrained refinement
$\Delta\rho_{\max}, \Delta\rho_{\min}$ (e Å ⁻³)	0.647, -0.847

5.2.2 Crystallographic study of [Fe(H-5-Br-thsa-Et)₂](NO₃)·H₂O

The crystal structure of bis(5-bromosalicylaldehyde 4-ethylthiosemicarbazonato(1-)- κ^3 -*O,N',S*)ferrate(III) nitrate monohydrate, [Fe(H-5-Br-thsa-Et)₂](NO₃)·H₂O (Figure 5.2.1), was determined at 100 K. The present compound crystallises in the orthorhombic system in the space group *Pnna*. The asymmetric unit is comprised from the [Fe(H-5-Br-thsa-Et)₂]⁺ fragment, nitrate

anion and a water solvent molecule. Selected geometric parameters are given in Table 5.2.2. The Fe^{III} cation is coordinated by two singly deprotonated thione O,N,S-ligands. The Fe^{III}O₂N₂S₂ unit displays a distorted octahedral geometry, as corroborated by the bond angles of the donor atoms and Fe1 atom. The 5-bromosalicylaldehyde 4-ethylthiosemicarbazone(1-) ligands are deprotonated at the phenolate-O atoms.

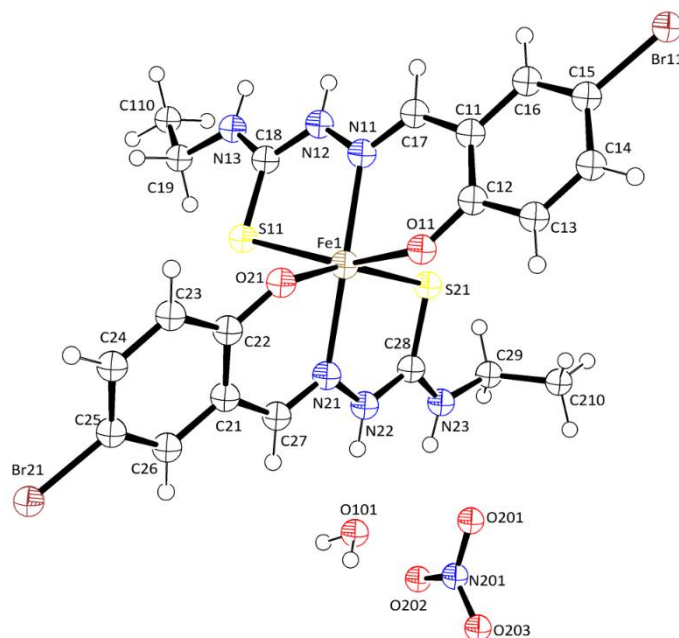


Figure 5.2.1 The molecular structure and atom-numbering scheme for [Fe(H-5-Br-thsa-Et)₂](NO₃)·H₂O. Displacement ellipsoids are drawn at the 50% probability level.

Table 5.2.2 Selected geometric parameters of [Fe(H-5-Br-thsa-Et)₂](NO₃)·H₂O (Å, °)

Fe1–S11	2.4406(15)	Fe1–S21	2.4635(15)
Fe1–O11	1.958(4)	Fe1–O21	1.945(3)
Fe1–N11	2.175(4)	Fe1–N21	2.162(4)
S11–Fe1–S21	98.78(5)	O11–C12–C11	123.1(5)
S11–Fe1–N11	78.94(11)	C12–C11–C17	123.9(5)
S11–Fe1–O11	158.08(11)	C11–C17–N11	125.3(5)
S11–Fe1–O21	89.97(11)	C17–N11–Fe1	126.5(3)
S11–Fe1–N21	88.36(11)	Fe1–O21–C22	134.6(3)
S21–Fe1–O11	92.88(11)	O21–C22–C21	121.1(4)
S21–Fe1–O21	160.34(11)	C22–C21–C27	123.6(4)

Table 5.2.2 Selected geometric parameters of [Fe(H-5-Br-thsa-Et)₂](NO₃)·H₂O (Å, °) (continued)

S21–Fe1–N11	84.91(11)	C21–C27–N21	125.7(4)
S21–Fe1–N21	78.97(11)	C27–N21–Fe1	126.1(3)
O11–Fe1–O21	84.98(15)	C18–S11–Fe1	99.87(18)
O11–Fe1–N11	83.71(15)	N11–N12–C18	120.2(4)
O11–Fe1–N21	112.17(15)	N12–C18–S11	121.4(4)
O21–Fe1–N11	114.18(15)	C28–S21–Fe1	99.53(18)
O21–Fe1–N21	83.74(14)	N21–N22–C28	121.1(4)
N11–Fe1–N21	157.72(15)	N22–C28–S21	121.1(4)
Fe1–O11–C12	134.9(3)		

The Fe1 donor atom distances involving the two tridentate anionic H-5-Br-thsa-Et ligands are Fe1–S11 = 2.4406(15) Å, Fe1–S21 = 2.4635(15) Å, Fe1–O11 = 1.958(4) Å, Fe1–O21 = 1.945(3) Å, Fe1–N11 = 2.175(4) Å and Fe1–N21 = 2.162(4) Å. The Fe-donor atom bond distances suggest that the Fe^{III} cation in the present compound is in the high-spin state at 100 K. Typical distances for Fe–S, Fe–O and Fe–N bonds are 2.23-2.31, 1.93-1.95 and 1.88-1.96 Å, respectively, for low-spin Fe^{III} compounds of this family, and 2.40-2.44, 1.96-1.99 and 2.05-2.15 Å, respectively, for the corresponding high-spin Fe^{III} compounds [18].

The tridentate ligands in the present compound coordinate to the Fe^{III} cation to give rise to a Fe^{III}O₂N₂S₂ octahedral environment, forming six- and five-membered chelate rings. The values of the root-mean-square deviations from the least-squares planes of the atoms comprising the five membered [Fe1 N11 N12 C18 S11] and [Fe1 N21 N22 C28 S21] chelate rings are 0.072 Å and 0.007 Å, respectively; the corresponding values for the six-membered [Fe1 N11 C17 C11 C12 O11] and [Fe1 N21 C27 C21 C22 O21] chelate rings are 0.073 Å and 0.103 Å, respectively. These geometric features are associated with O11–Fe1–N11 and O21–Fe1–N21 bite angles of 83.71(15)° and 83.74(14)°, respectively; as expected the six-membered chelate ring's bite angles are larger than the values of the five-membered chelate ring's bite angles of S11–F1–N11 = 78.94(11)° and S21–Fe1–N21 = 78.97(11)°. The conformation of the five- and six-membered chelate rings of [Fe(H-5-Br-thsa-Et)₂](NO₃)·H₂O illustrates there is no major puckering.

5-Bromosalicylaldehyde 4-ethylthiosemicarbazone appears to be in its thione form, *i.e.* it is deprotonated at the phenolate-O atoms (O11 and O21) and possesses a hydrogen atom on the hydrazinic nitrogen atoms (N12 and N22). The protonation of the hydrazinic N atoms (N12 and N22) confirms the presence of the thione form of the tautomer which is corroborated by the C=S bond distances of the 5-bromosalicylaldehyde 4-ethylthiosemicarbazone(1-) ligands, as they are closer to a bond order of two. The C–S bond distances are C18–S11 = 1.686(5) Å and C28–S21 = 1.696(5)

Å. Furthermore, the N–N and C–N bond distances indicate there is electron delocalisation over the 5-membered chelate in both ligands coordinated to the Fe^{III} cation. These bond distances give rise to a bond order more than one, *i.e.* the N11–N12 and N21–N22 bond distances are 1.395(6) Å and 1.374(5) Å, respectively, and the N12–C18 and N22–C28 bond distances are 1.351(6) Å and 1.352(6) Å, respectively.

The hydrogen bonding interactions of [Fe(H-5-Br-thsa-Et)₂](NO₃)·H₂O are listed in Table 5.2.3 and displayed in Figure 5.2.2. The nitrate anion is involved in hydrogen bonding interactions with the 5-bromosalicylaldehyde 4-ethylthiosemicarbazonate(1-) ligand. These hydrogen bonding interactions include the terminal nitrogen atoms N13 and N23 forming contacts with the oxygen atoms of the nitrate anion, O203ⁱ (*i* = *x* + 1, *-y* + 1/2, *-z* + 3/2) and O201 atoms, respectively. The nitrogen atom N12 forms a contact N12–H12···O202ⁱ (*i* = *x* + 1, *-y* + 1/2, *-z* + 3/2) with the oxygen atom O202ⁱ of the nitrate anion. Also, the nitrate anion forms a hydrogen bonding interaction with the oxygen atom O101 of the water solvent molecule. The nitrate anion is involved in two hydrogen bonding ring systems which connect the Fe^{III} units. The first ring system is formed between two Fe^{III} units, two water solvent molecules and a nitrate anion. The ring system is formed by the following contacts N12–H12···O202ⁱ (*i* = *x* + 1, *-y* + 1/2, *-z* + 3/2), O101–H10B···O202ⁱⁱⁱ (*iii* = *x*, *-y* + 1/2, *-z* + 3/2), O101–H10A···O11ⁱⁱ (*ii* = *x* – 1/2, *y*, *-z* + 1), and N22–H22···O101, giving rise to a R⁵₄(18) ring system. Furthermore, the second ring system is created by the contacts N12–H12···O202ⁱ and N13–H13···O203ⁱ (*i* = *x* + 1, *-y* + 1/2, *-z* + 3/2), giving rise to a R²₂(8) ring system.

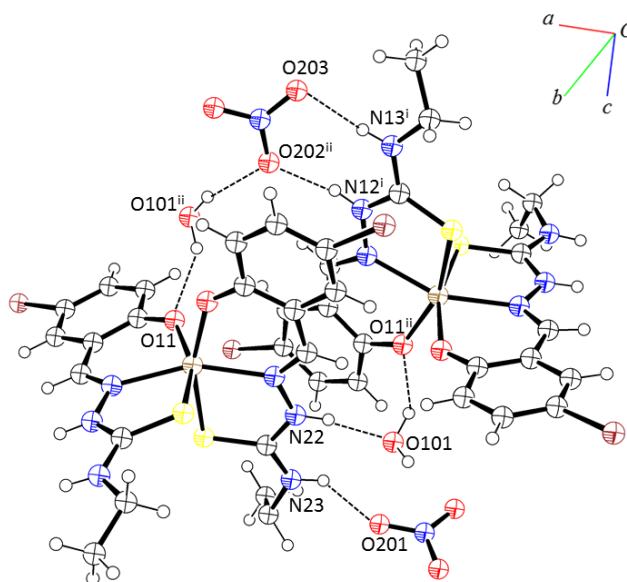


Figure 5.2.2 A projection showing the hydrogen bonding interactions of [Fe(H-5-Br-thsa-Et)₂](NO₃)·H₂O. Displacement ellipsoids are drawn at the 50% probability level. Dashed lines indicate hydrogen bonds. [Symmetry codes: (i) *x* + 1, *-y* + 1/2, *-z* + 3/2; (ii) *x* – 1/2, *y*, *-z* + 1; (iii) *x*, *-y* + 1/2, *-z* + 3/2].

Table 5.2.3 Hydrogen bond geometry of $[\text{Fe}(\text{H-5-Br-thsa-Et})_2](\text{NO}_3)\cdot\text{H}_2\text{O}$ (Å, °)

$D\text{-H}\cdots A$	$D\text{-H}$	$\text{H}\cdots A$	$D\cdots A$	$D\text{-H}\cdots A$
$\text{N12-H12}\cdots\text{O202}^{\text{i}}$	0.88	1.89	2.737(6)	161.5
$\text{N13-H13}\cdots\text{O203}^{\text{i}}$	0.88	2.01	2.892(6)	176.3
$\text{N22-H22}\cdots\text{O101}$	0.88	1.83	2.695(6)	167.3
$\text{N23-H23}\cdots\text{O201}$	0.88	2.24	2.898(6)	131.6
$\text{O101-H10A}\cdots\text{O11}^{\text{ii}}$	0.87	2.09	2.811(6)	139.7
$\text{O101-H10B}\cdots\text{O202}^{\text{iii}}$	0.87	1.89	2.692(6)	152.6

Symmetry codes: (i) $x + 1, -y + 1/2, -z + 3/2$; (ii) $x - 1/2, y, -z + 1$, (iii) $x, -y + 1/2, -z + 3/2$.

The assembly of the Fe^{III} units of the present compound is displayed in Figure 5.2.3. The presence of both the NO_3^- anion and the water solvent molecule of $[\text{Fe}(\text{H-5-Br-thsa-Et})_2](\text{NO}_3)\cdot\text{H}_2\text{O}$, might have some effect on how the Fe^{III} units are packed in the crystal lattice. $[\text{Fe}(\text{H-5-Br-thsa-Et})_2](\text{NO}_3)\cdot\text{H}_2\text{O}$ displays $\text{Fe}^{\text{III}}\cdots\text{Fe}^{\text{III}}$ ($1/2 + x, y, -z + 1$) separations of 6.788(7) Å and $\text{Fe}^{\text{III}}\cdots\text{Fe}^{\text{III}}$ ($x, 1/2 - y, 3/2 - z$) separations of 7.2135(16) Å. Despite the presence of the water solvent molecule and the nitrate anion the Fe^{III} units are packed relatively close together within the crystal lattice. This feature could be due to the hydrogen bonding ring systems (*vide supra*), which link the Fe^{III} units together using the hydrogen bonding interactions of the water solvent molecule and the nitrate anion.

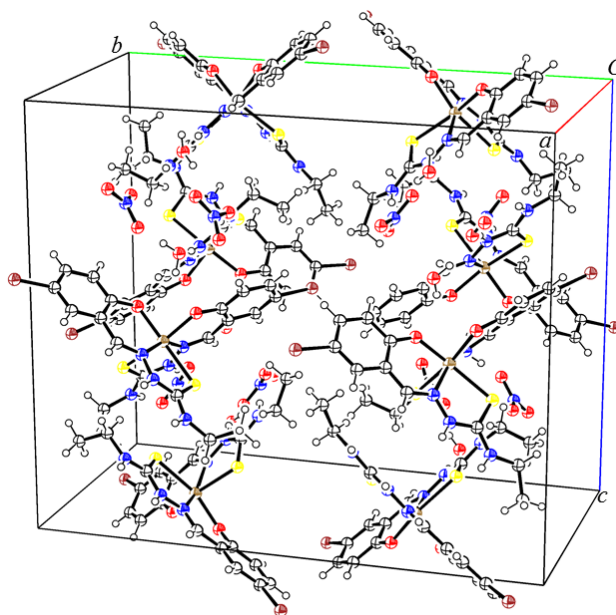


Figure 5.2.3 A projection showing the unit cell of $[\text{Fe}(\text{H-5-Br-thsa-Et})_2](\text{NO}_3)\cdot\text{H}_2\text{O}$. Displacement ellipsoids are drawn at the 50% probability level.

5.2.3 Infrared spectroscopic study of $[\text{Fe}(\text{H-5-Br-thsa-Et})_2](\text{NO}_3)\cdot\text{H}_2\text{O}$ and the free ligand 5-bromosalicylaldehyde 4-ethylthiosemicarbazone, $\text{H}_2\text{-5-Br-thsa-Et}$

The infrared spectra of the ferric compound bis(5-bromosalicylaldehyde 4-ethylthiosemicarbazonato(-1)- $\kappa^3\text{-O,N}^I\text{,S}$)ferrate nitrate monohydrate and the corresponding free ligand 5-bromosalicylaldehyde 4-ethylthiosemicarbazone are given in the appendix. The infrared spectrum of the free ligand, 5-bromosalicylaldehyde 4-ethylthiosemicarbazone ($\text{H}_2\text{-5-Br-thsa-Et}$), exhibits a strong band at 1613 cm^{-1} , which is assigned to the imine resulting from the condensation from the salicylaldehyde moiety and the thiosemicarbazone moiety. Furthermore, the infrared spectrum of the ligand exhibits a medium band at 3146 cm^{-1} , which is assigned to the $\nu\text{N-H}$ vibration. The presence of the $\nu\text{N-H}$ band in the spectrum of $[\text{Fe}(\text{H-5-Br-thsa-Et})_2](\text{NO}_3)\cdot\text{H}_2\text{O}$ shows evidence that the ligand is coordinated to the central Fe^{III} cation in the thione form of the tautomer. Upon coordination of the imine nitrogen, the $\nu\text{C=N}$ band shifts from 1613 cm^{-1} in the free ligand to 1600 cm^{-1} in the complex. The $\nu\text{N-N}$ band of the thiosemicarbazone moiety of the free ligand is found at 1105 cm^{-1} ; the wavenumber increases to 1312 cm^{-1} for the $\nu\text{N-N}$ band in the ferric complex. In comparison to the free ligand, the ferric complex does not show the presence of the νOH vibration; this is due to the phenolic oxygen having been deprotonated in order to coordinate the O,N,S-tridentate chelating ligand to the Fe^{III} cation in the $[\text{Fe}(\text{H-5-Br-thsa-Et})_2]^+$ fragment. The corresponding νOH band for the free ligand is found at 3299 cm^{-1} . The Fe^{III} cation is also coordinated to the sulfur atom of the thiosemicarbazone moiety of the ligand. The νCS band of the Fe^{III} coordinated ligand is assigned at 819 cm^{-1} in the ferric complex, but it is at a larger wavenumber in the free ligand, *i.e.* νCS at 1046 cm^{-1} . The decrease in the frequency of the νCS band in the thiosemicarbazone upon complexation of the ligand indicates coordination of the thione S atom to the Fe^{III} cation. In the infrared spectrum of the ferric complex there are two bands which represent the presence of the nitrate anion within the crystal lattice, the νNO bands of the NO_3^- anion are assigned at 866 and 1352 cm^{-1} , respectively. Furthermore, as evidenced from the crystallographic study of the complex $[\text{Fe}(\text{H-5-Br-thsa-Et})_2](\text{NO}_3)\cdot\text{H}_2\text{O}$ there is hydrogen bonding within the crystal lattice; which is supported by the broad peaks observed for the νNH bands assigned to the azomethine and terminal nitrogen atoms of the thiosemicarbazone moiety of the coordinated ligand.

5.2.4 Magnetic properties of $[\text{Fe}(\text{H-5-Br-thsa-Et})_2](\text{NO}_3)\cdot\text{H}_2\text{O}$

The temperature dependence of the $\chi_{\text{M}}T$ product (χ_{M} being the molar magnetic susceptibility, T being the temperature) for $[\text{Fe}(\text{H-5-Br-thsa-Et})_2](\text{NO}_3)\cdot\text{H}_2\text{O}$ is given in Figure 5.2.4 over the 5-300 K temperature range. The plot reveals the value of $\chi_{\text{M}}T$ varies from $4.17\text{ cm}^3\text{ mol}^{-1}\text{ K}$ at 300 K to $3.23\text{ cm}^3\text{ mol}^{-1}\text{ K}$ at 5 K. The temperature dependence of the $\chi_{\text{M}}T$ product clearly shows a plateau equal to $4.17\text{ cm}^3\text{ mol}^{-1}\text{ K}$ at high temperatures (300-50 K), which is close to the expected value of 4.37

$\text{cm}^3 \text{mol}^{-1} \text{K}$ ($g = 2.00$) for Fe^{III} in its high-spin state ($S=5/2$). As can be seen in Figure 5.2.4, the value of $\chi_{\text{M}}T$ drops rapidly below 20 K, reflecting the significant zero-field splitting of the ($S = 5/2$) ground state [19].

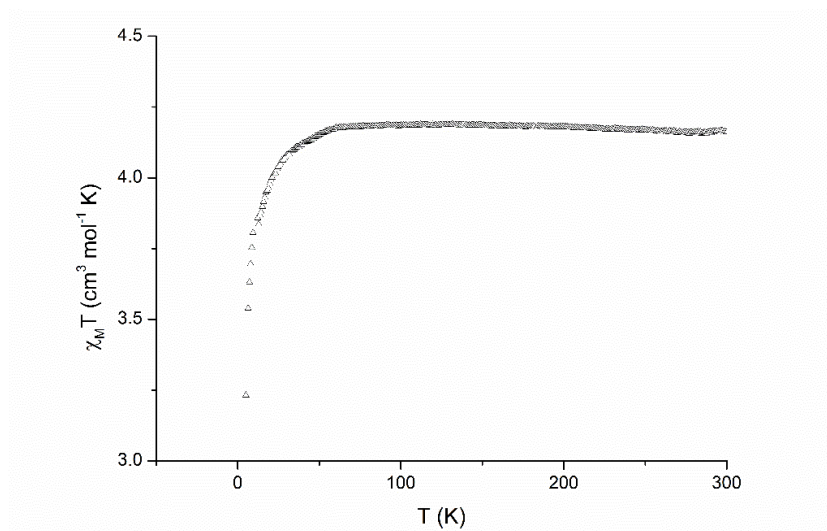


Figure 5.2.4 $\chi_{\text{M}}T$ vs T plot of $[\text{Fe}(\text{H-5-Br-thsa-Et})_2](\text{NO}_3) \cdot \text{H}_2\text{O}$ in the temperature range 5-300 K. The data were measured at a rate of 2 K min^{-1} .

The magnetic susceptibility, χ_{M} , data for $[\text{Fe}(\text{H-5-Br-thsa-Et})_2](\text{NO}_3) \cdot \text{H}_2\text{O}$ between the temperature range 5-300 K shown in Figure 5.2.5, were least-squares fitted to equation (1) to give the fitting parameters $D = 2.12 \text{ cm}^{-1}$ and $g = 2.22$, with a coefficient of determination value of 0.99 and a reduced χ^2 value of 0.00004.

$$\chi_{\text{M}} = \frac{Ng^2 \beta^2}{4kT} \left[\frac{0.14 + 5.12e^{-3.23X} + 23.85e^{-6.83X}}{1 + e^{-3.23X} + e^{-6.83X}} \right] \quad \text{Eqn (1)}$$

Where, $X = D/kT$, D is the zero-field splitting parameter, g is the average g tensor value and the other symbols have their standard meanings (as shown in Chapter I). As reported by Chen *et al.*, [19] equation (1) is the theoretical equation for the magnetic susceptibility resulting from the axial and rhombic zero-field splitting for a $\text{Fe}^{\text{III}} S = 5/2$ ion.

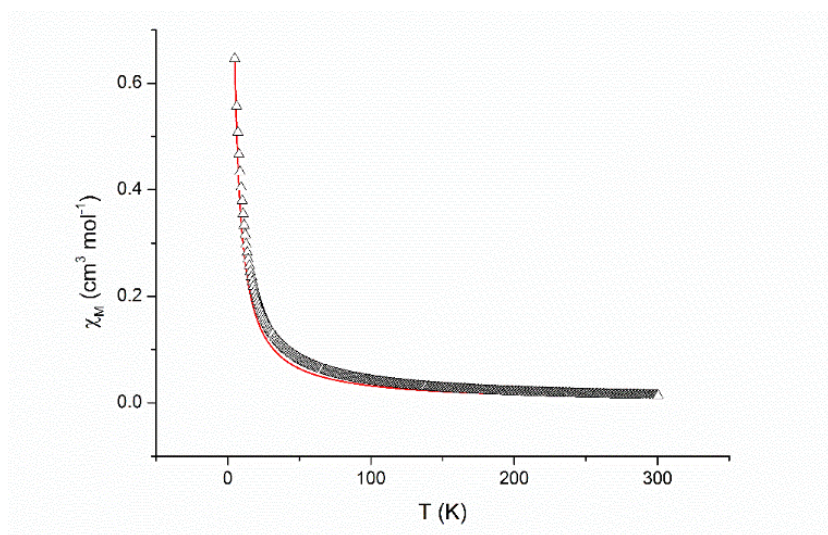


Figure 5.2.5 Temperature dependence of the molar magnetic susceptibility, χ_M , for the compound $[\text{Fe}(\text{H-5-Br-thsa-Et})_2](\text{NO}_3)\cdot\text{H}_2\text{O}$ in the range 5-300 K. Points are the experimental data; solid red line represents the least-squares fit of the data to Equation (1), where $D = 2.12 \text{ cm}^{-1}$ and $g = 2.22$.

5.3 The structure and magnetic properties of $[\text{Fe}(\text{H-4-OH-thsa})_2]_4\cdot(\text{SO}_4)_2\cdot 9\text{H}_2\text{O}$

In this section the crystallographic data (at 100 K) and magnetic properties of the ferric complex $[\text{Fe}(\text{H-4-OH-thsa})_2]_4\cdot(\text{SO}_4)_2\cdot 9\text{H}_2\text{O}$ are herein reported. Furthermore, the infrared spectroscopic studies of the free ligand, 2,4-dihydroxybenzaldehyde thiosemicarbazone, and the ferric complex, $[\text{Fe}(\text{H-4-OH-thsa})_2]_4\cdot(\text{SO}_4)_2\cdot 9\text{H}_2\text{O}$ are discussed.

The experimental data is reported in Chapter II for the synthesis of $[\text{Fe}(\text{H-4-OH-thsa})_2]_4\cdot(\text{SO}_4)_2\cdot 9\text{H}_2\text{O}$ and corresponding ligand, 2,4-dihydroxybenzaldehyde thiosemicarbazone.

5.3.1 Crystal Data and Structure Refinement Details of $[\text{Fe}(\text{H-4-OH-thsa})_2]_4\cdot(\text{SO}_4)_2\cdot 9\text{H}_2\text{O}$

Crystal data, data collection and structure refinement details are summarised in Table 5.3.1. The hydrogen atoms on all N–H and NH_2 groups were located in difference Fourier maps and refined with restrained N–H distances of $0.88(2) \text{ \AA}$ and with $U_{\text{iso}}(\text{H}) = 1.2U_{\text{eq}}(\text{N})$. The hydrogen atoms attached to hydroxy O atoms, *i.e.* O112, O122, O212, O222, O312, O322, as well as O412 and O422 positioned on the C4 atoms, *i.e.* C114, C124, C214, C224, C314, C324, C414 and C424, respectively, of the salicylaldehyde moiety were located in a difference Fourier map and refined with an O–H distance restraint of $0.84(2) \text{ \AA}$ and $U_{\text{iso}}(\text{H}) = 1.5U_{\text{eq}}(\text{O})$. The remaining hydrogen atoms were included in the refinement in calculated positions, and treated as riding on their parent atoms, with C–H = 0.95 \AA and $U_{\text{iso}}(\text{H}) = 1.2U_{\text{eq}}(\text{C})$ for aryl (–CH=) hydrogen atoms.

Table 5.3.1 Crystal data and structure refinement details of $[\text{Fe}(\text{H-4-OH-thsa})_2]_4 \cdot (\text{SO}_4)_2 \cdot 9\text{H}_2\text{O}$

Crystal data	
Chemical formula	$4(\text{C}_{16}\text{H}_{16}\text{FeN}_6\text{O}_4\text{S}_2) \cdot 2(\text{O}_4\text{S}) \cdot 9(\text{H}_2\text{O})$
M_r	2259.53
Crystal system, space group	Triclinic, $P-1$
Temperature (K)	100
a, b, c (Å)	12.1491(3), 19.4997(4), 19.6086(5)
α, β, γ (°)	85.8400(19), 88.3058(18), 84.3168(18)
V (Å ³)	4609.14(18)
Z	2
Radiation type	Mo $K\alpha$
μ (mm ⁻¹)	0.94
Crystal size (mm)	$0.03 \times 0.02 \times 0.01$
Colour	Black (plate)
Data collection	
Diffractometer	Rigaku AFC12 four-circle Kappa diffractometer
Absorption correction	Multi-scan (<i>CrystalClear-SM Expert</i> [20])
T_{\min}, T_{\max}	0.838, 1.000
No. of measured, independent and observed [$I > 2\sigma(I)$] reflections	60573, 21184, 14525
R_{int}	0.053
Refinement	
$R[F^2 > 2\sigma(F^2)], wR(F^2), S$	0.055, 0.141, 1.05
No. of reflections	21184
No. of parameters	1339
No. of restraints	32
H-atom treatment	H atoms treated by a mixture of independent and constrained refinement
$\Delta\rho_{\max}, \Delta\rho_{\min}$ (e Å ⁻³)	1.04, -0.48

The *CrystalClear-SM Expert* [20] program was used for the unit cell determination and data collection. The *CrysAlisPro* [14] program was used for the data reduction, cell refinement and absorption correction. The program used for the structure solution: *ShelXT* [21]; the structure refinement used the program *SHELXL* [16]. The *OLEX2* [13] and *ORTEP-3* for Windows [17] programs were used to produce the molecular graphics.

5.3.2 Crystallographic study of $[\text{Fe}(\text{H-4-OH-thsa})_2]_4 \cdot (\text{SO}_4)_2 \cdot 9\text{H}_2\text{O}$

The crystal structure of $[\text{Fe}(\text{H-4-OH-thsa})_2]_4 \cdot (\text{SO}_4)_2 \cdot 9\text{H}_2\text{O}$ (Figure 5.3.1) was determined at 100 K. The present compound crystallises in the triclinic space group $P-1$. The asymmetric unit (Figure 5.3.2) consists of four $[\text{Fe}(\text{HL})_2]^+$ fragments, two sulfate anions and nine water molecules, with no atoms in special positions. The four Fe^{III} units within the asymmetric unit display appreciably distorted octahedral geometries, created by two coordinating anionic tridentate 2,4-dihydroxybenzaldehyde thiosemicarbazonato(1-) ligands. Selected bond angles and bond lengths are listed in Table 5.3.2.

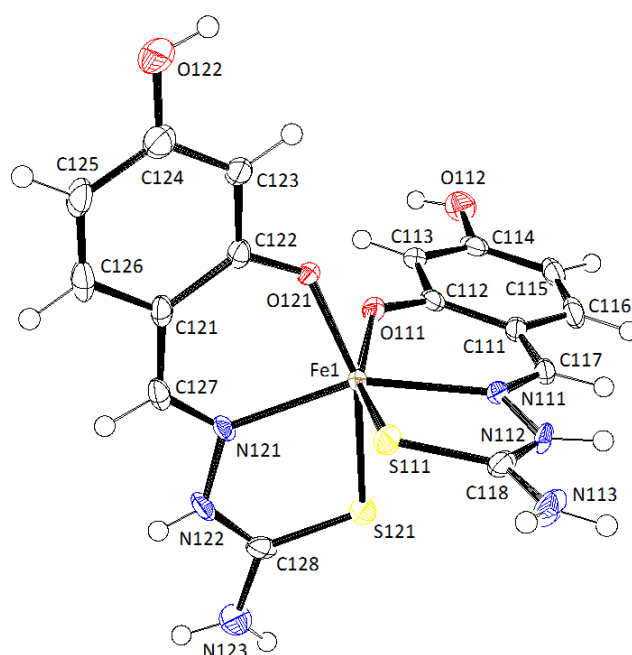


Figure 5.3.1 The molecular structure and atom-numbering scheme of the Fe1 unit for $[\text{Fe}(\text{H-4-OH-thsa})_2]_4 \cdot (\text{SO}_4)_2 \cdot 9\text{H}_2\text{O}$. Displacement ellipsoids are drawn at the 50% probability level.

The atom-numbering scheme of Fe2 unit of one of the HL fragments adopts the numbering scheme with a “21” in front of all numbers, *i.e.* O1 would become O211. For the second HL fragment adopts the numbering scheme with a “22” in front of all numbers, *i.e.* O1 would become O221. The atom-numbering scheme of Fe3 unit of one of the HL fragments adopts the numbering scheme with a “31” in front of all numbers, *i.e.* O1 would become O311. For the second HL fragment adopts the numbering scheme with a “32” in front of all numbers, *i.e.* O1 would become O321. The atom-numbering scheme of Fe4 unit of one of the HL fragments adopts the numbering scheme with a “41” in front of all numbers, *i.e.* O1 would become O411. For the second HL fragment adopts the numbering scheme with a “42” in front of all numbers, *i.e.* O1 would become O421.

Each Fe^{III} cation is coordinated by two anionic O,N,S-ligands, giving a FeO₂N₂S₂ octahedron. The donor atoms are located in mutually normal planes, the S and O-donor atoms being in the *cis* positions and the N-donor atoms in the *trans* positions. It has been acknowledged throughout the literature that the Fe-donor atom bond distances can be categorised into whether the Fe^{III} cation is in the high-spin or low-spin state at the measurement temperature. It is recognised that typical distances for Fe–S, Fe–O and Fe–N bonds are 2.23–2.31 Å, 1.93–1.95 Å and 1.88–1.96 Å, respectively, for low-spin Fe^{III} compounds of this family, and 2.40–2.44 Å, 1.96–1.99 Å and 2.05–2.15 Å, respectively, for the corresponding high-spin Fe^{III} compounds [18]. It can then be determined that for the four Fe^{III} units of the present compound, each Fe^{III} cation is in the high-spin state at 100 K.

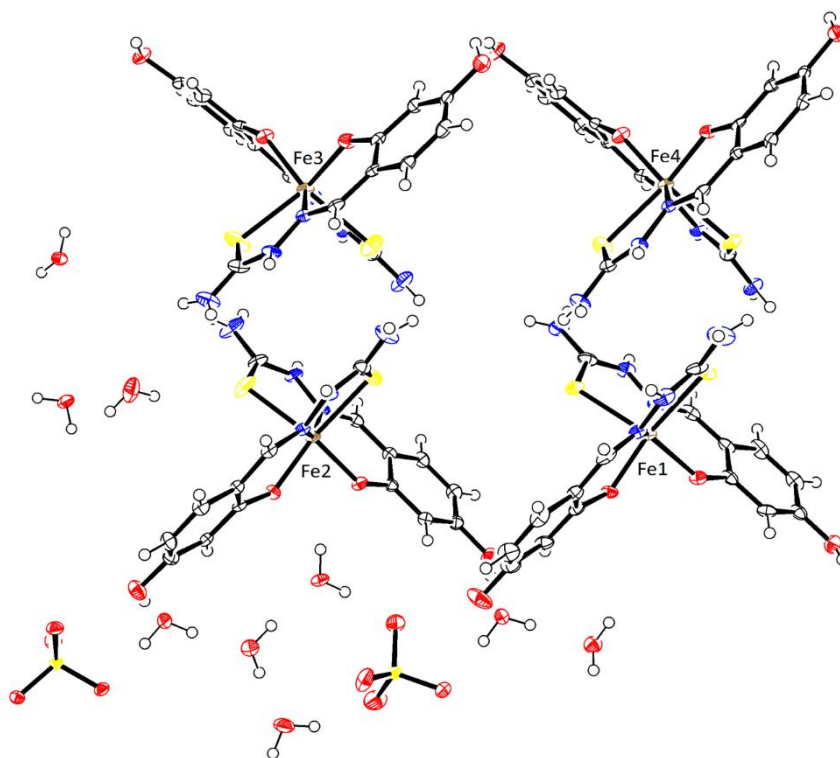


Figure 5.3.2 The molecular structure of the asymmetric unit of [Fe(H-4-OH-thsa)₂]₄·(SO₄)₂·9H₂O. Displacement ellipsoids are drawn at the 50% probability level.

The 2,4-dihydroxybenzaldehyde thiosemicarbazone(1-) is in the thione form of the tautomer when coordinated to the central Fe^{III} cation, *i.e.* deprotonation only occurs at the phenolate O-donor atoms, O111, O121, O211, O221, O311, O321, O411 and O421. Additionally, the protonation of the azomethine nitrogen atoms (N112, N122, N212, N222, N312, N322, N412 and N422) also indicates that the ligand is coordinated to the Fe^{III} cation in the thione form. This is further corroborated by the C=S distances of the ligand in each of the Fe^{III} units, which are closer to a bond order of two and that the adjacent C–N bonds are within the range expected for a bond order of one. Selected ligand bond distances are given in Table 5.3.2.

Table 5.3.2 Selected bond lengths and angles of [Fe(H-4-OH-thsa)₂]₄·(SO₄)₂·9H₂O (Å, °)

Fe1–S111	2.4391(10)	Fe1–S121	2.4422(11)
Fe1–O111	1.946(2)	Fe1–O121	1.945(2)
Fe1–N111	2.160(3)	Fe1–N121	2.173(3)
Fe2–S211	2.4331(10)	Fe2–S221	2.4369(11)
Fe2–O211	1.952(2)	Fe2–O221	1.935(2)
Fe2–N211	2.166(3)	Fe2–N221	2.175(3)
Fe3–S311	2.4655(11)	Fe3–S321	2.4268(12)
Fe3–O311	1.957(2)	Fe3–O321	1.929(2)
Fe3–N311	2.155(3)	Fe3–N321	2.182(3)
Fe4–S411	2.4587(10)	Fe4–S421	2.4506(11)
Fe4–O411	1.926(2)	Fe4–O421	1.950(2)
Fe4–N411	2.142(3)	Fe4–N421	2.143(3)
N111–C117	1.304(5)	N311–C317	1.307(4)
N121–C127	1.292(5)	N321–C327	1.300(4)
N112–C118	1.336(5)	N312–C318	1.340(5)
N122–C128	1.333(5)	N322–C328	1.337(5)
S111–C118	1.718(4)	S311–C318	1.690(4)
S121–C128	1.697(4)	S321–C328	1.707(4)
N211–C217	1.308(4)	N411–C417	1.302(4)
N221–C227	1.300(4)	N421–C427	1.301(4)
N212–C218	1.328(4)	N412–C418	1.344(4)
N222–C228	1.330(5)	N422–C428	1.321(4)
S211–C118	1.701(3)	S411–C418	1.702(3)
S221–C228	1.709(3)	S421–C428	1.706(3)
S111–Fe1–S121	101.08(3)	S211–Fe2–S221	97.85(4)
O111–Fe1–S121	84.51(10)	O211–Fe2–O221	83.68(9)
N111–Fe1–N121	155.09(10)	N211–Fe2–N221	153.16(10)
S311–Fe3–S321	101.90(4)	S411–Fe4–S421	94.92(4)
O311–Fe3–O321	85.66(10)	O411–Fe4–O421	84.91(10)
N311–Fe3–N321	153.64(10)	N411–Fe4–N421	155.72(10)

The four inequivalent Fe^{III} units are held together by a complex hydrogen bonding system involving both the sulfate anions and water molecules present in the crystal lattice. The hydrogen bond geometries for [Fe(H-4-OH-thsa)₂]₄·(SO₄)₂·9H₂O are listed in Table 5.3.3. The hydrogen bond

contacts among the Fe^{III} compound, sulfate anion and the water molecules form intramolecular ring systems in the lattice. Within the asymmetric unit of [Fe(H-4-OH-thsa)₂]₄·(SO₄)₂·9H₂O there are three different hydrogen bonding ring systems involving the Fe2 unit, as illustrated in Figure 5.3.3. The first ring system is formed by the contacts O212–H212···O7, O7–H7B···O501, O11–H11E···502 and O11–H11D···O221 giving rise to a R⁴₃(16) ring system. The ring system includes the phenolate-O atom, O221, of one of the coordinated ligands which is an Fe-donor atom; due to the interaction of the hydrogen bonding system with the Fe–O-donor atom, the ligand field strength of the ligand may be modified and this is determining the spin state of Fe^{III} ion. However, the hydrogen bonding interactions with the Fe–O donor atom have revealed that the Fe–O bond distances (displayed in Table 5.3.2) are shorter than expected for a high-spin compound (1.96-1.99 Å [18]).

Table 5.3.3 Hydrogen bond geometry of [Fe(H-4-OH-thsa)₂]₄·(SO₄)₂·9H₂O (Å, °)

<i>D–H···A</i>	<i>D–H</i>	<i>H···A</i>	<i>D···A</i>	<i>D–H···A</i>
O112–H112···O9 ⁱ	0.82(2)	1.90(2)	2.711(4)	171(5)
O122–H122···O7	0.85(2)	1.86(2)	2.706(4)	175(5)
N112–H11A···O603 ⁱⁱ	0.90(2)	1.96(2)	2.846(4)	173(4)
N113–H11B···O312 ⁱⁱⁱ	0.88(2)	2.12(3)	2.891(4)	145(4)
O212–H212···O7	0.84(2)	1.85(2)	2.681(4)	173(4)
O222–H222···O9	0.84(2)	1.91(2)	2.745(4)	175(5)
N212–H21A···O502 ⁱⁱ	0.87(2)	2.00(2)	2.859(4)	169(4)
N213–H21B···O412 ⁱⁱⁱ	0.85(2)	2.31(4)	2.889(4)	126(4)
N222–H22A···O11 ^{iv}	0.86(2)	2.03(2)	2.879(3)	170(3)
O312–H312···O601 ^v	0.82(2)	1.85(2)	2.661(3)	169(4)
O322–H322···O501 ^v	0.85(2)	1.87(2)	2.716(3)	177(4)
N312–H31A···O504 ⁱⁱ	0.84(2)	2.10(3)	2.845(4)	148(4)
N322–H32A···O503 ^{iv}	0.88(2)	1.89(2)	2.769(4)	177(4)
O412–H412···O501 ^v	0.82(2)	1.96(2)	2.738(3)	158(4)
O422–H422···O601 ^{vi}	0.81(2)	1.92(2)	2.720(3)	169(4)
N412–H41A···O17 ⁱ	0.89(2)	1.95(2)	2.821(3)	163(3)

Table 5.3.3 Hydrogen bond geometry of $[\text{Fe}(\text{H-4-OH-thsa})_2]_4 \cdot (\text{SO}_4)_2 \cdot 9\text{H}_2\text{O}$ (Å, °) (continued)

N422–H42A···O604 ^{iv}	0.86(2)	1.92(2)	2.782(3)	172(4)
O7–H7A···O8	0.87	1.88	2.726(4)	164
O7–H7B···O501	0.87	1.81	2.676(4)	175
O8–H8A···O12 ⁱⁱ	0.87	1.90	2.766(4)	175
O9–H9A···O601	0.87	1.88	2.745(3)	173
O9–H9B···O10	0.87	1.85	2.700(4)	166
O10–H10A···O14	0.87	1.88	2.751(4)	175
O10–H10B···O11	0.87	1.93	2.777(4)	163
O11–H11D···O221	0.87	2.17	2.849(3)	135
O11–H11E···O502	0.87	1.92	2.791(3)	174
O12–H12E···O121 ⁱⁱ	0.87	1.88	2.717(3)	161
O14–H14A···O311 ^{vii}	0.87	1.95	2.801(3)	166
O14–H14B···O504	0.87	1.94	2.752(4)	154
O16–H16B···O212 ⁱⁱ	0.87	1.98	2.847(4)	173
O17–H17B···O604 ^{viii}	0.87	1.85	2.698(3)	164

Symmetry codes: (i) $x, y, z - 1$; (ii) $-x + 1, -y + 1, -z + 1$; (iii) $-x + 1, -y, -z + 1$; (iv) $-x, -y + 1, -z + 1$; (v) $x, y - 1, z$; (vi) $x, y - 1, z - 1$; (vii) $x, y + 1, z$; (viii) $-x + 1, -y + 1, -z + 2$.

Furthermore, the second hydrogen bonding ring system formed with the Fe2 unit is created by the contacts O11–HD···O221, O222–H222···O9, O9–H9b···O10 and O10–H10b···O11, giving rise to a $R^3_4(12)$ ring system. The third hydrogen bonding system is formed between the O502 and O504 atoms of the sulfate anion and three of the solvent water molecules via the contacts O11–H11e···O502, O14–H14b···O504, O10–H10a···O14 and O10–H10b···O11, creating a $R^4_3(10)$ ring system. The Fe2 unit is linked to the Fe1 unit by the hydrogen bonds formed via the water molecule with the labelled O-atom, O7.

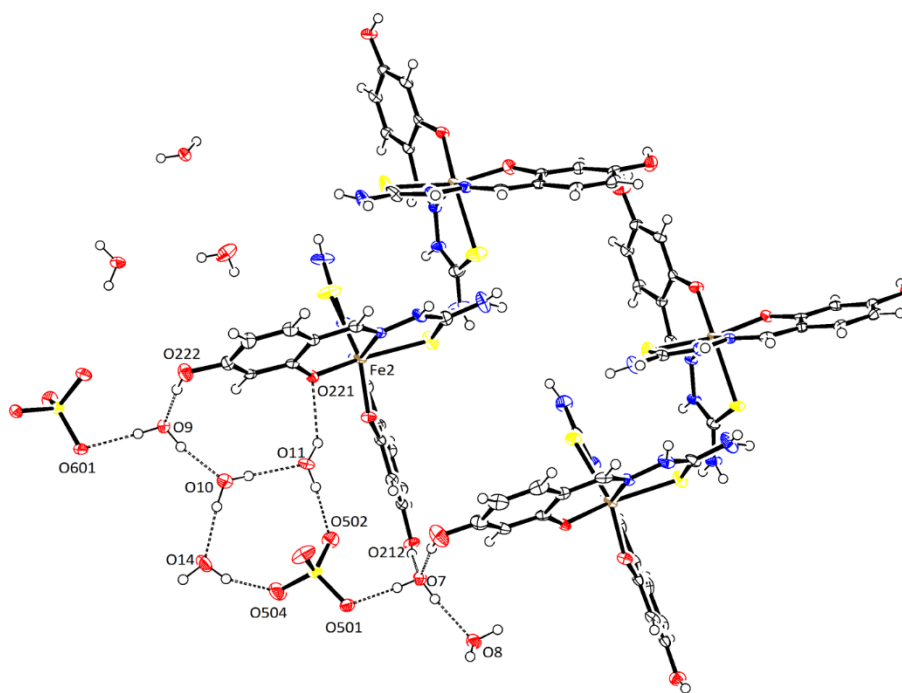


Figure 5.3.3 A projection of selected hydrogen bonding ring systems within the asymmetric unit of $[\text{Fe}(\text{H-4-OH-thsa})_2]_4 \cdot (\text{SO}_4)_2 \cdot 9\text{H}_2\text{O}$. Displacement ellipsoids are drawn at the 50% probability level.

5.3.3 Infrared Spectroscopic studies of $[\text{Fe}(\text{H-4-OH-thsa})_2]_4 \cdot (\text{SO}_4)_2 \cdot 9\text{H}_2\text{O}$ and the ligand 2,4-dihydroxybenzaldehyde thiosemicarbazone, $\text{H}_2\text{-4-OH-thsa}$

The infrared spectrum of $[\text{Fe}(\text{H-4-OH-thsa})_2]_4 \cdot (\text{SO}_4)_2 \cdot 9\text{H}_2\text{O}$ displays the typical bands expected for a ferric complex containing the one-fold deprotonated form of the ligand, 2,4-dihydroxybenzaldehyde thiosemicarbazone. The assignments of selected infrared spectroscopic bands of the Fe^{III} complex and corresponding ligand are listed in Table 5.3.4.

Table 5.3.4 Selected infrared spectroscopic bands (cm^{-1}) with assignments of $[\text{Fe}(\text{H-4-OH-thsa})_2]_4 \cdot (\text{SO}_4)_2 \cdot 9\text{H}_2\text{O}$ and H_2L ligand, 2,4-dihydroxybenzaldehyde thiosemicarbazone.

Compound	νOH	$\nu\text{C}=\text{N}$	$\nu\text{N}=\text{C}$	νNN	νCS	νCO
H_2L	3167	1631	-	1167	1165	1121
$4[\text{Fe}(\text{H-4-OH-thsa})_2] \cdot 2(\text{SO}_4) \cdot 9\text{H}_2\text{O}$	3174	1597	1578	1341	1031	1224

The spectrum of the free ligand exhibits bands in the regions 1631 cm^{-1} and 1165 cm^{-1} , which are assigned to $\nu\text{C}=\text{N}$ and νCS bands, respectively, indicating the free ligand is in the thione form. The coordination of the ligand to the Fe^{III} is accompanied by a negative shift of the $\nu\text{C}=\text{N}$ and νCS bands

and a positive shift of the ν_{CO} band with regards to the free ligand, therefore indicating the coordination of the Fe^{III} ion to the O,N,S-donor atoms. In the infrared spectrum of the ferric complex there is a band which represents the presence of the sulfate anion within the crystal lattice; the ν_{SO} band of the SO_4^{2-} anion is assigned at 1432 cm^{-1} .

5.3.4 Magnetic properties of $[\text{Fe}(\text{H-4-OH-thsa})_2]_4 \cdot (\text{SO}_4)_2 \cdot 9\text{H}_2\text{O}$

The product of the magnetic susceptibility and the temperature ($\chi_{\text{M}}T$) measured in the temperature range 5-300 K is shown in Figure 5.3.4. At 300 K, the $\chi_{\text{M}}T$ value is $4.08\text{ cm}^3\text{ mol}^{-1}\text{ K}$, which is close to the spin-only value ($4.37\text{ cm}^3\text{ mol}^{-1}\text{ K}$, $g = 2.00$) for the high-spin Fe^{III} ion ($S = 5/2$).

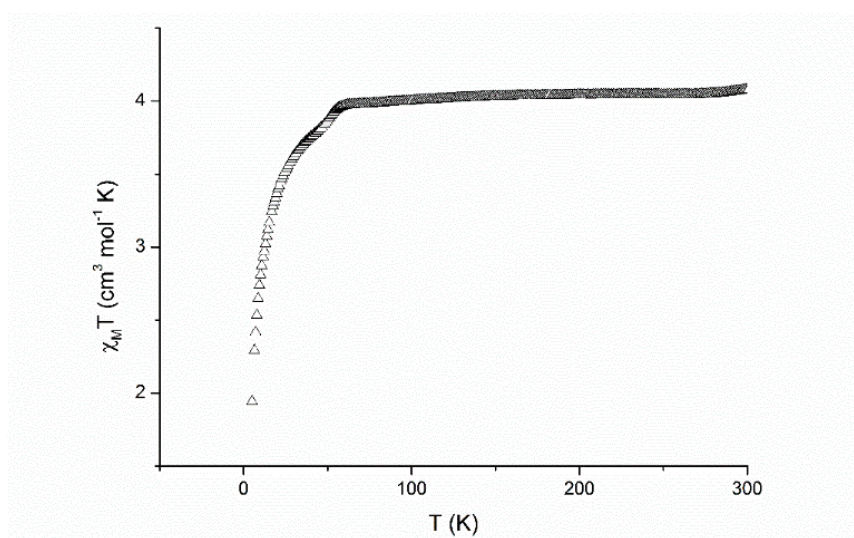


Figure 5.3.4 $\chi_{\text{M}}T$ vs T plot of $[\text{Fe}(\text{H-4-OH-thsa})_2]_4 \cdot (\text{SO}_4)_2 \cdot 9\text{H}_2\text{O}$ in the temperature range 5-300 K. The data were measured at a rate of 2 K min^{-1} .

Below 50 K, the value of $\chi_{\text{M}}T$ decreases abruptly reaching a value of $1.94\text{ cm}^3\text{ mol}^{-1}\text{ K}$ at 5 K. This behaviour is due to the presence of zero-field splitting of the high-spin Fe^{III} [19]. The magnetic data were least-squares fitted using equation (1):

$$\chi_{\text{M}} = \frac{Ng^2\beta^2}{4kT} \left[\frac{0.14 + 5.12e^{-3.23X} + 23.85e^{-6.83X}}{1 + e^{-3.23X} + e^{-6.83X}} \right] \quad \text{Eqn (1)}$$

In this equation, $X = D/kT$, D is the zero-field splitting parameter, g is the average g tensor value and the other symbols have their standard meanings (as shown in Chapter I). Equation (1) is the

theoretical equation for the magnetic susceptibility resulting from the axial and rhombic zero-field splitting for a Fe^{III} $S = 5/2$ ion [19]. The temperature dependence of the molar paramagnetic susceptibility, χ_{M} , was least-squares fitted (Figure 5.3.5) between the temperature range 5-300 K and yielded the parameters $D = 2.78 \text{ cm}^{-1}$ and $g = 2.10$, for $[\text{Fe}(\text{H-4-OH-thsa})_2]_4 \cdot (\text{SO}_4)_2 \cdot 9\text{H}_2\text{O}$, with a coefficient of determination value of 0.97 and a reduced χ^2 value of 0.000002.

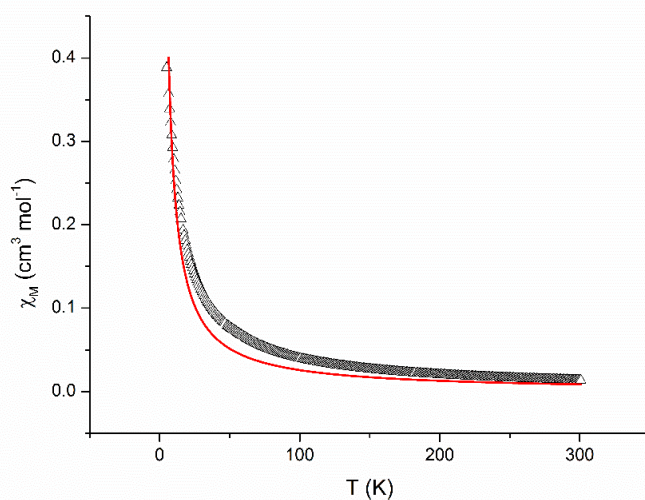


Figure 5.3.5 Temperature dependence of the molar magnetic susceptibility, χ_{M} , for the compound $[\text{Fe}(\text{H-4-OH-thsa})_2]_4 \cdot (\text{SO}_4)_2 \cdot 9\text{H}_2\text{O}$ in the range 5-300 K. Points are the experimental data; solid red line represents the least-squares fit of the data to Equation (1), where $D = 2.78 \text{ cm}^{-1}$ and $g = 2.10$.

5.4 Discussion

This chapter reports the structural characterisation and magnetic properties of two novel mononuclear Fe^{III} complexes based on R-salicylaldehyde 4R'-thiosemicarbazone, $[\text{Fe}(\text{HL}^-)_2]\text{X} \cdot n\text{H}_2\text{O}$, where $\text{X} = \text{NO}_3^-$ or SO_4^{2-} . The aim of this comparative study is to attempt to explain in which manner the spin state of the $[\text{Fe}(\text{HL}^-)_2]^+$ cation appears to be dependent on the accompanying non-coordinating anion, the R- and R'-substituent and the solvent molecules. It is noteworthy to mention, to the best of our knowledge, that the reported compounds $[\text{Fe}(\text{H-5-Br-thsa-Et})_2](\text{NO}_3) \cdot \text{H}_2\text{O}$ and $[\text{Fe}(\text{H-4-OH-thsa})_2]_4 \cdot (\text{SO}_4)_2 \cdot 9\text{H}_2\text{O}$ are the first type of $[\text{Fe}(\text{HL}^-)_2](\text{anion}^-) \cdot n\text{H}_2\text{O}$ compound to be described containing the R-salicylaldehyde 4R'-thiosemicarbazone ligand.

It is difficult to correlate the structure and the magnetic properties of spin-crossover systems, therefore studies of spin-crossover materials are essential for understanding how to govern the generation of a spin-transition. In the following, the crystallographic data of $[\text{Fe}(\text{H-5-Br-thsa-Et})_2](\text{NO}_3) \cdot \text{H}_2\text{O}$ and $[\text{Fe}(\text{H-4-OH-thsa})_2]_4 \cdot (\text{SO}_4)_2 \cdot 9\text{H}_2\text{O}$ will be compared. The Fe-donor atom distances of the Fe^{III} bis(ligand) compounds in this chapter are listed in Table 5.4.1. The structures

of $[\text{Fe}(\text{H-5-Br-thsa-Et})_2](\text{NO}_3)\cdot\text{H}_2\text{O}$ and $[\text{Fe}(\text{H-4-OH-thsa})_2]_4\cdot(\text{SO}_4)_2\cdot 9\text{H}_2\text{O}$ consist of an $\text{Fe}^{\text{III}}\text{O}_2\text{N}_2\text{S}_2$ chromophore which is formed by two chelating tridentate anionic R-salicylaldehyde 4R'-thiosemicarbazonato(1-) ligands. The $\text{Fe}^{\text{III}}\text{O}_2\text{N}_2\text{S}_2$ chromophore exhibits a distorted octahedral geometry, where the O- and S-donor atoms are in the *cis* positions and the N-donor atoms are in the *trans* positions. The Fe^{III} cation in both $[\text{Fe}(\text{H-5-Br-thsa-Et})_2](\text{NO}_3)\cdot\text{H}_2\text{O}$ and $[\text{Fe}(\text{H-4-OH-thsa})_2]_4\cdot(\text{SO}_4)_2\cdot 9\text{H}_2\text{O}$ is in the high-spin state at 100 K.

Table 5.4.1 Fe-donor atom bonds for high-spin (HS) $[\text{Fe}(\text{HL}^-)_2](\text{anion}^-)\cdot n\text{H}_2\text{O}$ type compounds of R-salicylaldehyde 4R-thiosemicarbazone.

Compound ⁱ	T (K)	Space group	Fe-S (Å)	Fe-N (Å)	Fe-O (Å)
$[\text{Fe}(\text{H-5-Br-thsa-Et})_2](\text{NO}_3)\cdot\text{H}_2\text{O}$	100	<i>Pnna</i>	2.4406(15)	2.175(4)	1.958(4)
			2.4635(15)	2.162(4)	1.945(3)
$[\text{Fe}(\text{H-4-OH-thsa})_2]_4\cdot(\text{SO}_4)_2\cdot 9\text{H}_2\text{O}^{\text{ii}}$	100	<i>P-1</i>	2.4391(10)	2.160(3)	1.946(2)
			2.4422(11)	2.173(3)	1.945(2)
			2.4331(10)	2.166(3)	1.952(2)
			2.4369(11)	2.175(3)	1.935(2)
			2.4655(11)	2.155(3)	1.957(2)
			2.4268(12)	2.182(3)	1.929(2)
			2.4587(10)	2.142(3)	1.926(2)
			2.4506(11)	2.143(3)	1.950(2)

ⁱ In the case that there are different ligands coordinated to the Fe atom, the geometric parameters involving each ligand are given in separate lines.

ⁱⁱ Compound contains four crystallographically independent Fe sites (Fe1, Fe2, Fe3 and Fe4).

It has long been discussed that the nature of the spin transition can be strongly influenced by chemical contributions which affect the lattice interactions [1-12, 18, 25]. In this instance, several influences on the structural and magnetic properties of the reported $[\text{Fe}(\text{HL}^-)_2](\text{anion}^-)\cdot n\text{H}_2\text{O}$ compounds will be considered, these include: the nature of the non-coordinating anion associated with the complex system, the extent and nature of solvation of the complex and the variations in the ligand substituents.

The variation of the R and R'-substituent groups of the R-salicylaldehyde 4R'-thiosemicarbazone type ligand has been utilised with the aim of finely tuning the spin-crossover behaviours in Fe^{III} complexes. In Fe^{III} complexes, the R-salicylaldehyde 4R'-thiosemicarbazone type ligand has been known to form π - π stacking interactions which enhances the cooperativity and interactions between the Fe^{III} units and leads to the possibility to create an abrupt spin-transition [1-12, 18, 25]. In the case

of $[\text{Fe}(\text{H-5-Br-thsa-Et})_2](\text{NO}_3)\cdot\text{H}_2\text{O}$, the ligand contains the R-substituent, 5-bromo on the salicylaldehyde moiety, and an ethyl group as the R'-substituent on the thiosemicarbazone moiety, whereas, $[\text{Fe}(\text{H-4-OH-thsa})_2]_4\cdot(\text{SO}_4)_2\cdot 9\text{H}_2\text{O}$ contains R = 4-hydroxy group and R' = H. As stated, $[\text{Fe}(\text{H-5Br-thsa-Et})_2](\text{NO}_3)\cdot\text{H}_2\text{O}$ and $[\text{Fe}(\text{H-4-OH-thsa})_2]_4\cdot(\text{SO}_4)_2\cdot 9\text{H}_2\text{O}$ are both in the high-spin form over the temperature range 5-300 K. The R,R'-substituents of the ligand may exhibit steric and electronic effects, including being involved in hydrogen bonding, via the R,R'-substituents in the $[\text{Fe}(\text{HL}^-)_2](\text{anion}^-)\cdot n\text{H}_2\text{O}$ compounds (Table 5.4.1), these features may be harnessed to induce a particular spin state for Fe^{III} . The introduction of the alkyl chain into the ligand should slightly increase the ligand field strength of the ligand because of alkyl chains having a weak tendency to donate electrons. However, this may be outbalanced by the alkyl group in close proximity to the donating S atom, being able to bind less efficiently to Fe^{III} , elongating the Fe-S bond and hence decreasing the ligand field strength. Perhaps the latter effect is larger and the compound has Fe^{III} in the high-spin state, but that is difficult to conclude as many parameters are involved. Furthermore, the addition of the alkyl group would add steric bulk to the thiosemicarbazone moiety of the ligand, which may cause less efficient packing in the within the crystal lattice, in comparison to the ligand, 2,4-dihydroxybenzaldehyde thiosemicarbazone, which contains R' = H. The most significant of interactions found in the spin-crossover systems include π - π stacking and hydrogen bonding interactions. It has been determined that both high-spin compounds, $[\text{Fe}(\text{H-5Br-thsa-Et})_2](\text{NO}_3)\cdot\text{H}_2\text{O}$ and $[\text{Fe}(\text{H-4-OH-thsa})_2]_4\cdot(\text{SO}_4)_2\cdot 9\text{H}_2\text{O}$ do not exhibit π - π stacking interactions, but exhibit extensive hydrogen bonding interactions between the solvent molecules, non-coordinating anions and the coordinating ligands.

Over the past few decades, the influence of the non-coordinating anion on the spin-crossover process has included research on an abundance of Fe^{II} , Fe^{III} and Co^{II} spin-crossover salts [22-26]. Particular focus has been paid to the singly deprotonated form of the pyridoxal 4R-thiosemicarbazone ligand, which has been found to generate Fe^{III} spin-crossover [27-28]. Previous work by Yemeli Tido [8] focused on using derivatives of pyridoxal-4R-thiosemicarbazone for generating Fe^{III} spin-crossover, resulting in the three octahedral $\text{Fe}^{\text{III}}\text{O}_2\text{N}_2\text{S}_2$ entities of the molecular formula $[\text{Fe}^{\text{III}}(\text{HL}^-)]\text{X}\cdot n\text{H}_2\text{O}$, where HL^- is the monoanionic form of pyridoxal thiosemicarbazone (Hthpy) or pyridoxal-4-methylthiosemicarbazone (Hmthpy), respectively, and X = sulfate, nitrate or tosylate anion [8]. It was recognised that the magnetic behaviour of these salts was sensitive to the non-coordinating anion and the solvent molecules, both of which were involved in hydrogen bonding [8]. For instance, for the compounds $[\text{Fe}(\text{Hthpy})_2](\text{SO}_4)_{1/2}\cdot 3.5\text{H}_2\text{O}$ and $[\text{Fe}(\text{Hthpy})_2]\text{NO}_3\cdot 3\text{H}_2\text{O}$ where the ligand and its degree of deprotonation are identical, completely different magnetic behaviour is encountered. $[\text{Fe}(\text{Hthpy})_2](\text{SO}_4)_{1/2}\cdot 3.5\text{H}_2\text{O}$ shows an abrupt spin transition above room temperature upon release of its water solvent molecules on heating, whereas for $[\text{Fe}(\text{Hthpy})_2]\text{NO}_3\cdot 3\text{H}_2\text{O}$, the Fe^{III} ion remains in the low-spin state, even upon dehydration of the complex [8]. The variation of the non-

coordinating anion associated with the spin-crossover active complex cation $[\text{Fe}(\text{Hthpy})_2]^+$, SO_4^{2-} and NO_3^- apparently results in the spin-crossover behaviour being suppressed [8].

The main difference observed between the present compounds $[\text{Fe}(\text{H-5Br-thsa-Et})_2](\text{NO}_3)\cdot\text{H}_2\text{O}$ and $[\text{Fe}(\text{H-4-OH-thsa})_2]_4\cdot(\text{SO}_4)_2\cdot 9\text{H}_2\text{O}$ is the varying size, shape and charge of the associated non-coordinating anion. The two anions present in the two reported compounds $[\text{Fe}(\text{H-5Br-thsa-Et})_2](\text{NO}_3)\cdot\text{H}_2\text{O}$ and $[\text{Fe}(\text{H-4-OH-thsa})_2]_4\cdot(\text{SO}_4)_2\cdot 9\text{H}_2\text{O}$ are different such that NO_3^- anion having a trigonal planar configuration whereas the SO_4^{2-} anion has a tetrahedral configuration. Their differences are mainly in the aspects of size and electronic properties. It could be suggested that the size and the electronic properties of the non-coordinating anions exert an influence on the crystal packing and the cooperativity of the Fe^{III} units. Perhaps, investigating these compounds with smaller anions such as Cl^- to tune the spin-crossover is worth performing at a later stage, in order increase cooperativity between the Fe^{III} units. It should be duly noted that the effect of the R and R'-substituents of the salicylaldehyde and thiosemicarbazone moieties, respectively, cannot be excluded.

It is possible that the magnetic behaviour of $[\text{Fe}(\text{H-5Br-thsa-Et})_2](\text{NO}_3)\cdot\text{H}_2\text{O}$ and $[\text{Fe}(\text{H-4-OH-thsa})_2]_4\cdot(\text{SO}_4)_2\cdot 9\text{H}_2\text{O}$ may be caused by the intermolecular interactions created by the solvent molecules present in the crystal lattice. For instance, it is recognised that hydrogen bonding has been found to play a significant role in changes in the spin-crossover behaviour accompanying hydration or dehydration processes [25]. It has been suggested that hydration of the metal complex will generally result in a stabilisation of the low-spin state, through hydrogen bonding of the water with the ligand [25, 26, 29-32]. This does seem to be the case for most hydrates, but in a cationic spin-crossover system where the ligand is hydrogen bonded to the associated anion only and this in turn is hydrogen bonded to the water, the effect can be the reverse, *i.e.*, loss of water can also result in stabilisation of the low-spin state [25, 26, 29-32]. However, this turns out not to be the case, as for both compounds, $[\text{Fe}(\text{H-5Br-thsa-Et})_2](\text{NO}_3)\cdot\text{H}_2\text{O}$ and $[\text{Fe}(\text{H-4-OH-thsa})_2]_4\cdot(\text{SO}_4)_2\cdot 9\text{H}_2\text{O}$, the ligands form intermolecular interactions with both the non-coordinating anions and the water solvent molecules, therefore does not comply with the suggestion that the loss of water could result in the stabilisation of the low-spin state. The involvement of hydrogen bonding also plays an important role in the changes in the spin-crossover behaviour accompanying the hydration and/or dehydration processes, as reported by Yemeli Tido [8], Mohan *et al.* [28], and Timken *et al.* [33]. It is likely that the highly cooperative nature of the spin-transition of $[\text{Fe}(\text{HL}^-)_2](\text{anion}^-)\cdot n\text{H}_2\text{O}$ type compounds is due to the extended interaction of the metal ion units through intermolecular hydrogen bonds and π - π interactions.

To conclude, the rationalisation of the factors (*i.e.* the effect of the R,R'-substituents of the ligand, the non-coordinating anion, the degree of solvation and intermolecular interactions) that govern the

spin-crossover process in cationic Fe^{III} complexes, such as [Fe(H-5Br-thsa-Et)₂](NO₃)·H₂O and [Fe(H-4-OH-thsa)₂]₄·(SO₄)₂·9H₂O, is rather difficult as they are not always consistent from one system to another. The development of a strategy towards the synthesis of [Fe(HL⁻)₂](anion⁻)·nH₂O type compounds containing R-salicylaldehyde 4R'-thiosemicarbazone ligand, with a pre-determined spin state will require the measurement and analysis of crystallographic data of a larger number of cationic Fe^{III} complexes, including these having different R and/or R'-substituents and a variety of associated anions.

5.5 References

1. Zelentsov, V. V., Bogdanova, L. G., Ablov, V. V., Gerbelev, N. V. and Dyatlova, Ch. V. (1973). *Russ. J. Inorg. Chem.* **18**(10), pp. 1410-1412.
2. Ryabova, N. A., Ponomarev, V. I., Zelentsov, V. V. and Atovmyan, L. O. (1981). *Kristallografiya*. **26**, pp. 101-108.
3. Zelentsov, V. V., Ablov, A. V., Turta, K. I., Stukan, R. A., Gerbelev, N. V., Ivanov, E. V., Bogdanov, A. P., Barba, N. A. and Bodyu, V. G. (1972). *Russ. J. Inorg. Chem.* **17**(7), pp. 1000-1003.
4. Ryabova, N. A., Ponomarev, V. I., Zelentsov, V. V., Shipilov, V. I. and Atovmyan, L. O. (1981). *J. Struct. Chem.* **22**, pp. 111-115.
5. Ryabova, N. A., Ponomarev, V. I., Atovmyan, L. O., Zelentsov, V. V. and Shipilov, V. I. (1978). *Koord Khim.* **4**, pp. 119-126.
6. Zelentsov, V. V. (1983). *Advances in Inorganic Chemistry*. 6th Ed. MIR Publishers.
7. Ryabova, N. A., Ponomarev, V. I., Zelentsov, V. V. and Atovmyan, L. O. (1982). *Sov. Phys. Crystallogr.* **27**, pp. 46.
8. Yemeli Tido, E. W. (2010). PhD Thesis, University of Groningen, The Netherlands.
9. Li, Z.-Y., Dai, J.-W., Gagnon, K. J., Cai, H.-L., Yamamoto, T., Einaga, Y., Zhao, H.-H., Kanegawa, S., Sato, O., Dunbar, K. R. and Xiong, R.-R. (2013). *J. Chem. Soc., Dalton. Trans.* **42**, pp. 14685-14688.
10. Floquet, S., Boillot, M.-L., Rivière, E., Varret, F., Boukheddaden, K., Morineau, D. and Négrier, P. (2003). *New. J. Chem.* **27**, pp. 341-348.
11. Floquet, S., Guillou, N., Négrier, P., Rivière, E. and Boillot, M.-L. (2006). *New. J. Chem.* **30**, pp. 1621-1627.
12. Li, Z.-Y., Dai, J.-W., Shiota, Y., Yoshizawa, K., Kanegawa, S. and Sato, O. (2013). *Chem. Eur. J.* **19**, pp. 12948-12952.
13. Dolomanov, O.V., Bourhis, L. J., Gildea, R. J., Howard, J. A. K. and Puschmann, H. (2009). *J. Appl. Cryst.* **42**, pp. 339-341.

14. Agilent (2014). *CrysAlisPro*. Agilent Technologies UK Ltd, Yarnton, England.
15. Palatinus, L. and Chapuis, G. (2007). *J. Appl. Cryst.* **40**, pp. 786-790.
16. Sheldrick, G. M. (2008). *Acta Cryst.* **A64**, pp. 112-122.
17. Farrugia, L. J. (2012). *J. Appl. Cryst.* **45**, pp. 849-854.
18. Koningsbruggen, P. J. van., Maeda, Y. and Oshio, H. (2004). *Spin Crossover in Transition Metal Compounds I*, edited by Gülich, P. and Goodwin, H. A., *Top. Curr. Chem.* Berlin: Springer, **233**, pp. 259-324.
19. Chen, C.-H., Lee, Y.-Y., Liau, B.-C., Shanmugham, E., Chen, J.-H., Hsieh, H.-Y, Liao, F.-L. Wang, S.-L. and Hwang, L.-P. (2002). *J. Chem. Soc., Dalton. Trans.*, pp. 3001-3006.
20. Rigaku (2013). *CrystalClear-SM Expert 2.1 b29*. Rigaku Corporation, The Woodlands, Texas, USA.
21. Sheldrick, G. M. (2015). *Acta Cryst.* **A71**, pp. 3-8.
22. Kremer, S., Henke, W. and Reinen, D. (1982). *Inorg. Chem.* **21**, pp. 3013.
23. Figgis, B. N., Kucharski, E. S. and White, A. W. (1983). *Aust. J. Chem.* **36**, pp. 1527.
24. Hogg, R. and Wilkins, R. G. (1962). *J. Chem. Soc.*, pp. 341-350.
25. Gülich, P. and Goodwin, H. A. (2004). Editors. *Spin Crossover in Transition Metal Compounds I-III*, edited by Gülich, P. and Goodwin, H. A., *Top. Curr. Chem.* Berlin: Springer, **233-235**.
26. Goodwin, H. A. (2004). *Spin Crossover in Transition Metal Compounds II*, edited by Gülich, P. and Goodwin, H. A., *Top. Curr. Chem.* Berlin: Springer, **234**, pp. 23-47.
27. Gupta, N. S., Mohan, M., Jha, N. K. and Antholine, W. E. (1991). *Inorg. Chim. Acta.* **184**, pp.13.
28. Mohan, M., Madhuranath, P. H., Kumar, A., Kumar, M. and Jha, N. K. (1989). *Inorg. Chem.* **28**, pp. 96.
29. Gülich, P., Hauser, A. and Spiering, H. (1994). *Angew. Chem., Int. Ed. Engl.* **33**, pp. 2024-2054.
30. Real, J. A., Gaspar, A. B., Niel, V. and Muñoz, M. C. (2003). *Coord. Chem. Rev.* **236**, pp. 121-141.
31. Real, J. A., Gaspar, A. B. and Muñoz, M. C. (2005). *J. Chem. Soc., Dalton Trans.* pp. 2062-2079.
32. Galet, A., Gaspar, A. B., Muñoz, M. C. and Real, J. A. (2006). *Inorg. Chem.* **45**, pp. 4413-4422.
33. Timken, M. D., Wilson, S. R. and Hendrickson, D. N. (1985). *Inorg. Chem.* **24**, pp. 3450.

Chapter VI

Conclusions and Outlook

6.0 Conclusions and Outlook

6.1 Conclusions

The motivation of this work was to synthesise a variety of functionalised R-salicylaldehyde 4R'-thiosemicarbazone ligands to obtain novel Fe^{III} compounds with the potential to display spin-crossover behaviour. The design of the derivatives was driven by the aim to successfully crystallise single crystalline systems, so that the interpretation of the magnetic properties could be supported with structural evidence. In this thesis, several ligands have been prepared based on R-salicylaldehyde 4R'-thiosemicarbazone, by varying the R- and R'-substituents appended to the salicylaldehyde and thiosemicarbazone moieties, respectively. Using these tridentate chelating ligands, ten Fe^{III} based compounds have been crystallised and structures have been elucidated, adding to this family of Fe^{III} bis(ligand) compounds found in the literature. The thermal magnetic behaviour of these compounds has been studied in detail, together with a study of the structural features that form the crystal lattice and the determination of the magnetic properties of this family of materials.

The investigation into the family of R-salicylaldehyde 4R'-thiosemicarbazone Fe^{III} compounds yielded three types of differently charged moieties of Fe^{III} bis(ligand) complexes (listed in Table 6.1), these include: (i) (cation⁺)[Fe^{III}(L²⁻)₂] \cdot x(solvate), (ii) [Fe^{III}(HL⁻)(L²⁻)] \cdot x(solvate) and (iii) [Fe^{III}(HL⁻)₂](anion⁻) \cdot x(solvate), reported in Chapters 3, 4 and 5, respectively.

The manifestation of a spin transition in a solid state system is subject to the operation of lattice forces. It has long been established that the nature of the spin transition can be strongly influenced by chemical contributions which affect the lattice interactions. In this instance, several influences on the structural features and the magnetic properties of the reported Fe^{III} compounds were considered throughout this thesis. These include:

- (v) The nature of the anion or cation associated with the metal fragment;
- (vi) The extent and nature of solvation of the complex;
- (vii) Variations in the ligand substituents.

The study of (cation⁺)[Fe^{III}(L²⁻)₂] \cdot x(solvate) type complexes (Chapter III) containing two dianionic R-salicylaldehyde 4R'-thiosemicarbazone(2-) ligands, focused upon investigating the effect of varying R- and R'-substituents, cations and solvent molecules within the lattice on the crystal packing and magnetic properties. Chapter IV provided a study of three mononuclear [Fe^{III}(HL⁻)(L²⁻)] \cdot H₂O type complexes, containing one anionic and one dianionic R-salicylaldehyde 4R'-thiosemicarbazone ligand. Correlations between the steric and electronic effects imposed by the R- and R'-substituents of the ligands bound to the Fe^{III} ions and the magnetic properties observed were discussed. Chapter V investigated [Fe^{III}(HL⁻)₂](anion⁻) \cdot xH₂O type complexes, with focus upon the

effect of varying the anions and the R- and R'-substituents of the coordinated one-fold deprotonated ligands within the crystal lattice on the magnetic properties and crystal packing of Fe^{III} units.

Table 6.1 Selected crystallographic data and spin state of the Fe^{III} bis(R-salicylaldehyde 4R'-thiosemicarbazone) compounds

Compound ⁱ	T (K)	Space group	Fe–S (Å)	Fe–N (Å)	Fe–O (Å)	Spin State ⁱⁱ
Cs[Fe(3-OEt-thsa-Me) ₂] \cdot CH ₃ OH	100	<i>P</i> -1	2.2686	1.933	1.904	LS
			2.265	1.939	1.918	
Cs[Fe(5-Br-thsa) ₂]	293	<i>P</i> 2 ₁ / <i>c</i>	2.2321	1.947	1.942	LS
			2.2422	1.938	1.956	
NH ₄ [Fe(thsa) ₂]	100	<i>P</i> 2 ₁ / <i>n</i>	2.2366	1.930	1.938	LS
			2.2373	1.948	1.950	
NH ₄ [Fe(5-Br-thsa) ₂]	100	<i>Pbcn</i>	2.263	1.942	1.938	LS
(CH ₃) ₂ NH ₂ [Fe(3-OEt-thsa) ₂]	100	<i>P</i> 2 ₁ / <i>n</i>	2.4320	2.167	1.9806	HS
			2.4389	2.131	1.9595	
[Fe(H-thsa-Me)(thsa-Me)] \cdot H ₂ O	100	<i>Aea</i> 2	2.249	1.946	1.932	LS
[Fe(H-3-OEt-thsa-Me)(3-OEt-thsa-Me)] \cdot H ₂ O ⁱⁱⁱ	100	<i>P</i> -1	2.473	2.168	1.939	Fe1
			2.442	2.085	1.996	HS
			2.482	2.146	1.958	Fe11
			2.417	2.096	1.994	HS
[Fe(H-5-Cl-thsa-Me)(5-Cl-thsa-Me)] \cdot H ₂ O	100	<i>Aea</i> 2	2.255	1.969	1.951	LS sco
[Fe(H-5-Br-thsa-Et) ₂](NO ₃) \cdot H ₂ O	100	<i>Pnna</i>	2.4406	2.175	1.958	HS
			2.4635	2.162	1.945	
[Fe(H-4-OH-thsa) ₂] ₄ \cdot (SO ₄) ₂ \cdot 9H ₂ O ^{iv}	100	<i>P</i> -1	2.4391	2.160	1.946	Fe1
			2.4422	2.173	1.945	HS
			2.4331	2.166	1.952	Fe2
			2.4369	2.175	1.935	HS
			2.4655	2.155	1.957	Fe3
			2.4268	2.182	1.929	HS
			2.4587	2.142	1.926	Fe4
			2.4506	2.143	1.950	HS

ⁱ In the case that there are different ligands coordinated to the Fe atom, the geometric parameters involving each ligand are given in separate lines.

ⁱⁱ The spin states are defined as low-spin (LS) and high-spin (HS); sco defines spin-crossover.

ⁱⁱⁱ Compound contains two crystallographically independent Fe sites (Fe1 and Fe11).

^{iv} Compound contains four crystallographically independent Fe sites (Fe1, Fe2, Fe3 and Fe4).

These studies have shown that all of the reported Fe^{III} bis(ligand) systems (listed in Table 6.1) consist of an Fe^{III}O₂N₂S₂ chromophore which is formed by two chelating tridentate R-salicylaldehyde 4R'-thiosemicarbazonato ligands. Furthermore, it has been found that the Fe^{III}O₂N₂S₂ chromophore exhibits a distorted octahedral geometry, where the O- and S-donor atoms are in the *cis* positions and N-donor atoms are in the *trans* positions.

6.1.1 Anionic Fe^{III} complexes of R-salicylaldehyde 4R'-thiosemicarbazones

The correlations between the structural features and magnetic behaviour of the (cation⁺)[Fe(L²⁻)₂] \cdot x(solvate) type compounds revealed two major effects which influence the magnetic properties of this family of compounds: (i) the associated non-coordinating cation in the complex system and (ii) the R-substituents at the benzene ring of the salicylaldehyde moiety and/or the introduction of R'-substituents into the thioamide group of the thiosemicarbazide moiety. The variation of the cation (either NH₄⁺, Cs⁺ or (CH₃)₂NH₂⁺) in the crystal lattice may have an indirect impact on the spin state of Fe^{III} ion by influencing the crystal packing. In addition to the difference in the size between NH₄⁺, (CH₃)₂NH₂⁺ and Cs⁺ ions, the two former may engage in directed interactions through hydrogen bonding, while the Cs⁺ ion presents a more uniform electrostatic field without a preferred direction for hydrogen bonds. The R,R'-substituents of the ligand may exhibit steric and electronic effects as well as being involved in hydrogen bonding, via the R,R'-substituents in the (cation⁺)[Fe(L²⁻)₂] \cdot x(solvate) type compounds. It appears the steric effect induced by the R-substituent was more pronounced in the systems containing the bulkier 3-ethoxysalicylaldehyde 4R'-thiosemicarbazone ligand, especially with respect to the compound (CH₃)₂NH₂[Fe(3-OEt-thsa)₂], in which the Fe^{III} ion was found to be in the high-spin state at 100 K. Furthermore, an important feature of spin-crossover materials is cooperativity, which is a measure of the degree to which a spin transition in one Fe^{III} unit affects neighbouring Fe^{III} units. The Δ_o required for the Fe^{III} units to exhibit thermal spin-crossover does not seem have been reached for the reported (cation⁺)[Fe(L²⁻)₂] \cdot x(solvate) type compounds (as listed in Table 6.1), as these compounds do not exhibit spin-crossover. However, the magnetic behaviour of NH₄[Fe(5-Br-thsa)₂] proved interesting as the magnetic properties revealed an estimated fraction of about 12% of Fe^{III} ions converting into the high-spin state at 200 K.

6.1.2 Neutral Fe^{III} complexes of R-salicylaldehyde 4R'-thiosemicarbazones

The [Fe(HL⁻)(L²⁻)] \cdot H₂O compounds are an interesting example of how the R and R'-substituents of the R-salicylaldehyde 4R'-thiosemicarbazonato ligand may influence the nature of the spin transition of the Fe^{III} ion. The three compounds reported in Chapter IV, [Fe(H-5-Cl-thsa-Me)(5-Cl-thsa-Me)] \cdot H₂O, [Fe(H-thsa-Me)(thsa-Me)] \cdot H₂O and [Fe(H-3-OEt-thsa-Me)(3-OEt-thsa-Me)] \cdot H₂O, all

contain the R'-substituent, R' = Me, whereas their R-substituents differ, giving R = 5-Cl, R = H and R = 3-OEt, respectively. The isostructural compounds [Fe(H-5-Cl-thsa-Me)(5-Cl-thsa-Me)]·H₂O and [Fe(H-thsa-Me)(thsa-Me)]·H₂O, were found to be chiral, although this is a rare occurrence due to the fact no chiral compounds were used in the synthesis of the ferric complexes to induce chirality. It is clear that the electronic and steric implications of the R-substituents affect the spin state of the Fe^{III} complex, and also whether the compound exhibits spin-crossover or remains in either the low-spin or high-spin state. A rare two-step spin transition with hysteresis was observed for the compound [Fe(H-5-Cl-thsa-Me)(5-Cl-thsa-Me)]·H₂O. Upon changing the R-group from R = 5-Cl to R = -H, the isostructural compound [Fe(H-thsa-Me)(thsa-Me)]·H₂O was obtained, however, the latter material exhibits very different magnetic behaviour in comparison to [Fe(H-5-Cl-thsa-Me)(5-Cl-thsa-Me)]·H₂O. The value of $\chi_M T$ (χ_M being the molar magnetic susceptibility and T the temperature) for [Fe(H-thsa-Me)(thsa-Me)]·H₂O indicated that the Fe^{III} ion was in the low-spin state between the temperature range 5-300 K, however, higher temperature magnetic measurements between 200-400 K revealed an incomplete spin transition, whereby the $\chi_M T$ value at 400 K is 2.52 cm³ mol⁻¹ K, which corresponds to an estimated high-spin fraction of 54%. Moreover, replacing the R-group with a sterically bulky group, R = 3-OEt, yielded the high-spin compound [Fe(H-3-OEt-thsa-Me)(3-OEt-thsa-Me)]·H₂O. It may be proposed that the strong steric bulkiness of the 3-ethoxy group on the benzene ring of the salicylaldehyde moiety in the complex causes the compound to remain in the high-spin state between the temperature range 5-300K, as the bulky substituents are close to the donor atoms of the Fe^{III} entities, so prevents the shortening of the Fe-donor atom bond distances. Furthermore, for this series of compounds, the electronic effect on the spin-crossover behaviour of the R-groups suggests that the larger the electron withdrawing effect the lower the T_{1/2} which is corroborated by the linear relationship between T_{1/2} and the Hammett parameters, (σ).

6.1.3 Cationic Fe^{III} complexes of R-salicylaldehyde 4R'-thiosemicarbazones

Structural studies of [Fe(HL⁻)₂](anion⁻)·xH₂O type compounds, where HL⁻ is the one-fold deprotonated R-salicylaldehyde 4R'-thiosemicarbazonato(1-) ligand, are still an unexploited avenue with regards to the synthesis of spin-crossover compounds with this type of ligand. However, [Fe(H-5-Br-thsa-Et)₂](NO₃)·H₂O and [Fe(H-4-OH-thsa)₂]₄·(SO₄)₂·9H₂O are particularly interesting first examples of this type of material. The spin state of the Fe^{III} ions of [Fe(H-5-Br-thsa-Et)₂](NO₃)·H₂O and [Fe(H-4-OH-thsa)₂]₄·(SO₄)₂·9H₂O may have been influenced by the non-coordinating anion, the R,R'-substituents of the ligand and/or the solvent effect. The NO₃⁻ and SO₄²⁻ anions are different in size and electronic properties, such that NO₃⁻ has a trigonal planar configuration whereas the SO₄²⁻ anion has a tetrahedral configuration. The R,R'-substituents of the ligand may exhibit steric and electronic effects as well as being involved in hydrogen bonding via the R,R'-substituents in the

[Fe(HL⁻)₂](anion⁻)·x(solvate) type compounds. The crystal packing and cooperativity of the Fe^{III} units may be influenced by both the size and electronic properties of the non-coordinating anion, in addition to the electronic and steric effects due to the R and R'-substituents of the coordinated ligands. An interesting structural feature of [Fe(H-5-Br-thsa-Et)₂](NO₃)·H₂O and [Fe(H-4-OH-thsa)₂]₄·(SO₄)₂·9H₂O is how the hydrogen bonding interactions involving the water molecules and the non-coordinating anions within the crystal lattice of each compound may induce the stabilisation of the high-spin state. Hydrogen bonding has been found to play a significant role in the changes in the spin-crossover behaviour accompanying hydration or dehydration processes [1-6]. It has been suggested that hydration will generally result in a stabilisation of the low-spin state, through hydrogen bonding of the water with the ligand [1-6]. This does seem to be the case for most hydrates, but in a cationic spin-crossover system where the ligand is hydrogen bonded to the associated anion only and this in turn is hydrogen bonded to the water, the effect can be the reverse, *i.e.*, loss of water can also result in stabilisation of the low-spin state [1-6]. The study of the high-spin [Fe(HL⁻)₂](anion⁻)·xH₂O type systems has revealed that this is not the case for this family of compounds. The structural features of the [Fe(H-5-Br-thsa-Et)₂](NO₃)·H₂O and [Fe(H-4-OH-thsa)₂]₄·(SO₄)₂·9H₂O compounds has revealed that the ligands form intermolecular interactions with both the non-coordinating anions and water solvent molecules, it may be suggested that these intermolecular interactions do not comply with the evidence that the loss of water could result in the stabilisation of the low-spin state.

The work described in this thesis provides an in depth study of the structural and magnetic properties of a wide range of Fe^{III} bis(R-salicylaldehyde 4R'-thiosemicarbazonato) compounds with the following configurations: (i) (cation⁺)[Fe^{III}(L²⁻)₂]·x(solvate), (ii) [Fe^{III}(HL⁻)(L²⁻)]·x(solvate) and (iii) [Fe^{III}(HL⁻)₂](anion⁻)·x(solvate). This study includes the unique two step transition observed in the compound [Fe(H-5-Cl-thsa-Me)(5-Cl-thsa-Me)]·H₂O, in addition to the study of the two novel solvated [Fe^{III}(HL⁻)₂](anion⁻) complexes, [Fe(H-5-Br-thsa-Et)₂](NO₃)·H₂O and [Fe(H-4-OH-thsa)₂]₄·(SO₄)₂·9H₂O, this latter type of configuration of Fe^{III} complex containing the R-salicylaldehyde 4R'-thiosemicarbazone ligand are the first of this type and are still relatively unexploited in the literature.

6.2 Outlook

Although the spin-crossover phenomenon was first discovered in the 1930s, it has only been in recent decades that interest has been shown in the potential of Fe^{III} bis(R-salicylaldehyde 4R'-thiosemicarbazonato) compounds as spin-crossover systems. It has been realised that the most important features which are manifested in the nature of a spin transition are influenced by the chemical contributions which affect the crystal lattice interactions formed by the anion or cation

associated with the complex cation or complex anion, the extent and nature of solvation of the complex and/or the variations in the ligand substituents. The results of the studies herein provide a platform to devise further derivatives of R-salicylaldehyde 4R'-thiosemicarbazone type ligands, in order to design a library of Fe^{III} bis(R-salicylaldehyde 4R'-thiosemicarbazonato) compounds to increase the knowledge of the possible correlations between the structural and magnetic properties which lies behind our current understanding of this family of compounds. There are a number of ways in which the relationship between the structural and magnetic behaviour studies described here can be continued. The continuation of structural studies of this family of compounds is essential in the development of the strategy to predict the switching capabilities associated with the structural and electronic features. However, structural studies only are not sufficient for the complete understanding of spin-crossover, this leads to the approach of continued detailed crystallographic studies alongside detailed analysis of the magnetic properties of the ferric complexes by SQUID magnetometry measurements.

At this stage, it would appear that this family of compounds represents a unique and extremely versatile Fe^{III} model system that will allow for the target of further systematic and detailed modifications of the Fe^{III} system. This is especially true for the [Fe(HL⁻)(L²⁻)]·xH₂O type compound, as this configuration of the Fe^{III} systems with the R-salicylaldehyde 4R'-thiosemicarbazone ligand has been shown to exhibit spin-crossover frequently [7-9]. Furthermore, a systematic approach into the research of the structural and magnetic properties of the [Fe(HL⁻)₂](anion⁻)·xH₂O type compounds containing the R-salicylaldehyde 4R'-thiosemicarbazone ligand would be of great interest, as the two compounds reported in this thesis, are the first of this configuration. The next stage of the study would investigate several derivatives of the R-substituted salicylaldehyde moiety and the R'-substituted thiosemicarbazone moiety, as well as the unsubstituted salicylaldehyde thiosemicarbazone. In addition, investigate the variation of the non-coordinating anion, starting with a smaller anion *i.e.* Cl⁻, then continue the research by increasing the size of the anion. Therefore, within the process to synthesise numerous [Fe(HL⁻)₂](anion⁻)·xH₂O type compounds comprising a combination of varied ligands and non-coordinating anions, will not only add to the library of Fe^{III} bis(R-salicylaldehyde 4R'-thiosemicarbazonato) compounds, but will allow further understanding of the interactions of the ligand and the non-coordinating anions, and how these influence the nature of the spin transition. The nature of the different R,R'-substituents incorporated in the various R-salicylaldehyde 4R'-thiosemicarbazone ligands allows us to tune the steric and electronic features of the organic moiety. More precisely, this enables the selective tuning of the intra- and inter-molecular interactions between the Fe^{III} bis(ligand) entities. It is fair to say, that their true potential is yet to be unlocked, and that future research will reveal the full potential of this variously tuneable class of Fe^{III} systems.

After the aforementioned Fe^{III} systems have been subjected to an extensive characterisation focusing on obtaining information on the structural and electronic features associated with their unique magnetic behaviour, there have been very few systematic studies into the phenomenon in metal centres other than Fe^{II} and Co^{II} systems. Extension of this research to use other metal ions *i.e.* Cr^{III}, as this would create analogues of the Fe^{III} systems which would be a valuable addition to the work being performed in this area at present. This idea stems from the premise that one may use the Cr^{III} analogue instead of the Fe^{III} bis(R-salicylaldehyde 4R'-thiosemicarbazone) compound to assess the prospect of the Fe^{III} system displaying spin-crossover, simply by measuring the UV-Vis spectrum (thus determine Δ_o) of the Cr^{III} analogue. There is evidence of Cr^{III} salts bound to thiosemicarbazone type ligand systems being characterised with the purpose to understand the coordination of the ligands to the metal centres, as in this case for the analogous compounds [Fe^{III}(Hthpu)(thpu)]·H₂O and [Cr^{III}(Hthpu)(thpu)]·H₂O [10]. It should be duly noted that some Cr^{III} compounds may have ligands in an alternative orientation with respect to another, hence the Cr^{III} and Fe^{III} compounds are not isomorphous. The further study of the other 3d⁵ metal centres containing the R-salicylaldehyde 4R'-thiosemicarbazone ligand is likely to yield a wide range of compounds with interesting correlations between the structural and magnetic properties.

The advancement of experimental techniques over the next few decades will greatly widen the areas of research in which the electronic state can be detected. It is already recognised that for many spin transition systems, spin-crossover behaviour can be examined by solution NMR spectroscopy using the Evans Method [11-12]. It has been proposed that ¹³C solid state NMR spectroscopy could be used in an attempt to determine what spin state the metal centre exhibits at measurement temperature, although not without difficulty due to the paramagnetic behaviour of Fe^{III}. It has also been postulated that dependent upon spin state, either the low-spin state or the high-spin state, the signals observed would shift up or down field depending upon the electronic state of the metal ion. If this would be the case, it would be an interesting new technique to utilise in the determination of the spin state of the metal compound in question.

In conclusion, a continuation of the research into this family of Fe^{III} bis(R-salicylaldehyde 4R'-thiosemicarbazone) compounds is likely to provide new and exciting insights into the theory behind the nature of the spin-crossover phenomenon. Furthermore, it may be suggested that detailed crystallographic studies coupled with corresponding magnetic measurements will play a critical role in the future research and development of this field. Moreover, the discovery of coordination compounds with the ability to switch spin state, which is accompanied by the modification of the macroscopic properties of the material, such as those materials belonging to the family of Fe^{III} bis(R-salicylaldehyde 4R'-thiosemicarbazone) compounds, will gain more and more interest due to their potential applications in spintronics, display devices and sensors [13-19]. It is well documented that despite their great potential these type of materials present a number of problems such as chemical instability on a molecular level. Further research is required to solve these issues, which currently

involves the field of nanoscience with an aim to customize future spintronic devices. Thus the research into this family of Fe^{III} bis(R-salicylaldehyde 4R'-thiosemicarbazone) compounds on the macroscopic level must be continued not only on the macroscopic level but also on the nano-scale, in order to discover their full potential as molecular switches and for applications in spintronic, display devices and sensors.

6.3 References

1. Gütlich, P. and Goodwin, H. A. (2004). Editors. *Spin Crossover in Transition Metal Compounds I-III*, edited by Gütlich, P. and Goodwin, H. A., *Top. Curr. Chem.* Berlin: Springer, **233-235**.
2. Goodwin, H. A. (2004). *Spin Crossover in Transition Metal Compounds II*, edited by Gütlich, P. and Goodwin, H. A., *Top. Curr. Chem.* Berlin: Springer, **234**, pp. 23-47.
3. Gütlich, P., Hauser, A. and Spiering, H. (1994). *Angew. Chem., Int. Ed. Engl.* **33**, pp. 2024-2054.
4. Real, J. A., Gaspar, A. B., Niel, V. and Muñoz, M. C. (2003). *Coord. Chem. Rev.* **236**, pp. 121-141.
5. Real, J. A., Gaspar, A. B. and Muñoz, M. C. (2005). *Dalton Trans.* pp. 2062-2079.
6. Galet, A., Gaspar, A. B., Muñoz, M. C. and Real, J. A. (2006). *Inorg. Chem.* **45**, pp. 4413-4422.
7. Li, Z.-Y., Dai, J. W., Shiota, Y., Yoshizawa, K., Kanegawa, S. and Sato, O. (2013). *Chem. Eur. J.* **19**(39), pp. 12948-12952.
8. Li, Z.-Y., Dai, J.-W., Gagnon, K. J., Cai, H.-L., Yamamoto, T., Einaga, Y., Zhao, H.-H., Kanegawa, S., Sato, O., Dunbar, K. R. and Xiong, R.-R. (2013). *Dalton Trans.* **42**, pp. 14685-14688.
9. Floquet, S., Rivière, E., Boukheddaden, K., Morineau, D. and Boillot, M.-L. (2014). *Polyhedron.*, **80**, pp. 60-68.
10. Timken, M. D., Wilson, S. R. and Hendrickson, D. N. (1985). *Inorg. Chem.*, **24**, pp. 3450-3457.
11. Evans, D. F. (1959). *J. Chem. Soc.* pp. 2003-2005.
12. Evans, D. F., Fazakerley, G. V. and Phillips, R. F. (1971). *J. Chem. Soc.* pp. 1931-1934.
13. Muñoz, M. C. and Real, J. A. (2011). *Coord. Chem. Rev.* **255**, pp.2068–2093.
14. Gamez, P., Costa, J. S., Quesada, M. and Aromi, G. (2009). *Dalton Trans.* pp. 7845-7853.
15. Garcia, Y., Ksenofontov, V. and Gütlich, P. (2002). *Hyperfine Interact.* **129**, pp. 543-551.
16. Linares, J., Codjovi, E. and Garcia, Y. (2012). *Sensors.* **12**, pp. 4479-4192.
17. Jureschi, C. M., Linares, J., Rotaru, A., Ritti, M. H., Parlier, M., Dîrtu, M. M., Wolff, M. and Garcia, Y. (2015). *Sensors.* **15**, pp. 2388-2398.

18. Lefter, C., Ran, R., Tricard, S., Dugay, J., Molnar, G., Salmon, L., Carrey, J., Rotaru, A. and Bousseksou, A. (2015). *Polyhedron*. **102**, pp. 434-440.
19. Lefter, C., Davesne, L., Salmon, L., Molnár, G., Demont, P., Rotaru, M. and Bousseksou, A. (2016). *Magnetochemistry*. **2**, pp. 18.

Appendix

Appendix A

List of Publications

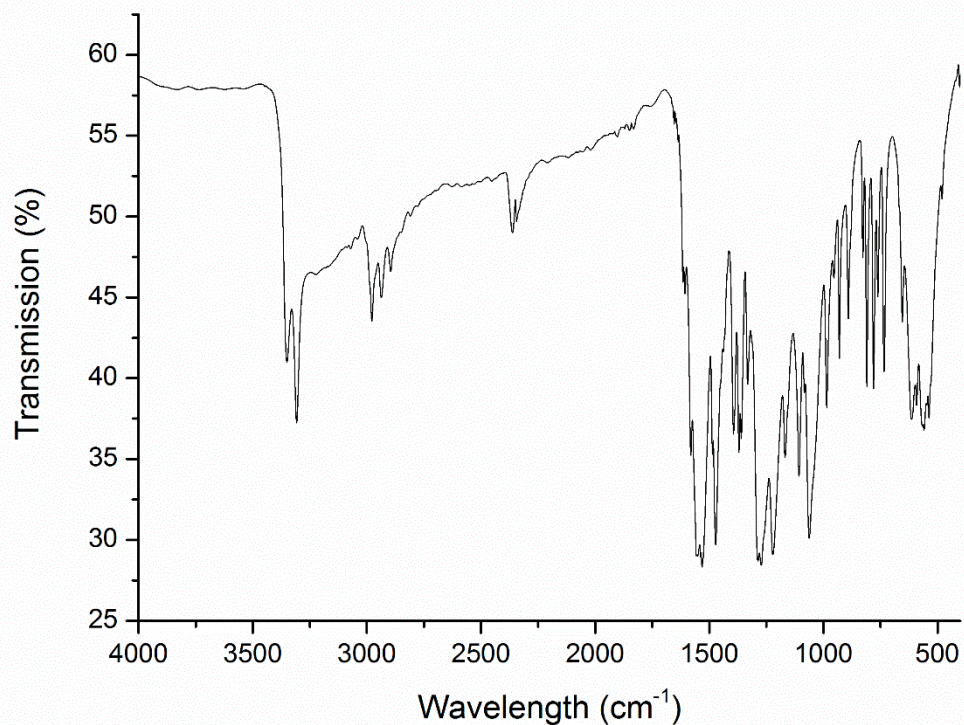
Powell, R. E., Schwalbe, C. H., Tizzard, G. J. and van Koningsbruggen, P. J. (2014). *Acta. Cryst.* **C70**, pp. 595-598.

Powell, R. E., Schwalbe, C. H., Tizzard, G. J. and van Koningsbruggen, P. J. (2015). *Acta. Cryst.* **C71**, pp. 169-174.

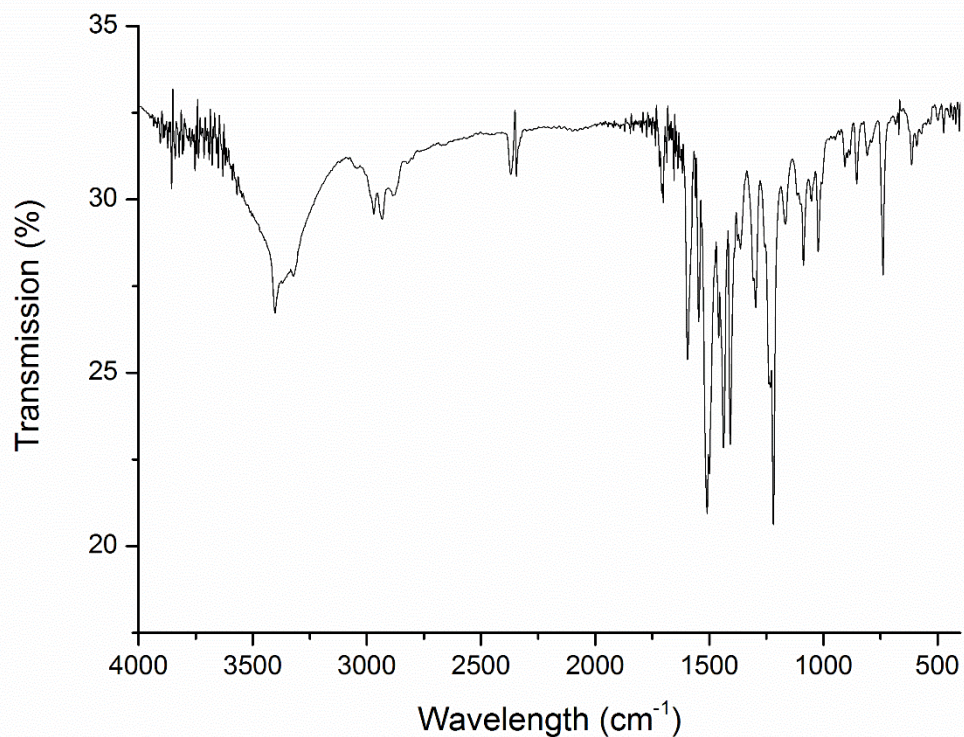
Appendix B

Infrared Spectra of R-salicylaldehyde 4R'-thiosemicarbazone ligands and ferric complexes

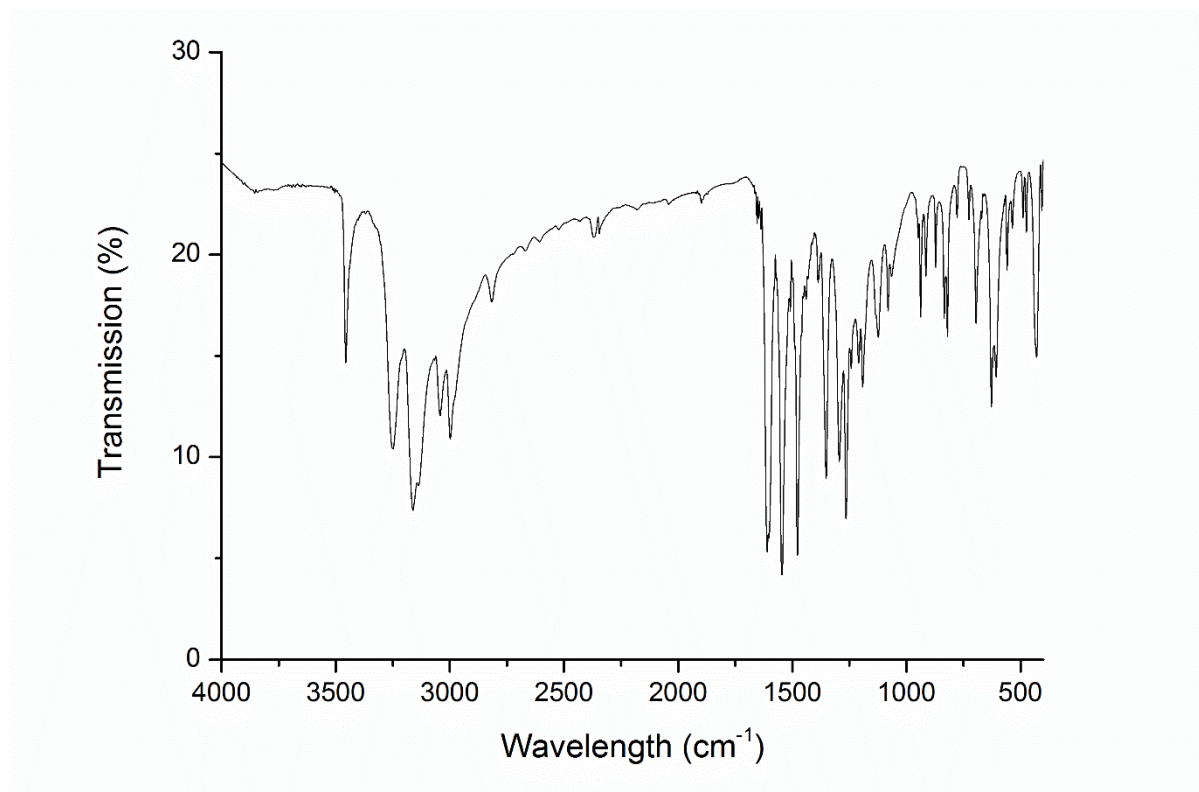
B1. Infrared spectrum of 3-ethoxysalicylaldehyde 4-methylthiosemicarbazone, H₂-3-OEt-thsa-Me



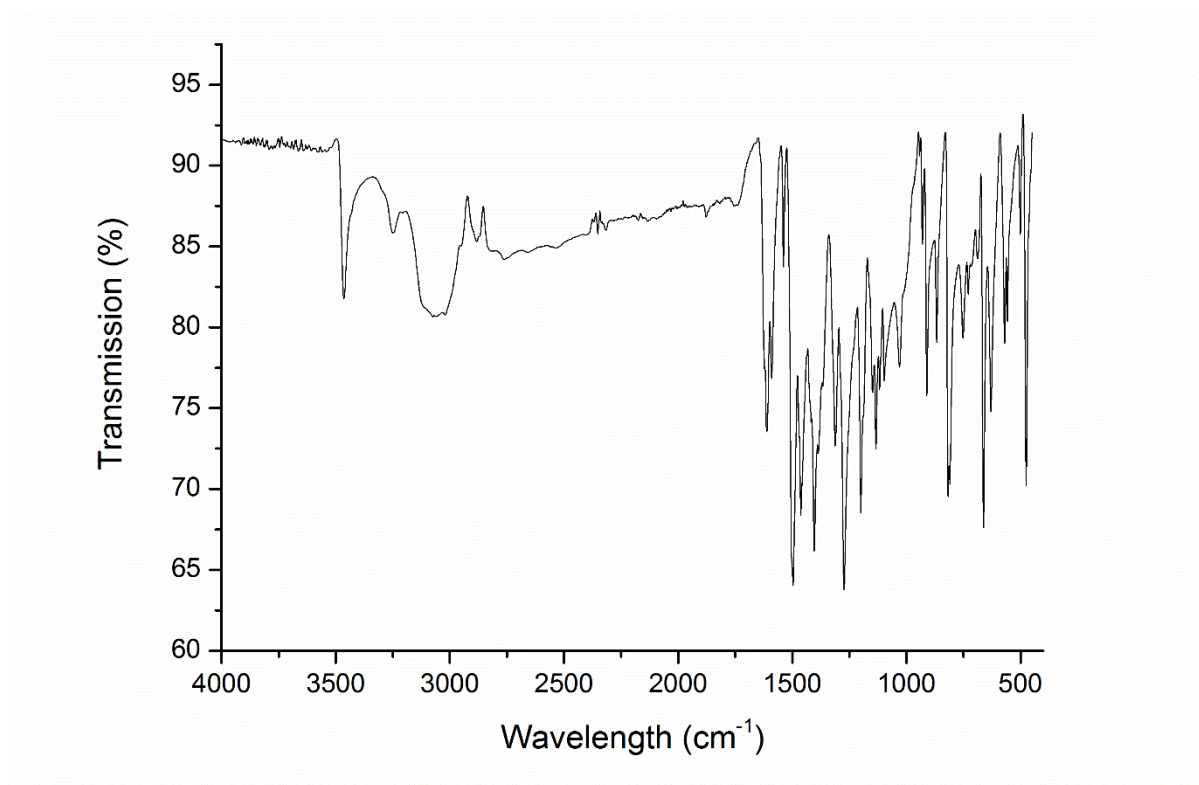
B2. Infrared spectrum of Cs[Fe(3-OEt-thsa-Me)₂]:CH₃OH



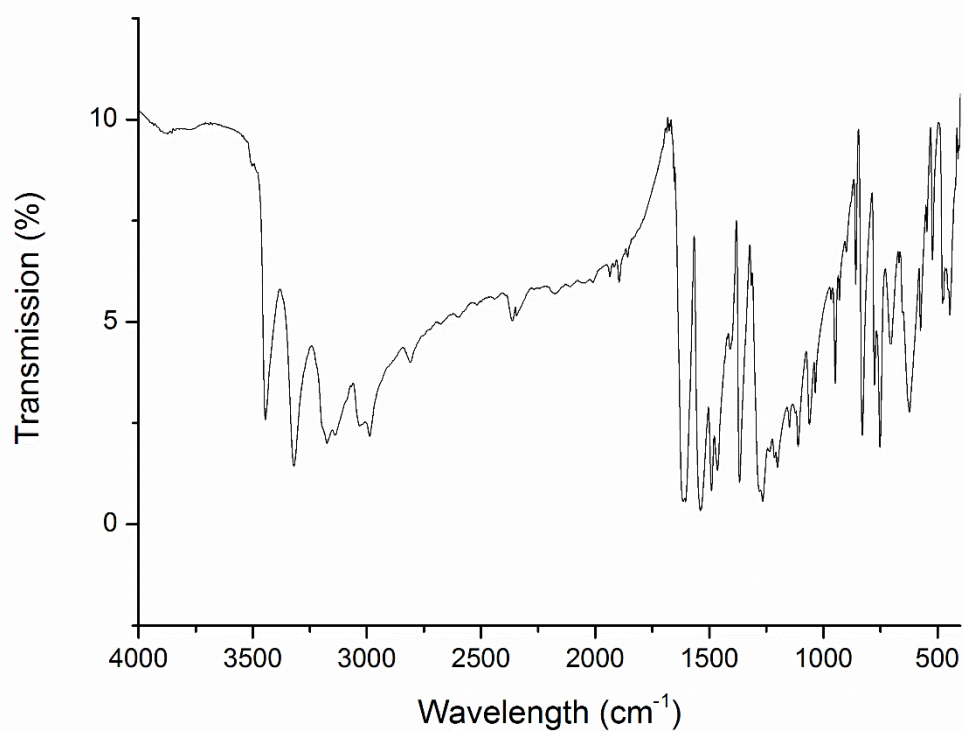
B3. Infrared spectrum of 5-bromosalicylaldehyde thiosemicarbazone, H₂-5-Br-thsa



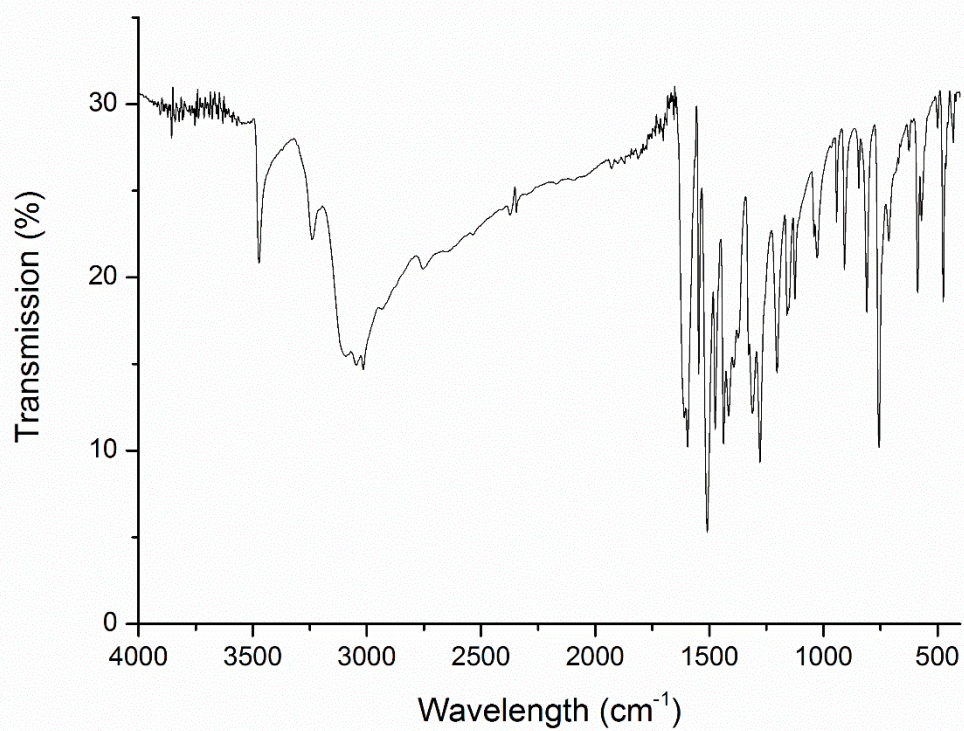
B4. Infrared spectrum of Cs[Fe(5-Br-thsa)₂]



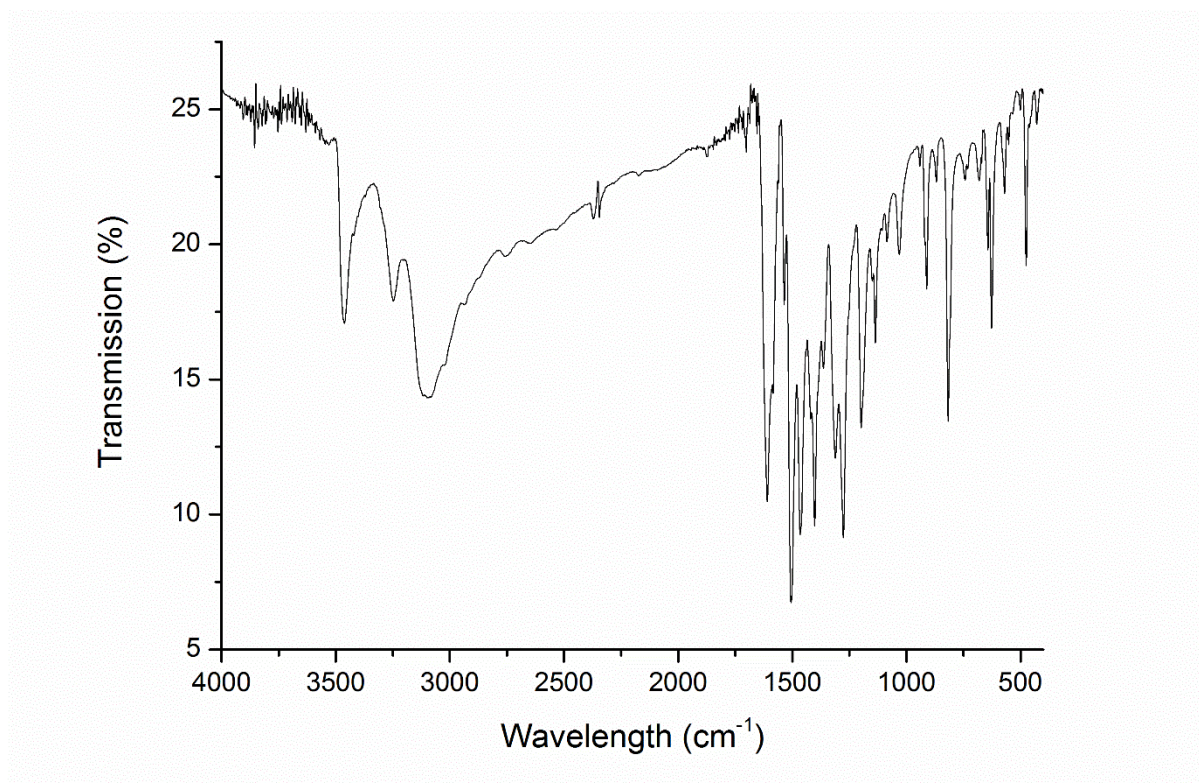
B5. Infrared spectrum of salicylaldehyde thiosemicarbazone, H₂-thsa



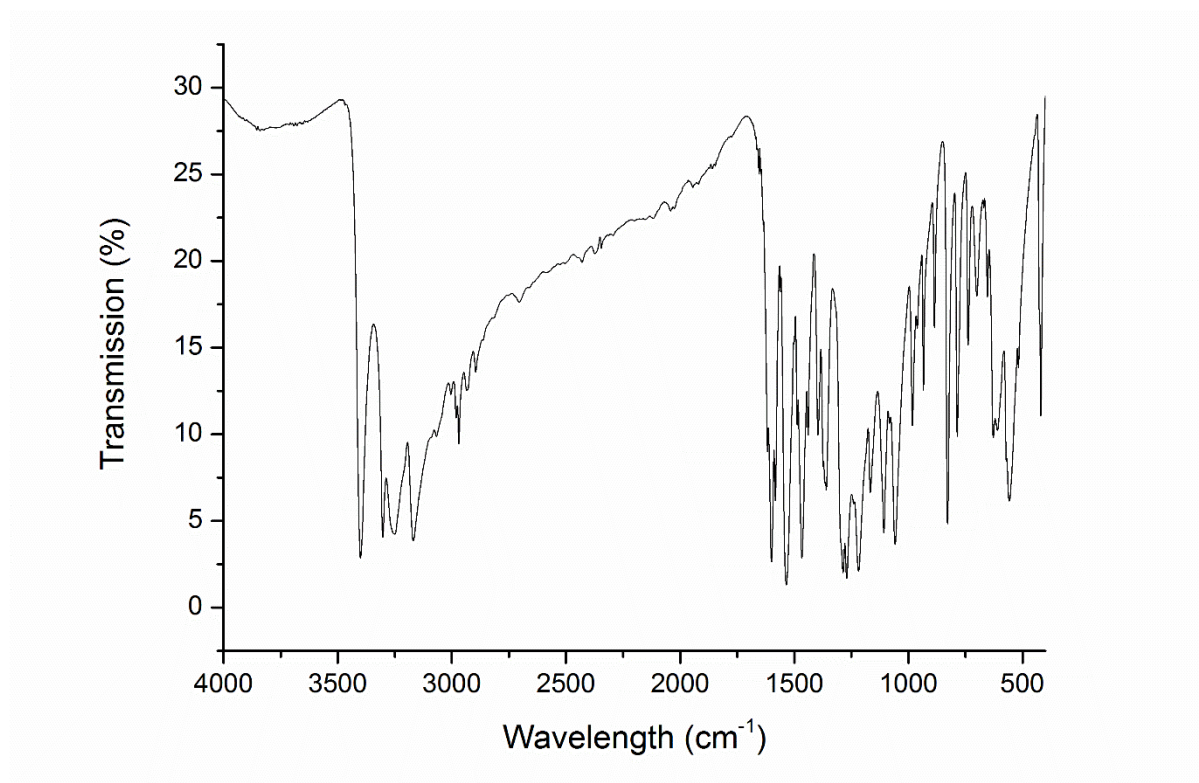
B6. Infrared spectrum of NH₄[Fe(thsa)₂]



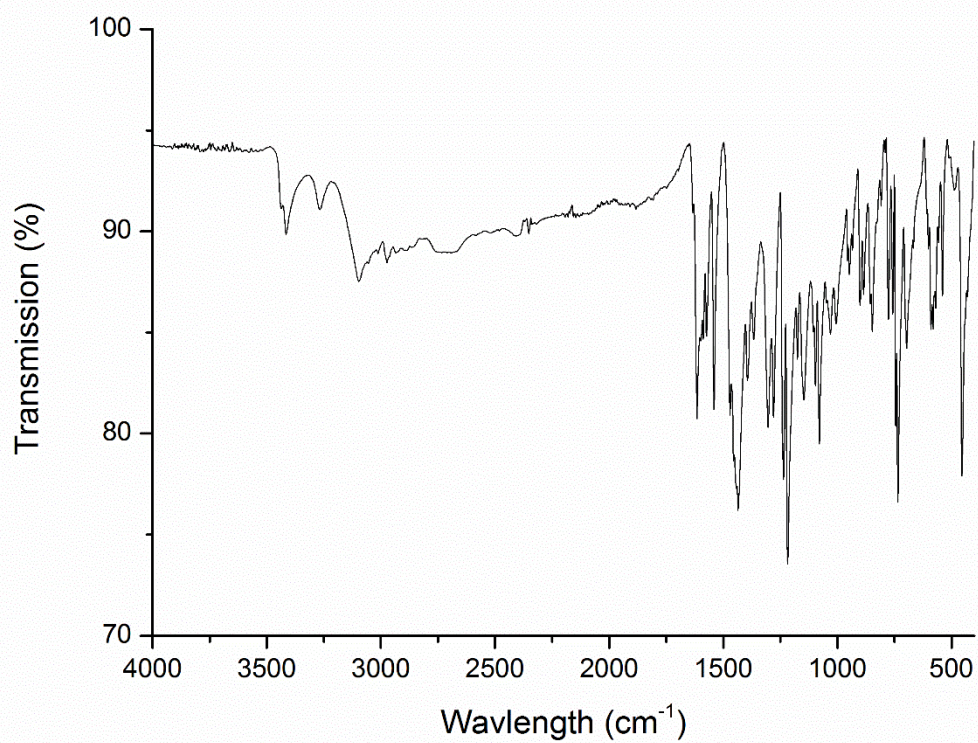
B7. Infrared spectrum of $\text{NH}_4[\text{Fe}(\text{5-Br-thsa})_2]$



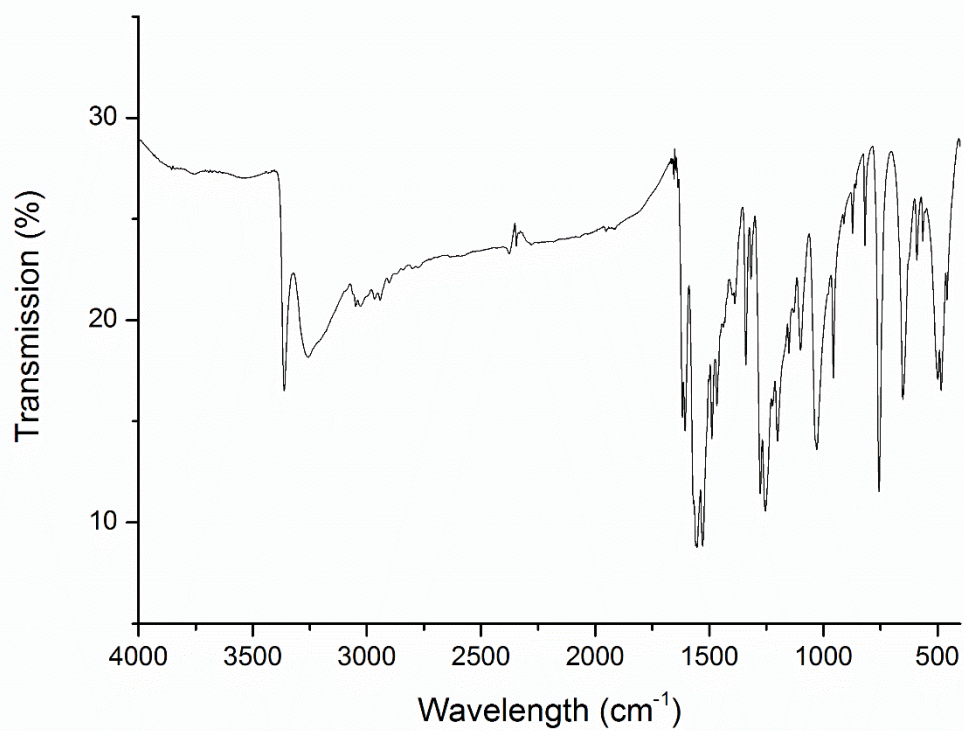
B8. Infrared spectrum of 3-ethoxysalicylaldehyde thiosemicarbazone, $\text{H}_2\text{-3-OEt-thsa}$



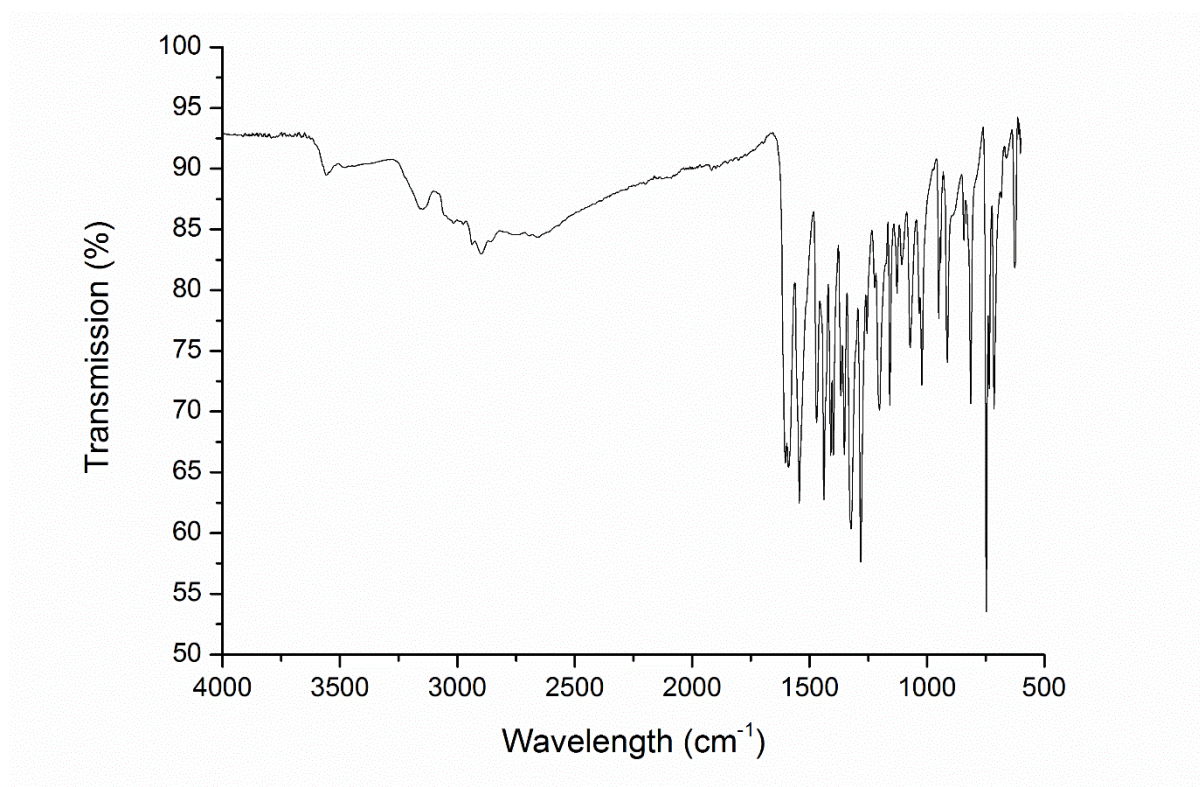
B9. Infrared spectrum of $(\text{CH}_3)_2\text{NH}_2[\text{Fe}(\text{3-OEt-thsa})_2]$



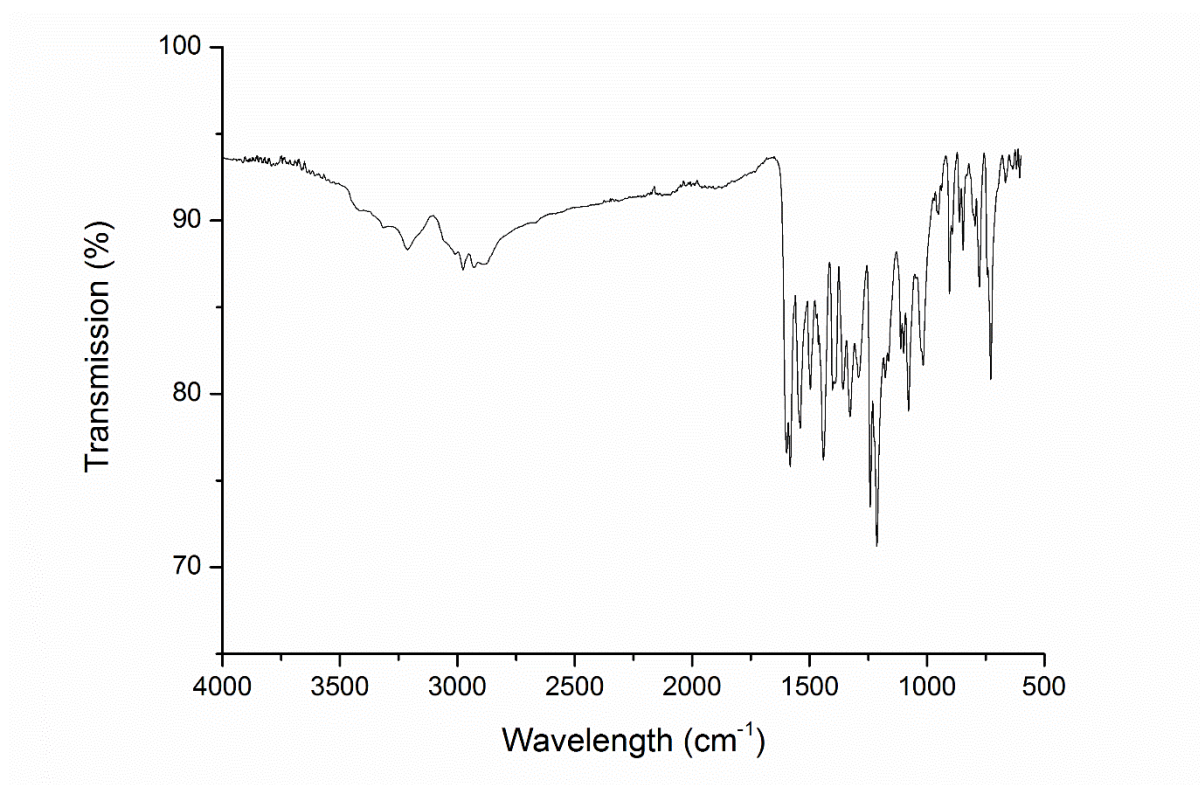
B10. Infrared spectrum of salicylaldehyde 4-methylthiosemicarbazone, $\text{H}_2\text{-thsa-Me}$



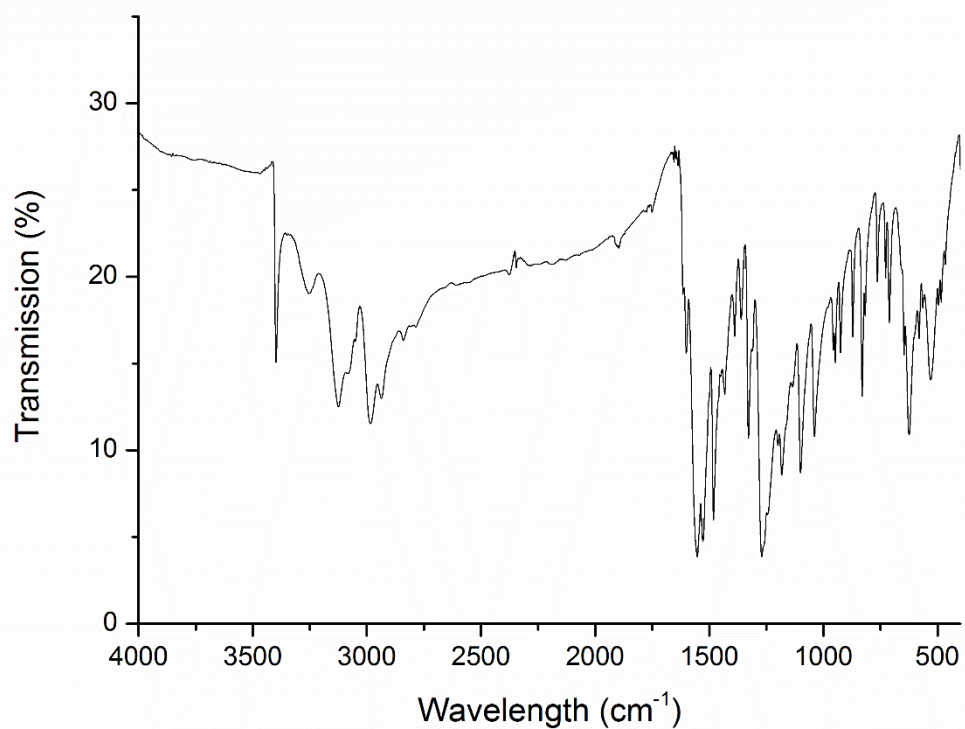
B11. Infrared spectrum of $[\text{Fe}(\text{H-thsa-Me})(\text{thsa-Me})]\cdot\text{H}_2\text{O}$



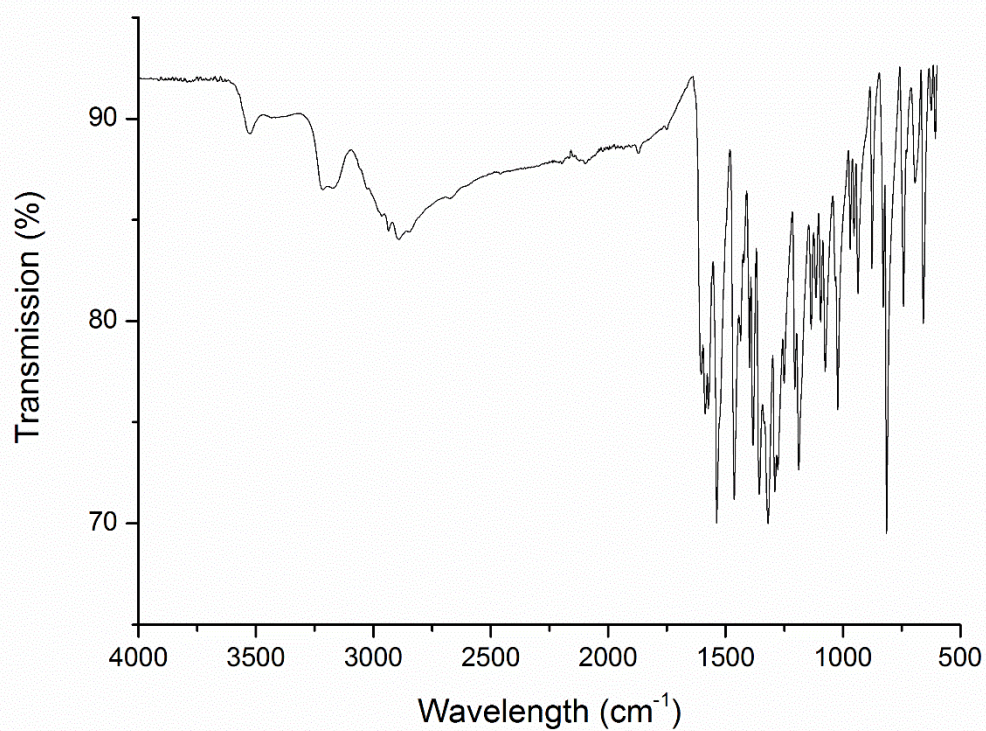
B12. Infrared spectrum of $[\text{Fe}(\text{H-3-OEt-thsa-Me})(3\text{-OEt-thsa-Me})]\cdot\text{H}_2\text{O}$



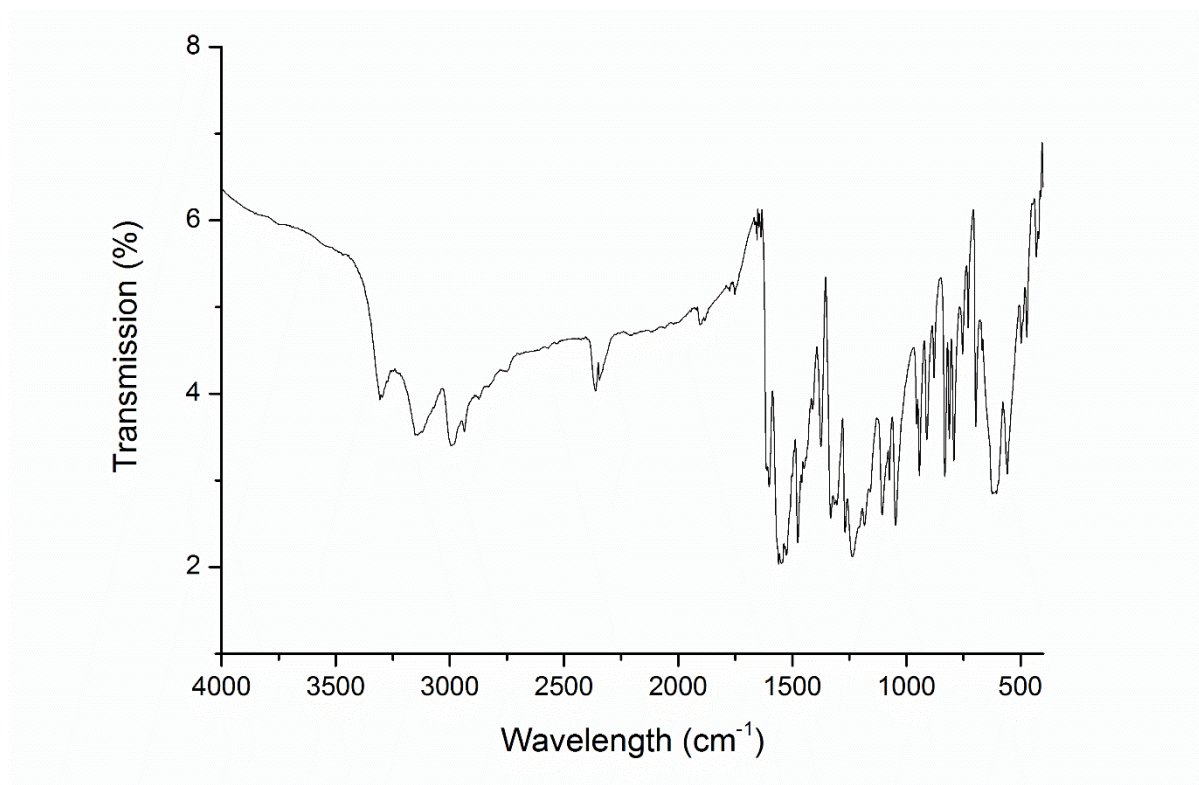
B13. Infrared spectrum of 5-chlorosalicylaldehyde 4-methylthiosemicarbazone, H₂-5-Cl-thsa-Me



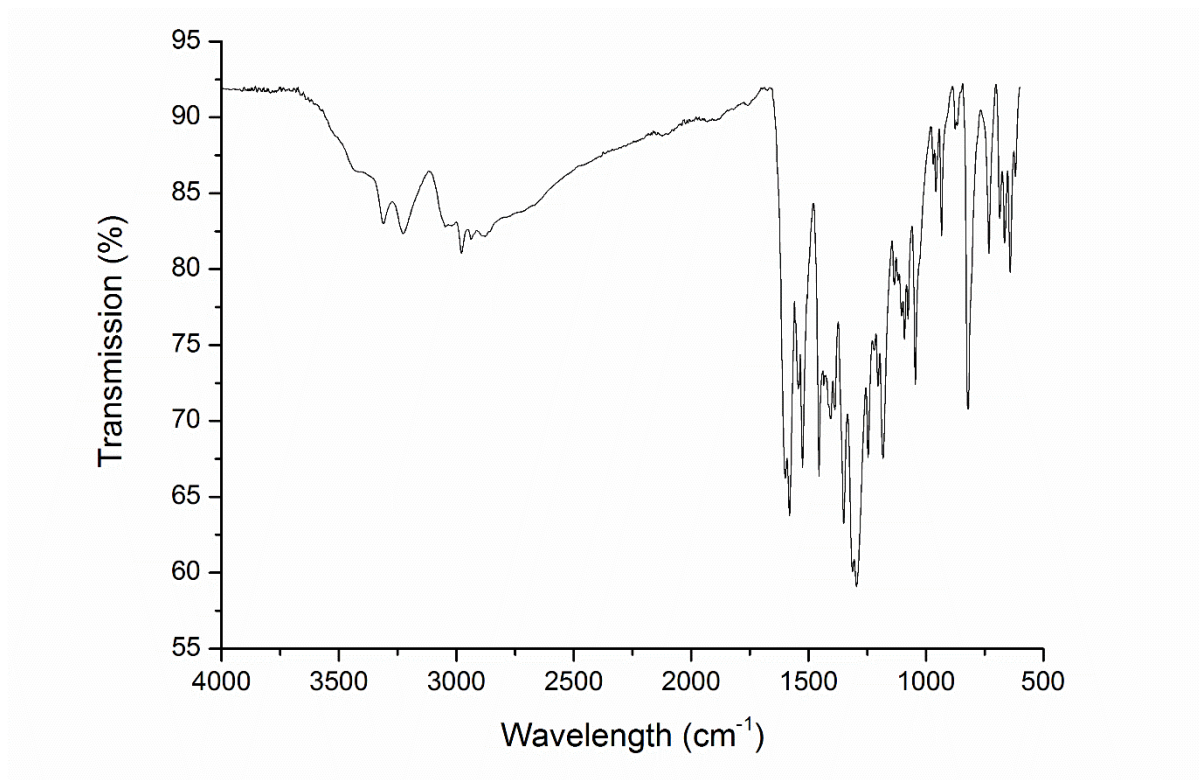
B14. Infrared spectrum of [Fe(H-5-Cl-thsa-Me)(5-Cl-thsa-Me)]·H₂O



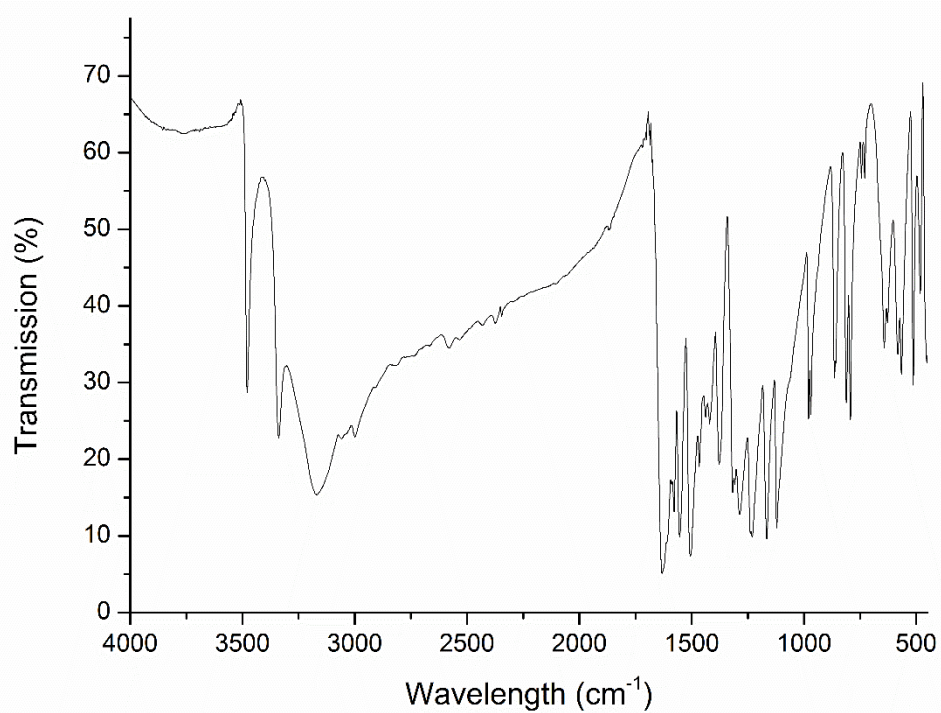
B15. Infrared spectrum of 5-bromosalicylaldehyde 4-ethylthiosemicarbazone, H₂-5-Br-thsa-Et



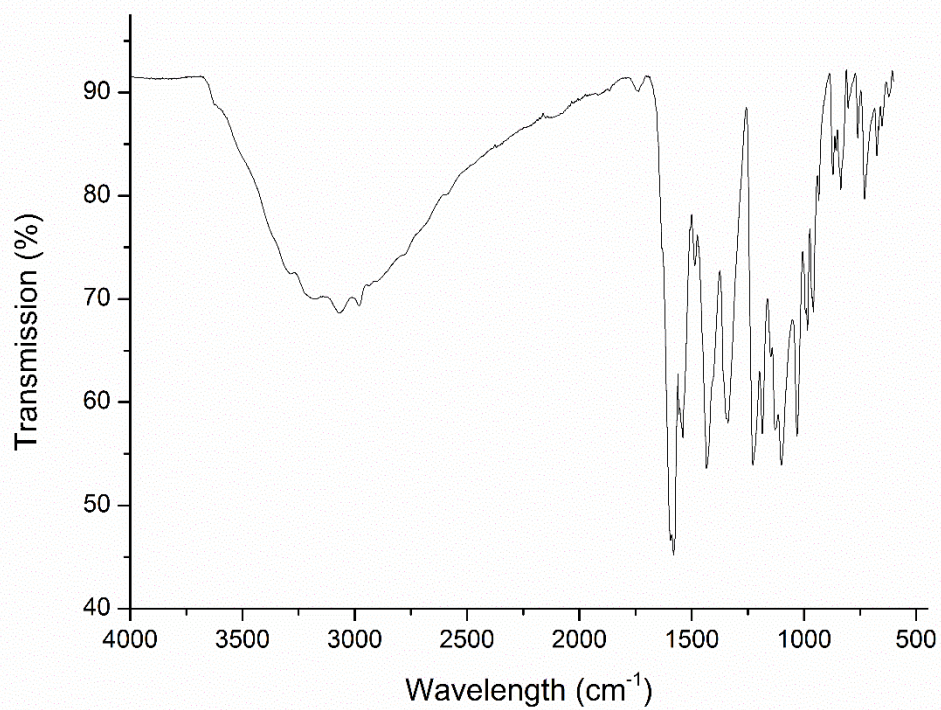
B16. Infrared spectrum of [Fe(H-5-Br-thsa-Et)₂](NO₃)·H₂O



B17. Infrared spectrum of 2,4-dihydroxybenzaldehyde thiosemicarbazone, H₂-4-OH-thsa



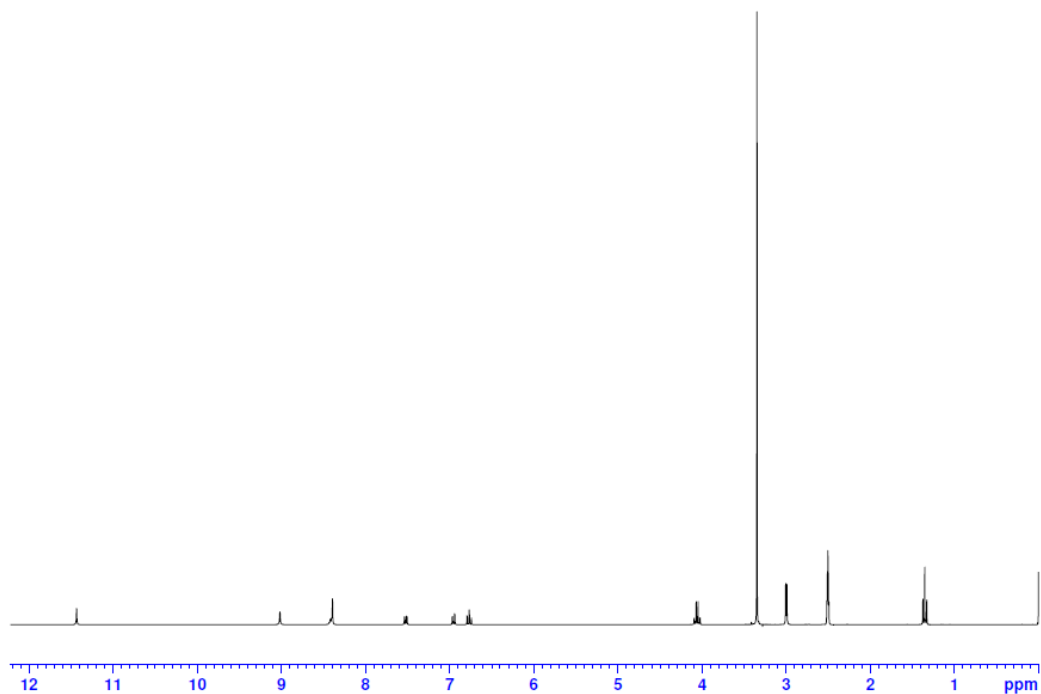
B18. Infrared spectrum of [Fe(H-4-OH-thsa)₂]₄·(SO₄)₂·H₂O



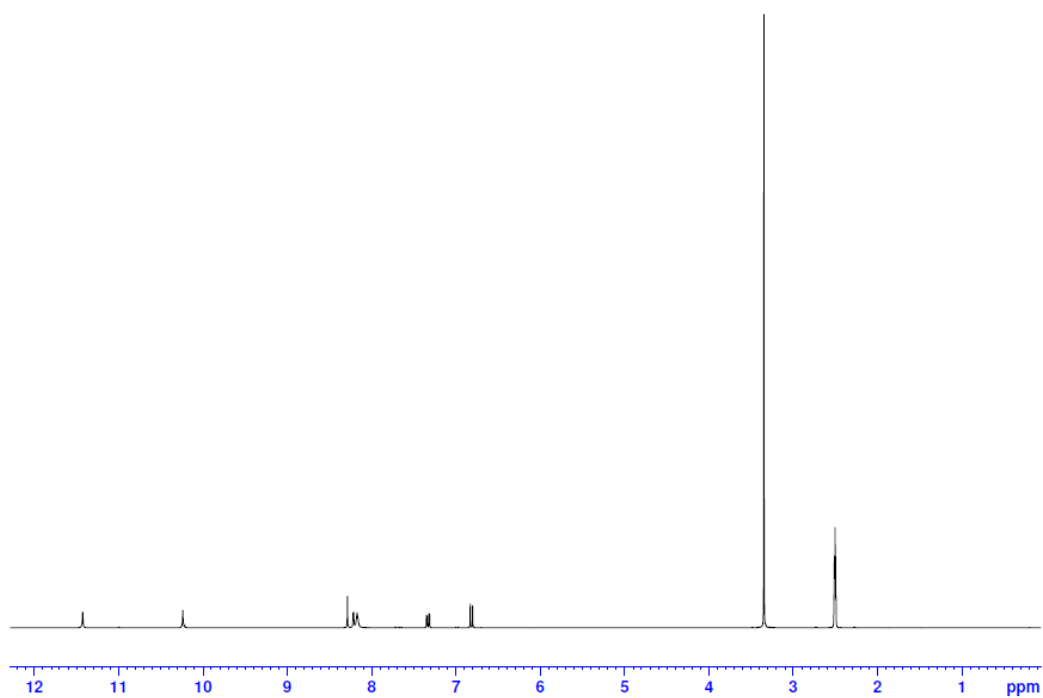
Appendix C.

^1H NMR Spectra of R-salicylaldehyde 4R'-thiosemicarbazone ligands in DMSO-d_6

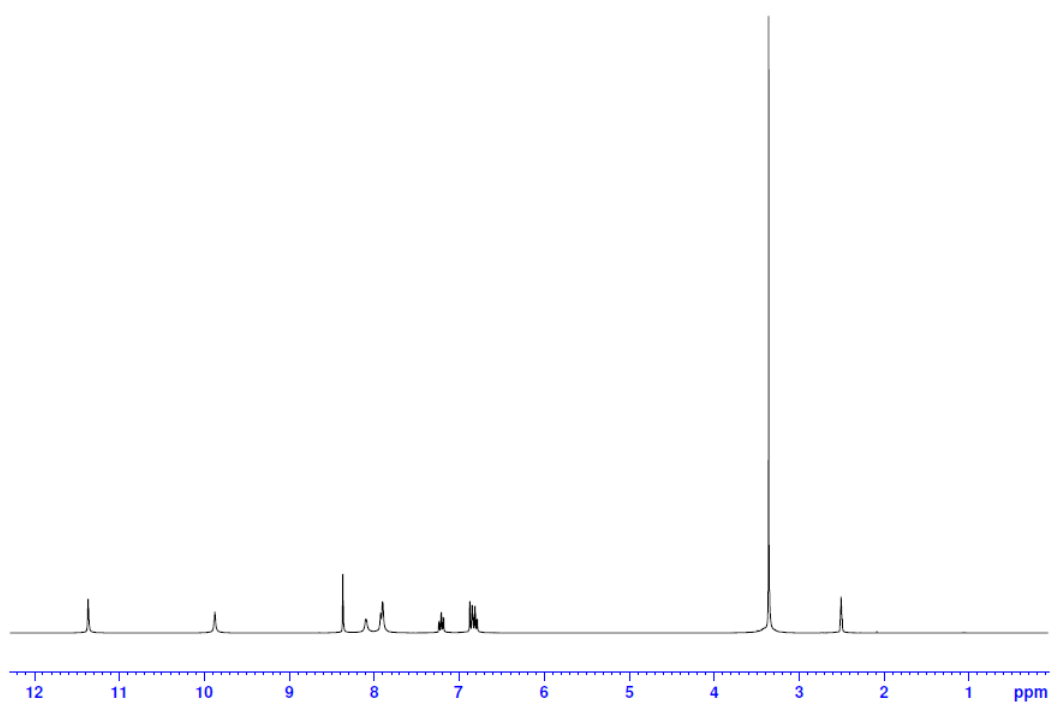
C1. ^1H NMR spectrum of 3-ethoxysalicylaldehyde 4-methylthiosemicarbazone, $\text{H}_2\text{-3-OEt-thsa-Me}$



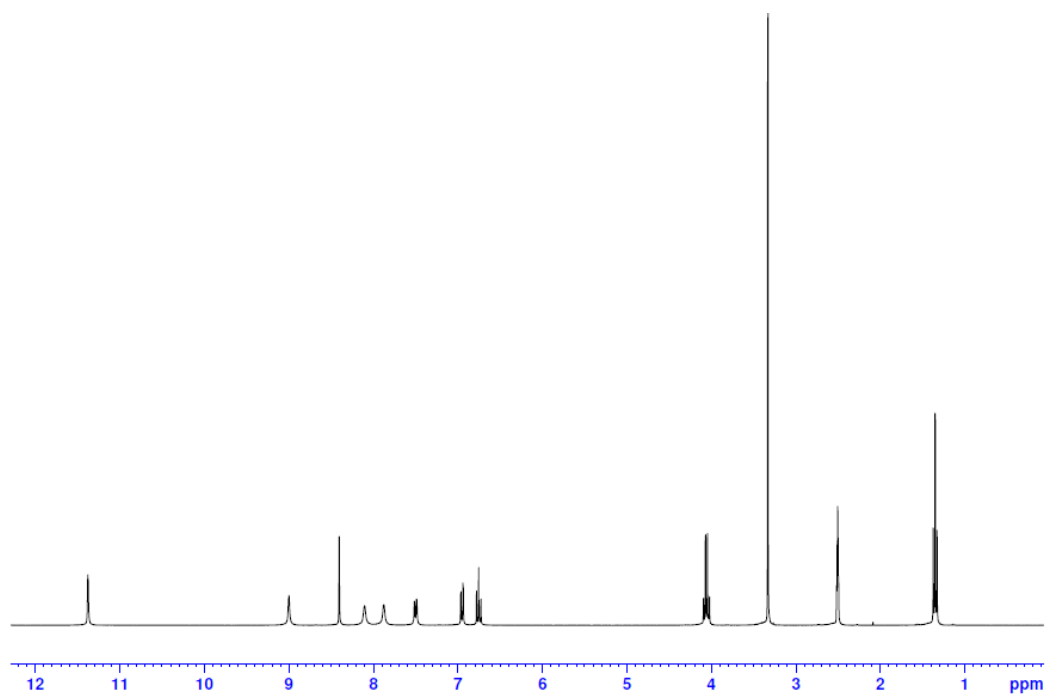
C2. ^1H NMR spectrum of 5-bromosalicylaldehyde thiosemicarbazone, $\text{H}_2\text{-5-Br-thsa}$



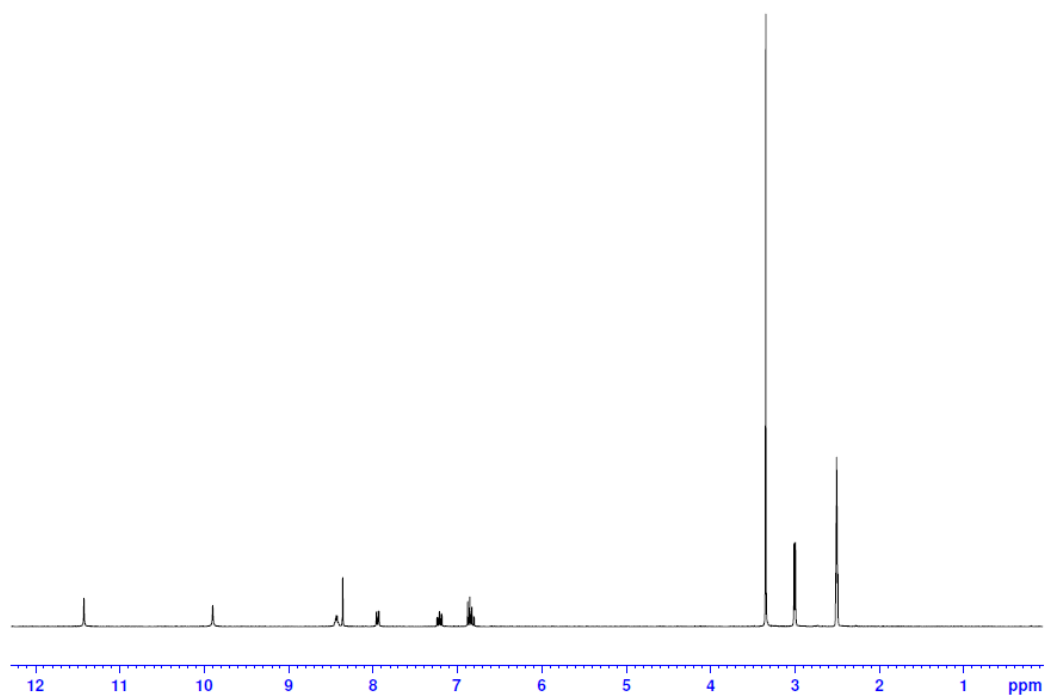
C3. ^1H NMR spectrum of salicylaldehyde thiosemicarbazone, $\text{H}_2\text{-thsa}$



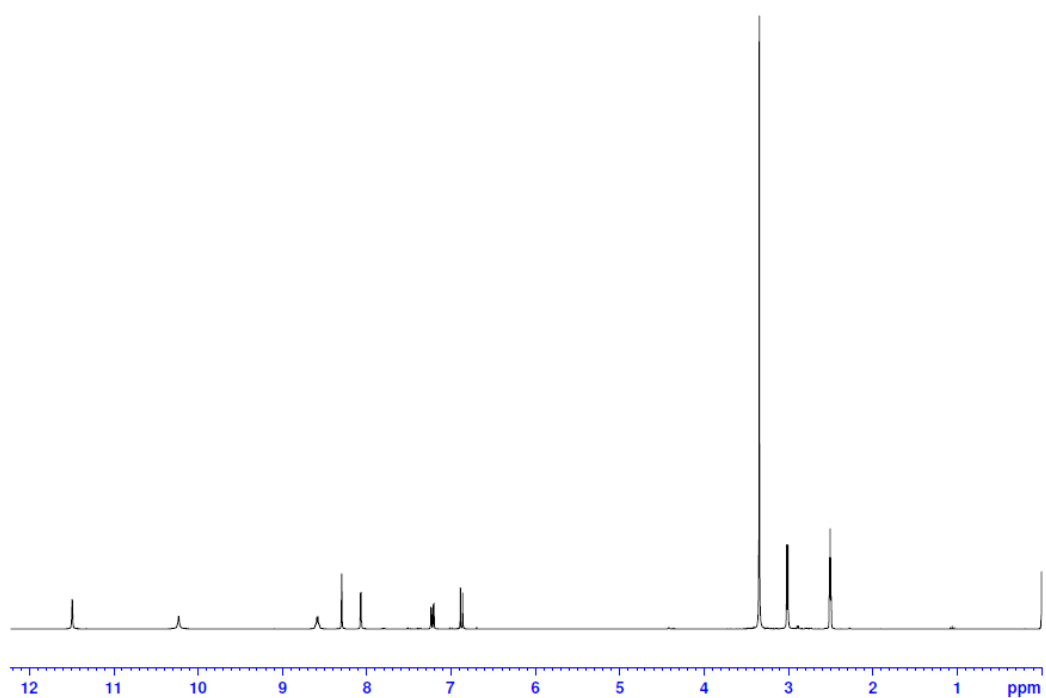
C4. ^1H NMR spectrum of 3-ethoxysalicylaldehyde thiosemicarbazone, $\text{H}_2\text{-3-OEt-thsa}$



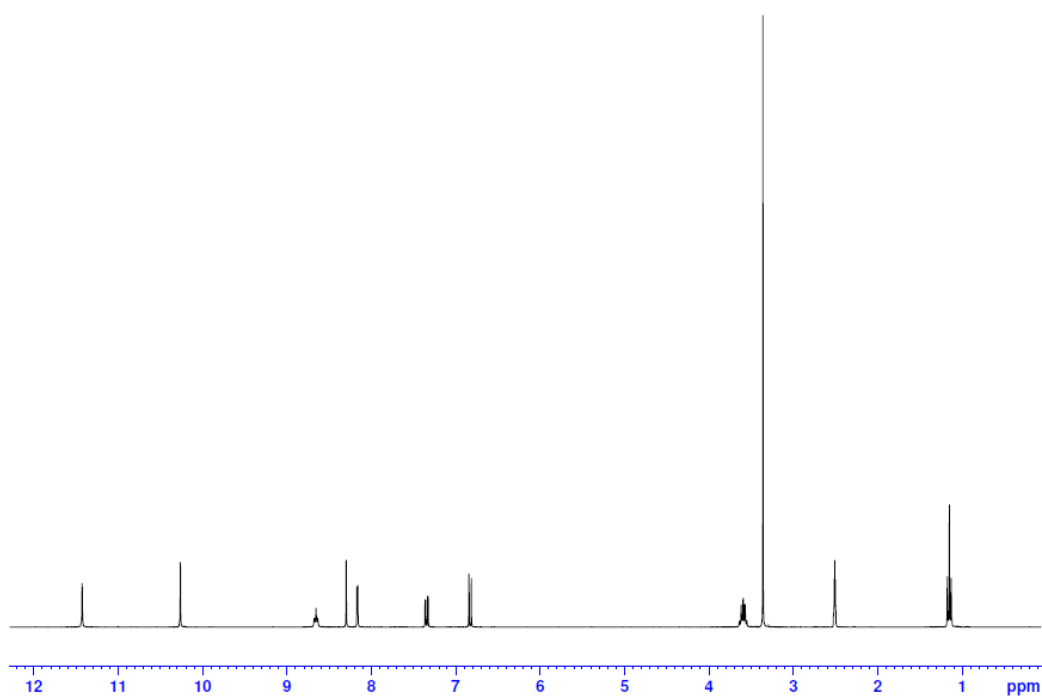
C5. ^1H NMR spectrum of salicylaldehyde 4-methylthiosemicarbazone, $\text{H}_2\text{-tHsa-Me}$



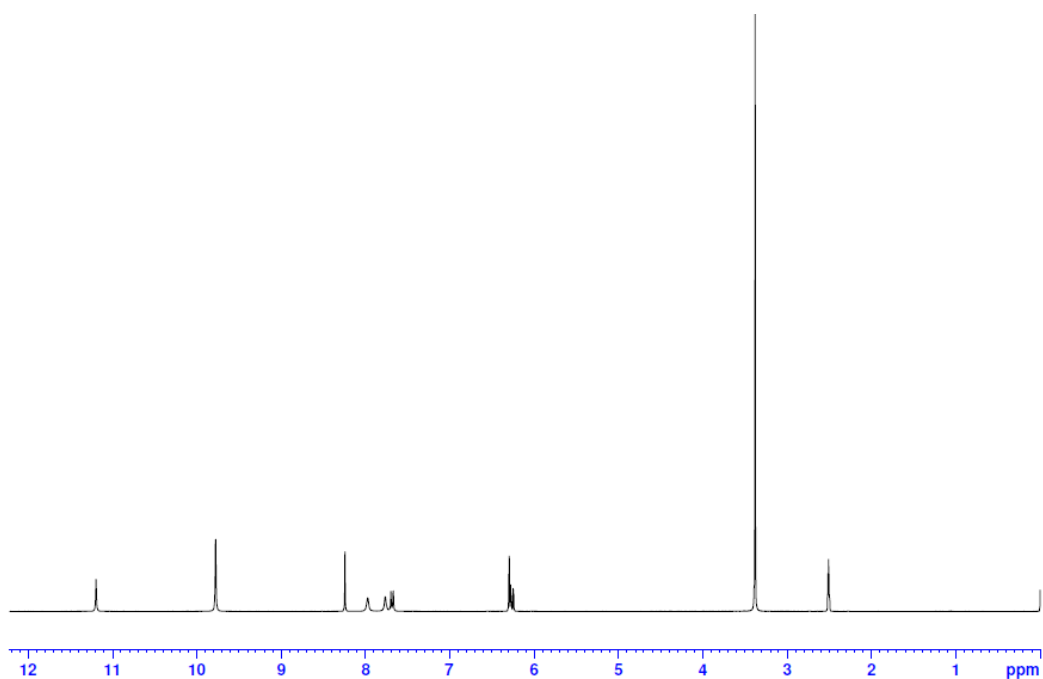
C6. ^1H NMR spectrum of 5-chlorosalicylaldehyde 4-methylthiosemicarbazone, $\text{H}_2\text{-5-Cl-tHsa-Me}$



C7. ^1H NMR spectrum of 5-bromosalicylaldehyde 4-ethylthiosemicarbazone, $\text{H}_2\text{-5-Br-thsa-Et}$



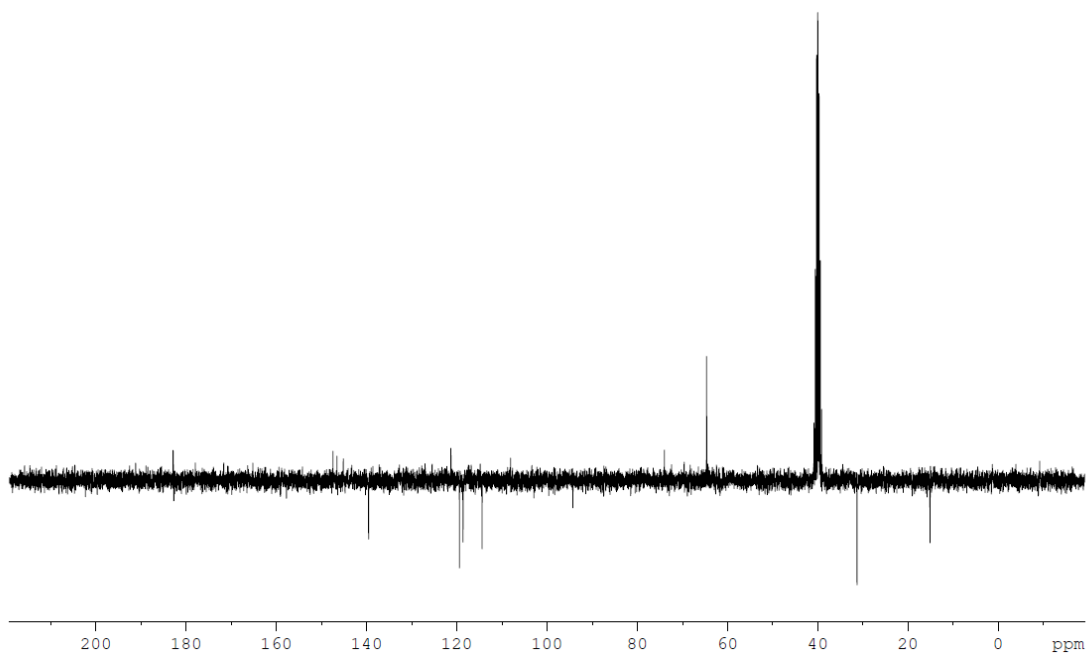
C8. ^1H NMR spectrum of 2,4-dihydroxybenzaldehyde thiosemicarbazone, $\text{H}_2\text{-4-OH-thsa}$



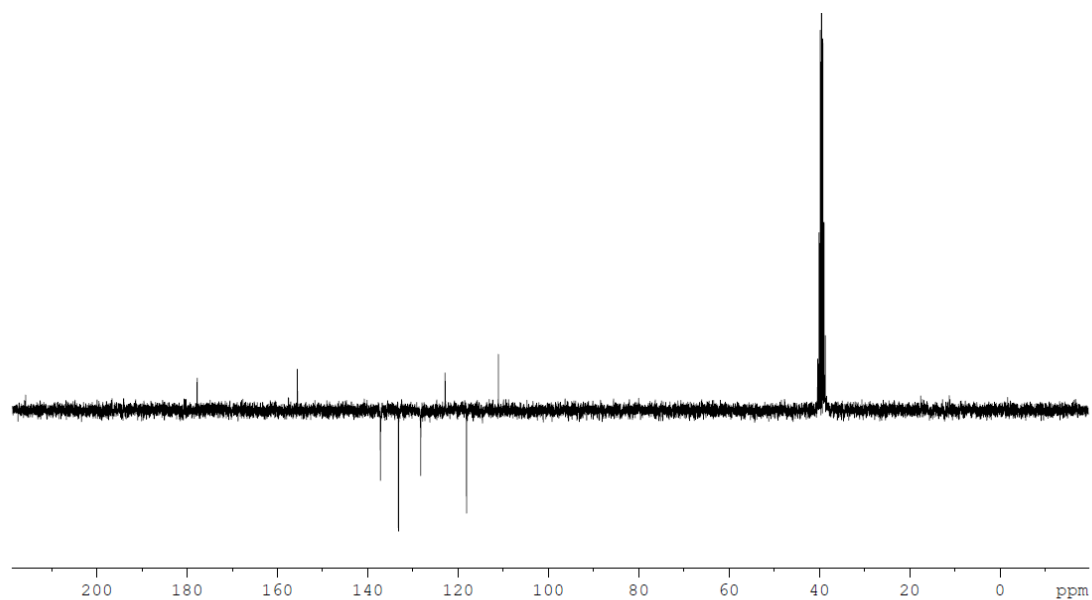
Appendix D.

^{13}C NMR Spectra of R-salicylaldehyde 4R'-thiosemicarbazone ligands in DMSO- d_6

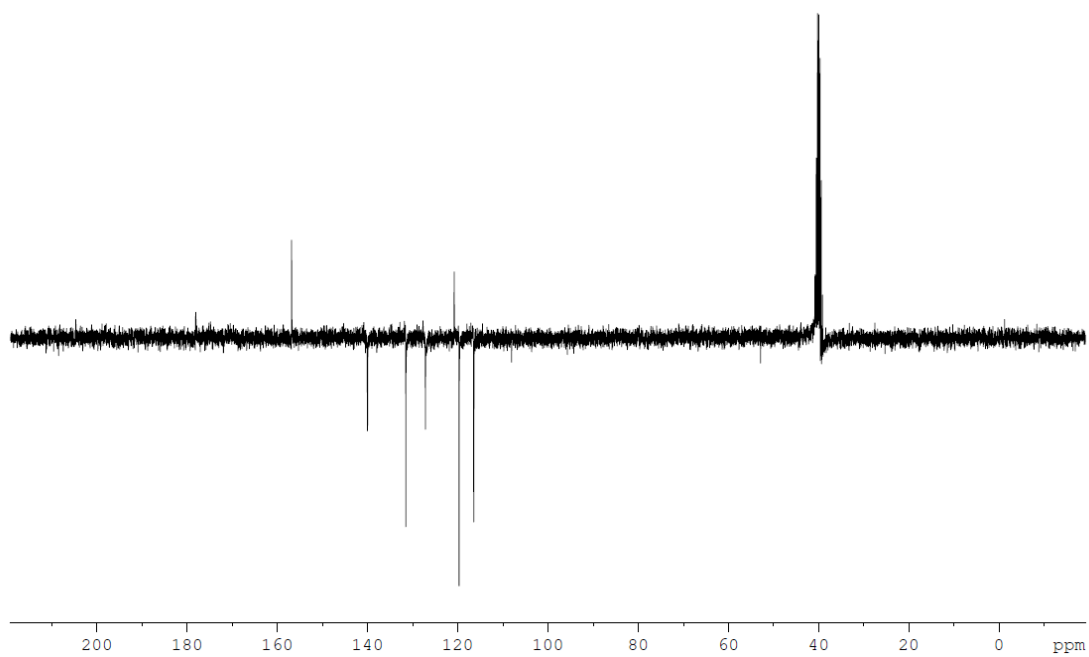
D1. ^{13}C NMR spectrum of 3-ethoxysalicylaldehyde 4-methylthiosemicarbazone, H₂-3-OEt-thsa-Me



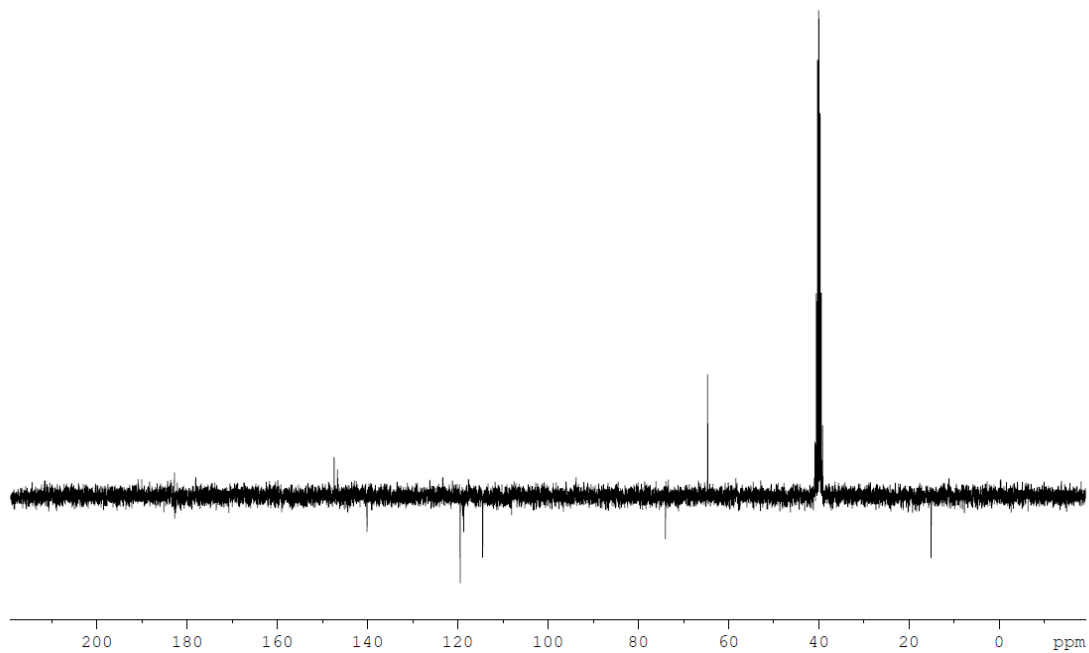
D2. ^{13}C NMR spectrum of 5-bromosalicylaldehyde thiosemicarbazone, H₂-5-Br-thsa



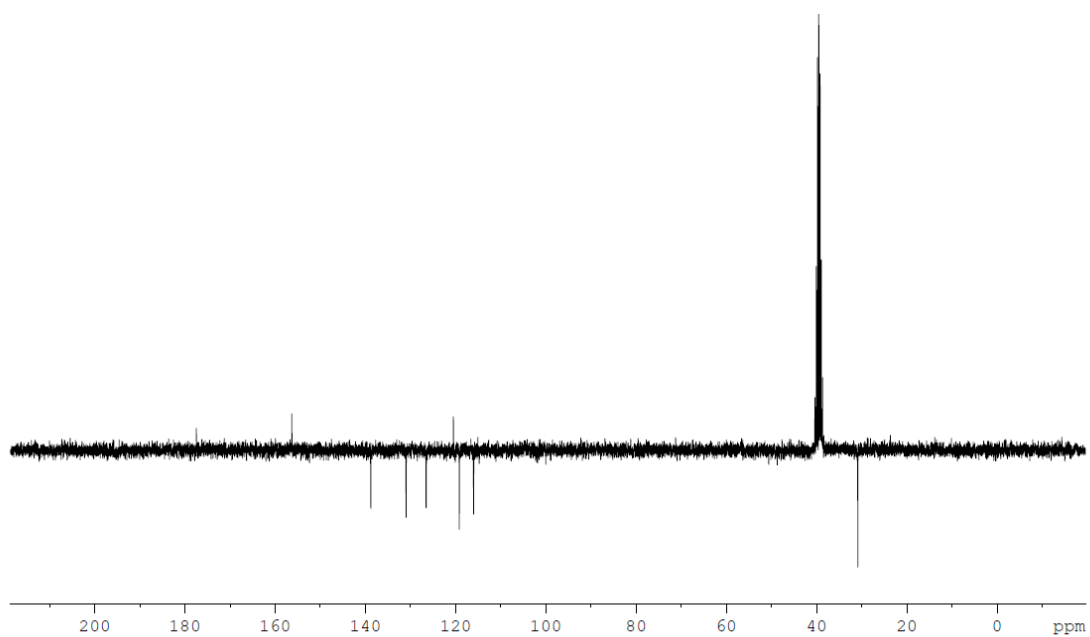
D3. ^{13}C NMR spectrum of salicylaldehyde thiosemicarbazone, $\text{H}_2\text{-thsa}$



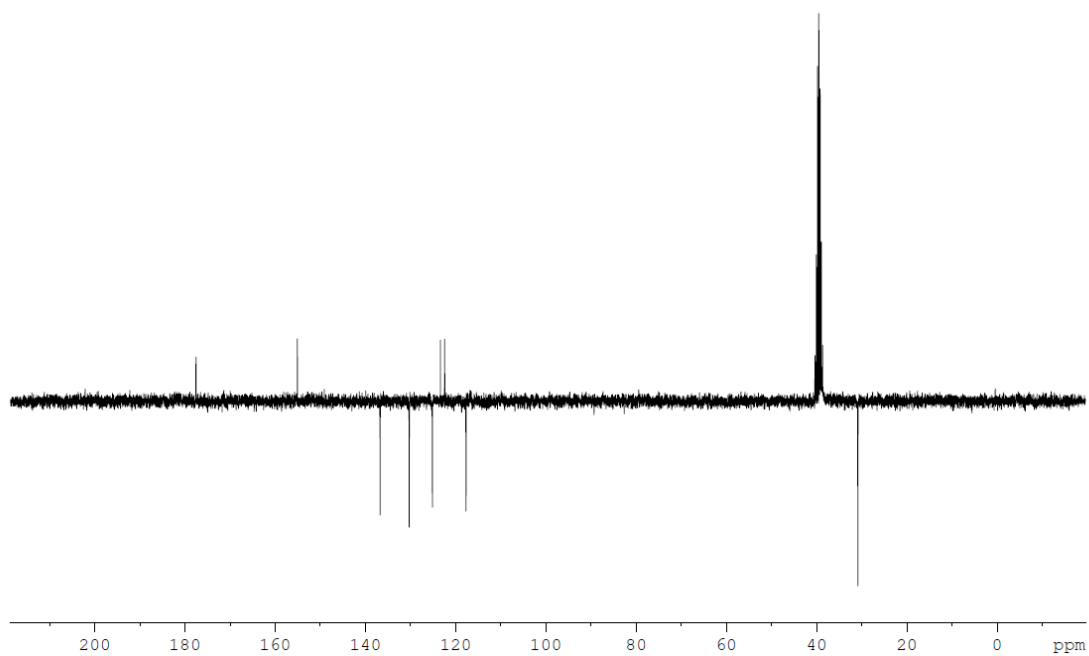
D4. ^{13}C NMR spectrum of 3-ethoxysalicylaldehyde thiosemicarbazone, $\text{H}_2\text{-3-OEt-thsa}$



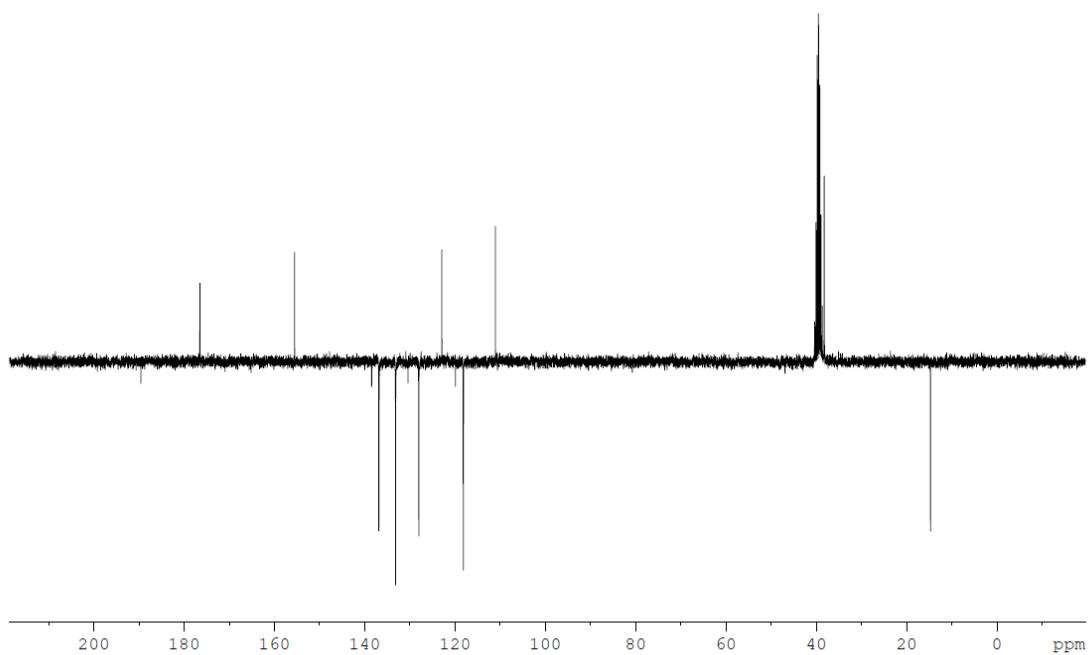
D5. ^{13}C NMR spectrum of salicylaldehyde 4-methylthiosemicarbazone, H₂-thsa-Me



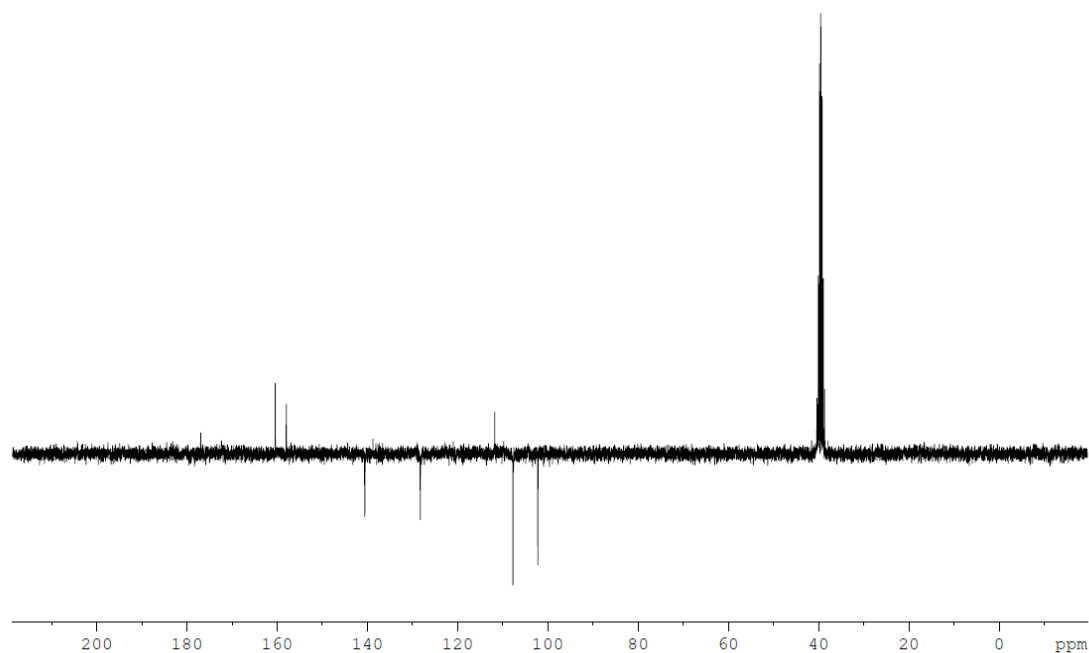
D6. ^{13}C NMR spectrum of 5-chlorosalicylaldehyde 4-methylthiosemicarbazone, H₂-5-Cl-thsa-Me



D7. ^{13}C NMR spectrum of 5-bromosalicylaldehyde 4-ethylthiosemicarbazone, $\text{H}_2\text{-5-Br-thsa-Et}$



D8. ^{13}C NMR spectrum of 2,4-dihydroxybenzaldehyde thiosemicarbazone, $\text{H}_2\text{-4-OH-thsa}$

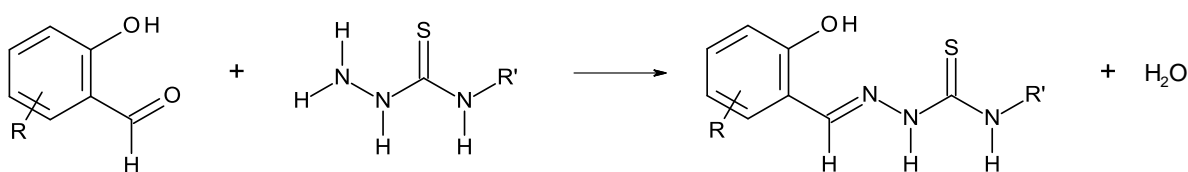


Appendix E.

Synthesis of R-salicylaldehyde 4R'-thiosemicarbazone and Fe^{III} compounds not presented in the thesis

E1. Synthesis of R-salicylaldehyde 4R'-thiosemicarbazone (H₂L) based ligands

The preparation of the desired R-salicylaldehyde 4R'-thiosemicarbazone ligands incorporated the synthesis between thiosemicarbazide and an R-substituted salicylaldehyde in ethanolic solution. The general reaction scheme is illustrated in Scheme E1.1.



Scheme E1.1

49 mmol of R-substituted salicylaldehyde was dissolved in 80 mL of ethanol with constant stirring, and was added to 49 mmol of the 4R'-thiosemicarbazide dissolved in 40 mL of ethanol. The corresponding mixture was refluxed for 120 minutes. The resulting solution was cooled to room temperature, the solid isolated by filtration, washed with ether and dried in a vacuum for two days.

E1.1 List of Ligands

Salicylaldehyde thiosemicarbazone, H₂-thsa (Data reported in Chapter II, Section 2.3)

5-Bromosalicylaldehyde thiosemicarbazone, H₂-5-Br-thsa (Data reported in Chapter II, Section 2.3)

3-Ethoxysalicylaldehyde thiosemicarbazone, H₂-3-OEt-thsa (Data reported in Chapter II, Section 2.3)

2,4-Dihydroxybenzaldehyde thiosemicarbazone, H₂-4-OH-thsa (Data reported in Chapter II, Section 2.3)

2-Hydroxy-5-methoxybenzaldehyde thiosemicarbazone, H₂-5-OMe-thsa Yield: 2.94 g (13.05 mmol, 79.9%). IR (cm⁻¹, KBr): 3413.63 (νOH), 3122.52 (νNH), 3309.05 (νNH₂), 1626.69 (νC=N), 1580.46–1602.41 (νC=C), 1267.19 (νC–N), 1112.29 (νC=S), 2835.58 (νCH₃). ¹H NMR (300 MHz, DMSO-d₆) δ (ppm): 11.38 (1H, s, OH), 9.47 (1H, s, S=C–NH), 8.34 (1H, s, N=C–H), 8.03–8.15 (2H, m, S=C–NH₂), 6.76–7.49 (aromatic 3H, m, C–H), 3.72 (3H, s, C–H₃).

2-Hydroxy-4-methoxybenzaldehyde thiosemicarbazone, H₂-4-OMe-thsa Yield: 4.78 g (21.22 mmol, 86.6%). IR (cm⁻¹, KBr): 3471.72 (νOH), 3152.99 (νNH), 3361.18 (νNH₂), 1631.09 (νC=N), 1546.92–1611.33 (νC=C), 1273.68 (νC–N), 1164.12 (νC=S), 2833.97 (νCH₃). ¹H NMR (300 MHz, DMSO-d₆) δ (ppm): 11.25 (1H, s, OH), 9.95 (1H, s, S=C–NH), 8.27 (1H, s, N=C–H), 7.80–8.04 (2H, m, S=C–NH₂), 6.40–6.45 (aromatic 3H, m, C–H), 3.73 (3H, s, C–H₃).

5-Chlorosalicylaldehyde thiosemicarbazone, H₂-5-Cl-thsa Yield: 10.20 g (44.41 mmol, 90.6%). IR (cm⁻¹, KBr): 3404.08 (νOH), 3165.92 (νNH), 3237.35 (νNH₂), 1611.73 (νC=N), 1598.37, 1542.13 (νC=C), 1264.20 (νC–N), 1188.90 (νC=S). ¹H NMR (300 MHz, DMSO-d₆) δ (ppm): 11.42 (1H, s, OH), 10.23 (1H, s, S=C–NH), 8.29 (1H, s, N=C–H), 8.10–8.17 (2H, m, C–NH₂), 6.85–7.24 (aromatic 3H, m, C–H).

Salicylaldehyde 4-methylthiosemicarbazone, H₂-thsa-Me (Data reported in Chapter II, Section 2.3)

5-Bromosalicylaldehyde 4-methylthiosemicarbazone, H₂-5-Br-thsa-Me Yield: 11.37 g (39.46 mmol, 80.5%). IR (cm⁻¹, KBr): 3455.54 (νOH), 3248.86, 3161.64 (νNH), 2997.51 (νCH₃), 1610.40 (νC=N), 1601.43, 1545.49 (νC=C), 1263.71 (νC–N), 1190.95 (νC=S). ¹H NMR (300 MHz, DMSO-d₆) δ (ppm): 11.42 (1H, s, OH), 10.25 (1H, s, S=C–NH), 8.65 (1H, s, N=CH), 8.15–8.30 (1H, m, S=C–NH(CH₃)), 6.82–7.35 (aromatic 3H, m, C–H), 4.50 (3H, d, NH(CH₃)).

3-Ethoxysalicylaldehyde 4-methylthiosemicarbazone, H₂-3-OEt-thsa-Me (Data reported in Chapter II, Section 2.3)

2,4-Dihydroxybenzaldehyde 4-methylthiosemicarbazone, H₂-4-OH-thsa-Me Yield: 8.19 g (36.36 mmol, 74.2%). IR (cm⁻¹, KBr): 3381.61 (νOH), 3276.27 (νNH), 2976.05 (νCH₃), 1631.14 (νC=N), 1580.94, 1546.91 (νC=C), 1256.89 (νC–N), 1127.84 (νC=S). ¹H NMR (300 MHz, DMSO-d₆) δ (ppm): 11.20 (1H, s, OH), 9.70 (1H, s, S=C–NH), 8.22 (1H, s, N=CH), 6.24–7.68 (aromatic 3H, m, C–H), 3.02 (3H, d, NH(CH₃)).

5-Chlorosalicylaldehyde 4-methylthiosemicarbazone, H₂-5-Cl-thsa-Me (Data reported in Chapter II, Section 2.3)

Salicylaldehyde 4-ethylthiosemicarbazone, H₂-thsa-Et Yield: 10.27 g (45.99 mmol, 93.9%). IR (cm⁻¹, KBr): 3355.41 (νOH), 3251.74 (νNH), 2974.19 (νCH₃), 2870.50 (νCH₂), 1618.14 (νC=N), 1601.56, 1551.55 (νC=C), 1233.98 (νC–N), 1156.25 (νC=S). ¹H NMR (300 MHz, DMSO-d₆) δ (ppm): 11.42 (1H, s, OH), 10.28 (1H, s, S=C–NH), 8.32 (1H, m, N=CH), 8.66 (1H, t, S=C–NH(CH₂CH₃)), 6.80–7.38 (aromatic 3H, m, C–H), 3.60 (2H, p, NH–CH₂), 1.15 (3H t, NHCH₂–CH₃).

5-Bromosalicylaldehyde 4-ethylthiosemicarbazone, H₂-5-Br-thsa-Et (Data reported in Chapter II, Section 2.3)

3-Ethoxysalicylaldehyde 4-ethylthiosemicarbazone, H₂-3-OEt-thsa-Et (Data reported in Chapter II, Section 2.3)

2,4-Dihydroxybenzaldehyde 4-ethylthiosemicarbazone, H₂-4-OH-thsa-Et Yield: 5.75 g (24.03 mmol, 98.1%). IR (cm⁻¹, KBr): 3410.70, 3400.98 (νOH), 3140.10 (νNH), 2976.79 (νCH₃), 2888.27 (νCH₂), 1637.77 (νC=N), 1612.22, 1542.04 (νC=C ring), 1246.05 (νC-N), 1157.02 (νC=S). ¹H NMR (300 MHz, DMSO-d₆) δ (ppm): 11.16 (1H, s, S=C-NH), 9.78–9.75 (2H, s, OH), 8.24 (1H, s, N=C-H), 8.33–8.29 (1H, t, S=C-NH), 6.30–7.72 (aromatic 3H, m, C-H), 3.56 (2H, m, C-H₂), 1.12 (3H, t, C-H₃).

5-Chlorosalicylaldehyde 4-ethylthiosemicarbazone, H₂-5-Cl-thsa-Et Yield: 5.00 g (19.39 mmol, 79.2%). IR (cm⁻¹, KBr): 3228.01 (νOH), 3301.00 (νNH), 2990.00 (νCH₃), 2936.00 (νCH₂), 1602.10 (νC=N), 1537.90 (νC=C), 1236.21 (νC-N), 1269.80 (νC=S). ¹H NMR (300 MHz, DMSO-d₆) δ (ppm): 11.38 (1H, s, OH), 10.33 (1H, s, S=C-NH), 8.15–8.32 (1H, m, N=CH), 8.66 (1H, t, S=C-NH(CH₂CH₃)), 6.85–7.24 (aromatic 3H, m, C-H), 3.61 (2H, m, NH-CH₂), 1.15 (3H t, NHCH₂-CH₃).

Salicylaldehyde 4-phenylthiosemicarbazone, H₂-thsa-Ph Yield: 12.21 g (45.00 mmol, 91.80%). IR (cm⁻¹, KBr): 3148.64 (νOH), 2990.54 (νNH), 1620.46 (νC=N), 1604.68, 1592.78, 1571.96, 1540.53 (νC=C), 1271.56 (νC-N), 1150.80 (νC=S). ¹H NMR (300 MHz, DMSO-d₆) δ (ppm): 11.80 (1H, s, OH), 10.04 (1H, s, S=C-NH), 8.48 (1H, s, N=CH), 10.19 (1H, t, S=C-NH(C₆H₅)), 6.83–8.04 (aromatic 9H, m, C-H).

5-Bromosalicylaldehyde 4-phenylthiosemicarbazone, H₂-5-Br-thsa-Ph Yield: 16.51 g (47.14 mmol, 96.2%). IR (cm⁻¹, KBr): 3445.60 (νOH), 3256.00 (νNH), 1618.5 (νC=N), 1605.92, 1581.09, 1554.21, 1546.90 (νC=C), 1221.49 (νC-N), 1117.00 (νC=S). ¹H NMR (300 MHz, DMSO-d₆) δ (ppm): 11.85 (1H, s, OH), 10.10 (1H, s, S=C-NH), 8.30 (1H, s, N=CH), 8.40 (1H, t, S=C-NH(C₆H₅)), 6.80–7.60 (aromatic 9H, m, C-H).

3-Ethoxysalicylaldehyde 4-phenylthiosemicarbazone, H₂-3-OEt-thsa-Ph Yield: 7.22 g (22.89 mmol, 93.4%). IR (cm⁻¹, KBr): 3301.18 (νOH), 3061.43 (νNH), 1615.82 (νC=N), 1595.59, 1581.43, 1551.59, 1519.67 (νC=C), 1281.41 (νC-N), 1192.04 (νC=S). ¹H NMR (300 MHz, DMSO-d₆) δ (ppm): 9.10 (1H, s, OH), 11.70 (1H, s, S=C-NH), 8.50 (1H, s, N=CH), 10.00 (1H, s, S=C-NH(C₆H₅)), 6.80–7.60 (aromatic 9H, m, C-H), 4.10 (2H, q, CH₂), 3.25 (3H, t, CH₃).

2,4-Dihydroxybenzaldehyde 4-phenylthiosemicarbazone, H₂-4-OH-thsa-Ph Yield: 3.98 g (13.85 mmol, 84.8%). IR (cm⁻¹, KBr): 3200.00 (νOH), 3152.07 (νNH), 1629.18 (νC=N), 1555.00, 1550.00, 1546.56, 1514.05 (νC=C), 1211.91 (νC-N), 1126.20 (νC=S). ¹H NMR (300 MHz, DMSO-d₆) δ (ppm): 8.60 (1H, s, OH), 11.70 (1H, s, S=C-NH), 8.30 (1H, s, N=CH), 9.90 (1H, s, S=C-NH(C₆H₅)), 6.80–7.60 (aromatic 9H, m, C-H).

5-Chlorosalicylaldehyde 4-phenylthiosemicarbazone, H₂-5-Cl-thsa-Ph Yield: 4.97 g (16.25 mmol, 66.3%). IR (cm⁻¹, KBr): 3273.70 (νOH), 3142.90 (νNH), 1600.00 (νC=N), 1590.00, 1581.50, 1550.40, 1525.25 (νC=C), 1266.20 (νC-N), 1085.70 (νC=S). ¹H NMR (300 MHz, DMSO-d₆) δ (ppm): 11.90 (1H, s, OH), 10.20 (1H, s, S=C-NH), 8.50 (1H, s, N=CH), 8.35 (1H, s, S=C-NH(C₆H₅)), 6.80-7.60 (aromatic 9H, m, C-H).

E2 Attempted syntheses of Fe^{III} compounds containing the ligand system: R-salicylaldehyde 4R'-thiosemicarbazone (H₂-R-thsa-R')

Various Fe^{III} compounds were synthesised throughout the preparation of this work, the details of the synthesis are displayed in Table E2.1, Table E2.1 includes the quantities of Fe^{III} salt, H₂L ligand, solvent and cation/anion used in the synthesis, and the state the compound is in, *i.e.* powder or crystalline.

Table E2.1 Quantities used in the synthesis of Fe^{III} complexes with R-salicylaldehyde 4R'-thiosemicarbazone (H₂-R-thsa-R') ligands.

Experimental code for Fe ^{III} Complex synthesis	T (°C)	Solvent (mL)	H ₂ -R-thsa-R' Ligand (g, mmol)	Cation (g, mmol)	Fe ^{III} (salt) (g, mmol)	Product Yield %	State of material
RP1:63:1	80	MeOH 35	H ₂ -3OEt-thsa 0.24, 1.0	CsOH 0.67, 4.0	FeCl ₃ ·6H ₂ O 0.27, 1.0	-	No result
RP1:63:2	80	MeOH 35	H ₂ -3OEt-thsa-Me 0.25, 1.0	CsOH 0.67, 4.0	FeCl ₃ ·6H ₂ O 0.27, 1.0	40.1	Crystalline
RP1:64:1	80	MeOH 35	H ₂ -3OEt-thsa-Et 0.28, 1.0	CsOH 0.67, 4.0	FeCl ₃ ·6H ₂ O 0.27, 1.0	-	No result
RP1:64:2	80	MeOH 35	H ₂ -3OEt-thsa-Ph 0.32, 1.0	CsOH 0.67, 4.0	FeCl ₃ ·6H ₂ O 0.27, 1.0	-	No result
RP1:65:1	80	MeOH 35	H ₂ -3OEt-thsa-Me 0.48, 2.0	CsOH 1.63, 8.0	FeCl ₃ ·6H ₂ O 0.54, 2.0	54.9	Crystalline
RP1:70:1	80	MeOH 30	H ₂ -3OEt-thsa 0.24, 1.0	CsOH 0.67, 4.0	Fe(CH ₃ C ₆ H ₄ SO ₃) ₃ ·6H ₂ O 0.68, 1.0	62.1	Powder
RP1:70:2	80	MeOH 35	H ₂ -3OEt-thsa-Me 0.25, 1.0	CsOH 0.67, 4.0	Fe(CH ₃ C ₆ H ₄ SO ₃) ₃ ·6H ₂ O 0.68, 1.0	34.5	Crystalline
RP1:71:1	80	MeOH 35	H ₂ -3OEt-thsa-Et 0.28, 1.0	CsOH 0.67, 4.0	Fe(CH ₃ C ₆ H ₄ SO ₃) ₃ ·6H ₂ O 0.68, 1.0	-	No result
RP1:71:2	80	MeOH 35	H ₂ -3OEt-thsa-Ph 0.32, 1.0	CsOH 0.67, 4.0	Fe(CH ₃ C ₆ H ₄ SO ₃) ₃ ·6H ₂ O 0.68, 1.0	44.6	Crystalline
RP1:72:1	80	MeOH 30	H ₂ -3OEt-thsa 0.24, 1.0	CsOH 0.67, 4.0	Fe(ClO ₄) ₃ ·6H ₂ O 0.35, 1.0	-	No result
RP1:72:2	80	MeOH 30	H ₂ -3OEt-thsa-Me 0.25, 1.0	CsOH 0.67, 4.0	Fe(ClO ₄) ₃ ·6H ₂ O 0.35, 1.0	-	No result
RP1:73:1	80	MeOH 30	H ₂ -3OEt-thsa-Et 0.28, 1.0	CsOH 0.67, 4.0	Fe(ClO ₄) ₃ ·6H ₂ O 0.35, 1.0	-	No result
RP1:73:2	80	MeOH 30	H ₂ -3OEt-thsa-Ph 0.32, 1.0	CsOH 0.67, 4.0	Fe(ClO ₄) ₃ ·6H ₂ O 0.35, 1.0	53.8	Crystalline

Table E2.1 Quantities used in the synthesis of Fe^{III} complexes with R-salicylaldehyde 4R'-thiosemicarbazone (H₂-R-thsa-R') ligands continued.

Experimental code for Fe ^{III} Complex synthesis	T (°C)	Solvent (mL)	H ₂ -R-thsa-R' Ligand (g, mmol)	Cation (g, mmol)	Fe ^{III} (salt) (g, mmol)	Product Yield %	State of material
RP1:74:1	80	MeOH 30	H ₂ -3OEt-thsa 0.24, 1.0	CsOH 0.67, 4.0	Fe(NO ₃) ₃ ·9H ₂ O 0.40, 1.0	76.7	Crystalline product + brown powder
RP1:74:2	80	MeOH 30	H ₂ -3OEt-thsa-Me 0.25, 1.0	CsOH 0.67, 4.0	Fe(NO ₃) ₃ ·9H ₂ O 0.40, 1.0	67.4	Crystalline product + brown powder
RP1:75:1	80	MeOH 30	H ₂ -3OEt-thsa-Et 0.28, 1.0	CsOH 0.67, 4.0	Fe(NO ₃) ₃ ·9H ₂ O 0.40, 1.0	56.9	Crystalline product + brown powder
RP1:75:2	80	MeOH 30	H ₂ -3OEt-thsa-Ph 0.32, 1.0	CsOH 0.67, 4.0	Fe(NO ₃) ₃ ·9H ₂ O 0.40, 1.0	67.0	Powder
RP1:76:1	80	MeOH 30	H ₂ -thsa 0.20, 1.0	NH ₄ OH 20 mL	Fe(CH ₃ C ₆ H ₄ SO ₃) ₃ ·6H ₂ O 0.68, 1.0	34.6	Crystalline
RP1:76:2	80	MeOH 30	H ₂ -3,5-Br-thsa 0.35, 1.0	NH ₄ OH 20 mL	Fe(CH ₃ C ₆ H ₄ SO ₃) ₃ ·6H ₂ O 0.68, 1.0	62.3	Powder
RP1:77:1	80	MeOH 30	H ₂ -5-Br-thsa 0.27, 1.0	NH ₄ OH 20 mL	Fe(CH ₃ C ₆ H ₄ SO ₃) ₃ ·6H ₂ O 0.68, 1.0	44.2	Crystalline product
RP1:77:2	80	MeOH 30	H ₂ -4-OH-thsa 0.21, 1.0	NH ₄ OH 20 mL	Fe(CH ₃ C ₆ H ₄ SO ₃) ₃ ·6H ₂ O 0.68, 1.0	55.2	Powder
RP1:78:1	80	MeOH 30	H ₂ -thsa 0.20, 1.0	NH ₄ OH 20 mL	FeCl ₃ ·6H ₂ O 0.27, 1.0	-	No result
RP1:78:2	80	MeOH 30	H ₂ -3,5-Br-thsa 0.35, 1.0	NH ₄ OH 20 mL	FeCl ₃ ·6H ₂ O 0.27, 1.0		No result
RP1:79:1	80	MeOH 30	H ₂ -5-Br-thsa 0.27, 1.0	NH ₄ OH 20 mL	FeCl ₃ ·6H ₂ O 0.27, 1.0	27.9	Crystalline product
RP1:79:2	80	MeOH 30	H ₂ -4-OH-thsa 0.21, 1.0	NH ₄ OH 20 mL	FeCl ₃ ·6H ₂ O 0.27, 1.0	61.9	Crystalline product + brown powder
RP1:80:2	80	MeOH 35	H ₂ -3OEt-thsa-Ph 0.32, 1.0	CsOH 0.67, 4.0	Fe(NO ₃) ₃ ·9H ₂ O 0.40, 1.0	57.3	Crystalline product + brown powder

Table E2.1 Quantities used in the synthesis of Fe^{III} complexes with R-salicylaldehyde 4R'-thiosemicarbazone (H₂-R-thsa-R') ligands continued.

Experimental code for Fe ^{III} Complex synthesis	T (°C)	Solvent (mL)	H ₂ -R-thsa-R' Ligand (g, mmol)	Cation (g, mmol)	Fe ^{III} (salt) (g, mmol)	Product Yield %	State of material
RP1:80:3	80	MeOH 70	H ₂ -3OEt-thsa-Ph 0.64, 2.0	CsOH 0.67, 4.0	Fe(NO ₃) ₃ ·9H ₂ O 0.40, 1.0	33.7	Crystalline
RP1:81:4	80	MeOH 35	H ₂ -3OEt-thsa-Ph 0.32, 1.0	CsOH 0.34, 2.0	Fe(NO ₃) ₃ ·9H ₂ O 0.40, 1.0	-	No result
RP1:81:5	80	MeOH 70	H ₂ -3OEt-thsa-Ph 0.64, 2.0	CsOH 0.50, 3.0	Fe(NO ₃) ₃ ·9H ₂ O 0.40, 1.0	55.0	Powder
RP1:82:6	80	MeOH 70	H ₂ -3OEt-thsa-Ph 0.64, 2.0	CsOH 0.67, 4.0	Fe(NO ₃) ₃ ·9H ₂ O 0.40, 1.0	41.6	Crystalline
RP1:82:2	80	MeOH 70	H ₂ -3OEt-thsa-Et 0.27, 1.0	CsOH 0.67, 4.0	Fe(NO ₃) ₃ ·9H ₂ O 0.40, 1.0	66.2	Crystalline product + brown powder
RP1:83:3	80	MeOH 70	H ₂ -3OEt-thsa-Et 0.54, 2.0	CsOH 0.67, 4.0	Fe(NO ₃) ₃ ·9H ₂ O 0.40, 1.0	38.9	Crystalline needles
RP1:83:1	80	MeOH 35	H ₂ -thsa-Ph 0.27, 1.0	CsOH 0.34, 2.0	Fe(NO ₃) ₃ ·9H ₂ O 0.40, 1.0	33.1	Brown powder
RP1:84:2	80	MeOH 70	H ₂ -thsa-Ph 0.54, 2.0	CsOH 0.67, 4.0	Fe(NO ₃) ₃ ·9H ₂ O 0.40, 1.0	22.7	Crystalline
RP1:84:3	80	MeOH 35	H ₂ -thsa-Ph 0.27, 1.0	NH ₄ OH 20 mL	Fe(NO ₃) ₃ ·9H ₂ O 0.40, 1.0	36.7	Crystalline
RP1:86:1	80	MeOH 35	H ₂ -4-OH-thsa-Ph 0.29, 1.0	CsOH 0.34, 2.0	Fe(NO ₃) ₃ ·9H ₂ O 0.40, 1.0	-	No result
RP1:87:2	80	MeOH 35	H ₂ -4-OH-thsa-Ph 0.58, 2.0	CsOH 0.67, 4.0	Fe(NO ₃) ₃ ·9H ₂ O 0.40, 1.0	45.6	Brown powder
RP1:87:3	80	MeOH 35	H ₂ -4-OH-thsa-Ph 0.29, 1.0	NH ₄ OH 20 mL	Fe(NO ₃) ₃ ·9H ₂ O 0.40, 1.0	55.2	Brown powder
RP1:88:1	80	MeOH 35	H ₂ -thsa-Ph 0.27, 1.0	NH ₄ OH 20 mL	Fe(CH ₃ C ₆ H ₅ SO ₃) ₃ ·6H ₂ O 0.68, 1.0	-	No result

Table E2.1 Quantities used in the synthesis of Fe^{III} complexes with R-salicylaldehyde 4R'-thiosemicarbazone (H₂-R-thsa-R') ligands continued.

Experimental code for Fe ^{III} Complex synthesis	T (°C)	Solvent (mL)	H ₂ -R-thsa-R' Ligand (g, mmol)	Cation (g, mmol)	Fe ^{III} (salt) (g, mmol)	Product Yield %	State of material
RP1:88:2	80	MeOH 70	H ₂ -thsa-Ph 0.54, 2.0	NH ₄ OH 20 mL	Fe(CH ₃ C ₆ H ₅ SO ₃) ₃ ·6H ₂ O 0.68, 1.0	-	No result
RP1:89:1	80	MeOH 35	H ₂ -4-OH-thsa-Ph 0.29, 1.0	NH ₄ OH 20 mL	Fe(CH ₃ C ₆ H ₅ SO ₃) ₃ ·6H ₂ O 0.68, 1.0	-	No result
RP1:89:2	80	MeOH 70	H ₂ -4-OH-thsa-Ph 0.58, 2.0	NH ₄ OH 20 mL	Fe(CH ₃ C ₆ H ₅ SO ₃) ₃ ·6H ₂ O 0.68, 1.0	-	No result
RP1:90:2	80	MeOH 30	H ₂ -thsa 0.20, 1.0	NH ₄ OH 20 mL	Fe(CH ₃ C ₆ H ₅ SO ₃) ₃ ·6H ₂ O 0.68, 1.0	29.1	Crystalline
RP1:90:3	80	MeOH 70	H ₂ -thsa 0.40, 2.0	NH ₄ OH 20 mL	Fe(CH ₃ C ₆ H ₅ SO ₃) ₃ ·6H ₂ O 0.68, 1.0	41.7	Crystalline
RP1:91:2	80	MeOH 35	H ₂ -5-Br-thsa 0.27, 1.0	NH ₄ OH 20 mL	FeCl ₃ ·6H ₂ O 0.27, 1.0	62.8	Crystalline + brown powder
RP1:91:3	80	MeOH 70	H ₂ -5-Br-thsa 0.54, 2.0	NH ₄ OH 20 mL	FeCl ₃ ·6H ₂ O 0.27, 1.0	-	No result
RP1:92:1	80	MeOH 70	H ₂ -3-OEt-thsa-Ph 0.64, 2.0	CsOH 0.67, 4.0	Fe(NO ₃) ₃ ·9H ₂ O 0.40, 1.0	42.4	Crystalline
RP1:92:4	80	MeOH 70	H ₂ -3-OEt-thsa-Et 0.54, 2.0	CsOH 0.67, 4.0	Fe(NO ₃) ₃ ·9H ₂ O 0.40, 1.0	-	No result
RP1:95:1	80	MeOH 70	H ₂ -3-OEt-thsa-Et 0.54, 2.0	CsOH 0.67, 4.0	Fe(CH ₃ C ₆ H ₅ SO ₃) ₃ ·6H ₂ O 0.68, 1.0	38.5	Crystalline
RP1:96:1	80	MeOH 30	H ₂ -5-Br-thsa 0.27, 1.0	CsOH 0.67, 4.0	Fe(CH ₃ C ₆ H ₅ SO ₃) ₃ ·6H ₂ O 0.68, 1.0	48.5	Powder
RP1:96:2	80	MeOH 70	H ₂ -5-Br-thsa 0.54, 2.0	CsOH 0.67, 4.0	Fe(CH ₃ C ₆ H ₅ SO ₃) ₃ ·6H ₂ O 0.68, 1.0	56.2	Crystalline product + brown powder
RP1:97:3	80	MeOH 30	H ₂ -5-Br-thsa 0.27, 1.0	CsOH 0.67, 4.0	Fe(NO ₃) ₃ ·9H ₂ O 0.40, 1.0	49.1	Powder

Table E2.1 Quantities used in the synthesis of Fe^{III} complexes with R-salicylaldehyde 4R'-thiosemicarbazone (H₂-R-thsa-R') ligands continued.

Experimental code for Fe ^{III} Complex synthesis	T (°C)	Solvent (mL)	H ₂ -R-thsa-R' Ligand (g, mmol)	Cation (g, mmol)	Fe ^{III} (salt) (g, mmol)	Product Yield %	State of material
RP1:97:4	80	MeOH 70	H ₂ -5-Br-thsa 0.54, 2.0	CsOH 0.67, 4.0	Fe(NO ₃) ₃ ·9H ₂ O 0.40, 1.0	28.8	Crystalline
RP1:98:5	80	MeOH 30	H ₂ -5-Br-thsa 0.27, 1.0	CsOH 0.67, 4.0	FeCl ₃ ·6H ₂ O 0.27, 1.0	35.8	Powder
RP1:98:6	80	MeOH 70	H ₂ -5-Br-thsa 0.54, 2.0	CsOH 0.67, 4.0	FeCl ₃ ·6H ₂ O 0.27, 1.0	48.2	Crystalline
RP1:99:1	80	MeOH 30	H ₂ -5-Br-thsa-Me 0.29, 1.0	CsOH 0.67, 4.0	Fe(CH ₃ C ₆ N ₅ SO ₃) ₃ ·6H ₂ O 0.68, 1.0	52.1	Powder
RP1:99:2	80	MeOH 70	H ₂ -5-Br-thsa-Me 0.58, 2.0	CsOH 0.67, 4.0	Fe(CH ₃ C ₆ N ₅ SO ₃) ₃ ·6H ₂ O 0.68, 1.0	58.3	Powder
RP1:100:3	80	MeOH 30	H ₂ -5-Br-thsa-Me 0.29, 1.0	CsOH 0.67, 4.0	Fe(NO ₃) ₃ ·9H ₂ O 0.40, 1.0	62.8	Crystalline product + brown powder
RP1:100:4	80	MeOH 70	H ₂ -5-Br-thsa-Me 0.58, 2.0	CsOH 0.67, 4.0	Fe(NO ₃) ₃ ·9H ₂ O 0.40, 1.0	45.8	Powder
RP1:101:5	80	MeOH 30	H ₂ -5-Br-thsa-Me 0.29, 1.0	CsOH 0.67, 4.0	FeCl ₃ ·6H ₂ O 0.27, 1.0	44.6	Crystalline product + brown powder
RP1:101:6	80	MeOH 70	H ₂ -5-Br-thsa-Me 0.58, 2.0	CsOH 0.67, 4.0	FeCl ₃ ·6H ₂ O 0.27, 1.0	54.3	Powder
RP1:102:7	80	MeOH 30	H ₂ -5-Br-thsa-Me 0.29, 1.0	NH ₄ OH 20 mL	Fe(CH ₃ C ₆ H ₅ SO ₃) ₃ ·6H ₂ O 0.68, 1.0	38.1	Crystalline product + brown powder
RP1:102:8	80	MeOH 70	H ₂ -5-Br-thsa-Me 0.58, 2.0	NH ₄ OH 20 mL	Fe(CH ₃ C ₆ H ₅ SO ₃) ₃ ·6H ₂ O 0.68, 1.0	-	No result
RP1:103:9	80	MeOH 30	H ₂ -5-Br-thsa-Me 0.29, 1.0	NH ₄ OH 20 mL	Fe(NO ₃) ₃ ·9H ₂ O 0.40, 1.0	32.8	Crystalline
RP1:103:10	80	MeOH 70	H ₂ -5-Br-thsa-Me 0.58, 2.0	NH ₄ OH 20 mL	Fe(NO ₃) ₃ ·9H ₂ O 0.40, 1.0	-	No result

Table E2.1 Quantities used in the synthesis of Fe^{III} complexes with R-salicylaldehyde 4R'-thiosemicarbazone (H₂-R-thsa-R') ligands continued.

Experimental code for Fe ^{III} Complex synthesis	T (°C)	Solvent (mL)	H ₂ -R-thsa-R' Ligand (g, mmol)	Cation (g, mmol)	Fe ^{III} (salt) (g, mmol)	Product Yield %	State of material
RP1:104:11	80	MeOH 30	H ₂ -5-Br-thsa-Me 0.29, 1.0	NH ₄ OH 20 mL	FeCl ₃ ·6H ₂ O 0.27, 1.0	28.7	Crystalline
RP1:104:12	80	MeOH 70	H ₂ -5-Br-thsa-Me 0.58, 2.0	NH ₄ OH 20 mL	FeCl ₃ ·6H ₂ O 0.27, 1.0	-	No result
RP1:106:1	80	MeOH 30	H ₂ -5-Br-thsa-Ph 0.35, 1.0	CsOH 0.67, 4.0	FeCl ₃ ·6H ₂ O 0.27, 1.0	-	No result
RP1:106:2	80	MeOH 70	H ₂ -5-Br-thsa-Ph 0.70, 2.0	NH ₄ OH 20 mL	FeCl ₃ ·6H ₂ O 0.27, 1.0	-	No result
RP1:107:3	80	MeOH 30	H ₂ -5-Br-thsa-Ph 0.35, 1.0	CsOH 0.67, 4.0	Fe(NO ₃) ₃ ·9H ₂ O 0.40, 1.0	-	No result
RP1:107:4	80	MeOH 70	H ₂ -5-Br-thsa-Ph 0.70, 2.0	NH ₄ OH 20 mL	Fe(NO ₃) ₃ ·9H ₂ O 0.40, 1.0	-	No result
RP1:108:5	80	MeOH 30	H ₂ -5-Br-thsa-Ph 0.35, 1.0	CsOH 0.67, 4.0	Fe(CH ₃ C ₆ H ₅ SO ₃) ₃ ·6H ₂ O 0.68, 1.0	37.6	Brown powder
RP1:108:6	80	MeOH 70	H ₂ -5-Br-thsa-Ph 0.70, 2.0	CsOH 0.67, 4.0	Fe(CH ₃ C ₆ H ₅ SO ₃) ₃ ·6H ₂ O 0.68, 1.0	-	No result
RP1:109:7	80	MeOH 30	H ₂ -5-Br-thsa-Ph 0.35, 1.0	NH ₄ OH 20 mL	FeCl ₃ ·6H ₂ O 0.27, 1.0	28.2	Brown powder
RP1:109:8	80	MeOH 70	H ₂ -5-Br-thsa-Ph 0.70, 2.0	NH ₄ OH 20 mL	FeCl ₃ ·6H ₂ O 0.27, 1.0	33.6	Brown/black powder
RP1:110:9	80	MeOH 30	H ₂ -5-Br-thsa-Ph 0.35, 1.0	NH ₄ OH 20 mL	Fe(NO ₃) ₃ ·9H ₂ O 0.40, 1.0	45.2	Brown/black powder
RP1:110:10	80	MeOH 70	H ₂ -5-Br-thsa-Ph 0.70, 2.0	NH ₄ OH 20 mL	Fe(NO ₃) ₃ ·9H ₂ O 0.40, 1.0	51.2	Crystalline product + brown powder
RP1:111:11	80	MeOH 30	H ₂ -5-Br-thsa-Ph 0.35, 1.0	NH ₄ OH 20 mL	Fe(CH ₃ C ₆ H ₅ SO ₃) ₃ ·6H ₂ O 0.68, 1.0	21.9	Brown powder

Table E2.1 Quantities used in the synthesis of Fe^{III} complexes with R-salicylaldehyde 4R'-thiosemicarbazone (H₂-R-thsa-R') ligands continued.

Experimental code for Fe ^{III} Complex synthesis	T (°C)	Solvent (mL)	H ₂ -R-thsa-R' Ligand (g, mmol)	Cation (g, mmol)	Fe ^{III} (salt) (g, mmol)	Product Yield %	State of material
RP1:111:12	80	MeOH 70	H ₂ -5-Br-thsa-Ph 0.70, 2.0	NH ₄ OH 20 mL	Fe(CH ₃ C ₆ H ₅ SO ₃) ₃ ·6H ₂ O 0.68, 1.0	28.3	Brown/black powder
RP1:112:1	80	MeOH 30	H ₂ -5-Br-thsa-Et 0.30, 1.0	NH ₄ OH 20 mL	FeCl ₃ ·6H ₂ O 0.27, 1.0	34.2	Crystalline
RP1:112:2	80	MeOH 70	H ₂ -5-Br-thsa-Et 0.60, 2.0	NH ₄ OH 20 mL	FeCl ₃ ·6H ₂ O 0.27, 1.0	38.5	Crystalline
RP1:113:3	80	MeOH 30	H ₂ -5-Br-thsa-Et 0.30, 1.0	NH ₄ OH 20 mL	Fe(NO ₃) ₃ ·9H ₂ O 0.40, 1.0	43.6	Crystalline product + brown powder
RP1:113:4	80	MeOH 70	H ₂ -5-Br-thsa-Et 0.60, 2.0	NH ₄ OH 20 mL	Fe(NO ₃) ₃ ·9H ₂ O 0.40, 1.0	29.2	Crystalline
RP1:114:5	80	MeOH 30	H ₂ -5-Br-thsa-Et 0.30, 1.0	NH ₄ OH 20 mL	Fe(CH ₃ C ₆ H ₅ SO ₃) ₃ ·6H ₂ O 0.68, 1.0	43.2	Crystalline product + brown powder
RP1:114:6	80	MeOH 70	H ₂ -5-Br-thsa-Et 0.60, 2.0	NH ₄ OH 20 mL	Fe(CH ₃ C ₆ H ₅ SO ₃) ₃ ·6H ₂ O 0.68, 1.0	39.1	Crystalline product + brown powder
RP1:118:1	80	MeOH 30	H ₂ -5-Cl-thsa 0.23, 1.0	CsOH 0.67, 4.0	FeCl ₃ ·6H ₂ O 0.27, 1.0	45.2	Powder
RP1:118:2	80	MeOH 70	H ₂ -5-Cl-thsa 0.46, 2.0	CsOH 0.67, 4.0	FeCl ₃ ·6H ₂ O 0.27, 1.0	57.3	Powder
RP1:119:3	80	MeOH 30	H ₂ -5-Cl-thsa 0.23, 1.0	CsOH 0.67, 4.0	Fe(NO ₃) ₃ ·9H ₂ O 0.40, 1.0	38.9	Powder
RP1:119:4	80	MeOH 70	H ₂ -5-Cl-thsa 0.46, 2.0	CsOH 0.67, 4.0	Fe(NO ₃) ₃ ·9H ₂ O 0.40, 1.0	66.1	Powder
RP1:120:5	80	MeOH 30	H ₂ -5-Cl-thsa 0.23, 1.0	CsOH 0.67, 4.0	Fe(CH ₃ C ₆ H ₅ SO ₃) ₃ ·6H ₂ O 0.68, 1.0	47.8	Powder
RP1:120:6	80	MeOH 70	H ₂ -5-Cl-thsa 0.46, 2.0	CsOH 0.67, 4.0	Fe(CH ₃ C ₆ H ₅ SO ₃) ₃ ·6H ₂ O 0.68, 1.0	55.7	Powder

Table E2.1 Quantities used in the synthesis of Fe^{III} complexes with R-salicylaldehyde 4R'-thiosemicarbazone (H₂-R-thsa-R') ligands continued.

Experimental code for Fe ^{III} Complex synthesis	T (°C)	Solvent (mL)	H ₂ -R-thsa-R' Ligand (g, mmol)	Cation (g, mmol)	Fe ^{III} (salt) (g, mmol)	Product Yield %	State of material
RP1:121:7	80	MeOH 30	H ₂ -5-Cl-thsa 0.23, 1.0	NH ₄ OH 20 mL	FeCl ₃ ·6H ₂ O 0.27, 1.0	45.2	Crystalline product + brown powder
RP1:121:8	80	MeOH 70	H ₂ -5-Cl-thsa 0.46, 2.0	NH ₄ OH 20 mL	FeCl ₃ ·6H ₂ O 0.27, 1.0	34.2	Crystalline
RP1:122:9	80	MeOH 30	H ₂ -5-Cl-thsa 0.23, 1.0	NH ₄ OH 20 mL	Fe(NO ₃) ₃ ·9H ₂ O 0.40, 1.0	46.2	Crystalline product + brown powder
RP1:122:10	80	MeOH 70	H ₂ -5-Cl-thsa 0.46, 2.0	NH ₄ OH 20 mL	Fe(NO ₃) ₃ ·9H ₂ O 0.40, 1.0	28.3	Crystalline
RP1:123:11	80	MeOH 30	H ₂ -5-Cl-thsa 0.23, 1.0	NH ₄ OH 20 mL	Fe(CH ₃ C ₆ H ₅ SO ₃) ₃ ·6H ₂ O 0.68, 1.0	66.5	Powder
RP1:123:12	80	MeOH 70	H ₂ -5-Cl-thsa 0.46, 2.0	NH ₄ OH 20 mL	Fe(CH ₃ C ₆ H ₅ SO ₃) ₃ ·6H ₂ O 0.68, 1.0	25.4	Crystalline
RP1:124:1	80	MeOH 30	H ₂ -5-Cl-thsa-Me 0.24, 1.0	CsOH 0.67, 4.0	FeCl ₃ ·6H ₂ O 0.27, 1.0	38.2	Crystalline
RP1:124:2	80	MeOH 70	H ₂ -5-Cl-thsa-Me 0.48, 2.0	CsOH 0.67, 4.0	FeCl ₃ ·6H ₂ O 0.27, 1.0	55.3	Powder
RP1:125:3	80	MeOH 30	H ₂ -5-Cl-thsa-Me 0.24, 1.0	NH ₄ OH 20 mL	FeCl ₃ ·6H ₂ O 0.27, 1.0	27.4	Crystalline
RP1:125:4	80	MeOH 70	H ₂ -5-Cl-thsa-Me 0.48, 2.0	NH ₄ OH 20 mL	FeCl ₃ ·6H ₂ O 0.27, 1.0	48.7	Crystalline product + brown powder
RP1:132:5	80	EtOH 65	H ₂ -thsa 0.40, 2.0	NH ₄ OH 0.035, 1.0	Fe(NO ₃) ₃ ·9H ₂ O 0.40, 1.0	-	No result
RP1:132:6	80	MeOH 65	H ₂ -thsa 0.46, 2.0	NH ₄ OH 0.035, 1.0	Fe(NO ₃) ₃ ·9H ₂ O 0.40, 1.0	-	No result
RP1:133:7	80	H ₂ O 65	H ₂ -thsa 0.40, 2.0	NH ₄ OH 0.07, 2.0	Fe(NO ₃) ₃ ·9H ₂ O 0.40, 1.0	-	No result

Table E2.1 Quantities used in the synthesis of Fe^{III} complexes with R-salicylaldehyde 4R'-thiosemicarbazone (H₂-R-thsa-R') ligands continued.

Experimental code for Fe ^{III} Complex synthesis	T (°C)	Solvent (mL)	H ₂ -R-thsa-R' Ligand (g, mmol)	Cation (g, mmol)	Fe ^{III} (salt) (g, mmol)	Product Yield %	State of material
RP1:133:8	80	EtOH 65	H ₂ -thsa 0.46, 2.0	NH ₄ OH 0.07, 2.0	Fe(NO ₃) ₃ ·9H ₂ O 0.40, 1.0	54.7	Crystalline
RP1:134:9	80	MeOH 65	H ₂ -thsa 0.46, 2.0	NH ₄ OH 0.07, 2.0	Fe(NO ₃) ₃ ·9H ₂ O 0.40, 1.0	-	No result
RP1:134:10	80	H ₂ O 65	H ₂ -thsa 0.40, 2.0	NH ₄ OH 0.07, 2.0	Fe(NO ₃) ₃ ·9H ₂ O 0.40, 1.0	-	No result
RP1:135:11	80	EtOH 65	H ₂ -thsa 0.40, 2.0	NH ₄ OH 0.105, 3.0	Fe(NO ₃) ₃ ·9H ₂ O 0.40, 1.0	62.1	Crystalline
RP1:135:12	80	MeOH 65	H ₂ -thsa 0.40, 2.0	NH ₄ OH 0.105, 3.0	Fe(NO ₃) ₃ ·9H ₂ O 0.40, 1.0	-	No result
RP1:49:5	80	MeOH 30	H ₂ -5Cl-thsa-Me 0.24, 1.0	CsOH 0.67, 4.0	Fe(NO ₃) ₃ ·9H ₂ O 0.40, 1.0	78.2	Powder
RP1:49:6	80	MeOH 30	H ₂ -5Cl-thsa-Me 0.48, 2.0	CsOH 0.67, 4.0	Fe(NO ₃) ₃ ·9H ₂ O 0.40, 1.0	69.2	Powder
RP1:50:7	80	MeOH 30	H ₂ -5Cl-thsa-Me 0.24, 1.0	NH ₄ OH 20 mL	Fe(NO ₃) ₃ ·9H ₂ O 0.40, 1.0	37.1	Crystalline
RP1:50:8	80	MeOH 65	H ₂ -5Cl-thsa-Me 0.48, 2.0	NH ₄ OH 20 mL	Fe(NO ₃) ₃ ·9H ₂ O 0.40, 1.0	66.5	Powder
RP1:54:1	80	EtOH 70	H ₂ -4OH-thsa 0.42, 2.0	-	Fe(NO ₃) ₃ ·9H ₂ O 0.40, 1.0	34.7	Crystalline
RP1:54:2	80	EtOH 70	H ₂ -4OH-thsa 0.42, 2.0	NH ₄ OH 0.035, 1.0	Fe(NO ₃) ₃ ·9H ₂ O 0.40, 1.0	28.8	Crystalline
RP1:55:3	80	EtOH 70	H ₂ -4OH-thsa 0.42, 2.0	NH ₄ OH 0.70, 2.0	Fe(NO ₃) ₃ ·9H ₂ O 0.40, 1.0	37.2	Crystalline
RP1:55:4	80	EtOH 70	H ₂ -4OH-thsa 0.42, 2.0	NH ₄ OH 0.105, 3.0	Fe(NO ₃) ₃ ·9H ₂ O 0.40, 1.0	42.8	Crystalline

Table E2.1 Quantities used in the synthesis of Fe^{III} complexes with R-salicylaldehyde 4R'-thiosemicarbazone (H₂-R-thsa-R') ligands continued.

Experimental code for Fe ^{III} Complex synthesis	T (°C)	Solvent (mL)	H ₂ -R-thsa-R' Ligand (g, mmol)	Cation (g, mmol)	Fe ^{III} (salt) (g, mmol)	Product Yield %	State of material
RP1:56:5	80	EtOH 70	H ₂ -4OH-thsa 0.42, 2.0	CsOH 0.17, 1.0	Fe(NO ₃) ₃ ·9H ₂ O 0.40, 1.0	43.6	Crystalline
RP1:56:6	80	EtOH 70	H ₂ -4OH-thsa 0.42, 2.0	CsOH 0.34, 2.0	Fe(NO ₃) ₃ ·9H ₂ O 0.40, 1.0	34.5	Crystalline
RP1:57:7	80	EtOH 70	H ₂ -4OH-thsa 0.42, 2.0	CsOH 0.51, 3.0	Fe(NO ₃) ₃ ·9H ₂ O 0.40, 1.0	36.4	Crystalline
RP1:57:1	20	EtOH 70	H ₂ -5OMe-thsa 0.42, 2.0	-	Fe(NO ₃) ₃ ·9H ₂ O 0.40, 1.0	66.3	Powder
RP1:58:2	80	EtOH 70	H ₂ -5OMe-thsa 0.42, 2.0	NH ₄ OH 0.035, 1.0	Fe(NO ₃) ₃ ·9H ₂ O 0.40, 1.0	56.2	Mixture of crystals + powder
RP1:58:3	80	EtOH 70	H ₂ -5OMe-thsa 0.42, 2.0	NH ₄ OH 0.7, 2.0	Fe(NO ₃) ₃ ·9H ₂ O 0.40, 1.0	58.4	Mixture of crystals + powder
RP1:59:4	80	EtOH 70	H ₂ -5OMe-thsa 0.42, 2.0	NH ₄ OH 0.105, 3.0	Fe(NO ₃) ₃ ·9H ₂ O 0.40, 1.0	28.3	Crystalline
RP1:59:1	80	MeOH 35	H ₂ -3OEt-thsa-Ph 0.32, 1.0	CsOH 0.67, 4.0	Fe(NO ₃) ₃ ·9H ₂ O 0.40, 1.0	34.4	Crystalline
RP2:4:1	80	EtOH 70	H ₂ -thsa-Me 0.42, 2.0	-	Fe(NO ₃) ₃ ·9H ₂ O 0.40, 1.0	26.7	Crystalline
RP2:4:2	80	EtOH 70	H ₂ -thsa-Me 0.42, 2.0	NH ₄ OH 0.035, 1.0	Fe(NO ₃) ₃ ·9H ₂ O 0.40, 1.0	29.4	Crystalline
RP2:5:3	80	EtOH 70	H ₂ -thsa-Me 0.42, 2.0	NH ₄ OH 0.7, 2.0	Fe(NO ₃) ₃ ·9H ₂ O 0.40, 1.0	34.5	Crystalline
RP2:5:4	80	EtOH 70	H ₂ -thsa-Me 0.42, 2.0	NH ₄ OH 0.105, 3.0	Fe(NO ₃) ₃ ·9H ₂ O 0.40, 1.0	36.9	Crystalline
RP2:6:1	80	EtOH 70	H ₂ -thsa-Et 0.44, 2.0	-	Fe(NO ₃) ₃ ·9H ₂ O 0.40, 1.0	42.3	Crystalline

Table E2.1 Quantities used in the synthesis of Fe^{III} complexes with R-salicylaldehyde 4R'-thiosemicarbazone (H₂-R-thsa-R') ligands continued.

Experimental code for Fe ^{III} Complex synthesis	T (°C)	Solvent (mL)	H ₂ -R-thsa-R' Ligand (g, mmol)	Cation (g, mmol)	Fe ^{III} (salt) (g, mmol)	Product Yield %	State of material
RP2:6:2	80	EtOH 70	H ₂ -thsa-Et 0.44, 2.0	NH ₄ OH 0.035, 1.0	Fe(NO ₃) ₃ ·9H ₂ O 0.40, 1.0	34.6	Crystalline
RP2:7:3	80	EtOH 70	H ₂ -thsa-Et 0.44, 2.0	NH ₄ OH 0.7, 2.0	Fe(NO ₃) ₃ ·9H ₂ O 0.40, 1.0	54.4	Crystalline
RP2:7:4	80	EtOH 70	H ₂ -thsa-Et 0.44, 2.0	NH ₄ OH 0.105, 3.0	Fe(NO ₃) ₃ ·9H ₂ O 0.40, 1.0	48.6	Crystalline
RP2:8:1	80	EtOH 70	H ₂ -thsa-Ph 0.54, 2.0	-	Fe(NO ₃) ₃ ·9H ₂ O 0.40, 1.0	28.9	Crystalline
RP2:8:2	80	EtOH 70	H ₂ -thsa-Ph 0.54, 2.0	NH ₄ OH 0.035, 1.0	Fe(NO ₃) ₃ ·9H ₂ O 0.40, 1.0	45.3	Powder
RP2:9:3	80	EtOH 70	H ₂ -thsa-Ph 0.54, 2.0	NH ₄ OH 0.7, 2.0	Fe(NO ₃) ₃ ·9H ₂ O 0.40, 1.0	34.8	Crystalline
RP2:9:4	80	EtOH 70	H ₂ -thsa-Ph 0.54, 2.0	NH ₄ OH 0.105, 3.0	Fe(NO ₃) ₃ ·9H ₂ O 0.40, 1.0	56.1	Crystalline
RP2:10:1	80	MeOH 70	H ₂ -thsa 0.40, 2.0	-	Fe(NO ₃) ₃ ·9H ₂ O 0.40, 1.0	-	No result
RP2:10:2	80	MeOH 70	H ₂ -thsa 0.40, 2.0	Et ₃ N 0.10, 1.0	Fe(NO ₃) ₃ ·9H ₂ O 0.40, 1.0	-	No result
RP2:11:3	80	MeOH 70	H ₂ -thsa 0.40, 2.0	Et ₃ N 0.20, 2.0	Fe(NO ₃) ₃ ·9H ₂ O 0.40, 1.0	-	No result
RP2:11:4	80	MeOH 70	H ₂ -thsa 0.40, 2.0	Et ₃ N 0.30, 3.0	Fe(NO ₃) ₃ ·9H ₂ O 0.40, 1.0	66.9	Powder
RP2:12:1	80	MeOH 35	H ₂ -5Cl-thsa-Ph 0.31, 1.0	CsOH 0.67, 4.0	Fe(NO ₃) ₃ ·9H ₂ O 0.40, 1.0	-	No result
RP2:12:2	80	MeOH 70	H ₂ -5Cl-thsa-Ph 0.62, 2.0	CsOH 0.67, 4.0	Fe(NO ₃) ₃ ·9H ₂ O 0.40, 1.0	-	No result

Table E2.1 Quantities used in the synthesis of Fe^{III} complexes with R-salicylaldehyde 4R'-thiosemicarbazone (H₂-R-thsa-R') ligands continued.

Experimental code for Fe ^{III} Complex synthesis	T (°C)	Solvent (mL)	H ₂ -R-thsa-R' Ligand (g, mmol)	Cation (g, mmol)	Fe ^{III} (salt) (g, mmol)	Product Yield %	State of material
RP2:13:3	80	MeOH 70	H ₂ -5Cl-thsa-Ph 0.31, 1.0	NH ₄ OH 20 mL	Fe(NO ₃) ₃ ·9H ₂ O 0.40, 1.0	37.8	Crystalline
RP2:13:4	80	MeOH 70	H ₂ -5Cl-thsa-Ph 0.62, 2.0	NH ₄ OH 20 mL	Fe(NO ₃) ₃ ·9H ₂ O 0.40, 1.0	52.1	Crystalline
RP2:14:1	80	MeOH 25 EtOH 25 H ₂ O 10	H ₂ -thsa 04.0, 2.0	(CH ₃) ₂ NH 0.45, 10.0	Fe(NO ₃) ₃ ·9H ₂ O 0.40, 1.0	-	No result
RP2:14:2	80	MeOH 25 EtOH 25 H ₂ O 10	H ₂ -thsa-Me 0.42, 2.0	(CH ₃) ₂ NH 0.45, 10.0	Fe(NO ₃) ₃ ·9H ₂ O 0.40, 1.0	34.8	Crystalline
RP2:15:3	80	MeOH 25 EtOH 25 H ₂ O 10	H ₂ -thsa-Et 0.44, 2.0	(CH ₃) ₂ NH 0.45, 10.0	Fe(NO ₃) ₃ ·9H ₂ O 0.40, 1.0	62.3	Powder
RP2:15:4	80	MeOH 25 EtOH 25 H ₂ O 10	H ₂ -thsa-Ph 0.54, 2.0	(CH ₃) ₂ NH 0.45, 10.0	Fe(NO ₃) ₃ ·9H ₂ O 0.40, 1.0	-	No result
RP2:16:5	80	MeOH 60 H ₂ O 10	H ₂ -thsa 0.40, 2.0	NH ₄ OH 0.16, 4.0	Fe(NO ₃) ₃ ·9H ₂ O 0.40, 1.0	-	No result
RP2:16:6	80	MeOH 60 H ₂ O 10	H ₂ -thsa-Me 0.42, 2.0	NH ₄ OH 0.16, 4.0	Fe(NO ₃) ₃ ·9H ₂ O 0.40, 1.0	-	No result
RP2:17:7	80	MeOH 60 H ₂ O 10	H ₂ -thsa-Et 0.44, 2.0	NH ₄ OH 0.16, 4.0	Fe(NO ₃) ₃ ·9H ₂ O 0.40, 1.0	-	No result
RP2:17:8	80	MeOH 60 H ₂ O 10	H ₂ -thsa-Ph 0.54, 2.0	NH ₄ OH 0.16, 4.0	Fe(NO ₃) ₃ ·9H ₂ O 0.40, 1.0	-	No result
RP2:18:1	80	MeOH 25 EtOH 25 H ₂ O 10	H ₂ -5Br-thsa 0.54, 2.0	(CH ₃) ₂ NH 0.45, 10.0	Fe(NO ₃) ₃ ·9H ₂ O 0.40, 1.0	-	No result

Table E2.1 Quantities used in the synthesis of Fe^{III} complexes with R-salicylaldehyde 4R'-thiosemicarbazone (H₂-R-thsa-R') ligands continued.

Experimental code for Fe ^{III} Complex synthesis	T (°C)	Solvent (mL)	H ₂ -R-thsa-R' Ligand (g, mmol)	Cation (g, mmol)	Fe ^{III} (salt) (g, mmol)	Product Yield %	State of material
RP2:18:2	80	MeOH 25 EtOH 25 H ₂ O 10	H ₂ -5Br-thsa-Me 0.58, 2.0	(CH ₃) ₂ NH 0.45, 10.0	Fe(NO ₃) ₃ ·9H ₂ O 0.40, 1.0	44.7	Crystalline
RP2:19:3	80	MeOH 25 EtOH 25 H ₂ O 10	H ₂ -5Br-thsa-Et 0.60, 2.0	(CH ₃) ₂ NH 0.45, 10.0	Fe(NO ₃) ₃ ·9H ₂ O 0.40, 1.0	34.9	Crystalline
RP2:19:4	80	MeOH 25 EtOH 25 H ₂ O 10	H ₂ -5Br-thsa-Ph 0.70, 2.0	(CH ₃) ₂ NH 0.45, 10.0	Fe(NO ₃) ₃ ·9H ₂ O 0.40, 1.0	66.7	Powder
RP2:20:5	80	MeOH 60 H ₂ O 10	H ₂ -5Br-thsa 0.54, 2.0	NH ₄ OH 0.16, 4.0	Fe(NO ₃) ₃ ·9H ₂ O 0.40, 1.0	-	No result
RP2:20:6	80	MeOH 60 H ₂ O 10	H ₂ -5Br-thsa-Me 0.58, 2.0	NH ₄ OH 0.16, 4.0	Fe(NO ₃) ₃ ·9H ₂ O 0.40, 1.0	-	No result
RP2:21:7	80	MeOH 60 H ₂ O 10	H ₂ -5Br-thsa-Et 0.60, 2.0	NH ₄ OH 0.16, 4.0	Fe(NO ₃) ₃ ·9H ₂ O 0.40, 1.0	22.7	Crystalline
RP2:21:8	80	MeOH 60 H ₂ O 10	H ₂ -5Br-thsa-Ph 0.70, 2.0	NH ₄ OH 0.16, 4.0	Fe(NO ₃) ₃ ·9H ₂ O 0.40, 1.0	45.2	Crystalline
RP2:23:1	80	MeOH 25 EtOH 25 H ₂ O 10	H ₂ -3OEt-thsa 0.48, 2.0	(CH ₃) ₂ NH 0.45, 10.0	Fe(NO ₃) ₃ ·9H ₂ O 0.40, 1.0	-	No result
RP2:23:2	80	MeOH 25 EtOH 25 H ₂ O 10	H ₂ -3OEt-thsa-Me 0.50, 2.0	(CH ₃) ₂ NH 0.45, 10.0	Fe(NO ₃) ₃ ·9H ₂ O 0.40, 1.0	55.3	Powder
RP2:24:3	80	MeOH 25 EtOH 25 H ₂ O 10	H ₂ -3OEt-thsa-Et 0.54, 2.0	(CH ₃) ₂ NH 0.45, 10.0	Fe(NO ₃) ₃ ·9H ₂ O 0.40, 1.0	-	No result

Table E2.1 Quantities used in the synthesis of Fe^{III} complexes with R-salicylaldehyde 4R'-thiosemicarbazone (H₂-R-thsa-R') ligands continued.

Experimental code for Fe ^{III} Complex synthesis	T (°C)	Solvent (mL)	H ₂ -R-thsa-R' Ligand (g, mmol)	Cation (g, mmol)	Fe ^{III} (salt) (g, mmol)	Product Yield %	State of material
RP2:24:4	80	MeOH 25 EtOH 25 H ₂ O 10	H ₂ -3OEt-thsa-Ph 0.64, 2.0	(CH ₃) ₂ NH 0.45, 10.0	Fe(NO ₃) ₃ ·9H ₂ O 0.40, 1.0	-	No result
RP2:25:1	80	MeOH 60 H ₂ O 10	H ₂ -3OEt-thsa 0.48, 2.0	(CH ₃) ₂ NH 0.45, 10.0	Fe(NO ₃) ₃ ·9H ₂ O 0.40, 1.0	34.7	Crystalline
RP2:25:2	80	MeOH 60 H ₂ O 10	H ₂ -3OEt-thsa-Me 0.50, 2.0	(CH ₃) ₂ NH 0.45, 10.0	Fe(NO ₃) ₃ ·9H ₂ O 0.40, 1.0	55.4	Crystalline
RP2:26:3	80	MeOH 60 H ₂ O 10	H ₂ -3OEt-thsa-Et 0.54, 2.0	(CH ₃) ₂ NH 0.45, 10.0	Fe(NO ₃) ₃ ·9H ₂ O 0.40, 1.0	-	No result
RP2:26:4	80	MeOH 60 H ₂ O 10	H ₂ -3OEt-thsa-Ph 0.64, 2.0	(CH ₃) ₂ NH 0.45, 10.0	Fe(NO ₃) ₃ ·9H ₂ O 0.40, 1.0	-	No result
RP2:27:1	80	MeOH 60 H ₂ O 10	H ₂ -3OEt-thsa 0.48, 2.0	NH ₄ OH 0.04, 1.0	Fe(NO ₃) ₃ ·9H ₂ O 0.40, 1.0	65.8	Powder
RP2:27:2	80	MeOH 60 H ₂ O 10	H ₂ -3OEt-thsa 0.48, 2.0	NH ₄ OH 0.08, 2.0	Fe(NO ₃) ₃ ·9H ₂ O 0.40, 1.0	58.6	Powder
RP2:28:3	80	MeOH 60 H ₂ O 10	H ₂ -3OEt-thsa 0.48, 2.0	NH ₄ OH 0.12, 3.0	Fe(NO ₃) ₃ ·9H ₂ O 0.40, 1.0	58.7	Powder
RP2:28:4	80	MeOH 60 H ₂ O 10	H ₂ -3OEt-thsa 0.48, 2.0	NH ₄ OH 0.16, 4.0	Fe(NO ₃) ₃ ·9H ₂ O 0.40, 1.0	67.2	Powder
RP2:29:1	80	MeOH 60 H ₂ O 10	H ₂ -3OEt-thsa-Me 0.50, 2.0	NH ₄ OH 0.04, 1.0	Fe(NO ₃) ₃ ·9H ₂ O 0.40, 1.0	45.8	Powder
RP2:29:2	80	MeOH 60 H ₂ O 10	H ₂ -3OEt-thsa-Me 0.50, 2.0	NH ₄ OH 0.08, 2.0	Fe(NO ₃) ₃ ·9H ₂ O 0.40, 1.0	52.1	Powder
RP2:30:3	80	MeOH 60 H ₂ O 10	H ₂ -3OEt-thsa-Me 0.50, 2.0	NH ₄ OH 0.12, 3.0	Fe(NO ₃) ₃ ·9H ₂ O 0.40, 1.0	68.3	Crystalline product + powder
RP2:30:4	80	MeOH 60 H ₂ O 10	H ₂ -3OEt-thsa-Me 0.50, 2.0	NH ₄ OH 0.16, 4.0	Fe(NO ₃) ₃ ·9H ₂ O 0.40, 1.0	65.8	Crystalline product + powder

Table E2.1 Quantities used in the synthesis of Fe^{III} complexes with R-salicylaldehyde 4R'-thiosemicarbazone (H₂-R-thsa-R') ligands continued.

Experimental code for Fe ^{III} Complex synthesis	T (°C)	Solvent (mL)	H ₂ -R-thsa-R' Ligand (g, mmol)	Cation (g, mmol)	Fe ^{III} (salt) (g, mmol)	Product Yield %	State of material
RP2:31:1	80	MeOH 60 H ₂ O 10	H ₂ -3OEt-thsa-Et 0.54, 2.0	NH ₄ OH 0.04, 1.0	Fe(NO ₃) ₃ ·9H ₂ O 0.40, 1.0	38.2	Crystalline
RP2:31:2	80	MeOH 60 H ₂ O 10	H ₂ -3OEt-thsa-Et 0.54, 2.0	NH ₄ OH 0.08, 2.0	Fe(NO ₃) ₃ ·9H ₂ O 0.40, 1.0	41.3	Crystalline
RP2:32:3	80	MeOH 60 H ₂ O 10	H ₂ -3OEt-thsa-Et 0.54, 2.0	NH ₄ OH 0.12, 3.0	Fe(NO ₃) ₃ ·9H ₂ O 0.40, 1.0	-	No result
RP2:32:4	80	MeOH 60 H ₂ O 10	H ₂ -3OEt-thsa-Et 0.54, 2.0	NH ₄ OH 0.16, 4.0	Fe(NO ₃) ₃ ·9H ₂ O 0.40, 1.0	-	No result
RP2:33:1	80	MeOH 60 H ₂ O 10	H ₂ -3OEt-thsa-Ph 0.64, 2.0	NH ₄ OH 0.04, 1.0	Fe(NO ₃) ₃ ·9H ₂ O 0.40, 1.0	-	No result
RP2:33:2	80	MeOH 60 H ₂ O 10	H ₂ -3OEt-thsa-Ph 0.64, 2.0	NH ₄ OH 0.08, 2.0	Fe(NO ₃) ₃ ·9H ₂ O 0.40, 1.0	-	No result
RP2:34:3	80	MeOH 60 H ₂ O 10	H ₂ -3OEt-thsa-Ph 0.64, 2.0	NH ₄ OH 0.12, 3.0	Fe(NO ₃) ₃ ·9H ₂ O 0.40, 1.0	-	No result
RP2:34:4	80	MeOH 60 H ₂ O 10	H ₂ -3OEt-thsa-Ph 0.64, 2.0	NH ₄ OH 0.16, 4.0	Fe(NO ₃) ₃ ·9H ₂ O 0.40, 1.0	-	No result
RP2:36:1	80	MeOH 60 H ₂ O 10	H ₂ -5Cl-thsa 0.46, 2.0	-	Fe(NO ₃) ₃ ·9H ₂ O 0.40, 1.0	22.8	Powder
RP2:36:2	80	MeOH 60 H ₂ O 10	H ₂ -5Cl-thsa 0.46, 2.0	NH ₄ OH 0.04, 1.0	Fe(NO ₃) ₃ ·9H ₂ O 0.40, 1.0	28.4	Powder
RP2:37:3	80	MeOH 60 H ₂ O 10	H ₂ -5Cl-thsa 0.46, 2.0	NH ₄ OH 0.08, 2.0	Fe(NO ₃) ₃ ·9H ₂ O 0.40, 1.0	33.5	Powder
RP2:37:4	80	MeOH 60 H ₂ O 10	H ₂ -5Cl-thsa 0.46, 2.0	NH ₄ OH 0.12, 3.0	Fe(NO ₃) ₃ ·9H ₂ O 0.40, 1.0	34.8	Powder
RP2:38:5	80	MeOH 60 H ₂ O 10	H ₂ -5Cl-thsa 0.46, 2.0	NH ₄ OH 0.16, 4.0	Fe(NO ₃) ₃ ·9H ₂ O 0.40, 1.0	28.7	Powder

Table E2.1 Quantities used in the synthesis of Fe^{III} complexes with R-salicylaldehyde 4R'-thiosemicarbazone (H₂-R-thsa-R') ligands continued.

Experimental code for Fe ^{III} Complex synthesis	T (°C)	Solvent (mL)	H ₂ -R-thsa-R' Ligand (g, mmol)	Cation (g, mmol)	Fe ^{III} (salt) (g, mmol)	Product Yield %	State of material
RP2:38:1	80	MeOH 60 H ₂ O 10	H ₂ -5Cl-thsa-Me 0.48, 2.0	-	Fe(NO ₃) ₃ ·9H ₂ O 0.40, 1.0	34.6	Crystalline
RP2:39:2	80	MeOH 60 H ₂ O 10	H ₂ -5Cl-thsa-Me 0.48, 2.0	NH ₄ OH 0.04, 1.0	Fe(NO ₃) ₃ ·9H ₂ O 0.40, 1.0	35.8	Crystalline
RP2:39:3	80	MeOH 60 H ₂ O 10	H ₂ -5Cl-thsa-Me 0.48, 2.0	NH ₄ OH 0.08, 2.0	Fe(NO ₃) ₃ ·9H ₂ O 0.40, 1.0	38.5	Crystalline
RP2:40:4	80	MeOH 60 H ₂ O 10	H ₂ -5Cl-thsa-Me 0.48, 2.0	NH ₄ OH 0.12, 3.0	Fe(NO ₃) ₃ ·9H ₂ O 0.40, 1.0	41.2	Crystalline
RP2:40:5	80	MeOH 60 H ₂ O 10	H ₂ -5Cl-thsa-Me 0.48, 2.0	NH ₄ OH 0.16, 4.0	Fe(NO ₃) ₃ ·9H ₂ O 0.40, 1.0	38.7	Crystalline
RP2:41:1	80	MeOH 60 H ₂ O 10	H ₂ -5Cl-thsa-Ph 0.62, 2.0	-	Fe(NO ₃) ₃ ·9H ₂ O 0.40, 1.0	43.1	Crystalline
RP2:41:2	80	MeOH 60 H ₂ O 10	H ₂ -5Cl-thsa-Ph 0.62, 2.0	NH ₄ OH 0.04, 1.0	Fe(NO ₃) ₃ ·9H ₂ O 0.40, 1.0	45.6	Crystalline
RP2:42:3	80	MeOH 60 H ₂ O 10	H ₂ -5Cl-thsa-Ph 0.62, 2.0	NH ₄ OH 0.08, 2.0	Fe(NO ₃) ₃ ·9H ₂ O 0.40, 1.0	42.8	Crystalline
RP2:44:1	80	MeOH 70	H ₂ -thsa-Me 0.42, 2.0	Et ₃ N 0.137 mL, 1.0	Fe(NO ₃) ₃ ·9H ₂ O 0.40, 1.0	43.6	Powder
RP2:44:2	80	MeOH 70	H ₂ -thsa-Me 0.42, 2.0	Et ₃ N 0.275 mL, 2.0	Fe(NO ₃) ₃ ·9H ₂ O 0.40, 1.0	54.7	Powder
RP2:45:3	80	MeOH 70	H ₂ -thsa-Me 0.42, 2.0	Et ₃ N 0.41 mL, 3.0	Fe(NO ₃) ₃ ·9H ₂ O 0.40, 1.0	41.2	Crystalline
RP2:45:1	80	MeOH 70	H ₂ -thsa-Et 0.44, 2.0	Et ₃ N 0.137 mL, 1.0	Fe(NO ₃) ₃ ·9H ₂ O 0.40, 1.0	38.7	Crystalline
RP2:46:2	80	MeOH 70	H ₂ -thsa-Et 0.44, 2.0	Et ₃ N 0.275 mL, 2.0	Fe(NO ₃) ₃ ·9H ₂ O 0.40, 1.0	48.7	Crystalline

Table E2.1 Quantities used in the synthesis of Fe^{III} complexes with R-salicylaldehyde 4R'-thiosemicarbazone (H₂-R-thsa-R') ligands continued.

Experimental code for Fe ^{III} Complex synthesis	T (°C)	Solvent (mL)	H ₂ -R-thsa-R' Ligand (g, mmol)	Cation (g, mmol)	Fe ^{III} (salt) (g, mmol)	Product Yield %	State of material
RP2:46:3	80	MeOH 70	H ₂ -thsa-Et 0.44, 2.0	Et ₃ N 0.41 mL, 3.0	Fe(NO ₃) ₃ ·9H ₂ O 0.40, 1.0	54.2	Crystalline
RP2:47:1	80	MeOH 70	H ₂ -thsa-Ph 0.54, 2.0	Et ₃ N 0.137 mL, 1.0	Fe(NO ₃) ₃ ·9H ₂ O 0.40, 1.0	-	No result
RP2:47:2	80	MeOH 70	H ₂ -thsa-Ph 0.54, 2.0	Et ₃ N 0.275 mL, 2.0	Fe(NO ₃) ₃ ·9H ₂ O 0.40, 1.0	72.1	Black powder
RP2:48:3	80	MeOH 70	H ₂ -thsa-Ph 0.54, 2.0	Et ₃ N 0.41 mL, 3.0	Fe(NO ₃) ₃ ·9H ₂ O 0.40, 1.0	66.5	Powder
RP2:48:1	80	MeOH 70	H ₂ -5Cl-thsa 0.46, 2.0	(CH ₃) ₂ NH 0.45, 10.0	Fe(NO ₃) ₃ ·9H ₂ O 0.40, 1.0	-	No result
RP2:49:2	80	MeOH 70	H ₂ -5Cl-thsa-Me 0.48, 2.0	(CH ₃) ₂ NH 0.45, 10.0	Fe(NO ₃) ₃ ·9H ₂ O 0.40, 1.0	56.4	Powder
RP2:49:3	80	MeOH 70	H ₂ -5Cl-thsa-Ph 0.62, 2.0	(CH ₃) ₂ NH 0.45, 10.0	Fe(NO ₃) ₃ ·9H ₂ O 0.40, 1.0	64.8	Powder
RP2:50:1	80	MeOH 70	H ₂ -5Cl-thsa-Ph 0.62, 2.0	NH ₄ OH 0.105 mL, 3.0	Fe(NO ₃) ₃ ·9H ₂ O 0.40, 1.0	45.2	Powder
RP2:50:2	80	MeOH 70	H ₂ -5Cl-thsa-Ph 0.62, 2.0	NH ₄ OH 0.14 mL, 4.0	Fe(NO ₃) ₃ ·9H ₂ O 0.40, 1.0	42.8	Powder
RP2:51:1	80	MeOH 70	H ₂ -3,5Br-thsa 0.70, 2.0	NH ₄ OH 0.035 mL, 1.0	Fe(NO ₃) ₃ ·9H ₂ O 0.40, 1.0	38.8	Brown powder
RP2:51:2	80	EtOH 85	H ₂ -3,5Br-thsa 0.70, 2.0	NH ₄ OH 0.035 mL, 1.0	Fe(NO ₃) ₃ ·9H ₂ O 0.40, 1.0	45.6	Powder
RP2:52:3	80	H ₂ O 70	H ₂ -3,5Br-thsa 0.70, 2.0	NH ₄ OH 0.035 mL, 1.0	Fe(NO ₃) ₃ ·9H ₂ O 0.40, 1.0	-	No result
RP2:53:1	80	MeOH 70	H ₂ -4OH-thsa 0.42, 2.0	NH ₄ OH 0.035 mL, 1.0	FeCl ₃ ·6H ₂ O 0.27, 1.0	-	No result

Table E2.1 Quantities used in the synthesis of Fe^{III} complexes with R-salicylaldehyde 4R'-thiosemicarbazone (H₂-R-thsa-R') ligands continued.

Experimental code for Fe ^{III} Complex synthesis	T (°C)	Solvent (mL)	H ₂ -R-thsa-R' Ligand (g, mmol)	Cation (g, mmol)	Fe ^{III} (salt) (g, mmol)	Product Yield %	State of material
RP2:53:2	80	MeOH 70	H ₂ -4OH-thsa 0.42, 2.0	NH ₄ OH 0.07 mL, 2.0	FeCl ₃ ·6H ₂ O 0.27, 1.0	-	No result
RP2:54:3	80	MeOH 70	H ₂ -4OH-thsa 0.42, 2.0	NH ₄ OH 0.105 mL, 3.0	FeCl ₃ ·6H ₂ O 0.27, 1.0	-	No result
RP2:54:4	80	MeOH 70	H ₂ -4OH-thsa 0.42, 2.0	NH ₄ OH 0.14 mL, 4.0	FeCl ₃ ·6H ₂ O 0.27, 1.0	-	No result
RP2:55:5	80	MeOH 70	H ₂ -4OH-thsa 0.42, 2.0	Et ₃ N 0.137 mL, 1.0	FeCl ₃ ·6H ₂ O 0.27, 1.0	-	No result
RP2:55:6	80	MeOH 70	H ₂ -4OH-thsa 0.42, 2.0	Et ₃ N 0.275 mL, 2.0	FeCl ₃ ·6H ₂ O 0.27, 1.0	-	No result
RP2:56:7	80	MeOH 70	H ₂ -4OH-thsa 0.42, 2.0	Et ₃ N 0.41 mL, 3.0	FeCl ₃ ·6H ₂ O 0.27, 1.0	-	No result
RP2:56:8	80	MeOH 70	H ₂ -4OH-thsa 0.42, 2.0	Et ₃ N 0.548 mL, 4.0	FeCl ₃ ·6H ₂ O 0.27, 1.0	-	No result
RP2:57:9	80	MeOH 70	H ₂ -4OH-thsa 0.42, 2.0	(CH ₃) ₂ NH 0.05 mL, 1.0	FeCl ₃ ·6H ₂ O 0.27, 1.0	-	No result
RP2:57:10	80	MeOH 70	H ₂ -4OH-thsa 0.42, 2.0	(CH ₃) ₂ NH 0.10 mL, 2.0	FeCl ₃ ·6H ₂ O 0.27, 1.0	-	No result
RP2:58:11	80	MeOH 70	H ₂ -4OH-thsa 0.42, 2.0	(CH ₃) ₂ NH 0.15 mL, 3.0	FeCl ₃ ·6H ₂ O 0.27, 1.0	-	No result
RP2:58:12	80	MeOH 70	H ₂ -4OH-thsa 0.42, 2.0	(CH ₃) ₂ NH 0.20 mL, 4.0	FeCl ₃ ·6H ₂ O 0.27, 1.0	-	No result
RP2:59:1	80	MeOH 70	H ₂ -4OH-thsa-Me 0.45, 2.0	Et ₃ N 0.137 mL, 1.0	FeCl ₃ ·6H ₂ O 0.27, 1.0	-	No result
RP2:59:2	80	MeOH 70	H ₂ -4OH-thsa-Me 0.45, 2.0	Et ₃ N 0.275 mL, 2.0	FeCl ₃ ·6H ₂ O 0.27, 1.0	-	No result

Table E2.1 Quantities used in the synthesis of Fe^{III} complexes with R-salicylaldehyde 4R'-thiosemicarbazone (H₂-R-thsa-R') ligands continued.

Experimental code for Fe ^{III} Complex synthesis	T (°C)	Solvent (mL)	H ₂ -R-thsa-R' Ligand (g, mmol)	Cation (g, mmol)	Fe ^{III} (salt) (g, mmol)	Product Yield %	State of material
RP2:60:3	80	MeOH 70	H ₂ -4OH-thsa-Me 0.45, 2.0	Et ₃ N 0.41 mL, 3.0	FeCl ₃ ·6H ₂ O 0.27, 1.0	45.7	Powder
RP2:60:4	80	MeOH 70	H ₂ -4OH-thsa-Me 0.45, 2.0	Et ₃ N 0.548 mL, 4.0	FeCl ₃ ·6H ₂ O 0.27, 1.0	57.8	Powder
RP2:61:5	80	MeOH 70	H ₂ -4OH-thsa-Me 0.45, 2.0	(CH ₃) ₂ NH 0.05 mL, 1.0	FeCl ₃ ·6H ₂ O 0.27, 1.0	-	No result
RP2:61:6	80	MeOH 70	H ₂ -4OH-thsa-Me 0.45, 2.0	(CH ₃) ₂ NH 0.10 mL, 2.0	FeCl ₃ ·6H ₂ O 0.27, 1.0	-	No result
RP2:62:7	80	MeOH 70	H ₂ -4OH-thsa-Me 0.45, 2.0	(CH ₃) ₂ NH 0.15 mL, 3.0	FeCl ₃ ·6H ₂ O 0.27, 1.0	-	No result
RP2:62:8	80	MeOH 70	H ₂ -4OH-thsa-Me 0.45, 2.0	(CH ₃) ₂ NH 0.20 mL, 4.0	FeCl ₃ ·6H ₂ O 0.27, 1.0	34.6	Crystalline
RP2:63:9	80	MeOH 70	H ₂ -4OH-thsa-Me 0.45, 2.0	NH ₄ OH 0.035 mL, 1.0	FeCl ₃ ·6H ₂ O 0.27, 1.0	-	No result
RP2:63:10	80	MeOH 70	H ₂ -4OH-thsa-Me 0.45, 2.0	NH ₄ OH 0.07 mL, 2.0	FeCl ₃ ·6H ₂ O 0.27, 1.0	-	No result
RP2:64:11	80	MeOH 70	H ₂ -4OH-thsa-Me 0.45, 2.0	NH ₄ OH 0.105 mL, 3.0	FeCl ₃ ·6H ₂ O 0.27, 1.0	-	No result
RP2:64:12	80	MeOH 70	H ₂ -4OH-thsa-Me 0.45, 2.0	NH ₄ OH 0.14 mL, 4.0	FeCl ₃ ·6H ₂ O 0.27, 1.0	-	No result
RP2:65:1	80	MeOH 70	H ₂ -4OH-thsa-Et 0.48, 2.0	Et ₃ N 0.137 mL, 1.0	FeCl ₃ ·6H ₂ O 0.27, 1.0	-	No result
RP2:65:2	80	MeOH 70	H ₂ -4OH-thsa-Et 0.48, 2.0	Et ₃ N 0.275 mL, 2.0	FeCl ₃ ·6H ₂ O 0.27, 1.0	-	No result
RP2:66:3	80	MeOH 70	H ₂ -4OH-thsa-Et 0.48, 2.0	Et ₃ N 0.41 mL, 3.0	FeCl ₃ ·6H ₂ O 0.27, 1.0	55.8	Powder

Table E2.1 Quantities used in the synthesis of Fe^{III} complexes with R-salicylaldehyde 4R'-thiosemicarbazone (H₂-R-thsa-R') ligands continued.

Experimental code for Fe ^{III} Complex synthesis	T (°C)	Solvent (mL)	H ₂ -R-thsa-R' Ligand (g, mmol)	Cation (g, mmol)	Fe ^{III} (salt) (g, mmol)	Product Yield %	State of material
RP2:66:4	80	MeOH 70	H ₂ -4OH-thsa-Et 0.48, 2.0	Et ₃ N 0.548 mL, 4.0	FeCl ₃ ·6H ₂ O 0.27, 1.0	65.9	Powder
RP2:67:5	80	MeOH 70	H ₂ -4OH-thsa-Et 0.48, 2.0	NH ₄ OH 0.035 mL, 1.0	FeCl ₃ ·6H ₂ O 0.27, 1.0	-	No result
RP2:67:6	80	MeOH 70	H ₂ -4OH-thsa-Et 0.48, 2.0	NH ₄ OH 0.07 mL, 2.0	FeCl ₃ ·6H ₂ O 0.27, 1.0	-	No result
RP2:68:7	80	MeOH 70	H ₂ -4OH-thsa-Et 0.48, 2.0	NH ₄ OH 0.105 mL, 3.0	FeCl ₃ ·6H ₂ O 0.27, 1.0	-	No result
RP2:68:8	80	MeOH 70	H ₂ -4OH-thsa-Et 0.48, 2.0	NH ₄ OH 0.14 mL, 4.0	FeCl ₃ ·6H ₂ O 0.27, 1.0	-	No result
RP2:69:9	80	MeOH 70	H ₂ -4OH-thsa-Et 0.48, 2.0	(CH ₃) ₂ NH 0.05 mL, 1.0	FeCl ₃ ·6H ₂ O 0.27, 1.0	-	No result
RP2:69:10	80	MeOH 70	H ₂ -4OH-thsa-Et 0.48, 2.0	(CH ₃) ₂ NH 0.10 mL, 2.0	FeCl ₃ ·6H ₂ O 0.27, 1.0	-	No result
RP2:70:11	80	MeOH 70	H ₂ -4OH-thsa-Et 0.48, 2.0	(CH ₃) ₂ NH 0.15 mL, 3.0	FeCl ₃ ·6H ₂ O 0.27, 1.0	-	No result
RP2:70:12	80	MeOH 70	H ₂ -4OH-thsa-Et 0.48, 2.0	(CH ₃) ₂ NH 0.20 mL, 4.0	FeCl ₃ ·6H ₂ O 0.27, 1.0	-	No result
RP2:72:1	80	MeOH 70	H ₂ -4OH-thsa-Ph 0.57, 2.0	Et ₃ N 0.137 mL, 1.0	FeCl ₃ ·6H ₂ O 0.27, 1.0	-	No result
RP2:72:2	80	MeOH 70	H ₂ -4OH-thsa-Ph 0.57, 2.0	Et ₃ N 0.275 mL, 2.0	FeCl ₃ ·6H ₂ O 0.27, 1.0	66.5	Powder
RP2:73:3	80	MeOH 70	H ₂ -4OH-thsa-Ph 0.57, 2.0	Et ₃ N 0.41 mL, 3.0	FeCl ₃ ·6H ₂ O 0.27, 1.0	57.8	Powder
RP2:73:4	80	MeOH 70	H ₂ -4OH-thsa-Ph 0.57, 2.0	Et ₃ N 0.548 mL, 4.0	FeCl ₃ ·6H ₂ O 0.27, 1.0	62.4	Powder

Table E2.1 Quantities used in the synthesis of Fe^{III} complexes with R-salicylaldehyde 4R'-thiosemicarbazone (H₂-R-thsa-R') ligands continued.

Experimental code for Fe ^{III} Complex synthesis	T (°C)	Solvent (mL)	H ₂ -R-thsa-R' Ligand (g, mmol)	Cation (g, mmol)	Fe ^{III} (salt) (g, mmol)	Product Yield %	State of material
RP2:76:1	80	MeOH 70	H ₂ -5Cl-thsa-Et 0.52, 2.0	Et ₃ N 0.137 mL, 1.0	FeCl ₃ ·6H ₂ O 0.27, 1.0	28.7	Crystalline
RP2:76:2	80	MeOH 70	H ₂ -5Cl-thsa-Et 0.52, 2.0	Et ₃ N 0.275 mL, 2.0	FeCl ₃ ·6H ₂ O 0.27, 1.0	33.5	Crystalline
RP2:77:3	80	MeOH 70	H ₂ -5Cl-thsa-Et 0.52, 2.0	Et ₃ N 0.41 mL, 3.0	FeCl ₃ ·6H ₂ O 0.27, 1.0	32.9	Crystalline
RP2:77:4	80	MeOH 70	H ₂ -5Cl-thsa-Et 0.52, 2.0	Et ₃ N 0.548 mL, 4.0	FeCl ₃ ·6H ₂ O 0.27, 1.0	-	No result
RP2:79:1	80	MeOH 70	H ₂ -4OH-thsa-Ph 0.57, 2.0	(CH ₃) ₂ NH 0.05 mL, 1.0	FeCl ₃ ·6H ₂ O 0.27, 1.0	-	No result
RP2:79:2	80	MeOH 70	H ₂ -4OH-thsa-Ph 0.57, 2.0	(CH ₃) ₂ NH 0.10 mL, 2.0	FeCl ₃ ·6H ₂ O 0.27, 1.0	-	No result
RP2:80:3	80	MeOH 70	H ₂ -4OH-thsa-Ph 0.57, 2.0	(CH ₃) ₂ NH 0.15 mL, 3.0	FeCl ₃ ·6H ₂ O 0.27, 1.0	-	No result
RP2:80:4	80	MeOH 70	H ₂ -4OH-thsa-Ph 0.57, 2.0	(CH ₃) ₂ NH 0.20 mL, 4.0	FeCl ₃ ·6H ₂ O 0.27, 1.0	-	No result
RP2:81:5	80	MeOH 70	H ₂ -4OH-thsa-Ph 0.57, 2.0	NH ₄ OH 0.035 mL, 1.0	FeCl ₃ ·6H ₂ O 0.27, 1.0	-	No result
RP2:81:6	80	MeOH 70	H ₂ -4OH-thsa-Ph 0.57, 2.0	NH ₄ OH 0.07 mL, 2.0	FeCl ₃ ·6H ₂ O 0.27, 1.0	-	No result
RP2:82:7	80	MeOH 70	H ₂ -4OH-thsa-Ph 0.57, 2.0	NH ₄ OH 0.105 mL, 3.0	FeCl ₃ ·6H ₂ O 0.27, 1.0	-	No result
RP2:82:8	80	MeOH 70	H ₂ -4OH-thsa-Ph 0.57, 2.0	NH ₄ OH 0.14 mL, 4.0	FeCl ₃ ·6H ₂ O 0.27, 1.0	-	No result
RP2:84:4	80	MeOH 70	H ₂ -5Cl-thsa-Et 0.52, 2.0	NH ₄ OH 0.035 mL, 1.0	Fe(NO ₃) ₃ ·9H ₂ O 0.40, 1.0	-	No result

Table E2.1 Quantities used in the synthesis of Fe^{III} complexes with R-salicylaldehyde 4R'-thiosemicarbazone (H₂-R-thsa-R') ligands continued.

Experimental code for Fe ^{III} Complex synthesis	T (°C)	Solvent (mL)	H ₂ -R-thsa-R' Ligand (g, mmol)	Cation (g, mmol)	Fe ^{III} (salt) (g, mmol)	Product Yield %	State of material
RP2:84:5	80	MeOH 70	H ₂ -5Cl-thsa-Et 0.52, 2.0	NH ₄ OH 0.07 mL, 2.0	Fe(NO ₃) ₃ ·9H ₂ O 0.40, 1.0	-	No result
RP2:85:6	80	MeOH 70	H ₂ -5Cl-thsa-Et 0.52, 2.0	NH ₄ OH 0.105 mL, 3.0	Fe(NO ₃) ₃ ·9H ₂ O 0.40, 1.0	48.7	Powder
RP2:85:7	80	MeOH 70	H ₂ -5Cl-thsa-Et 0.52, 2.0	NH ₄ OH 0.14 mL, 4.0	Fe(NO ₃) ₃ ·9H ₂ O 0.40, 1.0	52.5	Powder
RP2:92:1	80	MeOH 70	H ₂ -4OMe-thsa 0.45, 2.0	Et ₃ N 0.137 mL, 1.0	Fe(NO ₃) ₃ ·9H ₂ O 0.40, 1.0	-	No result
RP2:92:2	80	MeOH 70	H ₂ -4OMe-thsa 0.45, 2.0	Et ₃ N 0.275 mL, 2.0	Fe(NO ₃) ₃ ·9H ₂ O 0.40, 1.0	65.2	Powder
RP2:93:3	80	MeOH 70	H ₂ -4OMe-thsa 0.45, 2.0	Et ₃ N 0.41 mL, 3.0	Fe(NO ₃) ₃ ·9H ₂ O 0.40, 1.0	43.7	Crystalline
RP2:93:4	80	MeOH 70	H ₂ -4OMe-thsa 0.45, 2.0	Et ₃ N 0.548 mL, 4.0	Fe(NO ₃) ₃ ·9H ₂ O 0.40, 1.0	-	No result
RP2:95:5	80	MeOH 70	H ₂ -4OMe-thsa 0.45, 2.0	NH ₄ OH 0.035 mL, 1.0	Fe(NO ₃) ₃ ·9H ₂ O 0.40, 1.0	-	No result
RP2:95:6	80	MeOH 70	H ₂ -4OMe-thsa 0.45, 2.0	NH ₄ OH 0.07 mL, 2.0	Fe(NO ₃) ₃ ·9H ₂ O 0.40, 1.0	52.6	Crystalline
RP2:96:7	80	MeOH 70	H ₂ -4OMe-thsa 0.45, 2.0	NH ₄ OH 0.105 mL, 3.0	Fe(NO ₃) ₃ ·9H ₂ O 0.40, 1.0	-	No result
RP2:96:8	80	MeOH 70	H ₂ -4OMe-thsa 0.45, 2.0	NH ₄ OH 0.14 mL, 4.0	Fe(NO ₃) ₃ ·9H ₂ O 0.40, 1.0	-	No result
RP2:97:9	80	MeOH 70	H ₂ -4OMe-thsa 0.45, 2.0	(CH ₃) ₂ NH 0.05 mL, 1.0	Fe(NO ₃) ₃ ·9H ₂ O 0.40, 1.0	-	No result
RP2:97:10	80	MeOH 70	H ₂ -4OMe-thsa 0.45, 2.0	(CH ₃) ₂ NH 0.10 mL, 2.0	Fe(NO ₃) ₃ ·9H ₂ O 0.40, 1.0	54.8	Powder

Table E2.1 Quantities used in the synthesis of Fe^{III} complexes with R-salicylaldehyde 4R'-thiosemicarbazone (H₂-R-thsa-R') ligands continued.

Experimental code for Fe ^{III} Complex synthesis	T (°C)	Solvent (mL)	H ₂ -R-thsa-R' Ligand (g, mmol)	Cation (g, mmol)	Fe ^{III} (salt) (g, mmol)	Product Yield %	State of material
RP2:98:1	80	MeOH 70	H ₂ -5Cl-thsa-Me 0.48, 2.0	NH ₄ OH 0.035 mL, 1.0	Fe(NO ₃) ₃ ·9H ₂ O 0.40, 1.0	32.7	Crystalline
RP2:98:2	80	MeOH 70	H ₂ -5Cl-thsa-Me 0.48, 2.0	NH ₄ OH 0.07 mL, 2.0	Fe(NO ₃) ₃ ·9H ₂ O 0.40, 1.0	43.5	Crystalline
RP2:99:3	80	MeOH 70	H ₂ -5Cl-thsa-Me 0.48, 2.0	NH ₄ OH 0.105 mL, 3.0	Fe(NO ₃) ₃ ·9H ₂ O 0.40, 1.0	45.2	Crystalline
RP2:99:4	80	MeOH 70	H ₂ -5Cl-thsa-Me 0.48, 2.0	NH ₄ OH 0.14 mL, 4.0	Fe(NO ₃) ₃ ·9H ₂ O 0.40, 1.0	52.8	Crystalline
RP2:100:8	80	MeOH 70	H ₂ -5Cl-thsa-Et 0.52, 2.0	(CH ₃) ₂ NH 0.05 mL, 1.0	Fe(NO ₃) ₃ ·9H ₂ O 0.40, 1.0	55.4	Powder
RP2:100:9	80	MeOH 70	H ₂ -5Cl-thsa-Et 0.52, 2.0	(CH ₃) ₂ NH 0.10 mL, 2.0	Fe(NO ₃) ₃ ·9H ₂ O 0.40, 1.0	58.6	Powder
RP2:101:10	80	MeOH 70	H ₂ -5Cl-thsa-Et 0.52, 2.0	(CH ₃) ₂ NH 0.15 mL, 3.0	Fe(NO ₃) ₃ ·9H ₂ O 0.40, 1.0	62.5	Powder
RP2:101:12	80	MeOH 70	H ₂ -5Cl-thsa-Et 0.52, 2.0	(CH ₃) ₂ NH 0.20 mL, 4.0	Fe(NO ₃) ₃ ·9H ₂ O 0.40, 1.0	61.9	Powder
RP2:106:1	80	MeOH 70	H ₂ -3OEt-thsa-Et 0.54, 2.0	Et ₃ N 0.137 mL, 1.0	FeCl ₃ ·6H ₂ O 0.27, 1.0	32.7	Crystalline
RP2:106:2	80	MeOH 70	H ₂ -3OEt-thsa-Et 0.54, 2.0	Et ₃ N 0.275 mL, 2.0	FeCl ₃ ·6H ₂ O 0.27, 1.0	43.2	Crystalline
RP2:107:3	80	MeOH 70	H ₂ -3OEt-thsa-Et 0.54, 2.0	Et ₃ N 0.41 mL, 3.0	FeCl ₃ ·6H ₂ O 0.27, 1.0	42.1	Crystalline
RP2:107:4	80	MeOH 70	H ₂ -3OEt-thsa-Et 0.54, 2.0	Et ₃ N 0.548 mL, 4.0	FeCl ₃ ·6H ₂ O 0.27, 1.0	38.7	Crystalline
RP2:108:5	80	MeOH 70	H ₂ -3OEt-thsa-Et 0.54, 2.0	(CH ₃) ₂ NH 0.05 mL, 1.0	FeCl ₃ ·6H ₂ O 0.27, 1.0	28.6	Crystalline

Table E2.1 Quantities used in the synthesis of Fe^{III} complexes with R-salicylaldehyde 4R'-thiosemicarbazone (H₂-R-thsa-R') ligands continued.

Experimental code for Fe ^{III} Complex synthesis	T (°C)	Solvent (mL)	H ₂ -R-thsa-R' Ligand (g, mmol)	Cation (g, mmol)	Fe ^{III} (salt) (g, mmol)	Product Yield %	State of material
RP2:108:6	80	MeOH 70	H ₂ -3OEt-thsa-Et 0.54, 2.0	(CH ₃) ₂ NH 0.10 mL, 2.0	FeCl ₃ ·6H ₂ O 0.27, 1.0	36.3	Crystalline
RP2:109:7	80	MeOH 70	H ₂ -3OEt-thsa-Et 0.54, 2.0	(CH ₃) ₂ NH 0.15 mL, 3.0	FeCl ₃ ·6H ₂ O 0.27, 1.0	38.7	Crystalline
RP2:109:8	80	MeOH 70	H ₂ -3OEt-thsa-Et 0.54, 2.0	(CH ₃) ₂ NH 0.20 mL, 4.0	FeCl ₃ ·6H ₂ O 0.27, 1.0	26.4	Crystalline
RP2:110:1	80	MeOH 30	H ₂ -3OH-thsa 0.21, 1.0	(CH ₃) ₂ NH 0.05 mL, 1.0	Fe(NO ₃) ₃ ·9H ₂ O 0.20, 0.5	28.5	Crystalline
RP2:110:2	80	MeOH 30	H ₂ -3OH-thsa 0.21, 1.0	(CH ₃) ₂ NH 0.10 mL, 2.0	Fe(NO ₃) ₃ ·9H ₂ O 0.20, 0.5	55.7	Powder
RP2:111:3	80	MeOH 30	H ₂ -3OH-thsa 0.21, 1.0	(CH ₃) ₂ NH 0.15 mL, 3.0	Fe(NO ₃) ₃ ·9H ₂ O 0.20, 0.5	45.9	Powder
RP2:111:4	80	MeOH 30	H ₂ -3OH-thsa 0.21, 1.0	(CH ₃) ₂ NH 0.20 mL, 4.0	Fe(NO ₃) ₃ ·9H ₂ O 0.20, 0.05	62.3	Powder
RP2:112:5	80	MeOH 30	H ₂ -3OH-thsa 0.21, 1.0	NH ₄ OH 0.035 mL, 1.0	Fe(NO ₃) ₃ ·9H ₂ O 0.20, 0.5	45.8	Crystalline
RP2:112:6	80	MeOH 30	H ₂ -3OH-thsa 0.21, 1.0	NH ₄ OH 0.07 mL, 2.0	Fe(NO ₃) ₃ ·9H ₂ O 0.20, 0.5	32.6	Crystalline
RP2:113:7	80	MeOH 30	H ₂ -3OH-thsa 0.21, 1.0	NH ₄ OH 0.105 mL, 3.0	Fe(NO ₃) ₃ ·9H ₂ O 0.20, 0.5	42.7	Crystalline
RP2:113:8	80	MeOH 30	H ₂ -3OH-thsa 0.21, 1.0	NH ₄ OH 0.14 mL, 4.0	Fe(NO ₃) ₃ ·9H ₂ O 0.20, 0.5	-	No result
RP2:114:1	80	MeOH 30	H ₂ -3OH-thsa-Me 0.23, 1.0	NH ₄ OH 0.035 mL, 1.0	Fe(NO ₃) ₃ ·9H ₂ O 0.20, 0.5	66.4	Powder
RP2:114:2	80	MeOH 30	H ₂ -3OH-thsa-Me 0.23, 1.0	NH ₄ OH 0.07 mL, 2.0	Fe(NO ₃) ₃ ·9H ₂ O 0.20, 0.5	26.5	Crystalline

Table E2.1 Quantities used in the synthesis of Fe^{III} complexes with R-salicylaldehyde 4R'-thiosemicarbazone (H₂-R-thsa-R') ligands continued.

Experimental code for Fe ^{III} Complex synthesis	T (°C)	Solvent (mL)	H ₂ -R-thsa-R' Ligand (g, mmol)	Cation (g, mmol)	Fe ^{III} (salt) (g, mmol)	Product Yield %	State of material
RP2:115:3	80	MeOH 30	H ₂ -3OH-thsa-Me 0.23, 1.0	NH ₄ OH 0.105 mL, 3.0	Fe(NO ₃) ₃ ·9H ₂ O 0.20, 0.5	32.8	Crystalline
RP2:115:4	80	MeOH 30	H ₂ -3OH-thsa-Me 0.23, 1.0	NH ₄ OH 0.14 mL, 4.0	Fe(NO ₃) ₃ ·9H ₂ O 0.20, 0.5	28.7	Crystalline
RP2:116:1	80	MeOH 30	H ₂ -3OH-thsa-Et 0.24, 1.0	NH ₄ OH 0.035 mL, 1.0	Fe(NO ₃) ₃ ·9H ₂ O 0.20, 0.5	55.8	Powder
RP2:116:2	80	MeOH 30	H ₂ -3OH-thsa-Et 0.24, 1.0	NH ₄ OH 0.07 mL, 2.0	Fe(NO ₃) ₃ ·9H ₂ O 0.20, 0.5	47.6	Crystalline
RP2:117:3	80	MeOH 30	H ₂ -3OH-thsa-Et 0.24, 1.0	NH ₄ OH 0.105 mL, 3.0	Fe(NO ₃) ₃ ·9H ₂ O 0.20, 0.5	57.5	Crystalline
RP2:117:4	80	MeOH 30	H ₂ -3OH-thsa-Et 0.24, 1.0	NH ₄ OH 0.14 mL, 4.0	Fe(NO ₃) ₃ ·9H ₂ O 0.20, 0.5	48.9	Crystalline
RP2:120:1	80	MeOH 25 EtOH 25 H ₂ O 10	H ₂ -5Cl-thsa-Et 0.52, 2.0	(CH ₃) ₂ NH 0.51 mL, 10.0	Fe(NO ₃) ₃ ·9H ₂ O 0.40, 1.0	39.8	Crystalline
RP2:120:2	80	MeOH 60	H ₂ -5Cl-thsa-Et 0.52, 2.0	(CH ₃) ₂ NH 0.51 mL, 10.0	Fe(NO ₃) ₃ ·9H ₂ O 0.40, 1.0	43.7	Crystalline
RP2:121:3	80	MeOH 25 EtOH 25 H ₂ O 10	H ₂ -5Cl-thsa-Ph 0.62, 2.0	(CH ₃) ₂ NH 0.51 mL, 10.0	Fe(NO ₃) ₃ ·9H ₂ O 0.40, 1.0	68.2	Powder
RP2:121:4	80	MeOH 60	H ₂ -5Cl-thsa-Ph 0.62, 2.0	(CH ₃) ₂ NH 0.51 mL, 10.0	Fe(NO ₃) ₃ ·9H ₂ O 0.40, 1.0	56.8	Powder
RP2:122:1	80	MeOH 25 EtOH 25 H ₂ O 10	H ₂ -thsa-Et 0.44, 2.0	(CH ₃) ₂ NH 0.51 mL, 10.0	Fe(NO ₃) ₃ ·9H ₂ O 0.40, 1.0	65.8	Powder
RP2:122:2	80	MeOH 60	H ₂ -thsa-Et 0.44, 2.0	(CH ₃) ₂ NH 0.51 mL, 10.0	Fe(NO ₃) ₃ ·9H ₂ O 0.40, 1.0	61.4	Powder

Table E2.1 Quantities used in the synthesis of Fe^{III} complexes with R-salicylaldehyde 4R'-thiosemicarbazone (H₂-R-thsa-R') ligands continued.

Experimental code for Fe ^{III} Complex synthesis	T (°C)	Solvent (mL)	H ₂ -R-thsa-R' Ligand (g, mmol)	Cation (g, mmol)	Fe ^{III} (salt) (g, mmol)	Product Yield %	State of material
RP2:123:3	80	MeOH 25 EtOH 25 H ₂ O 10	H ₂ -thsa-Ph 0.54, 2.0	(CH ₃) ₂ NH 0.51 mL, 10.0	Fe(NO ₃) ₃ ·9H ₂ O 0.40, 1.0	64.5	Powder
RP2:123:4	80	MeOH 60	H ₂ -thsa-Ph 0.54, 2.0	(CH ₃) ₂ NH 0.51 mL, 10.0	Fe(NO ₃) ₃ ·9H ₂ O 0.40, 1.0	67.8	Powder
RP2:124:5	80	MeOH 25 EtOH 25 H ₂ O 10	H ₂ -thsa-Ph 0.54, 2.0	(CH ₃) ₂ NH 0.51 mL, 10.0	Fe(NO ₃) ₃ ·9H ₂ O 0.40, 1.0	63.7	Powder
RP2:124:6	80	MeOH 60	H ₂ -thsa-Ph 0.54, 2.0	(CH ₃) ₂ NH 0.51 mL, 10.0	Fe(NO ₃) ₃ ·9H ₂ O 0.40, 1.0	65.0	Powder
RP2:125:1	80	MeOH 25 EtOH 25 H ₂ O 10	H ₂ -5Br-thsa 0.54, 2.0	(CH ₃) ₂ NH 0.51 mL, 10.0	Fe(NO ₃) ₃ ·9H ₂ O 0.40, 1.0	56.7	Crystalline
RP2:125:2	80	MeOH 60	H ₂ -5Br-thsa 0.54, 2.0	(CH ₃) ₂ NH 0.51 mL, 10.0	Fe(NO ₃) ₃ ·9H ₂ O 0.40, 1.0	-	No result
RP2:126:3	80	MeOH 25 EtOH 25 H ₂ O 10	H ₂ -5Br-thsa-Me 0.58, 2.0	(CH ₃) ₂ NH 0.51 mL, 10.0	Fe(NO ₃) ₃ ·9H ₂ O 0.40, 1.0	54.9	Crystalline
RP2:126:4	80	MeOH 60	H ₂ -5BR-thsa-Me 0.58, 2.0	(CH ₃) ₂ NH 0.51 mL, 10.0	Fe(NO ₃) ₃ ·9H ₂ O 0.40, 1.0	-	No result
RP2:127:5	80	MeOH 25 EtOH 25 H ₂ O 10	H ₂ -5Br-thsa-Et 0.60, 2.0	(CH ₃) ₂ NH 0.51 mL, 10.0	Fe(NO ₃) ₃ ·9H ₂ O 0.40, 1.0	48.7	Crystalline
RP2:127:6	80	MeOH 60	H ₂ -5Br-thsa-Et 0.60, 2.0	(CH ₃) ₂ NH 0.51 mL, 10.0	Fe(NO ₃) ₃ ·9H ₂ O 0.40, 1.0	38.9	Crystalline

Table E2.1 Quantities used in the synthesis of Fe^{III} complexes with R-salicylaldehyde 4R'-thiosemicarbazone (H₂-R-thsa-R') ligands continued.

Experimental code for Fe ^{III} Complex synthesis	T (°C)	Solvent (mL)	H ₂ -R-thsa-R' Ligand (g, mmol)	Cation (g, mmol)	Fe ^{III} (salt) (g, mmol)	Product Yield %	State of material
RP2:128:7	80	MeOH 25 EtOH 25 H ₂ O 10	H ₂ -5Br-thsa-Ph 0.70, 2.0	(CH ₃) ₂ NH 0.51 mL, 10.0	Fe(NO ₃) ₃ ·9H ₂ O 0.40, 1.0	47.5	Powder
RP2:128:8	80	MeOH 60	H ₂ -5Br-thsa-Ph 0.70, 2.0	(CH ₃) ₂ NH 0.51 mL, 10.0	Fe(NO ₃) ₃ ·9H ₂ O 0.40, 1.0	-	No result
RP2:131:1	80	MeOH 30	H ₂ -4OH-thsa 0.21, 1.0	(CH ₃) ₂ NH 0.05 mL, 1.0	Fe(NO ₃) ₃ ·9H ₂ O 0.20, 0.5	57.8	Crystalline
RP2:131:2	80	MeOH 30	H ₂ -4OH-thsa-Et 0.54, 2.0	(CH ₃) ₂ NH 0.05 mL, 1.0	Fe(NO ₃) ₃ ·9H ₂ O 0.20, 0.5	63.4	Crystalline
RP2:134:1	80	MeOH 25 EtOH 25 H ₂ O 10	H ₂ -3OEt-thsa 0.48, 2.0	(CH ₃) ₂ NH 0.05 mL, 1.0	Fe(NO ₃) ₃ ·9H ₂ O 0.40, 1.0	-	No result
RP2:134:2	80	MeOH 25 EtOH 25 H ₂ O 10	H ₂ -3OEt-thsa 0.48, 2.0	(CH ₃) ₂ NH 0.10 mL, 2.0	Fe(NO ₃) ₃ ·9H ₂ O 0.40, 1.0	-	No result
RP2:135:3	80	MeOH 25 EtOH 25 H ₂ O 10	H ₂ -3OEt-thsa 0.48, 2.0	(CH ₃) ₂ NH 0.15 mL, 3.0	Fe(NO ₃) ₃ ·9H ₂ O 0.40, 1.0	-	No result
RP2:135:4	80	MeOH 25 EtOH 25 H ₂ O 10	H ₂ -3OEt-thsa 0.48, 2.0	(CH ₃) ₂ NH 0.20 mL, 4.0	Fe(NO ₃) ₃ ·9H ₂ O 0.40, 1.0	-	No result
RP2:136:5	80	MeOH 25 EtOH 25 H ₂ O 10	H ₂ -3OEt-thsa 0.48, 2.0	(CH ₃) ₂ NH 0.51 mL, 10.0	Fe(NO ₃) ₃ ·9H ₂ O 0.40, 1.0	-	No result
RP2:136:1	80	MeOH 25 EtOH 25 H ₂ O 10	H ₂ -3OEt-thsa-Me 0.50, 2.0	(CH ₃) ₂ NH 0.05 mL, 1.0	Fe(NO ₃) ₃ ·9H ₂ O 0.40, 1.0	-	No result

Table E2.1 Quantities used in the synthesis of Fe^{III} complexes with R-salicylaldehyde 4R'-thiosemicarbazone (H₂-R-thsa-R') ligands continued.

Experimental code for Fe ^{III} Complex synthesis	T (°C)	Solvent (mL)	H ₂ -R-thsa-R' Ligand (g, mmol)	Cation (g, mmol)	Fe ^{III} (salt) (g, mmol)	Product Yield %	State of material
RP2:137:2	80	MeOH 25 EtOH 25 H ₂ O 10	H ₂ -3OEt-thsa-Me 0.50, 2.0	(CH ₃) ₂ NH 0.10 mL, 2.0	Fe(NO ₃) ₃ ·9H ₂ O 0.40, 1.0	-	No result
RP2:137:3	80	MeOH 25 EtOH 25 H ₂ O 10	H ₂ -3OEt-thsa-Me 0.50, 2.0	(CH ₃) ₂ NH 0.15 mL, 3.0	Fe(NO ₃) ₃ ·9H ₂ O 0.40, 1.0	-	No result
RP2:140:4	80	MeOH 25 EtOH 25 H ₂ O 10	H ₂ -3OEt-thsa-Me 0.50, 2.0	(CH ₃) ₂ NH 0.20 mL, 4.0	Fe(NO ₃) ₃ ·9H ₂ O 0.40, 1.0	-	No result
RP2:140:5	80	MeOH 25 EtOH 25 H ₂ O 10	H ₂ -3OEt-thsa-Me 0.50, 2.0	(CH ₃) ₂ NH 0.51 mL, 10.0	Fe(NO ₃) ₃ ·9H ₂ O 0.40, 1.0	-	No result
RP2:141:1	80	MeOH 25 EtOH 25 H ₂ O 10	H ₂ -3OEt-thsa-Et 0.54, 2.0	(CH ₃) ₂ NH 0.05 mL, 1.0	Fe(NO ₃) ₃ ·9H ₂ O 0.40, 1.0	-	No result
RP2:141:2	80	MeOH 25 EtOH 25 H ₂ O 10	H ₂ -3OEt-thsa-Et 0.54, 2.0	(CH ₃) ₂ NH 0.10 mL, 2.0	Fe(NO ₃) ₃ ·9H ₂ O 0.40, 1.0	-	No result
RP2:142:3	80	MeOH 25 EtOH 25 H ₂ O 10	H ₂ -3OEt-thsa-Et 0.54, 2.0	(CH ₃) ₂ NH 0.15 mL, 3.0	Fe(NO ₃) ₃ ·9H ₂ O 0.40, 1.0	-	No result
RP2:142:4	80	MeOH 25 EtOH 25 H ₂ O 10	H ₂ -3OEt-thsa-Et 0.54, 2.0	(CH ₃) ₂ NH 0.20 mL, 4.0	Fe(NO ₃) ₃ ·9H ₂ O 0.40, 1.0	-	No result
RP2:143:5	80	MeOH 25 EtOH 25 H ₂ O 10	H ₂ -3OEt-thsa-Et 0.54, 2.0	(CH ₃) ₂ NH 0.51 mL, 10.0	Fe(NO ₃) ₃ ·9H ₂ O 0.40, 1.0	-	No result

Table E2.1 Quantities used in the synthesis of Fe^{III} complexes with R-salicylaldehyde 4R'-thiosemicarbazone (H₂-R-thsa-R') ligands continued.

Experimental code for Fe ^{III} Complex synthesis	T (°C)	Solvent (mL)	H ₂ -R-thsa-R' Ligand (g, mmol)	Cation (g, mmol)	Fe ^{III} (salt) (g, mmol)	Product Yield %	State of material
RP2:149:1	80	MeOH 60 H ₂ O 10	H ₂ -5Br-thsa-Ph 0.70, 2.0	(CH ₃) ₂ NH 0.51 mL, 10.0	Fe(NO ₃) ₃ ·9H ₂ O 0.40, 1.0	-	No result
RP2:155:1	80	MeOH 50 H ₂ O 10	H ₂ -5Br-thsa-Ph 0.35, 1.0	(CH ₃) ₂ NH 0.05 mL, 1.0	Fe(NO ₃) ₃ ·9H ₂ O 0.40, 1.0	-	No result
RP2:155:2	80	MeOH 50 H ₂ O 10	H ₂ -5Br-thsa-Ph 0.35, 1.0	(CH ₃) ₂ NH 0.10 mL, 2.0	Fe(NO ₃) ₃ ·9H ₂ O 0.40, 1.0	-	No result
RP2:156:3	80	MeOH 50 H ₂ O 10	H ₂ -5Br-thsa-Ph 0.35, 1.0	(CH ₃) ₂ NH 0.15 mL, 3.0	Fe(NO ₃) ₃ ·9H ₂ O 0.40, 1.0	-	No result
RP2:156:4	80	MeOH 50 H ₂ O 10	H ₂ -5Br-thsa-Ph 0.35, 1.0	(CH ₃) ₂ NH 0.20 mL, 4.0	Fe(NO ₃) ₃ ·9H ₂ O 0.40, 1.0	-	No result
RP2:157:5	80	MeOH 50 H ₂ O 10	H ₂ -5Br-thsa-Ph 0.35, 1.0	(CH ₃) ₂ NH 0.51 mL, 10.0	Fe(NO ₃) ₃ ·9H ₂ O 0.40, 1.0	-	No result
RP2:157:1	80	MeOH 50 H ₂ O 10	H ₂ -thsa-Ph 0.27, 1.0	(CH ₃) ₂ NH 0.51 mL, 10.0	Fe(NO ₃) ₃ ·9H ₂ O 0.40, 1.0	55.4	Powder
RP2:158:2	80	MeOH 50 H ₂ O 10	H ₂ -thsa-Ph 0.27, 1.0	(CH ₃) ₂ NH 0.05 mL, 1.0	Fe(NO ₃) ₃ ·9H ₂ O 0.40, 1.0	-	No result
RP2:158:3	80	MeOH 50 H ₂ O 10	H ₂ -thsa-Ph 0.27, 1.0	(CH ₃) ₂ NH 0.10 mL, 2.0	Fe(NO ₃) ₃ ·9H ₂ O 0.40, 1.0	-	No result
RP2:159:4	80	MeOH 50 H ₂ O 10	H ₂ -thsa-Ph 0.27, 1.0	(CH ₃) ₂ NH 0.15 mL, 3.0	Fe(NO ₃) ₃ ·9H ₂ O 0.40, 1.0	-	No result
RP2:159:5	80	MeOH 50 H ₂ O 10	H ₂ -thsa-Ph 0.27, 1.0	(CH ₃) ₂ NH 0.20 mL, 4.0	Fe(NO ₃) ₃ ·9H ₂ O 0.40, 1.0	-	No result
RP2:160:1	80	MeOH 50 H ₂ O 10	H ₂ -3,5Br-thsa-Ph 0.43, 1.0	(CH ₃) ₂ NH 0.51 mL, 10.0	Fe(NO ₃) ₃ ·9H ₂ O 0.40, 1.0	55.4	Powder
RP2:160:2	80	MeOH 50 H ₂ O 10	H ₂ -3,5Br-thsa-Ph 0.43, 1.0	(CH ₃) ₂ NH 0.05 mL, 1.0	Fe(NO ₃) ₃ ·9H ₂ O 0.40, 1.0	52.6	Powder

Table E2.1 Quantities used in the synthesis of Fe^{III} complexes with R-salicylaldehyde 4R'-thiosemicarbazone (H₂-R-thsa-R') ligands continued.

Experimental code for Fe ^{III} Complex synthesis	T (°C)	Solvent (mL)	H ₂ -R-thsa-R' Ligand (g, mmol)	Cation (g, mmol)	Fe ^{III} (salt) (g, mmol)	Product Yield %	State of material
RP2:161:3	80	MeOH 50 H ₂ O 10	H ₂ -3,5Br-thsa-Ph 0.43, 1.0	(CH ₃) ₂ NH 0.10 mL, 2.0	Fe(NO ₃) ₃ ·9H ₂ O 0.40, 1.0	43.7	Powder
RP2:161:4	80	MeOH 50 H ₂ O 10	H ₂ -3,5Br-thsa-Ph 0.43, 1.0	(CH ₃) ₂ NH 0.15 mL, 3.0	Fe(NO ₃) ₃ ·9H ₂ O 0.40, 1.0	62.7	Powder
RP2:162:5	80	MeOH 50 H ₂ O 10	H ₂ -3,5Br-thsa-Ph 0.43, 1.0	(CH ₃) ₂ NH 0.20 mL, 4.0	Fe(NO ₃) ₃ ·9H ₂ O 0.40, 1.0	61.2	Powder
RP2:172:5	80	MeOH 50 H ₂ O 10	H ₂ -5Br-thsa-Ph 0.35, 1.0	(CH ₃) ₂ NH 0.51 mL, 10.0	Fe(SO ₄) ₃ ·H ₂ O 0.40, 1.0	-	No result
RP2:172:6	80	MeOH 25 H ₂ O 10	H ₂ -3,5Br-thsa-Ph 0.43, 1.0	NH ₄ OH 0.04 mL, 1.0	Fe(SO ₄) ₃ ·H ₂ O 0.40, 1.0	-	No result
RP2:173:7	80	MeOH 25 H ₂ O 10	H ₂ -5Br-thsa-Ph 0.35, 1.0	NH ₄ OH 0.08 mL, 2.0	Fe(SO ₄) ₃ ·H ₂ O 0.40, 1.0	-	No result
RP2:173:8	80	MeOH 25 H ₂ O 10	H ₂ -5Br-thsa-Ph 0.35, 1.0	NH ₄ OH 0.12 mL, 3.0	Fe(SO ₄) ₃ ·H ₂ O 0.40, 1.0	47.6	Powder
RP2:174:9	80	MeOH 25 H ₂ O 10	H ₂ -5Br-thsa-Ph 0.35, 1.0	NH ₄ OH 0.16 mL, 4.0	Fe(SO ₄) ₃ ·H ₂ O 0.40, 1.0	56.3	Powder
RP2:174:10	80	MeOH 25 H ₂ O 10	H ₂ -5Br-thsa-Ph 0.35, 1.0	NH ₄ OH 0.4 mL, 10.0	Fe(SO ₄) ₃ ·H ₂ O 0.40, 1.0	65.7	Powder
RP2:175:11	80	MeOH 25 H ₂ O 10	H ₂ -5Br-thsa-Ph 0.35, 1.0	Et ₃ N 0.14 mL, 1.0	Fe(SO ₄) ₃ ·H ₂ O 0.40, 1.0	45.6	Powder
RP2:176:12	80	MeOH 25 H ₂ O 10	H ₂ -5Br-thsa-Ph 0.35, 1.0	Et ₃ N 0.28 mL, 2.0	Fe(SO ₄) ₃ ·H ₂ O 0.40, 1.0	56.3	Crystalline
RP2:176:13	80	MeOH 25 H ₂ O 10	H ₂ -5Br-thsa-Ph 0.35, 1.0	Et ₃ N 0.42 mL, 3.0	Fe(SO ₄) ₃ ·H ₂ O 0.40, 1.0	56.4	Crystalline
RP2:177:14	80	MeOH 25 H ₂ O 10	H ₂ -5Br-thsa-Ph 0.35, 1.0	Et ₃ N 0.56 mL, 4.0	Fe(SO ₄) ₃ ·H ₂ O 0.40, 1.0	34.2	Brown powder

Table E2.1 Quantities used in the synthesis of Fe^{III} complexes with R-salicylaldehyde 4R'-thiosemicarbazone (H₂-R-thsa-R') ligands continued.

Experimental code for Fe ^{III} Complex synthesis	T (°C)	Solvent (mL)	H ₂ -R-thsa-R' Ligand (g, mmol)	Cation (g, mmol)	Fe ^{III} (salt) (g, mmol)	Product Yield %	State of material
RP2:177:15	80	MeOH 25 H ₂ O 10	H ₂ -5Br-thsa-Ph 0.35, 1.0	Et ₃ N 1.4 mL, 10.0	Fe(SO ₄) ₃ ·H ₂ O 0.40, 1.0	55.1	Crystalline
RP2:178:1	80	MeOH 50 H ₂ O 10	H ₂ -thsa-Ph 0.54, 2.0	Et ₃ N 0.14 mL, 1.0	Fe(SO ₄) ₃ ·H ₂ O 0.40, 1.0	62.1	Black powder
RP2:178:2	80	MeOH 50 H ₂ O 10	H ₂ -thsa-Ph 0.54, 2.0	Et ₃ N 0.28 mL, 2.0	Fe(SO ₄) ₃ ·H ₂ O 0.40, 1.0	65.3	Black powder
RP2:179:3	80	MeOH 50 H ₂ O 10	H ₂ -thsa-Ph 0.54, 2.0	Et ₃ N 0.42 mL, 3.0	Fe(SO ₄) ₃ ·H ₂ O 0.40, 1.0	52.8	Black powder
RP2:179:4	80	MeOH 50 H ₂ O 10	H ₂ -thsa-Ph 0.54, 2.0	Et ₃ N 0.56 mL, 4.0	Fe(SO ₄) ₃ ·H ₂ O 0.40, 1.0	44.8	Black powder
RP2:180:5	80	MeOH 50 H ₂ O 10	H ₂ -thsa-Ph 0.54, 2.0	Et ₃ N 1.4 mL, 10.0	Fe(SO ₄) ₃ ·H ₂ O 0.40, 1.0	32.7	Crystalline
RP2:182:6	80	MeOH 50 H ₂ O 10	H ₂ -thsa-Ph 0.54, 2.0	NH ₄ OH 0.04 mL, 1.0	Fe(SO ₄) ₃ ·H ₂ O 0.40, 1.0	43.7	Black powder
RP2:182:7	80	MeOH 50 H ₂ O 10	H ₂ -thsa-Ph 0.54, 2.0	NH ₄ OH 0.08 mL, 2.0	Fe(SO ₄) ₃ ·H ₂ O 0.40, 1.0	53.8	Black powder
RP2:183:8	80	MeOH 250 H ₂ O 10	H ₂ -thsa-Ph 0.54, 2.0	NH ₄ OH 0.12 mL, 3.0	Fe(SO ₄) ₃ ·H ₂ O 0.40, 1.0	44.2	Black powder
RP2:183:9	80	MeOH 50 H ₂ O 10	H ₂ -thsa-Ph 0.54, 2.0	NH ₄ OH 0.16 mL, 4.0	Fe(SO ₄) ₃ ·H ₂ O 0.40, 1.0	46.5	Black powder
RP2:184:10	80	MeOH 50 H ₂ O 10	H ₂ -thsa-Ph 0.54, 2.0	NH ₄ OH 0.4 mL, 10.0	Fe(SO ₄) ₃ ·H ₂ O 0.40, 1.0	62.7	Black powder
RP2:184:11	80	MeOH 50 H ₂ O 10	H ₂ -thsa-Ph 0.54, 2.0	(CH ₃) ₂ NH 0.05 mL, 1.0	Fe(NO ₃) ₃ ·9H ₂ O 0.40, 1.0	52.6	Powder
RP2:185:12	80	MeOH 50 H ₂ O 10	H ₂ -thsa-Ph 0.54, 2.0	(CH ₃) ₂ NH 0.10 mL, 2.0	Fe(NO ₃) ₃ ·9H ₂ O 0.40, 1.0	43.7	Powder

Table E2.1 Quantities used in the synthesis of Fe^{III} complexes with R-salicylaldehyde 4R'-thiosemicarbazone (H₂-R-thsa-R') ligands continued.

Experimental code for Fe ^{III} Complex synthesis	T (°C)	Solvent (mL)	H ₂ -R-thsa-R' Ligand (g, mmol)	Cation (g, mmol)	Fe ^{III} (salt) (g, mmol)	Product Yield %	State of material
RP2:185:13	80	MeOH 50 H ₂ O 10	H ₂ -thsa-Ph 0.54, 2.0	(CH ₃) ₂ NH 0.15 mL, 3.0	Fe(NO ₃) ₃ ·9H ₂ O 0.40, 1.0	62.7	Powder
RP2:186:14	80	MeOH 50 H ₂ O 10	H ₂ -thsa-Ph 0.54, 2.0	(CH ₃) ₂ NH 0.20 mL, 4.0	Fe(NO ₃) ₃ ·9H ₂ O 0.40, 1.0	57.2	Powder
RP2:186:15	80	MeOH 50 H ₂ O 10	H ₂ -thsa-Ph 0.54, 2.0	(CH ₃) ₂ NH 0.51 mL, 10.0	Fe(SO ₄) ₃ ·H ₂ O 0.40, 1.0	59.4	Powder